Deliverable 7.1: INITIAL STATE-OF-THE-ART ON THM BEHAVIOUR OF I) BUFFER CLAY MATERIALS AND OF II) HOST CLAY MATERIALS

Work Package 7

The project leading to this application has received funding from the European Union's Horizon 2020 research and innovation programme under grant agreement No 847593.

Document information

Project Acronym	**EURAD**
Project Title	**European Joint Programme on Radioactive Waste Management**
Project Type	**European Joint Programme (EJP)**
EC grant agreement No.	**847593**
Project starting / end date	**1st June 2019 – 30 May 2024**
Work Package No.	**7**
Work Package Title	**Influence of Temperature on Clay-based Material Behaviour**
Work Package Acronym	**HITEC**
Deliverable No.	**7.1**
Deliverable Title	**Initial State-Of-The-Art on THM Behaviour of I) Buffer Clay Materials and of II) Host Clay Materials**
Lead Beneficiary	**CIEMAT**
Contractual Delivery Date	**November 2019**
Actual Delivery Date	**December 2020**
Type	**Report**
Dissemination level	**Public**
Authors	**María Victoria Villar (CIEMAT), Gilles Armand (ANDRA), Nathalie Co (ANDRA), Christophe de Lesquen (ANDRA), Philipp Herold (BGE), E (BGE), Juan Carlos Mayor (ENRESA), Arnaud Dizier (EURIDICE), Xia (EURIDICE), Guangjing Chen (EURIDICE), Olivier Leupin (NAGRA), M Niskanen (POSIVA), Matt Bailey (RWM), Sally Thompson (RWM), Da Svensson (SKB), Patrik Sellin (SKB) Lucie Hausmannova (SÚRAO)**

To be cited as:

Villar, M.V., Armand, G., Conil, N., de Lesquen, Ch., Herold, Ph., Simo, E., Mayor, J.C., Dizier, A., Li, X., Chen, G., Leupin, O., Niskanen, M., Bailey, M., Thompson, S., Svensson, D., Sellin, P., Hausmannova, L.(2020). D7.1 HITEC. Initial State-of-the-Art on THM behaviour of i) Buffer clay materials and of ii) Host clay materials. Deliverable D7.1 HITEC. EURAD Project, Horizon 2020 No 847593. 214 pp.

Disclaimer

Acknowledgement

This document is a deliverable of the European Joint Programme on Radioactive Waste Management (EURAD). EURAD has received funding from the European Union's Horizon 2020 research and innovation programme under grant agreement No 847593.

Status of deliverable		
	By	**Date**
Delivered (Lead Beneficiary)	CIEMAT	March 18th 2020
Verified (WP Leader)	VTT	June 12th 2020
Reviewed (Reviewers)	Patrik Sellin (SKB)	August 25th 2020
Reviewed (Reviewers)	Gilles Armand (ANDRA)	November 2nd 2020
Approved (PMO)	Robert Winsley (RWM)	February 2nd 2021
Submitted to EC (Coordinator)	ANDRA	February 2nd 2021

Executive summary

This report presents the main characteristics of the national concepts of the organizations involved in EURAD-WP7 HITEC (ANDRA, BGE, ENRESA, EURIDICE, NAGRA, POSIVA, RWM, SKB and SÚRAO) and particularly of their thermal limits. An overview of what is known about the clay materials to be used in the WP, both as buffer and as host rock, is given, including the effect of temperature on the materials' behaviour. Large-scale tests relevant in terms of the temperatures involved have been identified and described, and they could be later used as benchmark exercises during the Project. The state of modelling approaches is presented, mostly particularising their application to specific tests.

It has been shown that the effect of temperature on hydro-mechanical properties of bentonite has been systematically studied for temperatures of up to 100°C and is quite well established with respect to safety functions: temperature modifies some properties but they keep in values acceptable for complying with the safety functions. It is clear that temperature increases the hydraulic conductivity, although this increase cannot be explained in most cases solely by the increase in water kinematic viscosity, and other reasons, such as microstructural or pore fluid chemistry changes, have been invoked. In contrast, the effect on swelling capacity seems to depend on the predominant exchangeable cations. Less work has been done on the effect of temperature on the water retention curve and thermal conductivity. Likewise, most laboratory studies have focused on compacted bentonite, therefore it cannot be stated if the effect of temperature on some properties is affected by the initial fabric (compacted powder, grains, pellets) or not.

Although the effect of temperatures higher than 100°C has been considerably studied concerning mineralogical transformations (unfortunately not always in clearly representative conditions), less is known with respect to HM properties for this range of temperatures, mainly because of the testing experimental issues.

Concerning the modelling of the buffer behaviour, it is considered that the THM formulations developed and validated for temperatures below 100°C can be extended without modifications to temperatures above that value.

For the clay host rock previous knowledge indicate that an increase in temperature due to the presence of heat-emitting wastes will induce strong and anisotropic THM coupled responses within the clay. Thermal expansion of pore water and thermal-induced decrease of clay strength are to be considered as a potential risk. In contrast, thermal-induced plasticity, swelling and creep of clay are likely beneficial to the sealing of fractures. Considering anisotropic properties of clay in the numerical simulations improves significantly the predictive capability of the numerical models. Current knowledge indicates that the capacity of the repository host rock to perform its intended role as a barrier and to maintain the long-term safety functions of the system will be still preserved in spite of the combined effect of the inevitable EDZ and the thermal output from the waste.

Acronyms and symbols

ORGANIZATIONS

ANDRA	Agence Nationale pour la Gestion des Déchets Radioactifs (France)
BGE	Bundesgesellschaft für Endlagerung (Germany)
BGR	Bundesanstalt für Geowissenschaften und Rohstoffe (Germany)
CIEMAT	Centro de Investigaciones Energéticas, Medioambientales y Tecnológicas (Spain)
EC	European Commission
ENRESA	Empresa Nacional de Residuos Radiactivos (Spain)
EURIDICE	European Underground Research Infrastructure for Disposal of nuclear waste in a Clay Environment (Belgium)
GRS	Gesellschaft für Anlagen und Reaktorsicherheit (Germany)
NAGRA	Nationale Genossenschaft für die Lagerung radioaktiver Abfälle (Suiza)
NWMO	Nuclear Waste Management Organization
ONDRAF/NIRAS	Organisme national des déchets radioactifs et des matières fissiles enrichies / Nationale instelling voor radioactief afval en verrijkte Splijtstoffen (Belgium)
POSIVA	Expert organisation responsible for the final disposal of spent nuclear fuel of the owners (Finland)
RWM	Radioactive Waste Management (United Kingdom)
SCK•CEN	Studiecentrum voor Kernenergie / Centre d'Étude de l'énergie Nucléaire (Belgium)
SKB	Svensk Kärnbränslehantering (Sweden)
SÚRAO	Správa Úložišť Radioaktivních Odpadú (Czech Republic)
UPC	Universitat Politècnica de Catalunya (Spain)

PROJECTS/FACILITIES

ABM	Alternative Buffer Materials
ALC	Alvéoles HA et chemisage – HLW cell and lining
CRQ	Comportement THM Représentatif d'un Quartier HA – Representative THM Behaviour of a HLW disposal section
EB	Engineered Barrier Emplacement
ESDRED	Engineering Studies and Demonstration of Repository Designs
FE	Full-scale Emplacement Experiment
FEBEX	Full-scale Engineered Barriers Experiment
HADES	High-Activity Disposal Experimental Site
HE	Heating Experiment Series
LOT	Long term test of buffer material
LUCOEX	Large Underground Concept Experiments
MHM URL	Meuse/Haute-Marne Underground Research Laboratory
TED	experimentation T(h)Ermique Deux – Thermal Experiment #2
TER	experimentation T(h)ERmique - (T(h)ERmal experiment
TFW	
TIMODAZ	Thermal Impact on the Damaged Zone around a Radioactive Waste Disposal in Clay Host Rocks

SPECIFIC VOCABULARY

µCT	Microcomputerized Tomography
CD	Consolidated-Drained
COx	Callovo-Oxfordian Clay
CPM	Continuous Porous Media
CRZ	Containment-providing rock zone
CU	Consolidated Undrained Test
DFN	Discrete Fracture Network
DGR	Deep Geological Repository
DZ	Damaged zone
EBS	Engineered Barrier System
EDZ	Excavation Disturbed Zone
GBM	Granulated Bentonite Mixture
HHGW	High Heat Generating Wastes
HLW	High-Level Waste
HLW-LL	High-Level Waste, Long Life
ILW	Intermediate-Level Waste
ILW-LL	Intermediate Level Waste, Long Life
L/ILW	Low/Intermediate Level Waste
NCL	Normal Compression Line
OCR	Overconsolidation Ratio
OPA	Opalinus Clay
PA	Performance Assessment
RD&D	Research, Development and Demonstration
SF/SNF	Spent (Nuclear) Fuel
THM	Thermo-Hydro-Mechanical
THMC	Thermo-Hydro-Mechanical and Chemical
UCS	Uniaxial Compressive Strength
URF	Underground Research Facility
URL	Underground Research Laboratory
WP	Work Package
WRC	Water Retention Curve
ZFC	Connected Fractured Zone
ZFD	Discrete Fractured Zone

SYMBOLS

B	hardening parameter
c, c'	cohesion, effective cohesion
c_p	solid phase specific heat
C_α	secondary consolidation coefficient
C_p	volumetric heat capacity
C_s	swelling index

e	void ratio
E, E'	Young modulus, effective Young modulus
$E_{\perp}$, $E_{//}$	Young modulus perpendicular and parallel to bedding
G, G_v	shear modulus
k_i k_{iv} k_{ih}	intrinsic permeability, vertical, horizontal
k_w	Hydraulic conductivity (saturated water permeability)
M	critical state parameter
m, S	fitting parameters (as defined by Hoek & Brown)
n	porosity
N	parameter of the Cam-clay model defining the position of normal compression line
p p^m p^M	mean effective stress, microstructural, macrostructural
p_r p_e	reference stress, Hvorslev equivalent pressure
P_s, P_c	swelling pressure, confining pressure
P_w	pore water pressure
S_r S_{rl}	degree of saturation, liquid residual degree of saturation
T	temperature
w	water content
α α_s α_u	linear thermal expansion coefficient, of solid, undrained
ε ε^m ε^M	strain, micro, macro
ϕ'	effective friction angle
φ_c	critical state friction angle
κ κ^*	elastic compressibility, parameter controlling the slope of the isotropic unloading line
λ λ_h λ_v λ_0	thermal conductivity, horizontal, vertical, initial
λ_1 λ_2	parameters of the water retention curve
λ^*	parameter of the Cam-clay model defining the slope of normal compression line
Λ	thermal pressurisation coefficient
ν $\nu_{//}$ $\nu_{\perp}$	Poisson's ratio, paralel, perpendicular to bedding
ν' $\nu'_{//}$ $\nu'_{\perp}$	Effective Poisson's ratio, paralel, perpendicular to bedding
ρ_d ρ_s	dry density, solid density
σ, σ^m σ^M	stress, micro, macro
σ_1, σ_3	maximum and minimum principal stress at failure
σ'_3	
σ_H/σ_h	maximum and minimum horizontal stresses
σ_v	vertical stress
σ_c	uniaxial compressive strength of the intact rock
τ	shear stress
ψ	dilation angle

Table of content

1 Introduction

The WP7 "Influence of Temperature on Clay-based Material Behaviour" of the EURAD Project aims to develop and document improved thermo-hydro-mechanical (THM) understanding of clay-based materials (host rocks and buffers) exposed at high temperatures (>100°C) or having experienced high temperature transients for extended durations. The WP's raison d'être is to evaluate whether or not elevated temperature limits (of 100-150°C) are feasible for a variety of geological disposal concepts for high heat generating wastes (HHGW). HITEC will study clay host rock formations (exposed at temperatures up to 120°C), document and establish the possible extent of elevated temperature damage in the near or far field (e.g. from over-pressurisation) and also indicate the likely consequences of any such damage. The WP will also look at bentonite buffers and determine the temperature influence on buffer swelling pressure, hydraulic conductivity, erosion or transport properties and see where the buffer safety functions start to be unacceptably impaired.

For the disposal of HHGW it is important to understand the consequences of the heat produced on the properties (and their long-term performance) of the natural and engineered clay barriers. Most safety cases for disposal concepts that involve clay currently consider a temperature limit of 100°C. Being able to tolerate higher temperature, whilst still ensuring an appropriate performance, would have significant advantages (e.g. shorter above-ground cooling times, more efficient packaging, fewer disposal containers, fewer transport operations, smaller facility footprints, etc.). This WP has the potential to effectively integrate with the parallel SFC RD&D WP (i.e. interrogate the validity of the currently applied thermal limits and also the importance of the accuracy of the assumed radiological waste properties) and consequently is a first step toward optimization of the architecture of the deep geological disposal.

In this context, the objectives of this Deliverable are to present the state-of-the-art and compile existing data about clay materials at high temperature. Previous and ongoing national and Community-supported research programmes have led to detailed understanding of the various key thermo-hydro-mechanical and chemical (THM-C) processes taking place in the buffer material up to 100°C (e.g. FEBEX, PROTOTYPE, BACCHUS, RESEAL, ECOCLAY, PEBS, DOPAS, BELBaR, Beacon…) and in host claystone (e.g. SELFRAC, TIMODAZ, NF-PRO…). Those data on THM behaviour of clay materials (buffers and clay host rocks) at different temperature are the starting point of this document, including:

- a synthesis of the state of knowledge on the THM behaviour of different buffer materials at different temperatures.
- a synthesis of the state of knowledge on the THM behaviour of host claystone (Boom Clay, Opalinus Clay, Callovo-Oxfordian claystone), including the Excavation Damaged Zone (EDZ, extension, permeability properties, self-sealing processes…) and the thermal pressurization in the far field.

For a better contextualization of this information, the national geological waste disposal concepts of the participant organisations are initially summarised at a high level. The characteristics of the clay materials to be used in Tasks 2 and 3, i.e. bentonites and host rocks, are described and their thermal, hydraulic and mechanical properties are summarised.

Experimental procedures, processes, parameters and models available at low or high temperature for the different buffer material and host rock are summarised. Existing or ongoing large-scale in situ experiments which can be proposed in Tasks 2 and 3 as benchmark exercises have been identified and described.

In the final stage of the project, the state-of-the-art will be updated (D7.2) integrating the findings of all R&D tasks in this WP and relevant findings from other WPs. The main objective will be to highlight the significance of the findings of Tasks 2 and 3 on the THM behaviour in clay materials at high temperature and at repository scale and evaluate the consequences of these findings on safety and optimization of geological disposal systems (Task 4).

2 WMO conceptualisation

The following sections give background information on different national concepts for disposal of HHGW (e.g. spent fuel, SF and/or high-level waste, HLW). This will help identifying the role assigned to each component of the multiple barrier system and the way in which temperature may affect their performance.

2.1 ANDRA (France)

In the 1990s, the French National Radioactive Waste Management Agency (ANDRA) started a study on the Callovo-Oxfordian (COx) claystone as a possible host rock for radioactive waste disposal. A geological investigation covering more than 100 km^2 was carried out, involving geophysical survey and drilling of boreholes near the village of Bure, in the eastern part of the Paris Basin. In 2000, Andra began to build the so-called Meuse/Haute-Marne underground research laboratory (MHM URL) in order to conduct experiments to demonstrate the feasibility of constructing and operating a radioactive waste disposal facility in the COx claystone. Demonstration experiments are supposed to represent, test and optimise actual potential disposal systems and repository components. In 2007, following the 2006 Waste Act adopted by the French parliament, Andra started work in preparation for the licence application to construct a deep geological disposal facility, which will be submitted in 2020. Previous research conducted in the MHM URL to clearly define the host rock continued in order to consolidate existing knowledge and clarify the location of the future facility. At the same time, a new programme focussing more on technological improvements and demonstration of the different disposal systems was launched in line with the “technology readiness level” scale.

Figure 2-1 shows a possible architecture for Cigéo, the industrial geological disposal facility. Surface facilities will be divided into two parts: one for nuclear activities (taking delivery of primary waste packages such as rail terminal, inspecting packages, re-packing them into disposal packages) and the second for excavation activities (workshops, cement plant, storage, drainage basins, excavation muck “heap”, etc.). A ramp will be used to transport the waste packages down to the main level of the underground disposal facility. Shafts are mainly used for all the activities related to excavation/support works, ventilation and workers’ transportation. The main underground disposal area will be divided into two sections depending on the type of radioactive waste (intermediate level long life (ILW-LL) or high-level long life (HLW-LL)) and the type of works used to emplace the waste containers (tunnel of 9-11 m in diameter for ILW-LL waste and micro-tunnel of 0.9 m in diameter for HLW-LL waste).

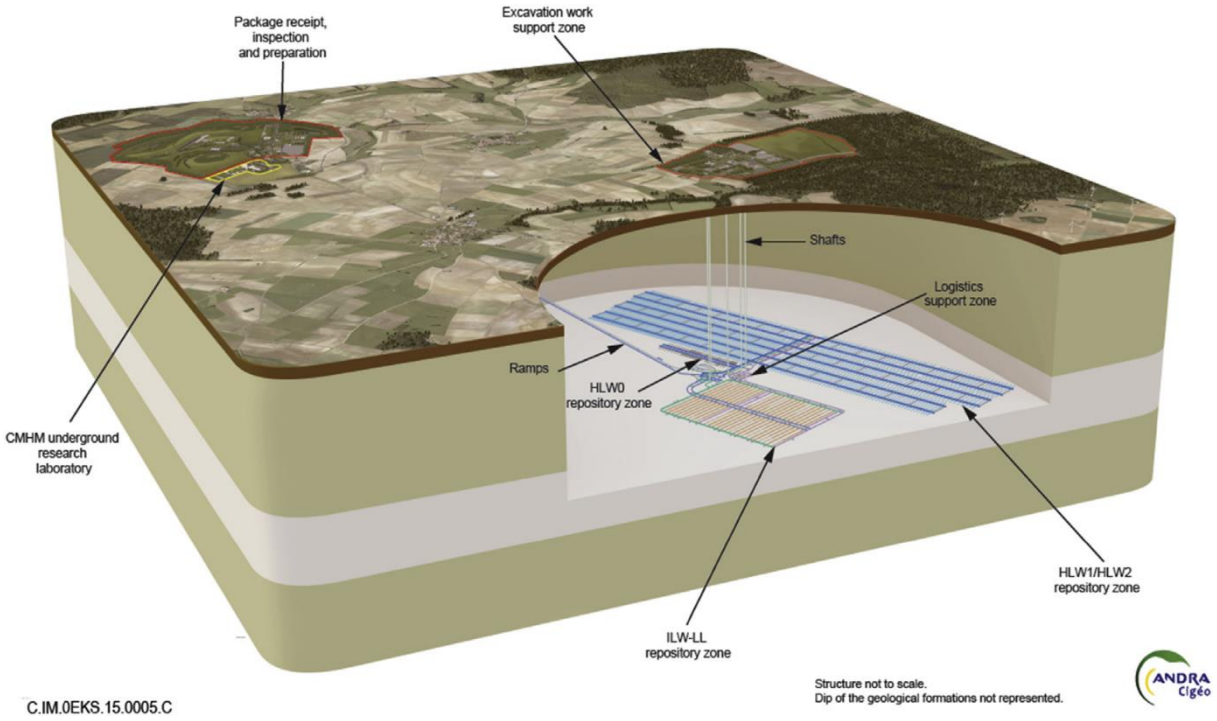

Figure 2-1. Possible architecture of Cigéo, the industrial geological disposal facility in north-eastern France

The waste package disposal facilities and the transfer and emplacement processes are designed with the aim of simplifying the waste package retrieval operations which may be decided in the future, using, if possible, technologies similar to those used for emplacement. As a result, clearances for handling purposes that must be maintained in the long-term are provided between the package and the cell walls.

Vitrified HLWs are hot cast into stainless steel canisters (primary waste) which will be conditioned in thick steel overpacks to prevent glass leaching during the thermal phase (i.e. time needed for the glass matrix temperature to decrease below 50/70°C depending on the type of waste). The main function of this overpack is to prevent water from reaching the glass matrix during 500 years for the most exothermic waste. The overpacks will be stored in dead-end, horizontal micro-tunnels with an excavated (drilled) diameter of approximately 0.9 m (Figure 2-2) and a steel casing.

In 2009, the length of the benchmark HLW cell had been limited to 40 m, but it was then extended to 80 m during the Cigéo basic design phase. The 2009 reference design is composed of a body section for package disposal, and a head section for cell closure. They are favourably aligned with respect to the stress field. To prevent rock deformation and enable potential retrieval of waste containers during the reversibility period, both cell body and cell head sections have a non-alloy steel casing. The diameter of the casing in the body is slightly smaller than that in the head, called the “insert”. This means that it can slide into the insert. Thus, the effects of the thrust produced by its dilation, due to heat generated by the exothermic packages, are absorbed without consequence for the cell head. The design of the cells has not been definitively finalized. Ongoing research and the technological programme may lead to changes and optimisation (with the same level of safety) of the concept. For example, for chemical reasons linked to corrosion rates, an alternative concept, in which the void between the steel casing and the rock must be filled with a concrete/bentonite mixture, emerged in 2013 and became the current reference design.

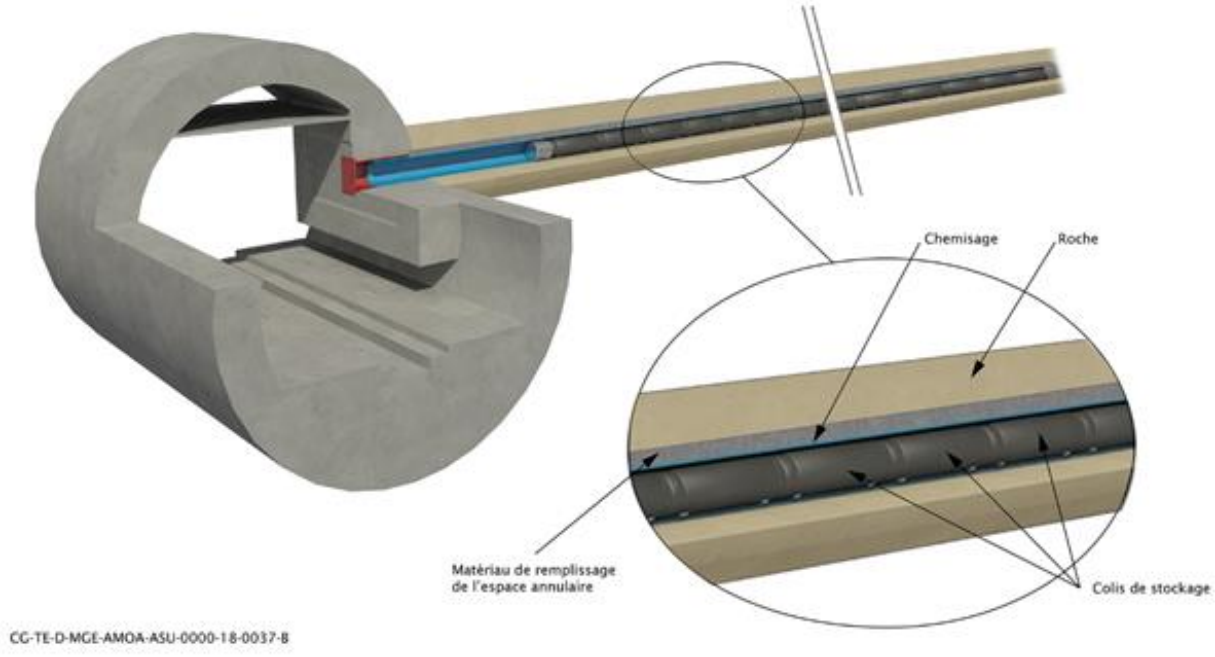

Figure 2-2. Concept of disposal cell for HLW-LL

In a longer term, if no retrieval operation is decided, the final closure of Cigeo will come about a century after the start of its operation. The drifts leading to the disposal sections as well as the shafts and ramps will then be backfilled and sealed. The disposal system is designed to robustly fulfil the following post-closure safety functions (ANDRA 2016):

- to isolate the waste from humans and from the biosphere so that the safety of the disposal facility is not significantly affected by climatic erosion or normal human activities,
- to prevent water circulation in the waste disposal facility,
- to limit the release of radionuclides and toxic chemicals and immobilise them in the repository,
- to delay and reduce the migration of radionuclides and toxic chemicals released.

The last three safety functions rely primarily on the favourable characteristics of the COx formation. The design of Cigeo (architecture, engineered components) and its operation aim to preserve these favourable characteristics. While the COx formation plays a central role in long-term safety, the packages and the repository's engineered components, specifically the underground facility's architecture on completion and closure structures, also contribute to containment of the waste and to maintaining the conditions for flows of water through the facility to be very slow.

THM response of COx claystone around a HLW cell

High-level waste (HLW) produces heat. As shown in Figure 2-3, temperature increases rapidly near the cell to reach a maximum around 80°C between 10 and 15 years after the waste packages (HA2 type in this case) are set. Further away, the temperature peaks are lower and are reached later. Half-way between two HLW cells, it is reached between 400 and 500 years with a magnitude of 40 to 50°C depending on the package type and their location in the HLW repository zone. At the top and base of the COx formation, the 40°C peak is reached after approximately 1000 years.

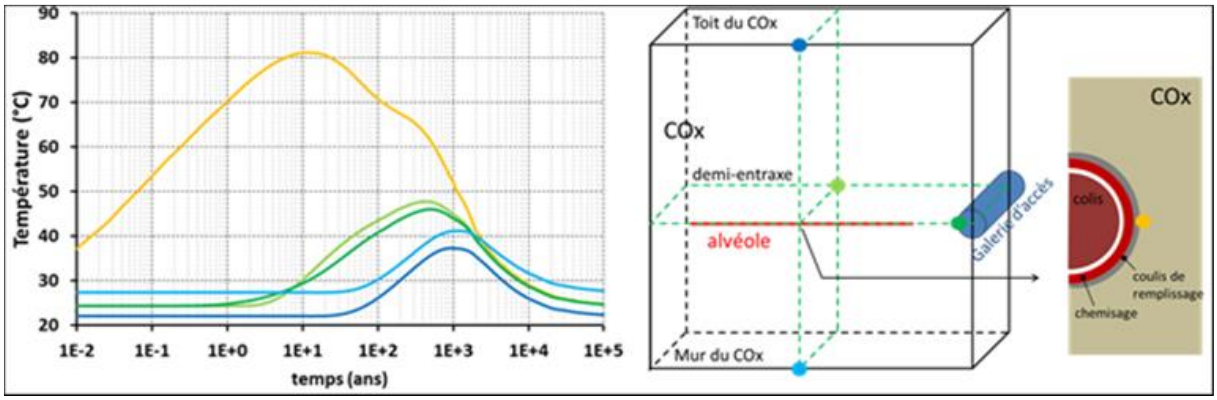

Figure 2-3. Temperature evolution over time at different locations around a HLW disposal cell

Therefore, the thermo-hydro-mechanical (THM) behaviour of the COx claystone is important in the rational design of an underground nuclear waste disposal facility. The size of the HLW repository zone is indeed dictated by temperature and THM criteria:

- The temperature should stay below 90°C in the COx claystone
- No formation damage should be caused by thermal loading

The architecture of the HLW sections comprised of a large number of parallel cells may be considered equivalent to a periodic configuration (except for the cells at the edge of the sections). In such a context, the THM behaviour of a section may be represented by considering a single cell with lateral symmetry (Figure 2-4). For this simplification, a simultaneous load for the adjacent cells is taken into consideration. This hypothesis is acceptable if the filling time is considered for two adjacent cells (a few years at the most) in relation to the time required for the most exothermic wastes to reach their thermal peak (several hundred years, approximately). It should be noted that, in this hypothesis, the pore pressures are very conservative for the design approach.

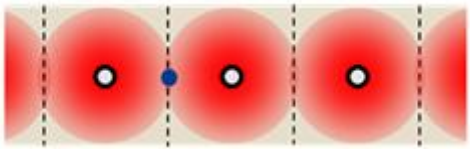

Figure 2-4. Conceptualisation of modelling and schematic representation of thermo-mechanical processes of a Representative Elemental Volume (REV) located at mid-point between two HLW cells

Symmetrical loading by two adjacent cells implies that the zone located at midpoint between two parallel cells is subject to loads from both cells. For a Representative Elementary Volume (REV) of the COx located in this zone (Figure 2-4), the increase in temperature will result in 1) an increase in the overall stress levels and 2) an increase in pore pressure (Figure 2-5). This overpressure does not have an isotropic impact on the stress levels. In fact, the lateral symmetrical conditions prevent horizontal expansion of the medium and horizontal dissipation of the pore pressure at the midpoint of the centre-to-centre distance between the cells. For this reason, the increase in temperature also results in a decrease in the total horizontal stresses (increased compression). In the vertical direction, the open surface area at the upper edge of the medium enables "free" vertical expansion, resulting in only negligible changes in total stresses. This situation results in the following:

- a significant increase in the effective vertical stress (the tensile stress is considered to be positive) due to thermal pressurisation that may cause effective tensile stresses;

- a decrease in total horizontal stresses due to thermo-mechanical compression stresses;
- an increase in the deviatoric stress (decrease in horizontal stresses and increase in vertical stress).

This load pathway may result in a rupture from cracks/fractures, in theory sub-horizontal (perpendicular to the tensile stress direction) in case of tensile failure. In cases where the deviatoric stress is sufficiently high, shear failure may also occur. The zone where the effective stresses are at their maximum is near the midpoint between the cells. This location is a direct result of the thermal (no flow), hydraulic (no flow) and mechanical (no displacement) boundary conditions in this zone.

The purpose of the thermal design is to prevent the appearance of any damage in this zone, located far away from the cells ("far-field"). Increasing the distance between the cells (centre-to-centre distance) attenuates the interaction between the cells and reduces the amplitude of the maximum stresses (Figure 2-5). On the other hand, reducing the spacing between two HLW cells would have a major impact on the size of the HLW repository zone and consequently on the cost of the project.

Several experiments were performed at the MHM URL, from small-scale tests to full-scale HLW cell demonstration experiments to study the THM effects of the thermal transient on the host clay and to demonstrate and optimise actual repository components (section 4.2.2). In parallel, Andra has also conducted theoretical work and characterisation on samples through collaborative work with academia.

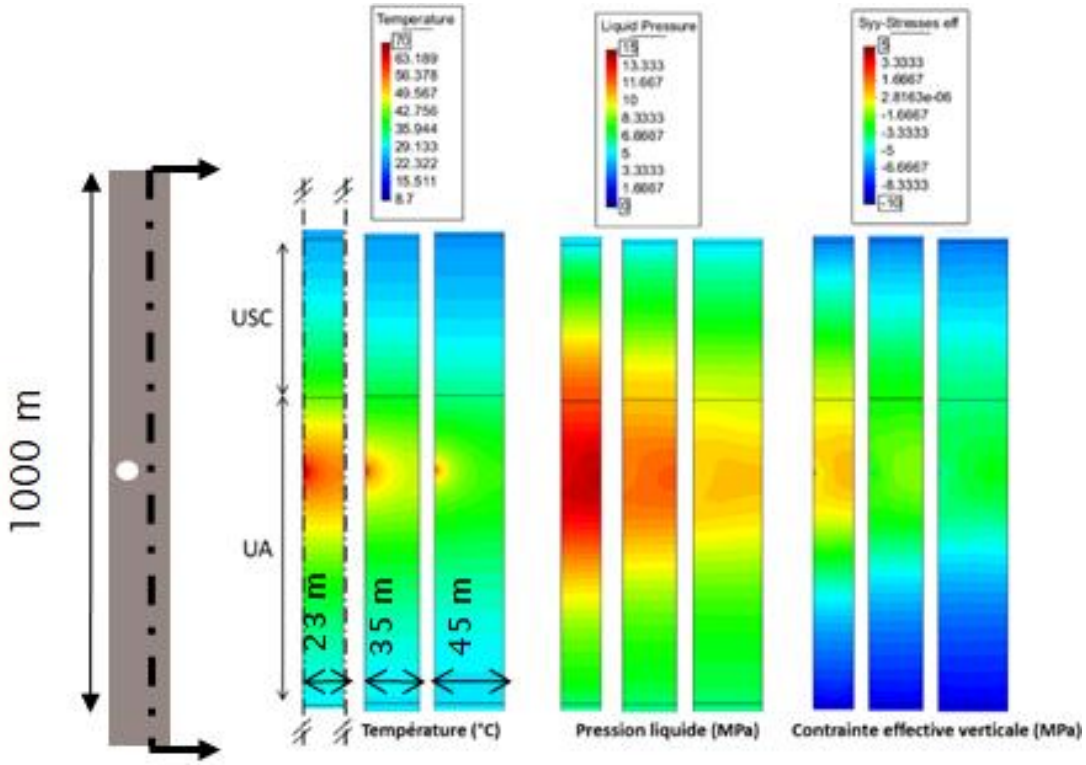

Figure 2-5. Temperature, pore pressure and effective stress disturbance caused by a heating HLW cell depending on the inter-cell spacing (23 to 45 m)

The results from laboratory experiments showed however a large scatter, due in large part to a poor control of the water saturation. Good practices for collecting and processing the samples have now been established (section 0) and it is expected that the laboratory experiments in the current Work Program will provide a better understanding of the THM properties, both in the near-field (EDZ) and in the far-field, and with a wider range of temperatures. In addition, the modelling of the most recent

heating experiments should give a better understanding of the THM processes both in the fractured zone around the HLW cells and in the virgin COx claystone. The main remaining uncertainties concern the influence of the non-linearity of the mechanical behaviour (fractured material properties, plasticity, thermal hardening) and the time-dependent behaviour of the COx (how it affects its response to a thermal load).

The closure structures

The closure structures consist of seals, HLW cell plugs and backfill (Figure 2-6).

- The seals are designed to prevent the water flows between the underground facility and the overlying formations and to limit the water circulation in the drifts. There are three categories of seals: vertical seals in the shafts, inclined seals in the ramps and horizontal seals at the main level of the repository. At this stage, they comprise a core based on swelling clay (swelling clay on its own or mixed with additives such as silica or limestone sand) occupying the entire cross-section area of the shaft/ramp/drift. The swelling clay is in direct contact on all its length with the clay rock in the shafts and ramps, the concrete linings being totally removed. For horizontal seals, only a few portions of the concrete lining are removed due to the nature of the clay rock, inducing partial contact between the swelling clay and the host rock. For all seal types, the swelling clay core is supported by two concrete containment walls.
- The backfill will be emplaced at the end of the operational phase in all the drifts. Its function is to limit the development of the fractured zone after the rupture of the lining strengthening the sides and roofs of the drifts in the underground facility. It helps to preserve the favourable characteristics of the COx. The backfill will consist of the excavated clay rock, possibly with the addition of additives such as bentonite or sand.

None of these will be subjected to very high temperatures. More details about the Cigéo repository concept can be found in ANDRA (2005).

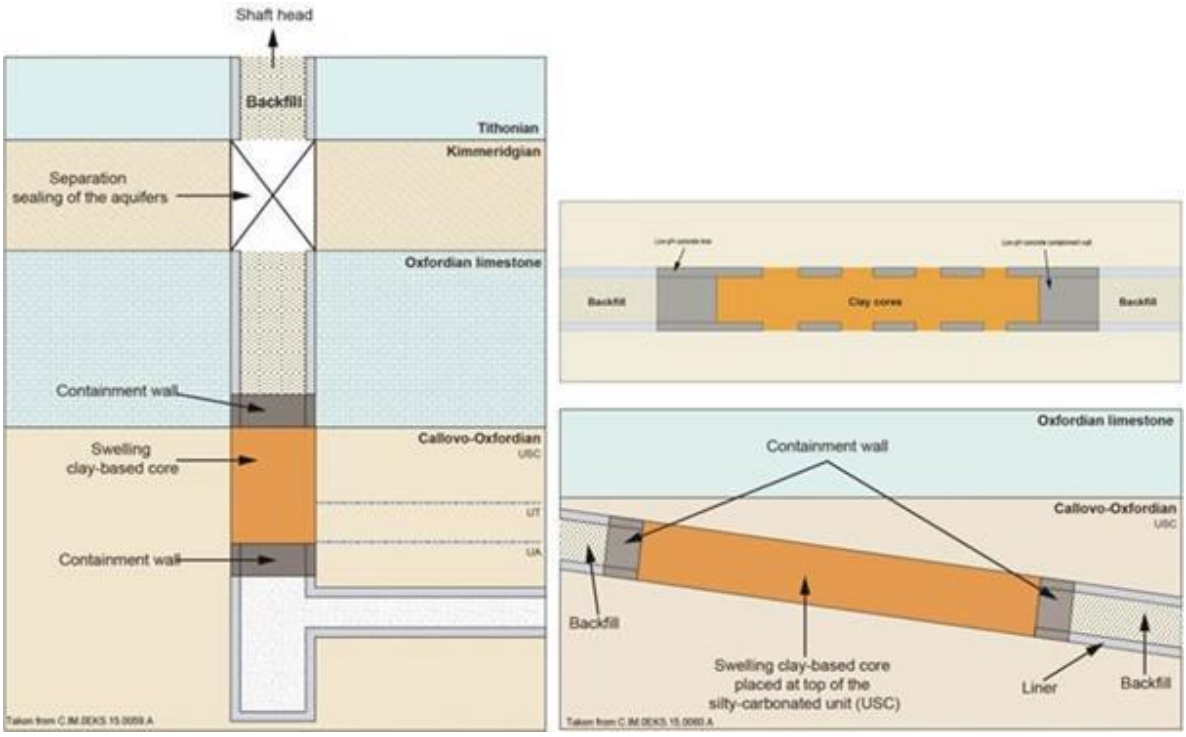

Figure 2-6. Block diagrams of the vertical, horizontal and inclined closure structures

2.2 BGE (Germany)

The Federal Company for Radioactive Waste Disposal mbH (Bundesgesellschaft für Endlagerung mbH, BGE) is a state-owned company established in September 2016 following the Act on the Organisational Restructuring in the Field of Radioactive Waste Storage. The Repository Site Selection Act (Standortauswahlgesetz May 5th 2017, June 19th 2020 – StandAG) defines the Site Selection Procedure, aiming to ensure the best possible safety for storing high-level radioactive waste in Germany for the duration of one million years. The procedure consists of three phases, after each phase, the legislator decides on the regions for further consideration in the next phase of the site selection procedure.

The first phase (Phase I) is divided into two steps. The objective of Step 1 of Phase I was to determine subareas of favourable geological conditions based on available data provided by the competent federal and state authorities. The BGE checked, homogenized and stored the data into databases and applied six legally defined exclusion criteria, related to e.g. seismicity, volcanic activity or vertical uplift. In addition, the data were used to identify regions satisfying legally defined minimum requirements such as host rock thickness and hydraulic conductivity. Due to the application of geoscientific weighing criteria, the BGE finally assessed the remaining regions with regard to their overall geological suitability. This selection procedure led to a number of 90 potentially suitable subareas considering rock salt, clay stone and crystalline rock as host rocks. The achieved results of Step 1 of Phase I were published in an interim report on subareas (BGE 2020a). In the current Step 2 of Phase I, representative preliminary safety assessments and the renewed application of geoscientific criteria and requirements will be implemented. The results will lead to identification of specific regions that will be considered for further surface-based geoscientific and geophysical exploration.

The interim report on the subareas (BGE 2020a) identified nine different subareas with clay formations for which favourable conditions for the disposal are expected. Clay formations in this context subsume both plastic clays and claystones, which are diagenetically hardened. According to Section 23(5) of the German site selection act, the containment providing rock zone (CRZ) of a repository system must have a hydraulic conductivity of less than 10^{-10} m/s, a minimum thickness of 100 m and must be located at least 300 m depth below the surface. Furthermore, there must be sufficient space to accommodate a repository and no findings or data have to be available that cast doubt on the preservation of the barrier function. The nine identified subareas include Opalinus clay formation (in the south of Germany), a large ensemble of Lower Cretaceous and Jurassic claystones in the north of Germany (in sum five subareas) and three subareas with younger, Tertiary formations located in the north and south. Figure 2-7 shows the selected subareas with pre-Tertiary and Tertiary clay formations in Germany.

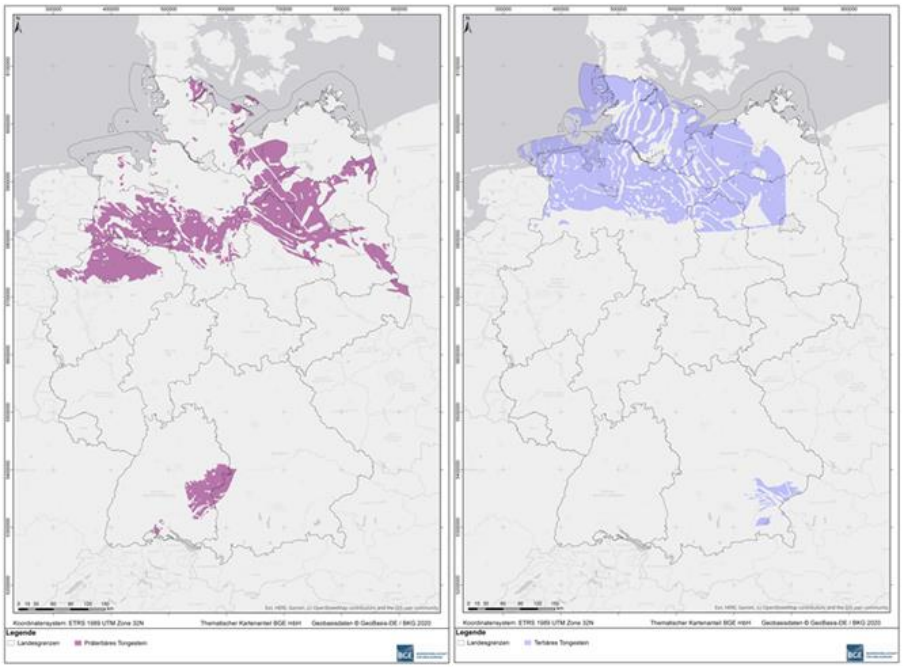

Figure 2-7. General map of the subareas in the host rock clay, based on (BGE 2020a). The subareas were identified according to stratigraphic units, therefore, this map representation shows a partial overlapping of several subareas in some cases, older, pre-Tertiary formations are marked in deep purple (left), younger, Tertiary formations are marked in blue (right)

Repository concepts of the BGE

An overview of the repository concepts of the German site selection procedure is given in BGE (2020b). The report summarizes the regulatory framework, basics of the German approach of containment providing rock zones and related safety concepts as well as basics of the repository designs as considered in the site selection procedure.

A large number of different repository concepts have already been developed on the national and international level. Whether one of these concepts can be transferred to a repository for high-level waste in Germany must be examined, particularly with regard to the safety concept, the regulatory requirements, especially those arising from the Site Selection Act (i.e. retrievability) and the Repository Safety Ordinance as well as the type and quantity of radioactive waste to be stored.

In the case of the safety concept of CRZ, safe confinement is essentially ensured by geology. One of the main functions of the containment providing rock zone is to spatially separate the emplacement area from possible transport routes (for radionuclides) into the biosphere. The StandAG defines the requirements for the geology to fulfil safe containment and retention. In addition, the technical and geotechnical engineered barrier systems (EBS) support the geological barrier in fulfilling its task. The technical barriers include the repository container and the disposed waste itself. The geotechnical barriers include, among others, the backfill material for backfilling the excavated cavities and the sealing structures (e.g. of a disposal route or the accesses to the repository mine from above ground). Depending on the host rock and the safety concept and the resulting repository concept, the individual barriers must be effective for different periods of time.

According to StandAG and the Repository Safety Ordinance, the crystalline host rock is a special case if no CRZ can be identified. The safe confinement has to be ensured by means of higher requirements for the engineered barriers, i.e. the technical barriers (disposal waste packages) and geotechnical barriers (e.g. bentonite buffer and sealing of mine openings).

The repository concept is an interaction of the emplacement concept, the technical and geotechnical barriers adapted to it and the geological situation. Accordingly, the repository concepts are developed on the basis of the underlying safety concept (CRZ principle or principle of confinement on the basis of EBS), the emplacement concept (including container concept) and the material selection.

On the national and international level, the emplacement concept was mainly considered as gallery disposal or borehole disposal. For borehole disposal, a distinction is made between vertical and horizontal disposal and the number of waste packages per borehole varies, in some cases considerably.

The materials selected for the EBS depend strongly on the safety concept. If the containment is primarily based on EBS (technical and geotechnical barriers), the requirements for the materials of these barriers are much higher than for the CRZ principle. The barrier system is always designed to ensure safe enclosure in the best possible way over the assessment period.

For the identification of the subareas (BGE 2020a), generic repository concepts, which are oriented to the different host rock configurations, have been used as a basis. These are the configurations:

- rock salt in stratiform formations,
- rock salt in steep formations,
- clay rock,
- crystalline rock represents the emplacement area and the CRZ
- crystalline rock represents the emplacement area and the safe confinement is formed by EBS,
- crystalline rock represents the emplacement area and the CRZ is formed by layers overlaying the crystalline.

Depending on the selected host rock configuration, different repository concepts were considered in Step 1 of Phase I. For rock salt in stratiform and steep formations, the CRZ principle is possible.

In clay rock, almost the same applies as for rock salt as the safety concept is based on the CRZ principle. Depending on the thickness and size of the layer various possibilities for the selection of the emplacement concept are given. If the thickness or the area is large enough, both gallery disposal and the vertical or horizontal borehole disposal are available. A limiting factor for narrowing the choice of different variations does not seem to be justifiable in Step 1 of Phase I of the German site selection procedure. The same applies to the selection of the possible container materials and the materials of the sealing structures. At the current stage, there are still too many variables available for the repository concept to be specified in more detail.

The safety concept according to the CRZ principle is also conceivable for the crystalline rock, in case it represents the emplacement area and the CRZ. Here, too, the range of possible areas and thicknesses is very wide, so that the most varied designs are conceivable. If CRZ cannot be identified in the crystalline rock, two further cases are conceivable. In the first case, the crystalline represents the emplacement area and the safe confinement is formed by the engineered barrier system and the corresponding safety concept is provided. BGE currently assumes that in some designated subareas only this safety concept based on the engineered barrier system (technical and geotechnical barriers) can be used to fulfil the long-term safe confinement. In the second case, the crystalline rock represents the emplacement area and the CRZ is formed by layers which overlay the crystalline. In this case, the repository is constructed in the crystalline rock, whereas the safe confinement is ensured by the overlying formation. Various repository concepts are conceivable here; a narrowing of the selection of these concepts cannot yet take place in Step 1 of Phase I.

For the representative preliminary safety studies in Step 2 of Phase l, a schematic description of the repository is sufficient according to the Repository Safety Ordinance. The spatial characterisation of the repository system must be roughly described. In addition, it can be assumed that the engineered barrier system, independent of the safety concept, will in principle fulfil its function as long it seems

possible according to the current state of science and technology. According to the Repository Safety Ordinance, the calculations of the discharged mass of radionuclides must also be performed in the preliminary safety investigations, but a dose calculation is not yet required in the representative preliminary safety investigations. An operational safety analysis is also not yet required. Accordingly, simple repository concepts adapted to the subarea are sufficient for the performance of the representative preliminary safety investigations. It is expected that a criteria-based restriction of all possible safety concepts to the promising variants will be carried out. These repository concepts must fulfil all regulatory requirements in interaction with the geological and spatial boundary conditions.

According to the Repository Safety Ordinance, a schematic description is no longer sufficient for the further developed preliminary safety investigations of the siting regions within the framework of StandAG and the comprehensive preliminary safety investigations of the sites. The Repository Safety Ordinance also does not contain a level of detail between the further developed and comprehensive preliminary safety investigations. This means that the preliminary safety investigations in Phases II and III require a higher level of detail in the repository concepts. Since the preliminary safety investigations build on each other, the corresponding repository concepts must also be further developed and detailed. This optimization is taken into account within the Repository Safety Ordinance. A substantial change of a previously based repository concept for the corresponding siting region or sites has to be justified. An example of an essential change would be the replanning of a disposal in galleries to a borehole disposal, if a better long-term safety could be expected.

National concepts and R&D activities

Generic R&D studies such as GENESIS (Jobmann et al. 2007), ERATO (Pöhler et al. 2010) and ANSICHT (Jobmann et al. 2017) investigated repositories in clay formations in Germany. These repository concepts and R&D activities were developed by national research institutes. Whether these concepts can be applied to the German Site Selection Procedure, especially with regard to the regulatory requirements, needs to be evaluated.

Based on generic reference models conceptual designs including gallery and borehole disposal were developed. Pöhler et al. (2010) developed concepts for vertical borehole disposal and horizontal gallery disposal in claystone for the first time. Both concepts served as basis for further development of the ANSICHT project where a safety assessment methodology for the two repository concepts in two generic reference formations has been carried out. In any case, the clay formations serve as geological barrier. Two shafts (one shaft for the transport of containers and the second for conventional mining operation) are considered to access the repository located at a depth between 700 and 900 m. In order to ensure the mechanical stability of the tunnels, a concrete liner is foreseen in all mine openings. The final layout and design of the liner is still under investigation. The tunnels are backfilled with expansive clay buffer like bentonite after the disposal of the waste packages. The function of the buffer is to retard possible fluid migrations from and to the waste packages and to ensure the retention of the radionuclides due to its sorption capacity. The buffer is composed of a high compacted pedestal block on which the waste package is emplaced and of expansive clay-based pellets used as backfill material in the remaining openings of the tunnel.

The clay formation in combination with the engineering barrier system guarantee the long-time confinement of the radioactive waste. It is expected that the remaining voids in the repository will be progressively closed due to the healing and sealing properties of claystone. Meanwhile the buffer will progressively saturate with water coming from the surrounding saturated rock. Following the saturation, the swelling process of the buffer takes place. Both phenomena lead to the closure of the gallery and therefore to the confinement of the disposed waste packages, although the closure of the excavated area in the repository will take some time to complete. Therefore, plugs and seals are

installed at several locations with redundant and diverse sealing elements in the repository to ensure the sealing of the repository in the early stage.

Thermal aspects, restrictions and motivation

The German site selection act demands that as long as the maximum physically possible temperatures in the respective host rocks have not yet been determined due to pending R&D activities, a temperature of 100°C at the outer surface of the waste packages can be assumed for precautionary reasons. This limitation is motivated by the fact that the influence of high temperature on clay materials is still not completely investigated. Based on generic repository concepts such as ANSICHT, influence of high temperatures on the buffer and the claystone can be expected. Within the R&D activities in Jobmann et al. (2017) scientific investigation of thermal effect up to temperatures of 150°C was initiated. Based on thermal analyses, the spacings between the waste packages with heat-generating radioactive waste in an emplacement tunnel and between the tunnels were optimized in order to limit the temperature peak in the repository. In addition to the existing knowledge of temperature effects to hydraulic, mechanical, chemical as well as biological processes, BGE intends with the participation in WP HITEC to deepen this knowledge and provide a contribution to the identification of temperature limits as defined in the German site selection act.

2.3 ENRESA (Spain)

The Spanish repository concept in plastic clay rock is based on the disposal of spent fuel in carbon steel canisters in long horizontal disposal galleries. Canisters are disposed of in cylindrical disposal cells constructed with pre-compacted bentonite blocks of 1,700 kg/m^3 dry density (in order to achieve a final dry density of 1,600 kg/m^3). The blocks are initially non-saturated (degree of saturation of 66%). The disposal galleries of 580 m in length and 2.4 m in diameter are located at a depth of 250 m in the host formation. A 0.3 m thick concrete liner is required to deal with the plastic nature of the clay host rock. The separation between canisters is determined mainly by thermal constraints. Separations of 1 m between canisters and 50 m between disposal galleries have been established, in order not to exceed a temperature of 100°C in the bentonite. Actual separation is a function of the properties of the host rock. Once a disposal gallery is completed, it is sealed with a 6-m long seal made of bentonite blocks and closed with a concrete plug at its entry. After completion of all the disposal galleries, the main drifts, ramp, shafts and other remaining rock cavities will be backfilled with compacted clay from the excavation of the repository, and subsequent projection of clay pellets in the remaining openings. The concept is shown in Figure 2-8.

The bentonite buffer is required to maintain a large diversity of safety functions, which can only be fulfilled once the bentonite saturates and swells, tightly closing the construction gaps between the bentonite blocks and the liner or the canister wall on the one hand and between the blocks themselves on the other. Nevertheless, there are no safety functional requirements applicable during the time when the canister provides absolute containment. During the re-saturation of the buffer, the main concern is the preservation of the favourable properties of the buffer material. As the safety functions assured by the buffer are assumed for the full duration of the quantitative safety assessment (on the scale of a million years), its properties have to be preserved at a sufficient level for commensurate periods of time.

The long-term safety functions of the bentonite buffer are to:

- Isolate the waste package from the geosphere by limiting advective transport of corroding agents to the canister.

- Avoid canister sinking in the disposal drift that could result in direct contact of the canister with the rock, hence short-circuiting the buffer.
- Avoid excessive swelling pressures that could contribute to total pressures that the canister cannot withstand.
- Avoid excessive temperatures (>100°C) that could result in chemical alteration of the bentonite and jeopardize its safety functions.
- The buffer is a containment barrier by itself, as it retains radionuclides based on its properties:
  - Low hydraulic conductivity, which makes radionuclide transport by advection negligible
  - Sorption of many radionuclides, especially actinides
  - Filtration of colloids and large complex molecules because of the small size of the pores
- Avoid the build-up of excessive gas pressure in the near-field, without undue impairment of the safety functions.
- Reduce microbial activity to minimize microbial corrosion of the canister.

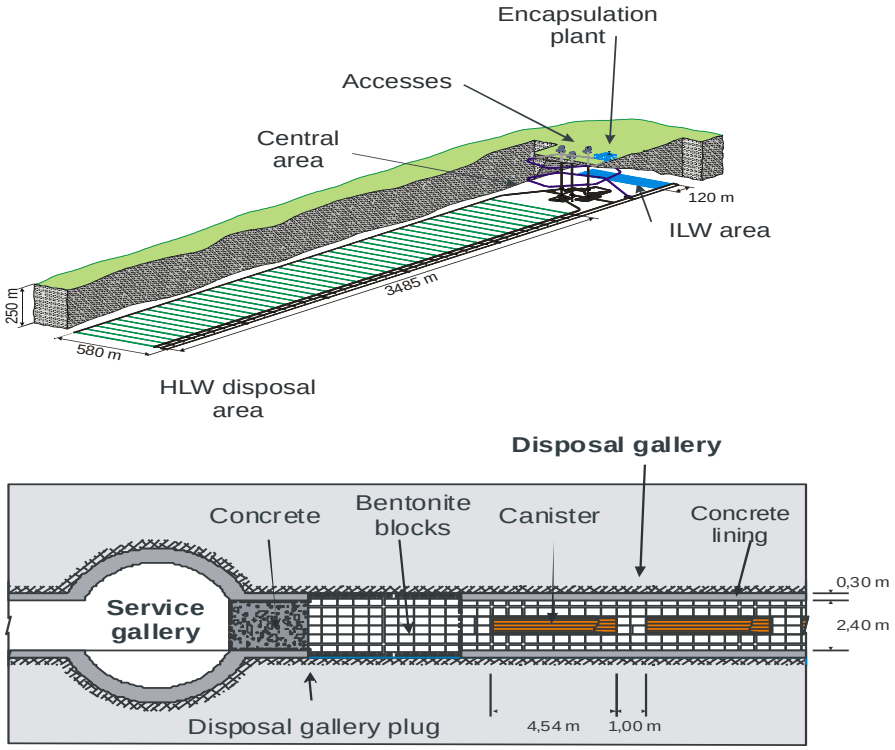

Figure 2-8. Schematic diagram of the geological repository in clay rock (Enresa 2004)

Thermal aspects and restrictions

The geometry of the repository, being understood as such the separations between canisters and between galleries, is determined, mainly, by limitations of thermal order and aspects of security and economy. A thermal analysis was carried out to define the geometry of the disposal area, optimizing its size as small as possible (for safety and economy) without exceeding thermal restrictions, namely the maximum permissible temperature increases in the upper aquifer (5°C) and on the land surface (0.5°C), and the maximum permissible temperature in the bentonite buffer (100°C).

Based on the established repository geological data (including a thermal conductivity value of the clay rock of 1.5 W/m·K), on the depth selected for the repository (250 m), and on the initial thermal power of 1,200 W per canister, the already mentioned separations of 1 m between canisters and 50 m

between disposal galleries have been established in order to comply with the thermal restrictions imposed.

2.4 NAGRA (Switzerland)

The concepts for implementing deep geological disposal currently under consideration in Switzerland are the result of many years of R&D, as well as of safety, design, cost, site evaluation and other studies performed by NAGRA and their reviews by the authorities. They also take into account the relevant national legal and regulatory guidance, as well as input from international developments.

For both the HLW and L/ILW repositories, it is envisaged that excavation will start with the construction and operation of a rock laboratory followed by construction of the main repository access and operation tunnels, pilot facility and shafts (Figure 2-9). This is followed by the successive opening of emplacement caverns or drifts, emplacement of the waste, and backfilling. Once an emplacement drift is backfilled, the access is plugged with a seal. Following emplacement of the waste, there will be monitoring phases during which the access and operation tunnels will be backfilled until repository closure, when all underground structures will have been backfilled and sealed.

After transport to the underground facilities, the disposal canisters are emplaced in 300 to 600-m long drifts with an inner diameter of about 2.5 m. In the reference configuration, the canisters are emplaced coaxially and centralized within the drifts, requiring a pedestal of compacted bentonite blocks (Na-bentonite from Wyoming, dry density 1,450 kg m^{-3}) to support the canisters prior to the backfilling of the remaining spaces with highly compacted bentonite granules (comprising ~80% by volume of dense granules ~2,100–2,200 kg m^{-3} and 20% powder). The bentonite blocks and granules together form a protective mechanical and chemical buffer around the canisters. A spacing of ~3 m is foreseen between individual canisters to limit the temperature increase in the surrounding buffer and rock due to heat generation in the canisters from radioactive decay. The current repository concept, published in NAGRA (2011), uses a cementitious liner to support the walls of the emplacement rooms and access tunnels, designed to withstand the highest mechanical loads expected to arise during the construction and operational phases. To avoid any hydraulic shortcuts along the walls of the SF/HLW emplacement drifts that could arise from the degradation of the liner, and to comply with the principle of compartmentalization, sealing sections comprised of granular and preformed bricks of buffer material (1,650-1,750 kg·m^{-3}) are emplaced at regular intervals along the drifts, about one for every 10 canisters, to provide a hydraulic barrier (NAGRA 2014a). There is no liner where these sealing sections are emplaced, so that bentonite forms a watertight contact directly with the Opalinus Clay. The concept is illustrated in Figure 2-10.

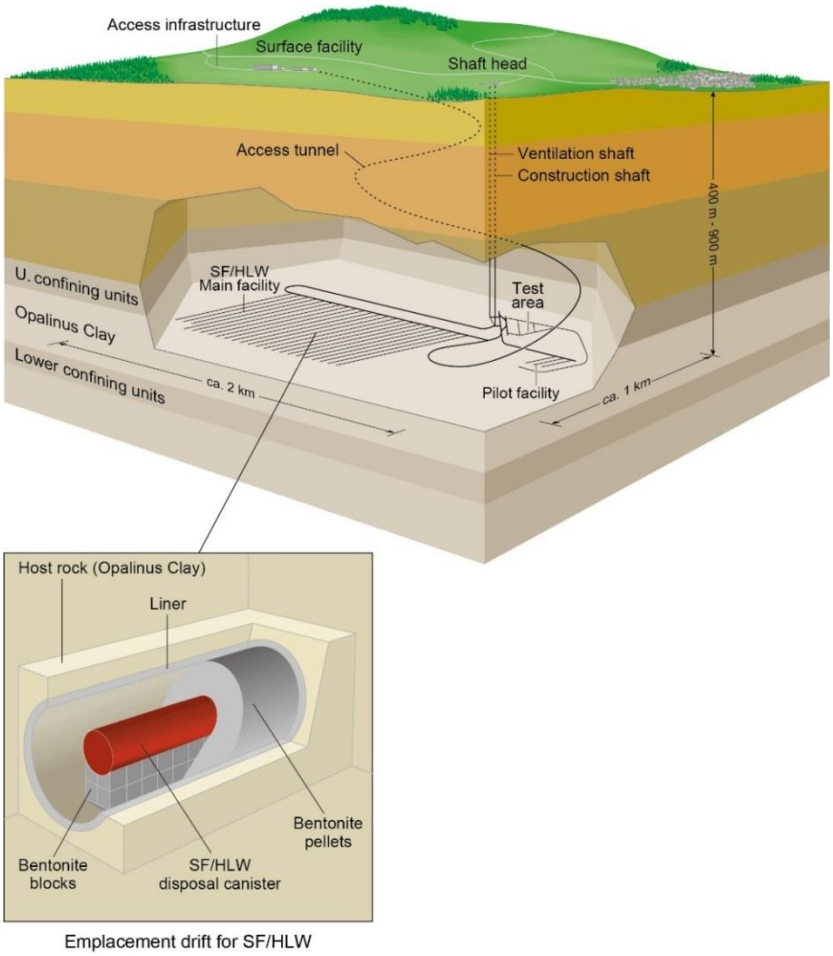

Figure 2-9. Example layout of the HLW repository with its main features

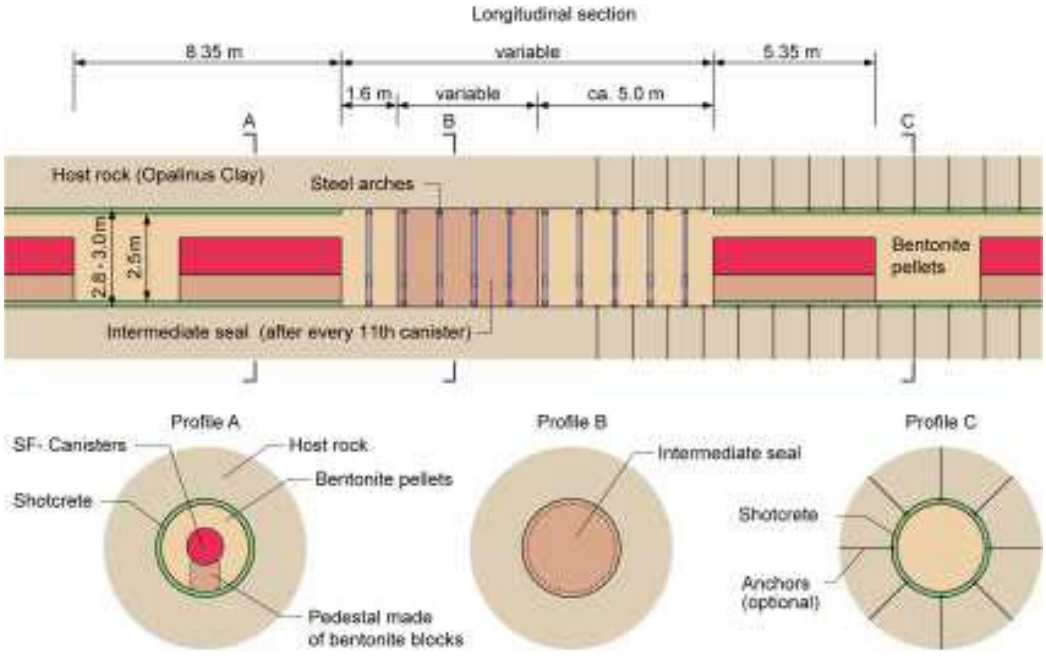

Figure 2-10 Schematic diagram of the near-field design of the Swiss SF/HLW repository based on NAGRA (2016a)

To safely contain the waste and to comply with the overriding safety principles, the key requirements for a buffer material in the case of high-level radioactive waste disposal independent of the host rock are: 1) low hydraulic permeability/conductivity; 2) self-sealing ability; and 3) durability of properties in the very long term. The safety-relevant properties of bentonite are:

- Swelling capacity providing mechanical stabilization of rooms and hence avoiding significant extension of the EDZ
- Chemical retention of radionuclides by retarding transport from the buffer
- Low hydraulic conductivity for ensuring diffusive transport
- Sufficiently high viscosity for mechanical support of the canister
- Sufficient gas transport capacity for ensuring gas transport without compromising the hydraulic barrier
- Minimizing microbial corrosion to ensure conditions favourable to slow corrosion (of the canister)
- Resistance to mineral transformation ensuring longevity of other safety-relevant attributes of the buffer
- Suitable heat conduction ensuring favourable maximum temperature conditions

To comply with these properties, it is generally accepted that a relatively high smectite content is required, e.g. the range defined in the Swedish concept is between 75% and 90% (SKB 2010). Leupin & Johnson (2013) indicate a range between 80 and 85%, considering the particular characteristics of MX-80 bentonite as a reference.

THM response of OPA claystone and buffer in and around a HLW drift

For SF canisters, the initial heat output is on average 1,350 W, which will result in a temperature at the canister interface with the buffer of about 130°C within about ten years (Senger et al. 2014). The temperature of the rock at the drift boundary will reach its maximum (about 90°C) after about 100 years. Heat transport to the far-field rock, which will become more effective once the buffer has saturated, will increase the temperature to a maximum value of ~75°C at a distance of 20 m above the drifts. Temperatures around the HLW canisters will be significantly lower.

The thermal conductivity of bentonite has significant impact on peak temperatures in the buffer and is particularly strongly coupled to the buffer saturation (NAGRA 2015). On the other hand, the evolution of the thermal conductivity of the buffer has little impact on the temperatures in the surrounding Opalinus Clay. By limiting the maximum thermal pulse such that temperatures in the rock remain below the reconstructed maximum paleotemperature of the Opalinus Clay, any detrimental chemical or mineralogical effects on the safety-relevant properties of the host rock can be excluded (NAGRA 2008c).

There are several types of chemical processes that might degrade the swelling capacity and reduce the plasticity of the bentonite buffer over time, all of which show temperature dependency. However, as discussed in Sellin & Leupin (2013), measurements on bentonites from short-term thermal studies and natural analogue studies show relatively minor changes of hydraulic properties (about 1 order of magnitude) below about 130°C, regardless of the experimental conditions. At temperatures of 150°C and above, the swelling pressure is reduced, and the hydraulic conductivity increases. Exposure of compacted bentonite to temperatures of 150°C and above may alter the plastic properties due to cementation effects (Johnson et al. 2014). Nonetheless, these hydrothermally altered bentonites are still characterised by very low hydraulic conductivities as well as reasonable plasticity and sorption capacity, even in cases where the content of expandable clays is low.

From experiments and a literature review reported in Leupin et al. (2014), it can be concluded that performance indicators, such as swelling pressure and hydraulic conductivity, are not adversely affected in the long-term by heat generated during the thermal transient.

Increasing temperature in the near-field rock will result in thermal stresses, rock heave and some increase in hydraulic conductivity due to reduced viscosity. Thermal expansion of groundwater/pore water in the rock and in the (saturated) buffer, coupled with their low hydraulic conductivity, will also result in an increase in pore water pressure; within about 20 m of the drifts, the pressure has been calculated to increase to as much as 70% of the lithostatic pressure after about 100 years. The potential mechanical impacts of pore water pressure increases are, however, expected to be minor. Thermally-induced pressures in the host rock around the EDZ will, however, also drive increased water flow into the EDZ and buffer, promoting saturation and consequent self-sealing of the EDZ (Lanyon 2019a, b) and increased saturation of the buffer.

Buffer saturation

It is possible that the near-field rock may have become substantially saturated by the time a SF/HLW emplacement drift is sealed. On the other hand, the SF/HLW buffer will require a significantly longer period to saturate. Flow of water from the near/field rock to the buffer through the liner will occur in only a few places at first, affected by heterogeneity in EDZ development (effective permeability and pore volumes) along and around the repository drifts. Later, as the liner integrity degrades, more general saturation will take place.

The water content in the bentonite adjacent to the canister surface (2-3 wt.% in granular bentonite and up to 18 wt.% in blocks used for the pedestal) will, in the early non-isothermal period, be redistributed by vapour diffusion within the near field. During the early post-emplacement period, a saturation front will develop due to the steep pressure gradient into high-suction bentonite material by vapour diffusion and/or liquid flow, resulting in early saturated conditions near the drift perimeter. Non-isothermal conditions will affect the subsequent saturation behaviour of the bentonite buffer. In particular, pore water in the buffer will be evaporated and transported away from the canister by vapour diffusion into cooler regions, where the vapour will condense, creating a counter flow of liquid water towards the canister. These processes are illustrated in Figure 2-11. Swelling of the outer parts of the bentonite buffer may result in additional compaction and increased density close to the canister (Figure 2-12).

Saturation of the buffer has been estimated to take around 100 years (Leupin et al. 2016). This re-saturation may be significantly slower in the case of very low permeability of the Opalinus clay. No adverse effects are expected from a slower re-saturation process. As defined here, the saturation phase ends with the close-to-full saturation of the buffer (a residual gas saturation of 1–2% is expected in the buffer at the end of the re-saturation phase as the trapped gas will eventually and largely dissolve into the pore water and diffuse into the geosphere, Figure 2-13). By then, it is likely that all construction and operation tunnels will have been backfilled and sealed, although the access tunnel and shafts will remain open to allow monitoring. The monitoring period will allow the saturation process to be followed in detail in the pilot facility, and any deviation from the expected evolution to be identified. Initially, upon saturation, pore water pressures within the buffer will be much lower than those in the surrounding host rock but will increase thereafter (model parametrization: Figure 2-14, model results: Figure 2-15, Figure 2-16).

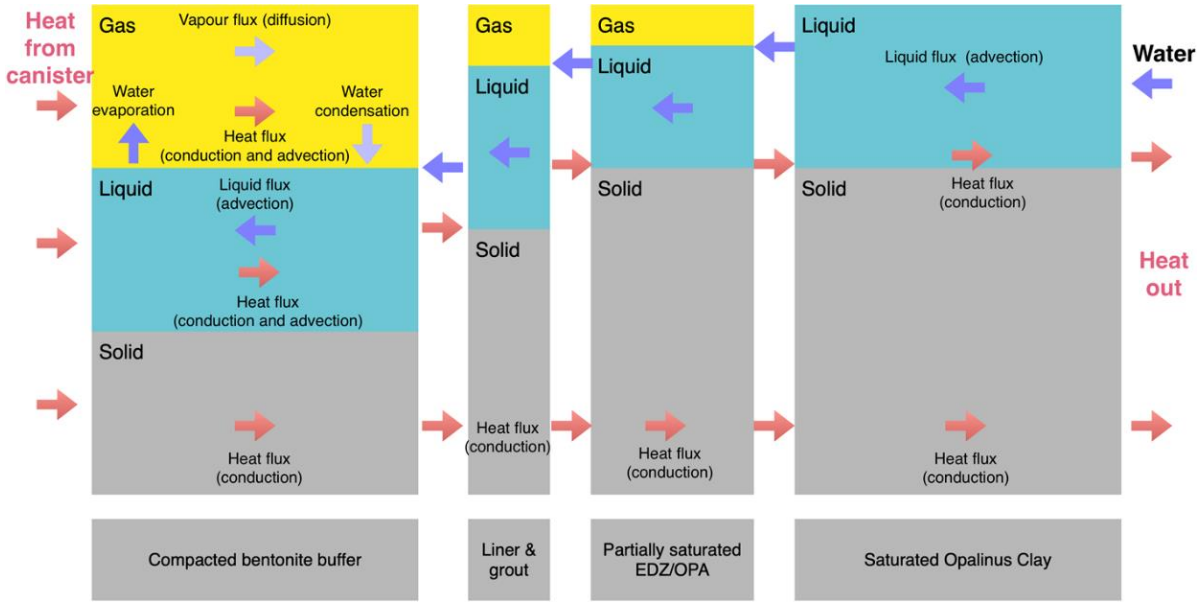

Figure 2-11. Schematic illustration of coupled processes associated with vapour transport (adapted from Gens 2003). The schematic is simplified and shows the initial state

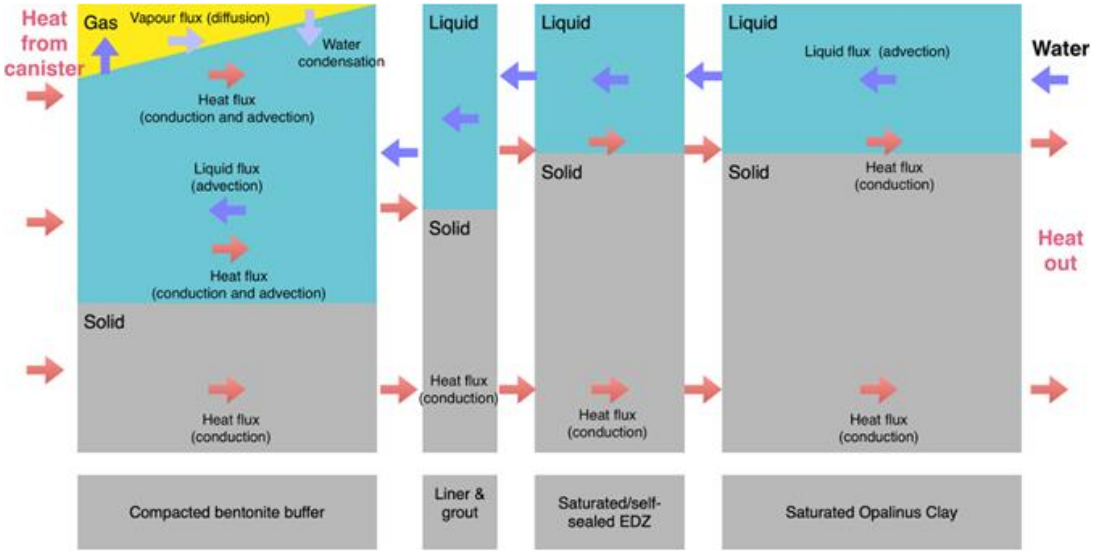

Figure 2-12. Schematic illustration of coupled processes associated with vapour transport (modified from Gens 2003) showing the saturation progress. Advective/diffusive flow in liquid/gas phase (two-phase flow) is assumed in all components of the multibarrier system

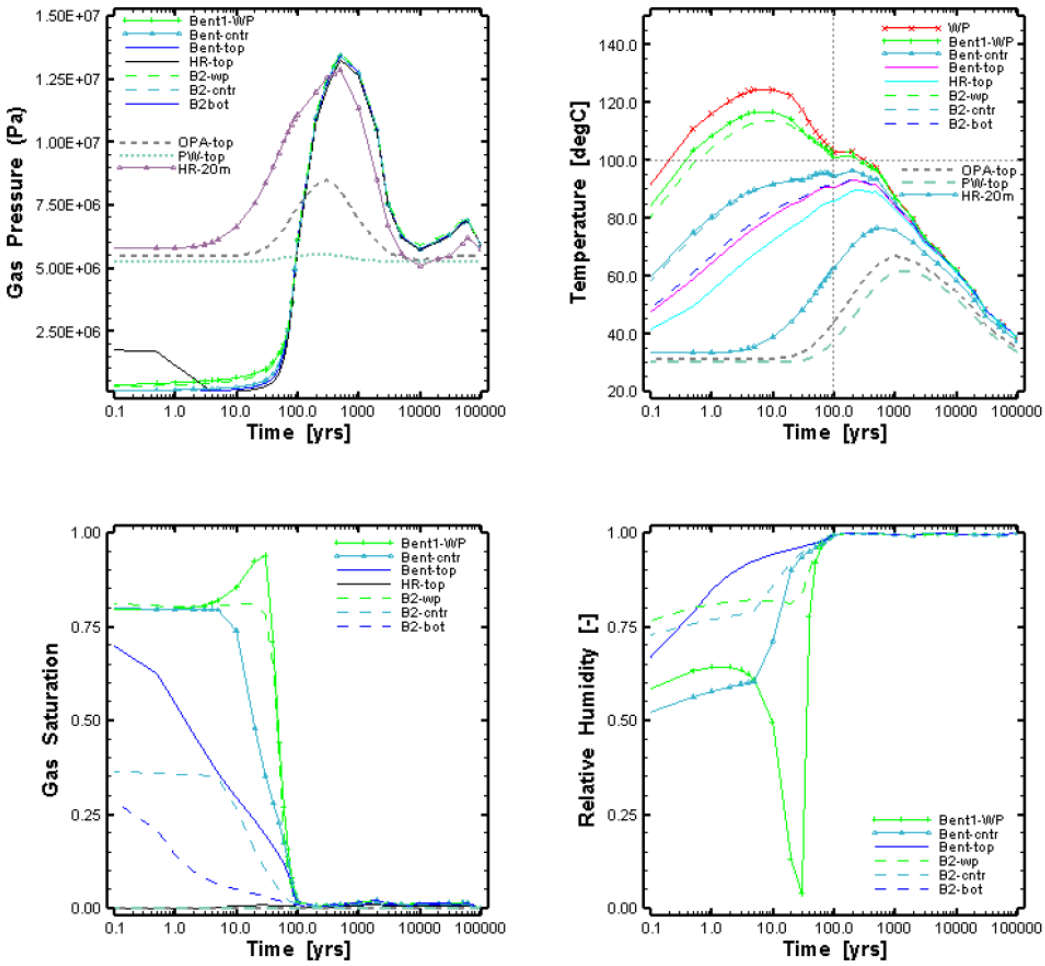

Figure 2-13. Base Case of simulation of heat and gas generation: time history at different locations in the bentonite buffer and surrounding host rock of pressures (upper left), temperatures (upper right), gas saturation (lower left), and computed relative humidity (lower right) (Senger et al. 2014)

	Intrinsic permeability	Reference [1] (600m)	Deep [2] (750m)	Shallow [3] (450m)
	(m^2)	Depth (m bgl)	Depth (mbgl)	Depth (m bgl)
Quaternary	1E-11	0-74	-	0-89
Tertiary	1E-16	74-205	0-325	-
Malm	1E-14	205-444	325-528	89-274
Effingen	1E-20	444-458	528-617	
Upper confining unit	5E-20	458-545	617-695	274-395
OPA	1E-20	545-655	695-805	395-505
Lower confining unit	5E-20	655-814	805-958	505-670
OMK	1E-14	814-877	958-1083	670-743
UMK	1E-16	877-979	1083-1130	743-848
Buntsandstein	1E-18	979-987	-	848-870
Permo-carbonif. Trough	1E-19	-	1130-2159	870-9000
Crystalline	1E-19	987-9000	2159-9000	-

[1]Corresponds to Benken lithostratigraphic profile.
[2]Corresponds to Weiach profile +139 m in Tertiary in order to shift tunnel depth to 750 m.
[3]Corresponds to Riniken profile +64 m in Quaternary in order to shift tunnel depth to 450 m.

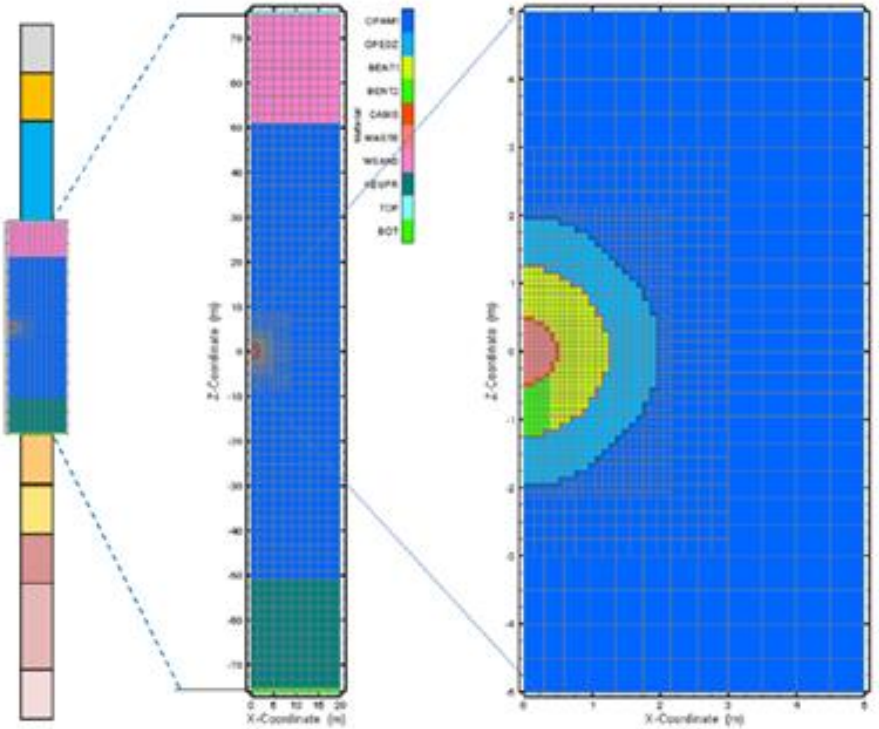

Figure 2-14. 2D model geometry of a SF/HLW emplacement tunnel in the Opalinus Clay with the 1D extension to the prescribed boundary conditions at the top (land surface) and at the bottom (crystalline) (Senger 2014)

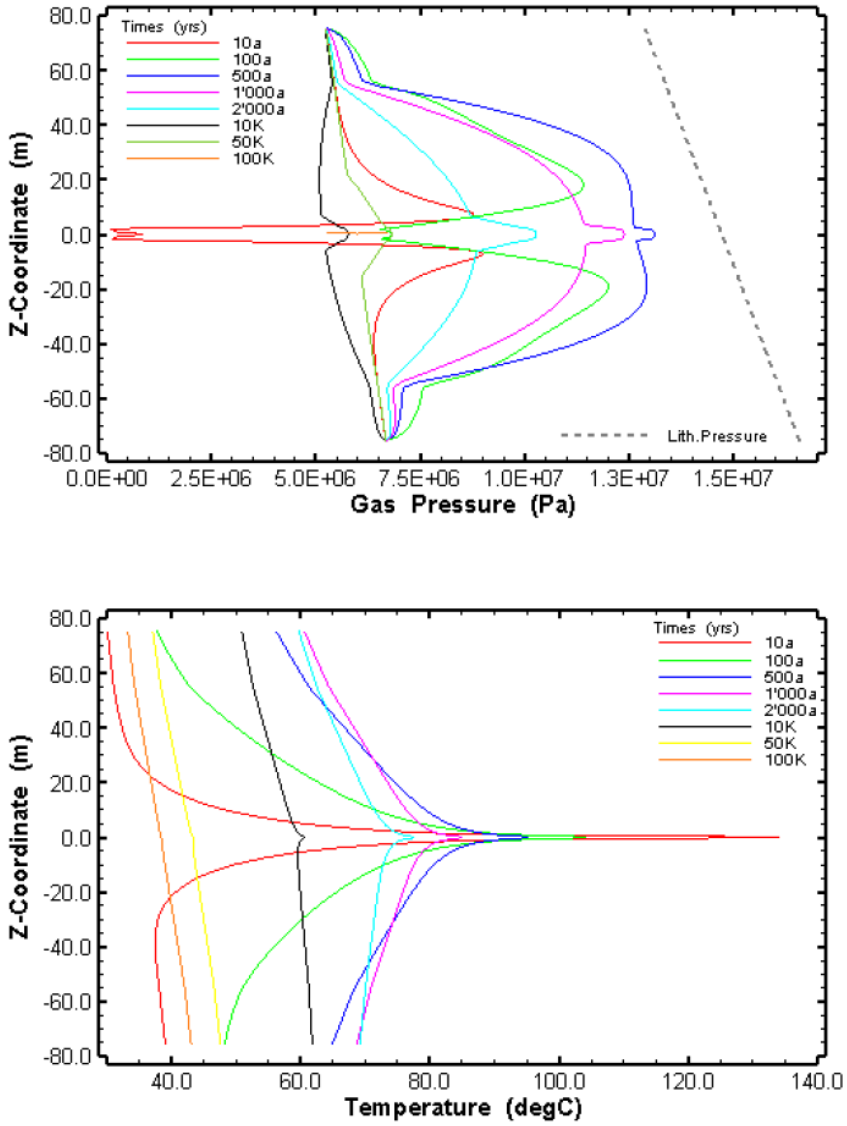

Figure 2-15. Base Case of simulation of heat and gas generation: vertical profiles of pressure (top) and temperatures (bottom) at different times (Senger et al. 2014)

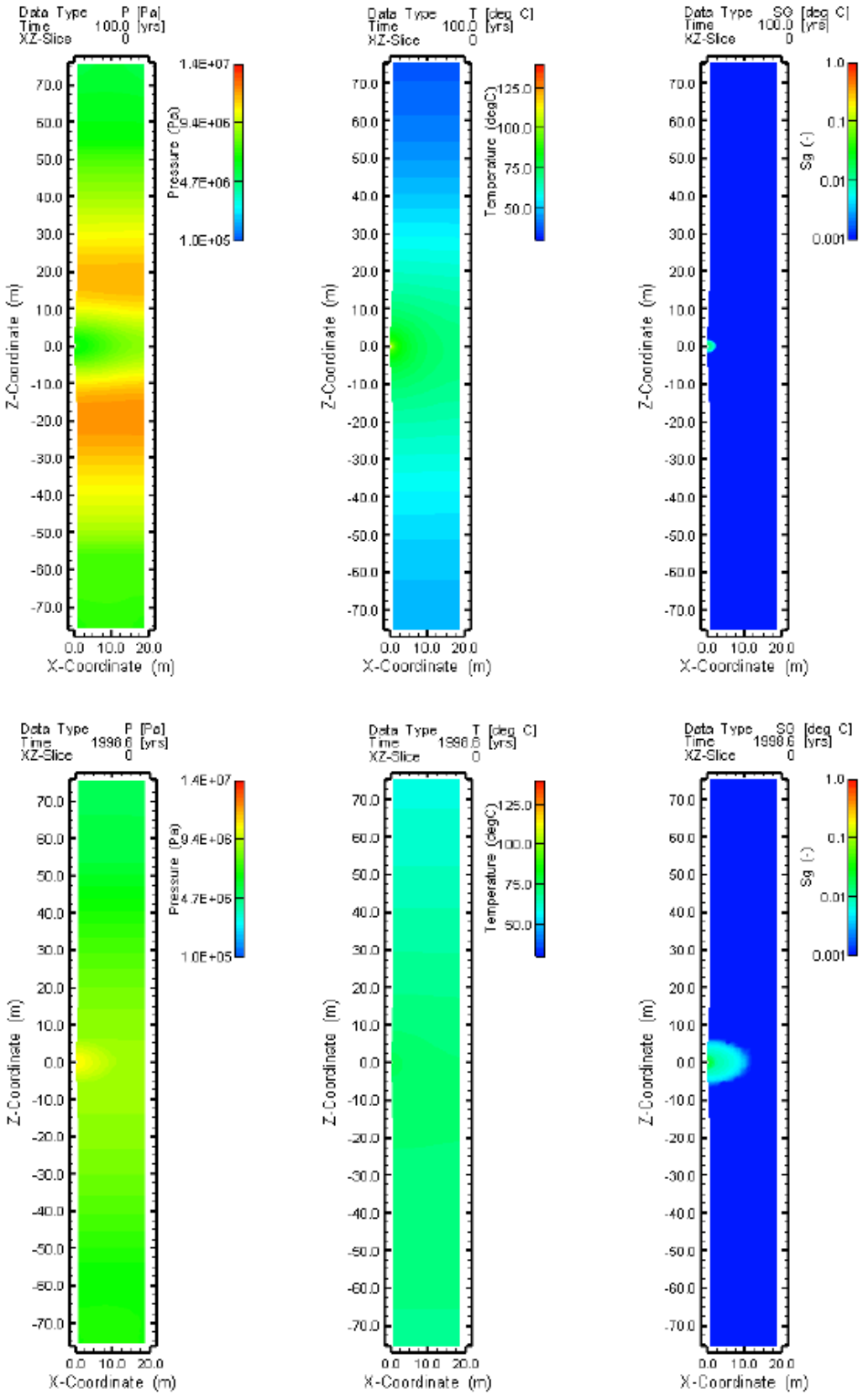

Figure 2-16. Base Case of simulation of heat- and gas generation: Vertical cross sections of pressures, temperatures, and gas saturations after 100 years (top) and after 2,000 years (bottom) (Senger et al. 2014)

2.5 ONDRAF/NIRAS (Belgium)

The Belgian concept for long-term radioactive waste management currently being studied foresees to condition B and C wastes in disposal packages, also called "Monoliths B" and "Supercontainers" respectively, that are intended to be disposed in the geological repository. Those conditioning operations will be performed in two dedicated surface facilities, usually called the "post-conditioning facilities" for B&C wastes. Monoliths B and Supercontainers will then be emplaced in the geological disposal facility (GDF), respectively in the B-zone and in the C-zone of the GDF. The supercontainer is a prefabricated concrete container that surrounds the Primary Waste Packages (PWPs) for category C waste as seen in Figure 2-17. More information concerning the design and the construction of the supercontainer for category C waste can be found in Leonard (2017).

The supercontainer consists of the following components:

- A carbon steel overpack that contains the primary waste package (CSD-V or SNFA encapsulated in a canister);
- A cylindrical buffer consisting of a concrete container and a concrete lid;
- A cementitious filler between the overpack and the concrete buffer, that fills the annular gap between the overpack and the pre-cast buffer component during fabrication of a supercontainer;
- A stainless steel sheet wrapping the concrete buffer.

Five types of supercontainers (from SC-1 to SC-5) will accommodate the different types of C wastes:

- SC-1 for the vitrified high level waste (CSD-V);
- SC-2 to SC-5 for the spent fuel nuclear assembly (SBNFA).

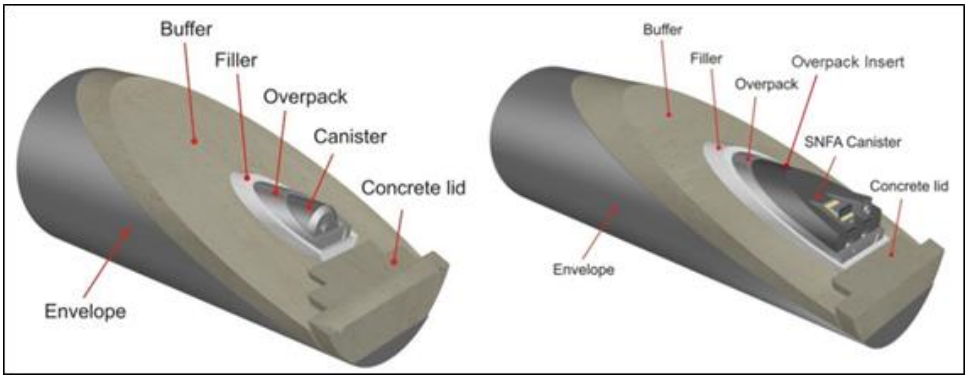

Figure 2-17. Supercontainer components

The C wastes (high level and long lived radioactive waste) emit large amount of heat. The supercontainer packages will be disposed in disposal galleries where a concrete lining guarantees the stability of these ones. A cement backfill fills the gap between the concrete lining and the supercontainer. Figure 2-18 presents a cross-section of the supercontainer inside the backfilled disposal gallery. The length of a supercontainer depends on the supercontainer type (depending on the wastes) while the size of the gallery is fixed, with an inner diameter of 3.5 m.

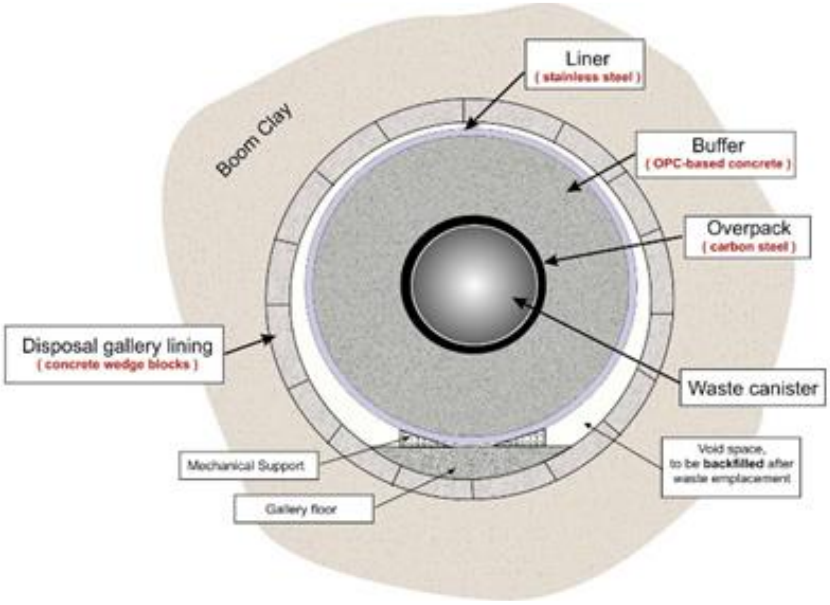

Figure 2-18. Supercontainer design in a geological repository, waste package, concrete lining and host rock formation (Boom or Ypresian clays) (© ONDRAF/NIRAS)

The present architecture of a geological disposal facility comprises two access shafts and two main access galleries. The disposal galleries are perpendicular to the access galleries. The length of these last ones is 1 km. An artistic view of a potential geological disposal facility is seen in Figure 2-19.

In the disposal galleries, the spacing between each supercontainer in a gallery is 10 cm and the inter-axis distance between the disposal galleries in the C-zone depends on the waste and is:

- 50 m for the vitrified wastes;
- 120 m for the SNFA (spent fuel: UOX-8 ft, UOX-12 ft, UOX-14 ft and MOX).

A multi-barrier system is defined in the geological disposal facility design:

1. The engineered barriers system (EBS), which is made up of the supercontainer (or monoliths B), the backfill of the disposal gallery and the concrete lining of the galleries (disposal and access galleries)
2. The natural barrier system, which is the host rock formation, i.e. the clay (Boom or Ypresian clays).

Each component has a chemical or/and mechanical function. The geological disposal facility has been designed in order to limit the evolution of the temperature at the overpack, in the supercontainer, and the clay formation – upper aquifer interface. Several parameters may be modified to accommodate the heat output: the number of primary packages in the supercontainer (the number of vitrified waste canister or the number of spent fuel assemblies), the spacing between supercontainers within a disposal gallery, the period of cooling prior to the disposal and the distance between the disposal galleries. The three first parameters control the near-field temperature while the last one the far-field temperature. The temperature at the overpack is limited to remain below 100°C while the temperature at the top of the host clay formation is restricted to be lower or equal to 25°C. The restriction at the overpack is driven by chemical reasons, in particular corrosion issues, while at the interface with the aquifer, the limitation is guided by drinkability of the upper aquifer.

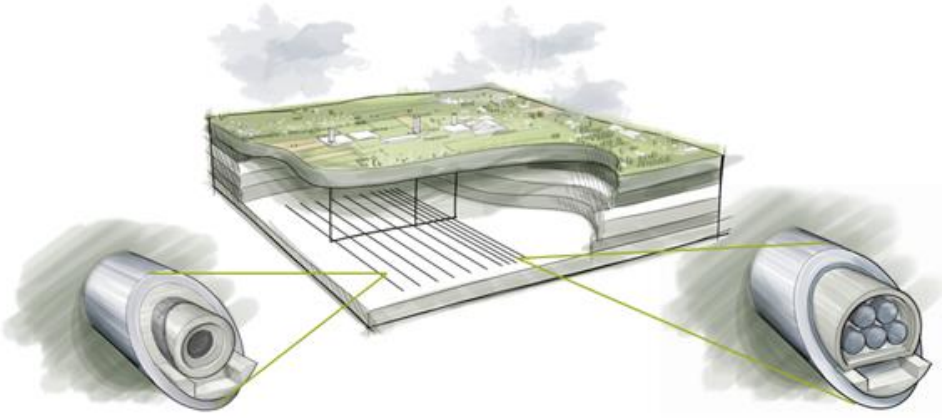

Figure 2-19. Artistic view of a geological disposal facility (Raymaeckers et al. 2019)

The disposal system has to provide three main safety functions (ONDRAF/NIRAS 2013, Figure 2-20):

1. *Engineered containment* (only for category C waste). Consists in preventing the release of contaminants from the waste disposal package during the thermal phase, where the thermal phase is the time frame during which the temperature of the host formation is expected to lie above the range of temperatures within which nominal migration properties can be relied upon, by using one or several engineered barriers. The component contributing to this safety function is a part of the supercontainer.
2. *Delay and attenuation of the releases* in order to retain the contaminants for as long as required within the disposal system. The components contributing to this safety function are the waste forms, the engineered barrier system and the host formation. Three sub-functions are defined:
   - *limitation of contaminant releases from the waste forms*: This function consists of limiting and spreading in time the releases of contaminants from the waste packages.
   - *limitation of the water flow through the disposal system*: This function consists of limiting the flow of water through the disposal system as much as possible, thus preventing or limiting the advective transport to the environment of the contaminants released from the waste packages.
   - *retardation of contaminant migration*: This function consists of retarding and spreading in time the migration to the environment of the contaminants released from the waste packages.
3. *Isolation* of the waste from man and the environment for as long as required, by preventing direct access to the waste and by protecting the repository from the potential detrimental processes occurring in its environment. The host formation and its geological coverage provide this safety function. Two sub-functions are defined:
   - *reduction of the likelihood of inadvertent human intrusion and of its possible consequences*: This function consists of limiting the likelihood of inadvertent human intrusion and, in case such intrusion does occur, of limiting its possible consequences in terms of radiological and chemical impact on humans and the environment.
   - *ensuring stable conditions for the disposed waste and the system components*: This function consists of protecting the waste and the engineered barrier system from changes and perturbations occurring in the environment of the facility, such as climatic variations, erosion, uplifting, seismic events or relatively rapid changes in chemical and physical conditions.

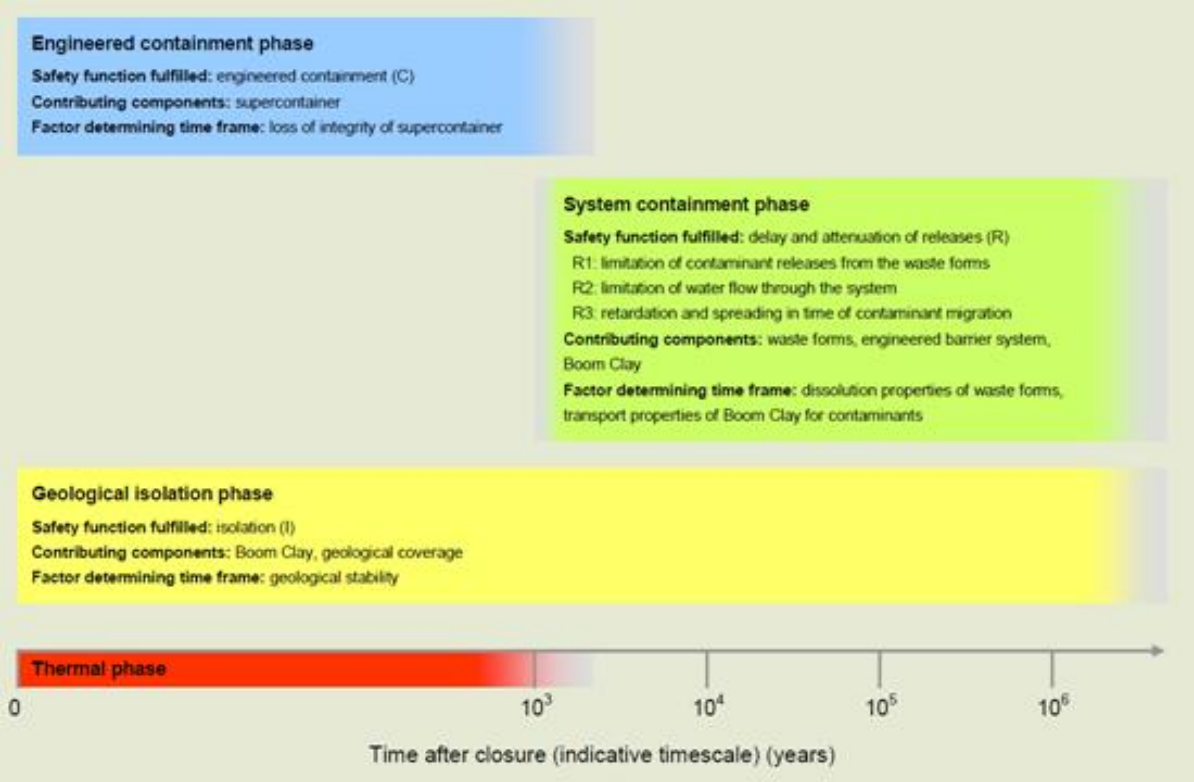

Figure 2-20. Safety functions provided by the main components of the disposal system in Boom Clay and its geological coverage and the time frames over which they are expected to be fulfilled. The engineered containment phase is specific to heat-generating waste (category C waste, that is, vitrified high-level waste and irradiated fuel) (ONDRAF/NIRAS 2013)

The primary component of the disposal system from the point of view of long-term safety is the host formation. The properties of the poorly indurated clays studied in Belgium are efficient natural barriers to the migration of radionuclides and chemical contaminants towards the surface environment:

- They have a *very low permeability*. There is therefore practically no water movement in these clays. As a result, transport is essentially diffusive, which means species migrate under the influence of their concentration gradient, not under the influence of the pore water movement.
- They have a *strong retention capacity* for many radionuclides and chemical contaminants (e.g. sorption capacity, favourable geochemical properties). Their migration through the clay is thus considerably delayed.
- They have a *capacity of self-sealing*. Fractures such as those induced by excavation works seal within weeks in Boom and Ypresian clays.

The EBS fulfils three main functions:

- next to operational safety aspects, it limits perturbations of the host formation by repository construction, operation and closure and it contains the category C waste during the thermal phase.
- it contributes to the delay and attenuation of the releases.
- the presence of backfill and seals will ensure that transport within the repository after closure will be diffusion-dominated.

Thermo-hydro-mechanical impact

Numerical predictions of a geological disposal facility had been done to assess the THM impact on the clay host formation. An example of such predictions showed that the temperature increased quickly

around the disposal gallery before rising slowly into the clay massif thanks of the heat dissipation (Figure 2-21). A maximum of 60°C was reached at the wall of the gallery. The distance between the disposal galleries is sufficient to not have a mutual interaction, i.e. the temperature evolution around one gallery does not affect the peak temperature of the neighbouring one.

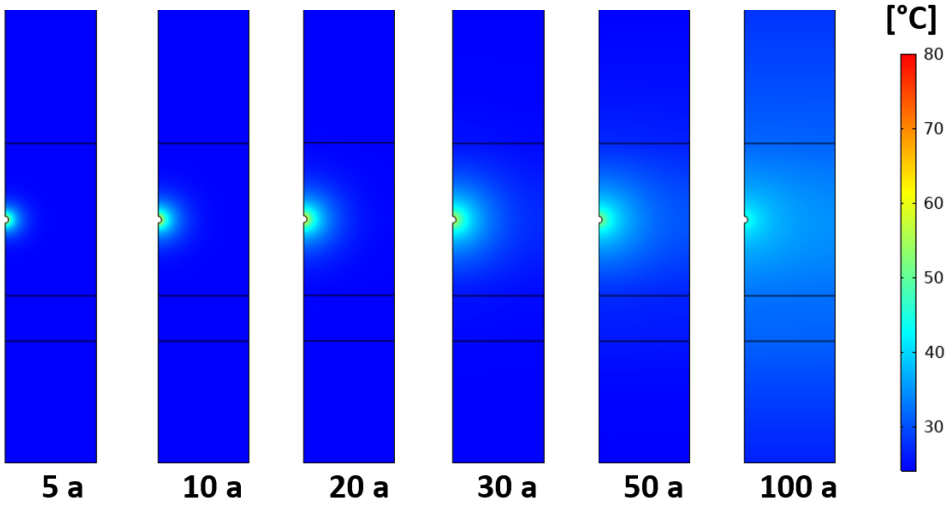

Figure 2-21. Numerical assessment of the temperature distribution around one disposal gallery at several intervals after 5, 10, 20, 30, 50 and 100 years of radioactive waste disposal (Dizier et al. 2020)

A closer look into the evolution of the temperature, obtained by numerical predictions of a geological disposal facility, showed that the temperature variation at the interface Boom Clay – lining has a maximum value of 50°C, the peak of the temperature is reached after one or two decades (Figure 2-22). The change in slope during the cooling period is influenced by the neighbouring galleries which affect only the long term cooling and has no consequence on the peak temperature.

At the interface Boom Clay – concrete lining, the pore water pressure increases because of the significant discrepancy between the thermal expansion coefficient of the solid and the one from the liquid phase (Figure 2-23, left). The pore water pressure rises quickly to a value close the undisturbed value of the pore pressure which pointed to 4 MPa in this case (repository at 400 m deep). The temperature at the wall of the gallery increases to value around 60°C before to cool down and to decrease. The peak of temperature evolution arrives after one or two decades similarly as what is observed in Figure 2-22. The analysis of the variation of the state of mechanical stress in Figure 2-23 (right) shows that the excavation process generates plastic strain which is consistent with the EDZ observed during the excavation of the connecting gallery in the HADES URF. The variation of temperature affects the mechanical state of stress by accumulating additional plastic strain around the gallery. This additional irreversible strain may modify the EDZ by extending the initial cracks, by increasing the permeability or by generating irreversible changes in the EDZ, affecting the favourable properties of the clay.

The large scale PRACLAY Heater test which has been running for more than four years aims at studying the combined effect of the hydro-mechanical perturbations induced by the excavation and the thermal loads coming from the wastes. Further explanations on this experiment are given in section 4.2.1.2.

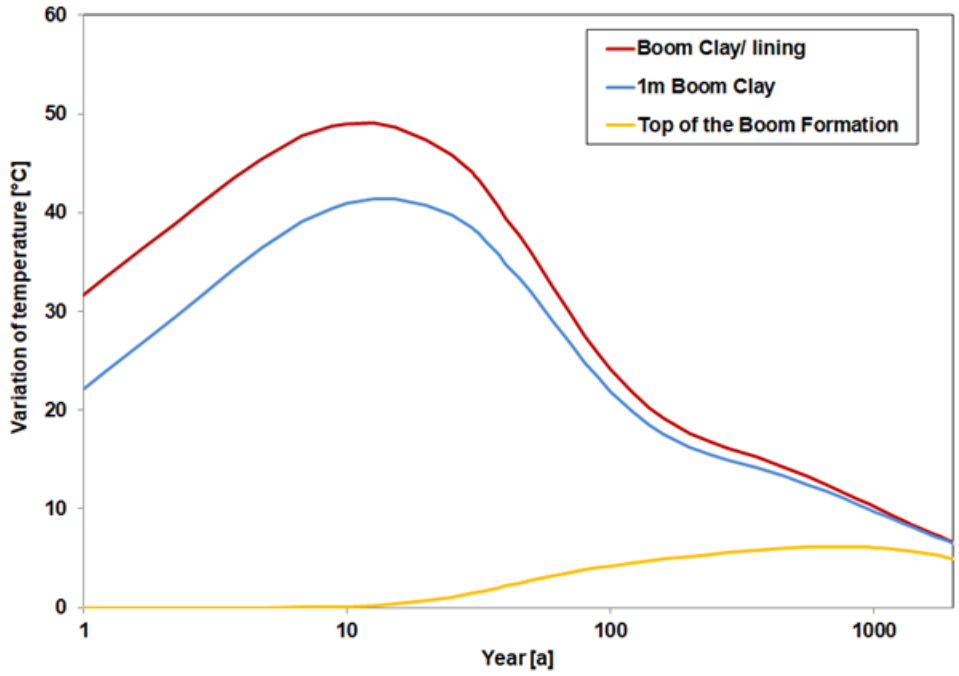

Figure 2-22. Temperature evolution at the interface between the lining support and the clay, 1 m deep into the clay and at the interface between the Boom Formation and the upper aquifer

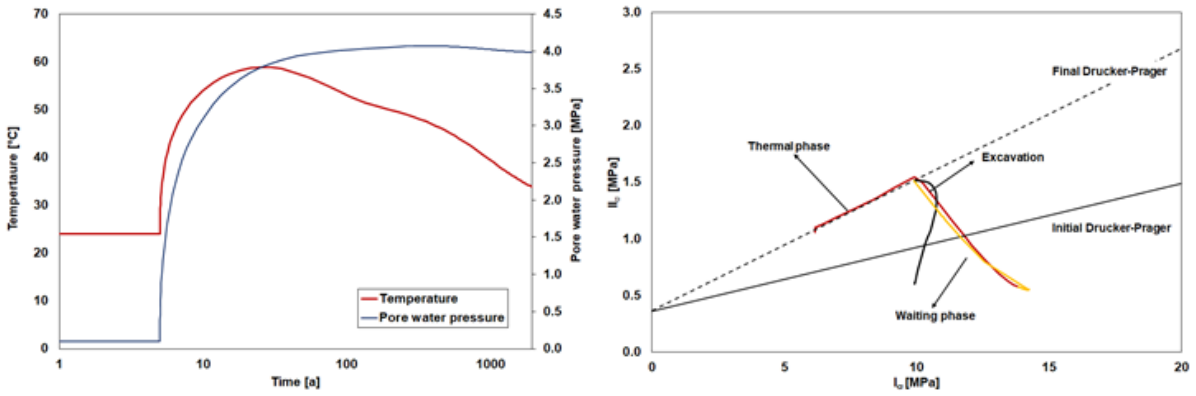

Figure 2-23. Pore water pressure and temperature evolution at the gallery wall obtained during a numerical prediction of geological disposal facility (left); Stress path in the plane of first invariant of the effective stress tensor and second invariant of the deviatoric effective stress tensor for appoint at the gallery's wall (right) (Dizier et al. 2020)

Thermal phase for a disposal in Boom Clay at 200 m deep (category C waste)

Once the category C waste is emplaced in the disposal gallery, the thermal phase starts. During this phase, which lasts some thousands of years, the temperature in the clay can increase up to almost 80°C. The EBS is designed in such a way that no radionuclide releases occur while a significant part of the clay formation is still hot. The increased temperature in the clay induces strongly coupled hydro-mechanical perturbations as summarised in Figure 2-24. It leads to a volumetric expansion of both the pore water and the rock minerals and thus also to an increase in pore water pressures and mean stresses. This may cause a decrease in effective stress in the clay.

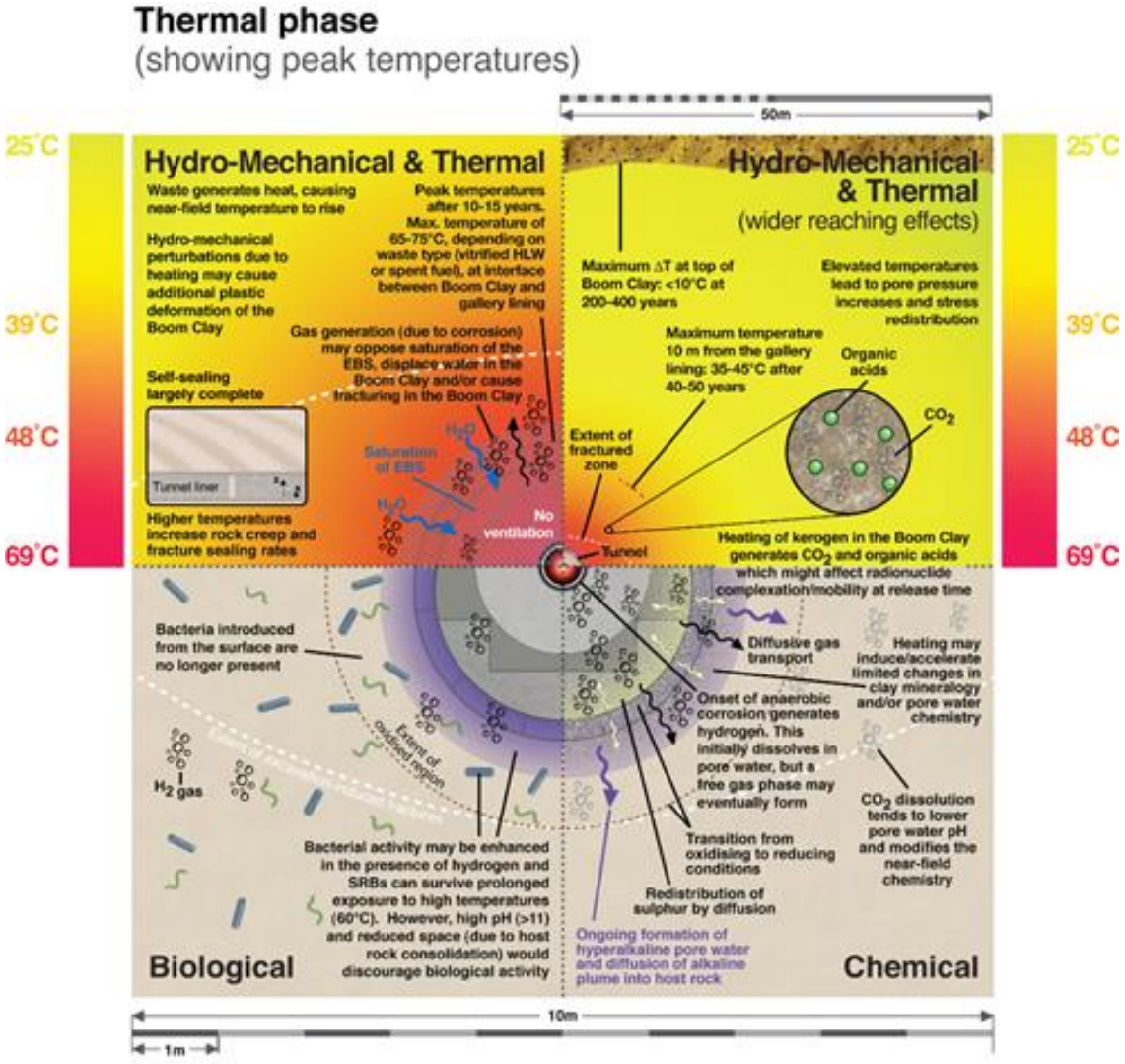

Figure 2-24. Transverse cross-sections through a disposal tunnel for category C waste and the surrounding Boom Clay illustrating the processes occurring in the disturbed zone during the thermal phase

Uncertainties

In the TIMODAZ project the impact of the temperature increase on the evolution of the disturbed zone was investigated and the consequences on the performance of the disposal system were evaluated. However, based on results to date, uncertainty remains on the large-scale hydromechanical response of the Boom Clay to heat. In particular, the anisotropy of the thermal conductivity in the Boom Clay, in combination with the anisotropy in the hydromechanical properties and in-situ stresses, and the consequences of these anisotropies are only examined by an in-situ test representative for the far field (ATLAS III, section 4.2.1.1). In the PRACLAY Heater Test a gallery in the Boom Clay is being heated up to 80°C over a gallery length of 35 m for 10 years. This allows a characterization of the THM behaviour of the Boom Clay on large-scale that is not only relevant to the far field, but also to the near field behaviour. The WP HITEC of the EURAD EC project will contribute to the evaluation of this near field THM behaviour of the Boom Clay.

The heating of the clay can also induce changes in the mineralogy and geochemistry of the Boom Clay. Up till now no significant changes in the clay mineralogy or geochemistry were observed, but research is still on-going, mainly on the effect of a combined thermal and alkaline perturbation.

Furthermore the thermal reactivity of the Boom Clay kerogen constitutes a factor of uncertainty. Because the kerogen in the Boom Clay is thermally immature, significant amounts of CO_2 and organic acids will be released during heating. This release may affect the mobility of radionuclides by complexation, while the dissolution of CO_2 in water, leading to pH reduction, may modify the near-field chemistry of the clay.

Another important phenomenon occurring after the closure of the disposal gallery is the generation of gas due to anaerobic corrosion, radioactive decay, radiolysis and microbial activity. Scoping calculations reveal that the large bulk of the gas that will be generated is hydrogen coming from anaerobic corrosion of the steel components used in the EBS. Depending on the amount of gas generated and the diffusion capacity of the clay, a free gas phase and a gas pressure might build up in the clay. This could lead to a fracturing of the clay. Another research project of EURAD (WP GAS) is on-going and will contribute to the evaluation of the risk of a gas phase on the Boom Clay behaviour.

2.6 POSIVA (Finland)

In Finland, spent nuclear fuel from the nuclear power plants of Teollisuuden Voima and Fortum will be embedded in Olkiluoto bedrock at a depth of 400-450 metres. Posiva's final disposal plans are based on the KBS-3V concept, developed by Swedish SKB. The solution is based on the multiple barriers principle. Radioactive substances are contained within several overlapping protective barriers so that no deficiency in one barrier and no predictable geological or other change will endanger the isolation. The release barriers include the physical state of the fuel, the disposal canister, the bentonite buffer, the backfilling of the tunnels and the surrounding rock (Figure 2-25).

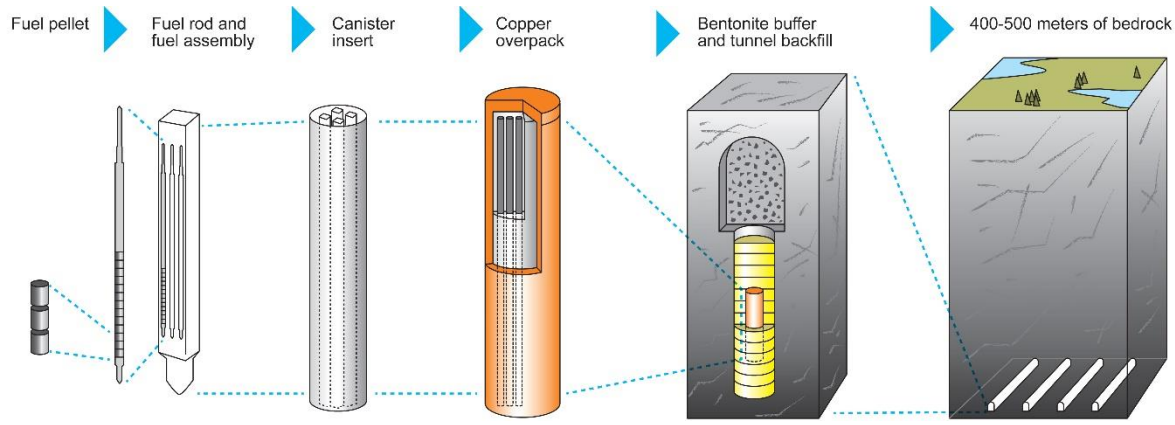

Figure 2-25. Multiple barriers and KBS-3V design

The bentonite buffer that surrounds the vertically installed copper canisters is composed of Wyoming Na-bentonite in form of compacted bentonite blocks (dry density 1650-1800 kg/m^3) and bentonite pellet filled gaps (dry density 880-960 kg/m^3) between canister and the compacted blocks as well as between the compacted blocks and host rock.

Performance target of maximum 100°C temperature for buffer has been set to ensure favourable early evolution of the engineered barriers. This target is taken into account in thermal dimensioning of the repository (Ikonen et al. 2018) that analyses allowed distance between disposal canisters and disposal tunnels and is basis for designing the repository layout.

Posiva has been involved only in limited number of buffer tests with higher than 100°C temperature due to the set 100°C performance target for the buffer.

2.7 RWM (United Kingdom)

The UK Government published its updated policy on geological disposal in December 2018, which marked the launch of the siting process in England. In Wales, the siting process was launched by the Welsh Government in January 2019. Both policies set out a consent-based approach of working in partnership with communities, where a geological disposal facility will only be built where both a willing community and a suitable site exist. At the time of writing, no disposal site or geology has been selected, and therefore illustrative designs have been adopted for suitable generic rock types. For lower strength sedimentary host rocks (e.g. clay) and higher strength host rocks (e.g. granite), a bentonite engineered barrier system is adopted, to surround high heat generating waste containers (RWM 2016). An evaporite concept is also being considered in the UK, but this does not involve any clay based barriers.

For illustrative purposes before a repository site is chosen, RWM has broadly adopted the NAGRA concept for a lower-strength sedimentary rock type, and the KBS-3V system developed by SKB for a higher strength rock type, for the disposal of high heat generating waste (Figure 2-26). Both disposal concepts assume the use of Na montmorillonite bentonite such as the Wyoming type for the buffer surrounding the waste container.

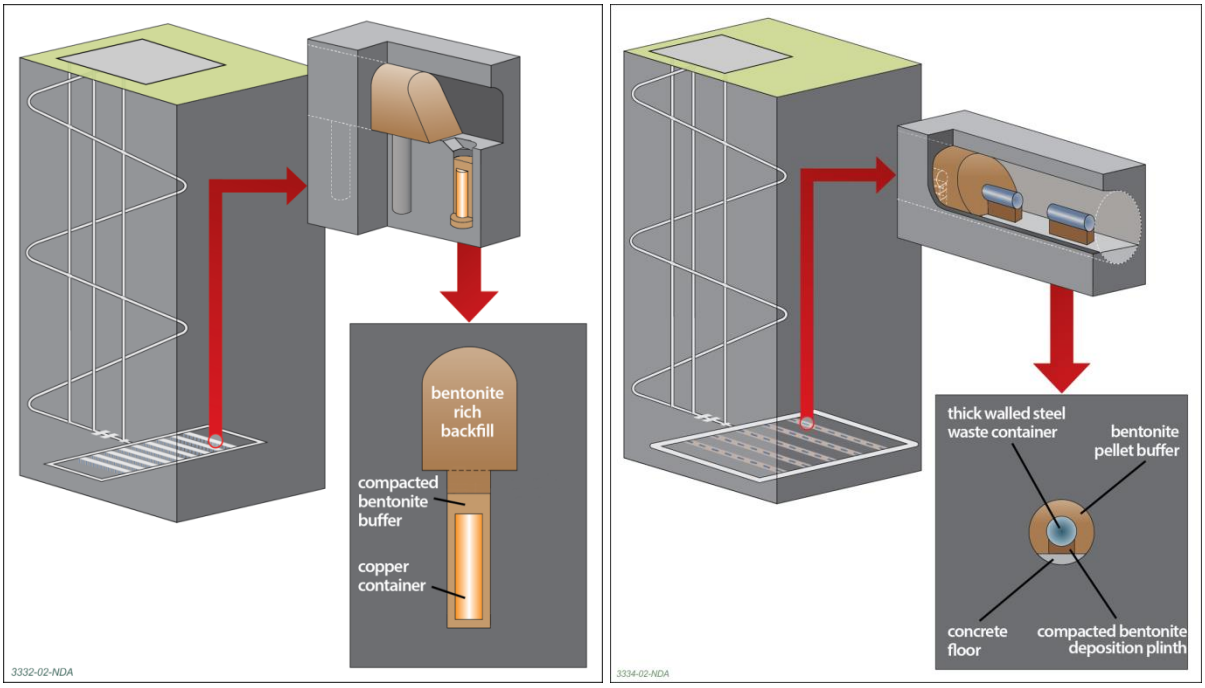

Figure 2-26. RWM illustrative designs for a higher strength rock (based upon KBS-3V, left) and lower strength sedimentary rock type (based upon NAGRA concept, right) after RWM (2016)

RWM acknowledges that the UK inventory differs from that in Sweden, Finland and Switzerland, and therefore tailored concepts will be developed for a UK disposal facility. Work is ongoing to consider the benefits and technical challenges of alternative concepts, such as mined borehole matrices or disposal vaults (Amec 2018a, b). Selection of final disposal concept will be driven by waste constraints, site specific characteristics (once these become available) as well as practical and economic considerations. It is relevant to mention that thermal dimensioning work by RWM has highlighted that significant repository footprint and waste cooling time reductions can be achieved through thermal optimisation (Amec 2016). This work is a key driver for RWM to better understand the thermal limits

of the bentonite buffer, since this component of the disposal system currently limits thermal loading in the proposed facility.

In the UK, there is a strategic need to further understand the thermal limits of engineered barriers, such that the implications of heat output can be considered when planning for the generation and packaging of wastes. The outcome of research into the behaviour of clays at high temperatures will be used to advise UK Government nuclear strategy, specifically in relation to possible re-use of the UK's civil plutonium stockpiles for the production of high burn up Mixed Oxide Fuels (MOx) which is a current planning assumption (Hinson 2019). Additionally, the research will help inform disposability assessments for other potential wastes such as legacy AGR and PWR SF and other possible future fuels from new nuclear power stations.

To-date, RWM has conducted limited research into the implications of elevated temperatures upon bentonite buffers since 2005. This has been because disposal planning has not been site specific and RWM has not yet identified its site specific disposal concepts.

2.8 SKB (Sweden)

In Sweden, used nuclear fuel will be emplaced in the Forsmark bedrock at a depth of approximately 500 metres. The final disposal plans are based on the KBS-3V concept, developed by SKB, also to be used by Posiva and explained above in further detail (section 2.6).

SKB has conducted a number of field experiments with bentonite at buffer densities and high temperature at the Äspö Hard Rock Laboratory, Oskarshamn (Sweden). Full scale experiments with both buffer and backfill, with a buffer temperature below 100°C (Prototype repository; e.g. Olsson et al. 2013), and smaller scale experiments (3-4 m high; 3 dm in diameter) using copper heater at 90 and 130°C (LOT; e.g. Karnland et al. 2009) and steel heater (ABM; e.g. Svensson et al. 2011) at typically 130°C. The exception ABM5 (Sandén et al. 2018) was at the hottest parts more than 200°C. The use of higher temperatures than 100°C (above the target temperature in the repository) is mainly aimed at acceleration of processes and increased understanding.

2.9 SÚRAO (Czech Republic)

SÚRAO is currently in the site selection and evaluation stage of the Czech Deep Geological Repository (DGR) development programme, which will be followed by the reduction in the number of potential sites (initially from 9 to 4) and the subsequent selection of the final and reserve sites by 2025. SÚRAO is also currently compiling a detailed RD&D plan which will provide a detailed overview of the various research activities to be conducted up to 2025.

The Czech DGR concept considers only crystalline rock environments, i.e. igneous or metamorphic rock (granites, gneisses) massifs at depths of approximately 500 metres below the earth's surface. The repository will serve for the disposal of spent nuclear fuel (SNF) and other high- and intermediate-level radioactive waste that cannot be disposed of in existing repositories. The two sections of the DGR (SNF and HLW/ILW) will be separated by a natural rock partition of sufficient thickness. The direct disposal of SNF is anticipated and it is expected that the encapsulation plant will be located within the DGR complex.

The final technical design of the repository has not yet been decided. Preliminary project design studies concerning DGR construction that have been compiled for each of the 9 potential sites consider four SNF disposal options, i.e. combinations of vertical and horizontal disposal and the fully-mechanised and conventional excavation of the underground complex. The vertical system involves the drilling of vertical disposal wells from horizontal disposal tunnels. The wells will have a diameter of 1.8 m and a

length of around 5.5 m for VVER-440-type containers and 7.2 m for VVER-1000-type containers. The horizontal disposal system considers the drilling of horizontal micro-tunnels with a diameter of 2.2 m and maximum lengths of 300 m (e.g. Špinka et al. 2018).

The design of the container for SNF is still under development, with 12 options currently being considered (Kotnour et al. 2017). The option that has been most extensively studied to date consists of a double-walled steel-based canister with an outer wall of carbon steel and inner containers made from stainless steel (Figure 2-27).

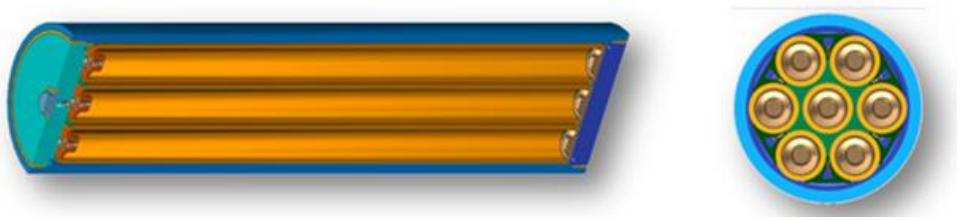

Figure 2-27. The most extensively studied Czech SNF disposal canister option with seven inner containers for the disposal of spent fuel from VVER 440 reactors (three such inner containers are envisaged for SNF from VVER 1000 reactors)

With respect to the buffer and backfill concept, while a basic design has been accepted in principle, the search for alternative approaches is ongoing. The basic buffer concept involves a combination of compacted bentonite blocks and pellets, while the backfill concept is based on a bentonite material only; however, the option of the use of a mixture of bentonite and crushed rock has not been rejected. Currently, it is planned that Czech bentonite will be used as the buffer and backfill material, the extensive testing of which has already been addressed by many research studies. The bentonite in question is mined in the western part of the Czech Republic and is of the Ca-Mg type with enhanced iron content in its octahedral positions (Hausmannová et al. 2018).

The research of the suitability of Czech bentonite as the buffer and backfill materials makes up one of SÚRAO's main priorities, with a final decision on its use expected no later than 2025. The various requirements relating to the buffer and backfill will be set according to the state of knowledge at the time and the DGR development phase.

Various bentonite materials will be tested at elevated temperatures as part of the HITEC project, the outcome of which will consist of an indication of which bentonite is most stable at higher temperatures. The information acquired from the project will assist in the determination of the design of the buffer and the various requirement settings.

2.10 Summary

Table 2-1 summarises some characteristics of the different national concepts presented. There are two concepts which do not consider the use of a clay buffer between the canister and the host rock, ANDRA and ONDRAF/NIRAS, and the contribution of these two agencies to the report focuses consequently on the clay host rock. NAGRA, which considers the use of a clay buffer in clay host rock, participates in both parts of the report. The rest of agencies contributed only to the buffer part, as their concepts are based on crystalline host rock (except for ENRESA). Of the agencies contributing to the buffer chapter, only ENRESA and SÚRAO use bentonites with a predominance of divalent cations in the interlayer of the smectite, whereas the others consider the use of sodium bentonite (MX-80).

Regarding temperature constrains, all the concepts presented assume that the temperature at any part of the buffer or host rock should be below 100°C, except for NAGRA, which allows a temperature of 130°C at the canister/buffer interface.

Table 2-1. Summary of characteristics of repository concepts

WMO	CONCEPT	CLAY BUFFER TYPE	THERMAL ASPECTS	UNCERTAINTIES
ANDRA	Cigéo	No	T<90°C in COx No formation damage	Non-linearity mechanical behaviour Time-dependent behaviour
BGE	ANSICHT	Yes, sodium bentonite	Preliminary cask surface T <100°C	
ENRESA	2004-concept clayrock	Yes, divalent bentonite	T <100°C in bentonite ΔT<5°C upper aquifer ΔT<0.5°C land surface	
NAGRA	HLW	Yes, sodium bentonite	130°C canister/buffer <90°C rock	
ONDRAF /NIRAS	Monoliths B and Supercontainer	No	<100°C overpack <25°C top clay formation	Large-scale response to heat Anisotropy of THM properties Changes in mineralogy/geochemistry (T, high pH) Thermal reactivity Gas role
POSIVA	KBS-3V	Yes, sodium bentonite	T <100°C in buffer	
RWM	preliminary	Yes, sodium bentonite		
SKB	KBS-3V	Yes	T <100°C in buffer	
SÚRAO	preliminary	Yes, divalent bentonite	T <100°C in bentonite	

3 Buffer materials

3.1 Materials to be used in HITEC

Three main bentonites have been identified as those better characterised and to be used by more participants in the HITEC project and in a wider variety of tests, including the large-scale ones (section 3.2). These are MX-80, FEBEX and BCV, described in the following subchapters. However, several other bentonites will also be used in the project, such as Ibeco, Imerys, Kunipia, PBA, PBC (see EURAD Milestone 47). In addition, some of the materials used in the ABM large-scale test (e.g. DepCAN, Asha505, Calcigel) are also briefly described below.

3.1.1 MX-80 bentonite

The MX-80 bentonite comes from Wyoming (USA) and is produced by American Colloid Co. It is a bentonite of volcanic origin, powdered and Na-homogenised. The deposit has been mined for decades, for which reason the characteristics of the bentonite found in the literature vary over time and also depending on the batches. Some of the initial characterisations of the material in the context of radioactive waste disposal were performed by Müller-Vonmoos & Kahr (1983), Borgesson et al. (1988), Madsen (1998) or Pusch (2001).

One of the batches of MX-80 bentonite used by POSIVA was obtained from Sibelco Nordic AB and has ID Be-Wy--BT0011-Sa-R and Be-Wy--VTT0002-BT1-Sa-R (Figure 3-1). Its characterisation can be found in Kiviranta & Kumpulainen (2011) and Kiviranta et al. (2018), where the methods for obtaining the data are discussed. Some of the results obtained are summarised here for reference, although the material batch is not intended to be used in HITEC. Tests aiming for thermo-hydro-mechanical simulation model parametrisation suchs as thermal conductivity measurements, infiltration tests, swelling pressure and hydraulic conductivity measurements, water retention curve and oedometer studies can be found for example in Pintado et al. (2013) and Toprak et al. (2018).

Figure 3-1. Photo of the Posiva MX-80 material Be-Wy--VTT002 (Kiviranta et al. 2011)

In the HE-E and FE tests (see sections 3.2.3.2 and 3.2.4) the MX-80 has been used in the form of irregular pellets of size <10 mm, dry density ~2.1 g/cm^3 and water content 6% (see Gaus et al. 2013 for manufacturing process).

The content of montmorillonite is between 80 and 90%, with quartz (contents between 4 and 15%), plagioclase and K-feldspars (2-9%), and minor quantities of cristobalite, tridymite, calcite, gypsum, pyrite, illite. In particular, the montmorillonite content of the Posiva MX-80 batch is 88.2±3.2 wt.%, with also quartz (3.5±0.1 wt.%), plagioclase (2.9±0.7 wt.%), K-felspar (2.4±1.5 wt.%), pyrite (0.8±0.2 wt.%), and rutile (0.5±0.4 wt.%). The purified montmorillonite of this batch had structural formula: exchangeable cation sites $Na_{0.46}Ca_{0.19}Mg_{0.07}$, octahedral sites $Al_{3.11}Fe^{3+}_{0.35}Fe^{2+}_{0.03}Mg_{0.47}$, tetrahedral sites $Si_{7.91}Al_{0.09}$, $O_{20}(OH)_4$.

The cation exchange capacity may be between 75 and 86 meq/100 g (86.3±0.3 meq/100 g for the Posiva batch. Na^+ is the main exchangeable cation (50-74 meq/100 g), with also Ca^{2+} (10-30 meq/100 g) and Mg^{2+} (3-8 meq/100g). The main soluble ions are sodium and sulphate.

The values of the plastic limit found in the literature vary between 46 and 70% and for the liquid limit between 450 and 550% (50% and 490% respectively for the Posiva batch). There is also variability in the values reported for the density of solid particles, which range between 2.76 and 2.82 g/cm^3 (2.78 g/cm^3 for the Posiva batch.) The as-received water cotent of the Posiva batch was 12.3±0.1%, the swelling index 22.0±0.3 mL/2g, the water absorption capacity 630% and the total specific surface area 624 m^2/g. The granule size distribution of this batch is shown in Figure 3-2.

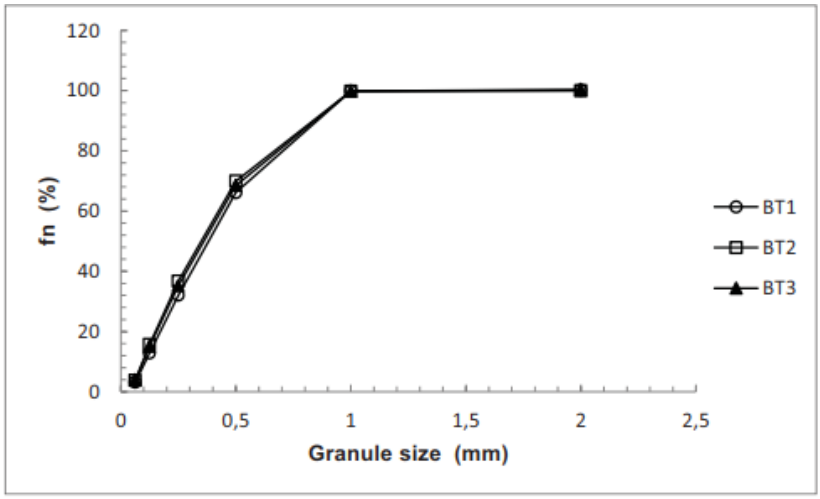

Figure 3-2. Granule size vs. percent passing different size sieves for three batches of MX-80 (Be-Wy--VTT002) (Kiviranta & Kumpulanien 2011)

The water retention capacity of MX-80 bentonite has also been checked by different authors, and the effect on the water retention curve (WRC) of dry density (e.g. Figure 3-3, Figure 3-4) and temperature have been analysed (e.g. Figure 3-5). Jacinto et al. (2009) found that the influence of dry density on the water retention capacity depends on the suction range, the limiting value being around 30 MPa. For suctions above this threshold value the retention capacity in terms of water content is slightly higher as the dry density is higher, whereas for lower suctions, the lower the dry density of the bentonite the higher its water content. The retention capacity decreases with temperature, more than predicted by the change in surface tension, especially for the high temperatures and the low suctions. Villar & Gómez-Espina (2008) reported some suction measurements on compacted MX-80 bentonite with different water contents at temperatures of up to 120°C.

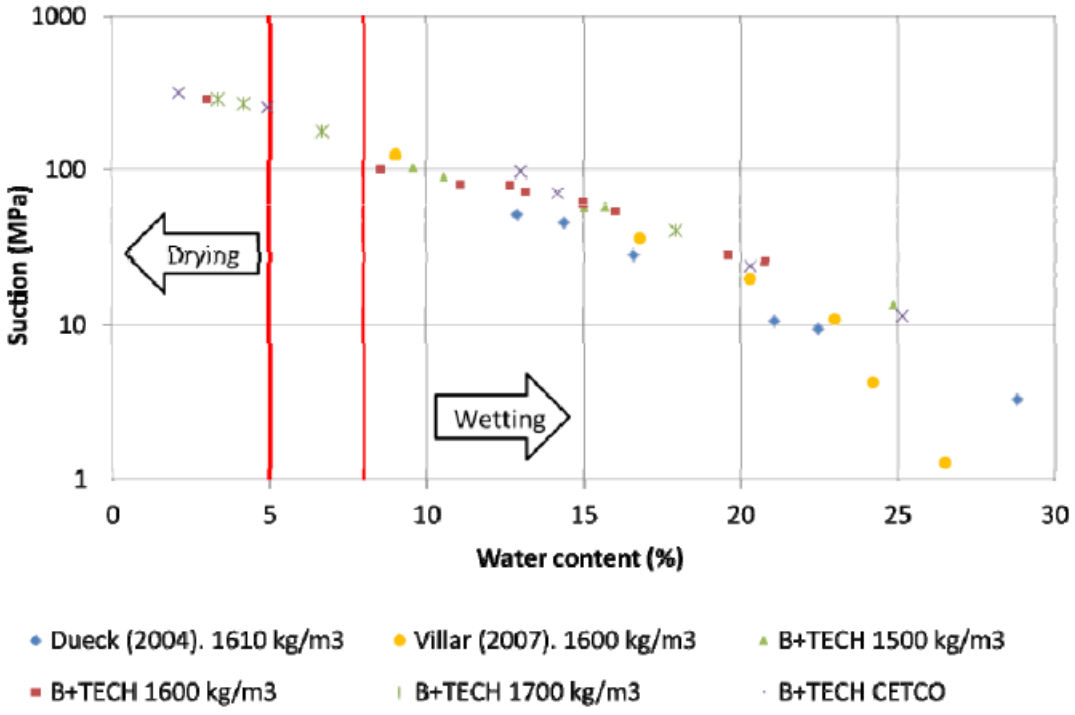

Figure 3-3. WRC of MX-80 samples of different dry density. The initial water content is 5-8% (Pintado et al. 2013)

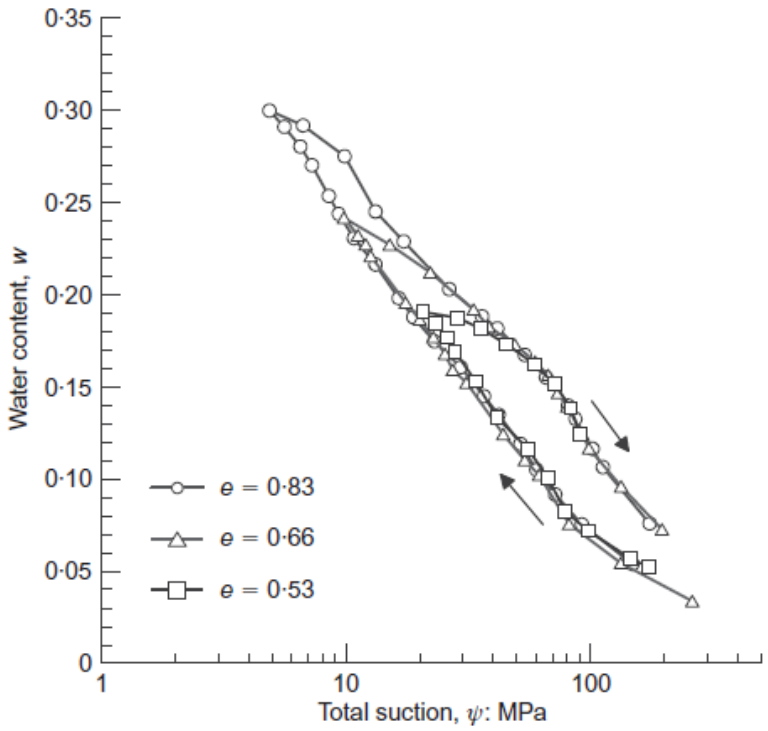

Figure 3-4. Effect of void ratio on the water retention behaviour of MX-80 granular bentonite (Seiphoori et al. 2014)

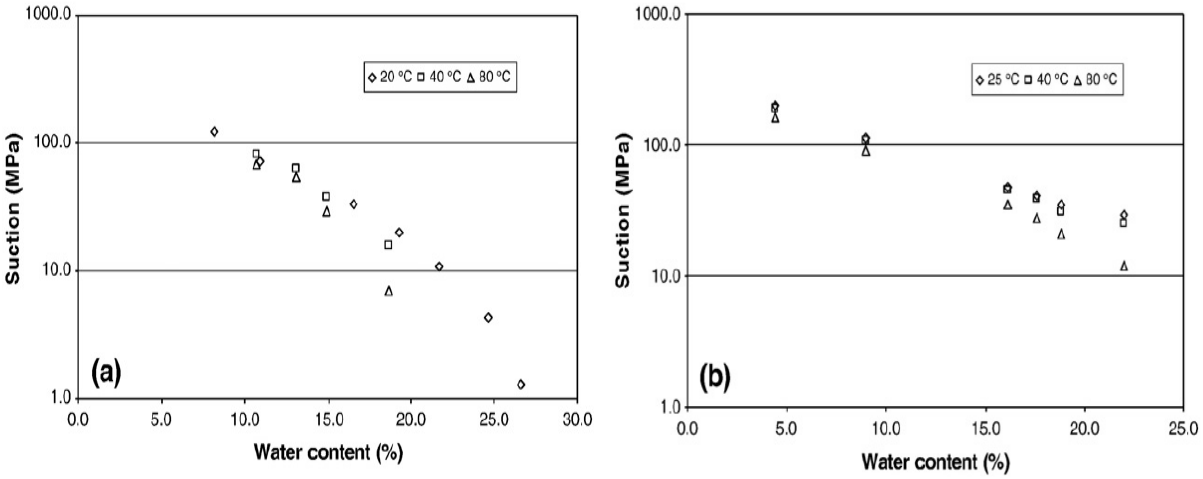

Figure 3-5. Experimental values of suction vs. water content at different temperatures for MX-80 compacted at dry densities of (a) 1.60 g/cm³ and (b) 1.75 g/cm³ (Jacinto et al. 2009).

Figure 3-6 shows an example of the swelling pressure and hydraulic conductivity for MX-80 samples of different dry density.

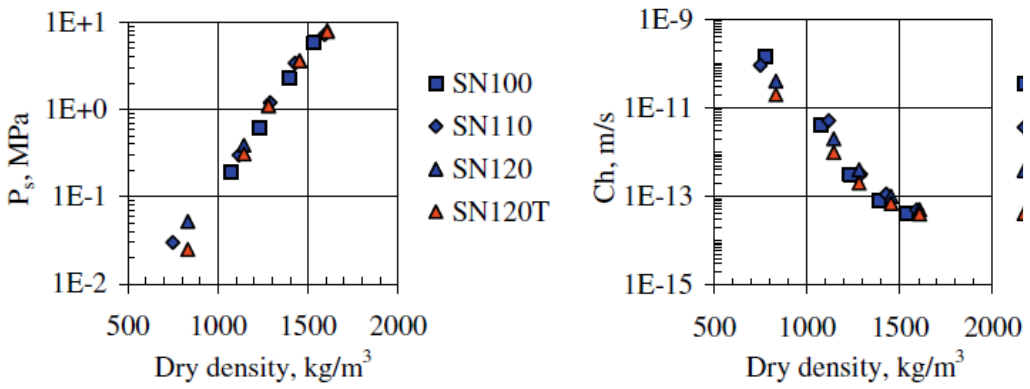

Figure 3-6. Swelling pressure (left) and hydraulic conductivity (right) as a function of dry density for samples of Wyoming bentonite (Karnland et al. 2008)

Unconfined compression test results are given in Figure 3-7 and tensile strength results are given in Figure 3-8.

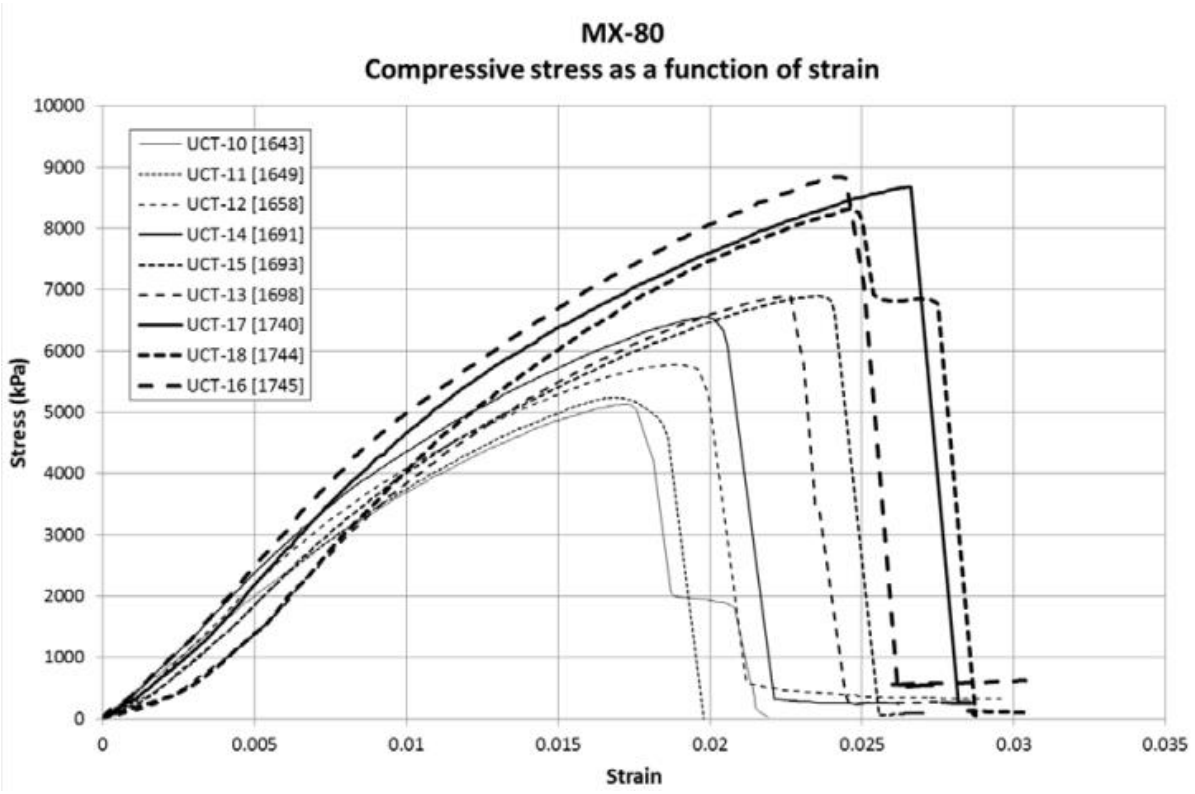

Figure 3-7. Stress-strain paths for the MX-80 bentonite samples. Dry densities are presented in brackets in kg/m^3 (Kiviranta et al. 2018)

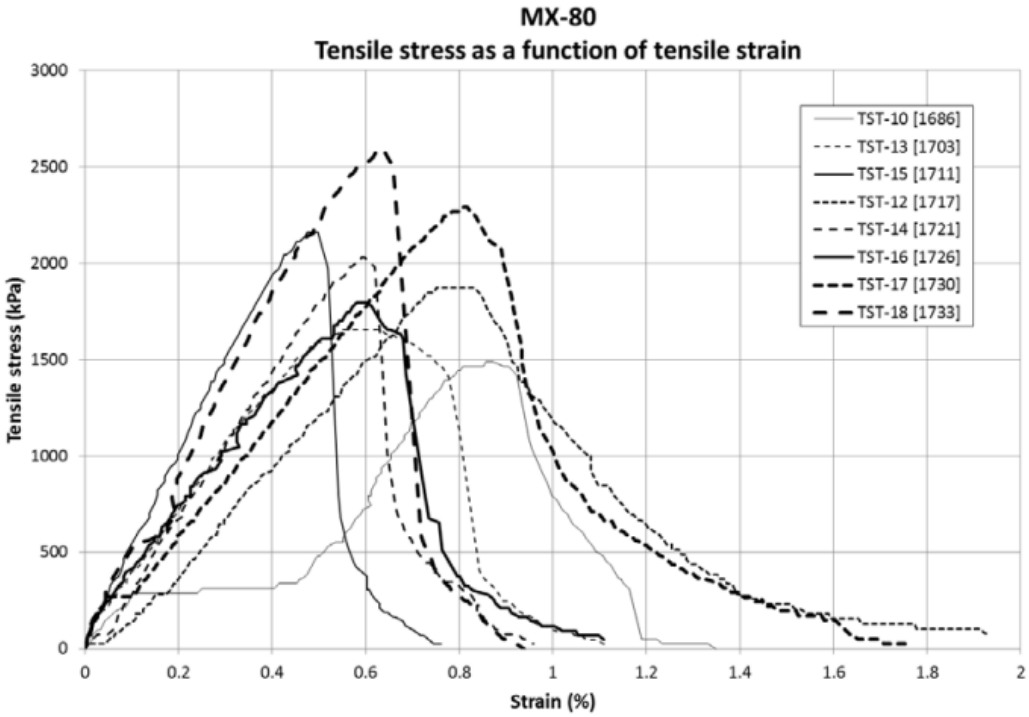

Figure 3-8. Tensile stress-strain curves of MX-80 samples. Dry densities are given in brackets in kg/m³ (Kiviranta et al. 2018)

Figure 3-9 and Figure 3-10 show examples of the increase of thermal conductivity of the MX-80 bentonite with dry density, water content and temperature taken from the literature.

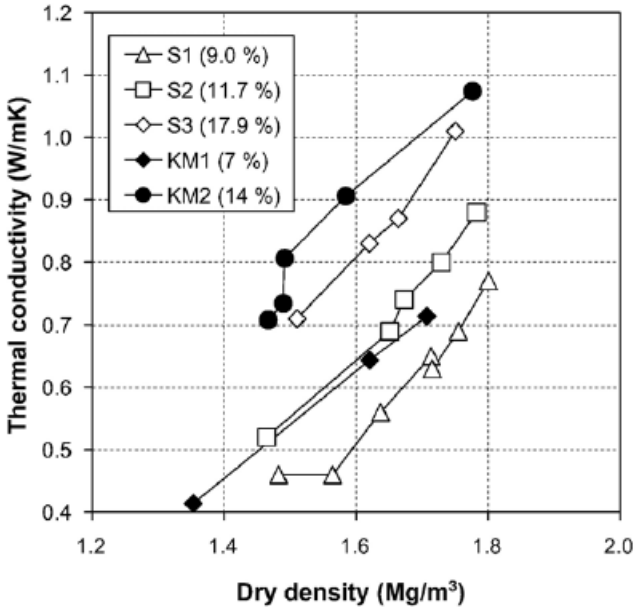

Figure 3-9: Dependence of thermal conductivity of MX-80 on dry density and water content (Tang et al. 2008a)

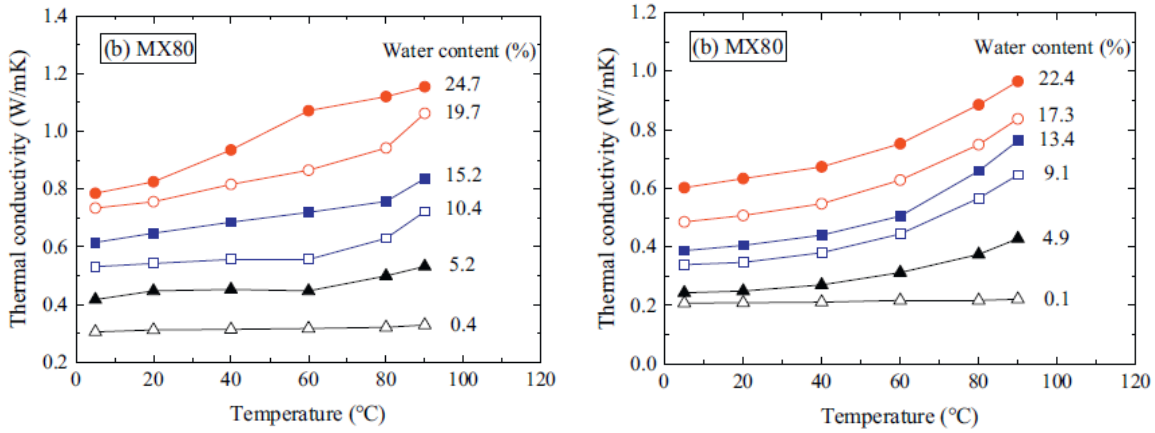

Figure 3-10: Dependence of MX-80 bentonite thermal conductivity on temperature for two dry densities: 1.6 g/cm³ (left) and 1.3 g/cm³ (right) according to Xu et al. (2019)

3.1.2 FEBEX bentonite

The FEBEX bentonite is a 900-t batch of bentonite that was extracted from the Cortijo de Archidona deposit and processed in 1996 for the FEBEX project. The processing consisted in homogenisation, air-drying and manual removal of volcanic pebbles on site and, at the factory, crumbling, drying in a rotary oven at temperatures between 50 and 60°C and sieving through a 5-mm mess. The blocks for the FEBEX *in-situ* test at Grimsel were manufactured from this material. During packaging, an approximately 9-kg bentonite sample was taken for every 2.5 t. These subsamples were mixed at CIEMAT facilities to obtain a very homogeneous material that was used for a comprehensive characterisation and different laboratory tests during the FEBEX I and FEBEX II projects. These initial studies can be found in the final report of the project (Enresa 2006) and in Villar (2002) and Fernández (2004). This material was also used for the NF-PRO and PEBS projects (Villar & Gómez-Espina 2009) and was distributed over the years to different laboratories to be used in different projects (e.g. ABM [Svensson et al. 2011], ESDRED [Alonso et al. 2008]).

The smectite content of the FEBEX bentonite is above 90 wt.% (92±3 %). The smectitic phases are actually made up of a montmorillonite-illite mixed layer, with 10-15 wt.% of illite layers. Besides, the bentonite contains variable quantities of quartz (2±1 wt.%), plagioclase (3±1 wt.%), K-felspar (traces), calcite (1±1 wt.%), and cristobalite-trydimite (2±1 wt.%).

The cation exchange capacity of the smectite is 98±2 meq/100g, the main exchangeable cations being calcium (33 meq/100g), magnesium (33 meq/100g) and sodium (28 meq/100g). The predominant soluble ions are chloride, sulphate, bicarbonate and sodium.

The liquid limit of the bentonite is 102±4 %, the plastic limit 53±3 %, the density of the solid particles 2.70±0.04 g/cm^3, and 67±3 % of particles are smaller than 2 µm. The hygroscopic water content in equilibrium with the laboratory atmosphere (relative humidity 50±10 %, temperature 21±3 °C, total suction about 100 MPa) is 13.7±1.3 %. The external specific surface area is 32±3 m^2/g and the total specific surface area is ~725 m^2/g.

The retention curve of the bentonite was determined in samples compacted to different dry densities at different temperatures (Lloret *et al*. 2004, Villar & Lloret 2004, Villar & Gómez-Espina 2009). The volume of the samples remained constant during the determinations, since they were confined in constant volume cells. Following an approach similar to that presented by Sánchez (2004) to fit the data from these laboratory determinations, the empirical Equation 1 was obtained:

$$w = \left(b \cdot n^{c} \cdot e^{-\alpha \cdot (T-T_0)}\right) \cdot \left[1 + \left(\frac{s}{P_0 \cdot e^{-\eta \cdot (n-n_0)} \cdot e^{-\alpha \cdot (T-T_0)}}\right)^{\frac{1}{1-\lambda_1}}\right]^{-\lambda_1} \cdot \left(1 - \left(\frac{s}{P_{sec}}\right)^{\lambda_2}\right) \cdot (S_r - S_{lr}) \quad [1]$$

where w is the water content (%), n and n_0 are the porosity and reference porosity, respectively, s is the suction (MPa), T and T_0 are the temperature and reference temperature, respectively, (°C), S_r and S_{lr} are the liquid degree of saturation and liquid residual degree of saturation, respectively, P_0, P_{sec}, λ_1 and λ_2 are the parameters to define the shape of the retention curve at the reference temperature and porosity, and b, c, α and η are fitting parameters that take into account the influence of temperature and porosity. The values of parameters are indicated in Table 3-1. The differences between measured values and the estimated values using Equation 4 are smaller than 2% in terms of water content.

Table 3-1. Values of parameters in Equation 4

b	c	P_0 (MPa)	λ_1	λ_2	η	n_0	α (1/°C)	T_0 (°C)	P_{sec} (MPa)	S_r	S_{lr}
145	1.9	25	0.2	1.1	20	0.4	0.0015	20	1000	1.0	0.01

The saturated hydraulic conductivity of compacted bentonite samples is exponentially related to their dry density (Eq. 1 and 2). For a dry density of 1.6 g/cm^3 the saturated permeability of the bentonite is approximately $5 \cdot 10^{-14}$ m/s at room temperature, either with diluted granitic or deionised water used as percolating fluid. The temperature increase tends to increase permeability.

for dry densities of less than 1.47 g/cm^3:

$$\log k_w = -6.00\ \rho_d - 4.09 \quad [2]$$

for dry densities in excess of 1.47 g/cm^3:

$$\log k_w = -2.96\ \rho_d - 8.57 \quad [3]$$

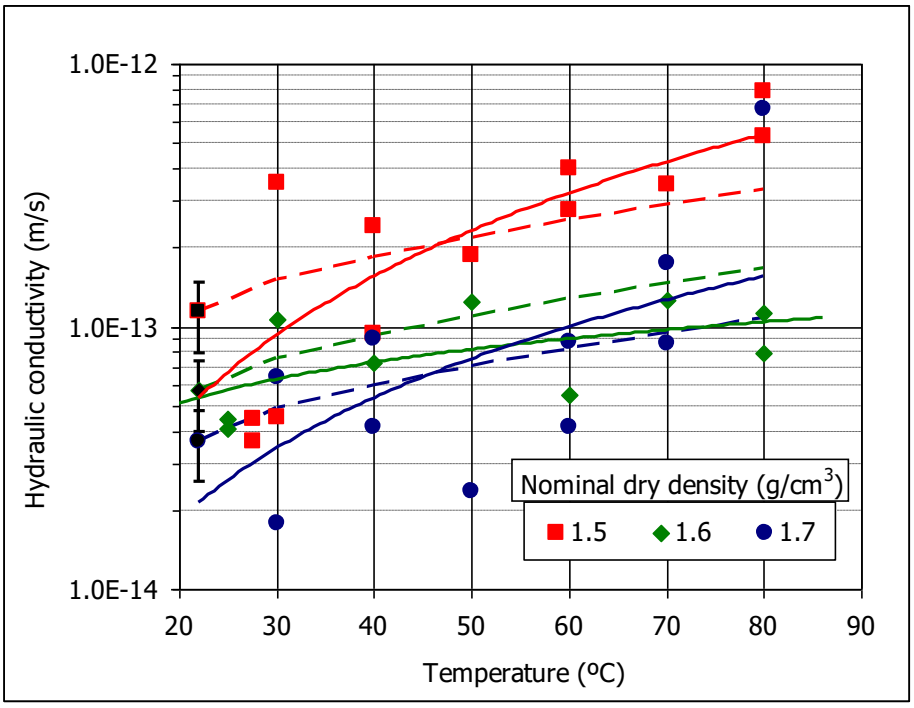

Figure 3-11. Hydraulic conductivity *vs*. temperature for saturated FEBEX clay compacted to different nominal dry densities (actual average dry densities are 1.48, 1.58 and 1.64 g/cm³). Error bars obtained with Equation 2. The dotted lines indicate the change of permeability expected on the basis of water properties changes with temperature (Villar & Gómez-Espina 2009)

Some isothermal infiltration tests and heat flow tests at constant overall water content were performed during FEBEX I project and they were backanalysed using CODEBRIGHT (Lloret *et al*. 2002, Pintado *et al*. 2002). It is possible to fit the experimental data using a cubic law for the relative permeability ($k_r = S_r^3$) and a value of 0.8 for the tortuosity factor (τ).

The swelling pressure of compacted samples is also exponentially related to the bentonite dry density (Eq 3). The bentonite compacted at dry density of 1.6 g/cm^3 and saturated with deionised water at room temperature develops a swelling pressure of about 6 MPa. Saturation with a Spanish diluted granitic water gives similar values, whereas temperature causes a decrease of them (Figure 3-12).

$$\ln P_s = 6.77\ \rho_d - 9.07 \qquad [4]$$

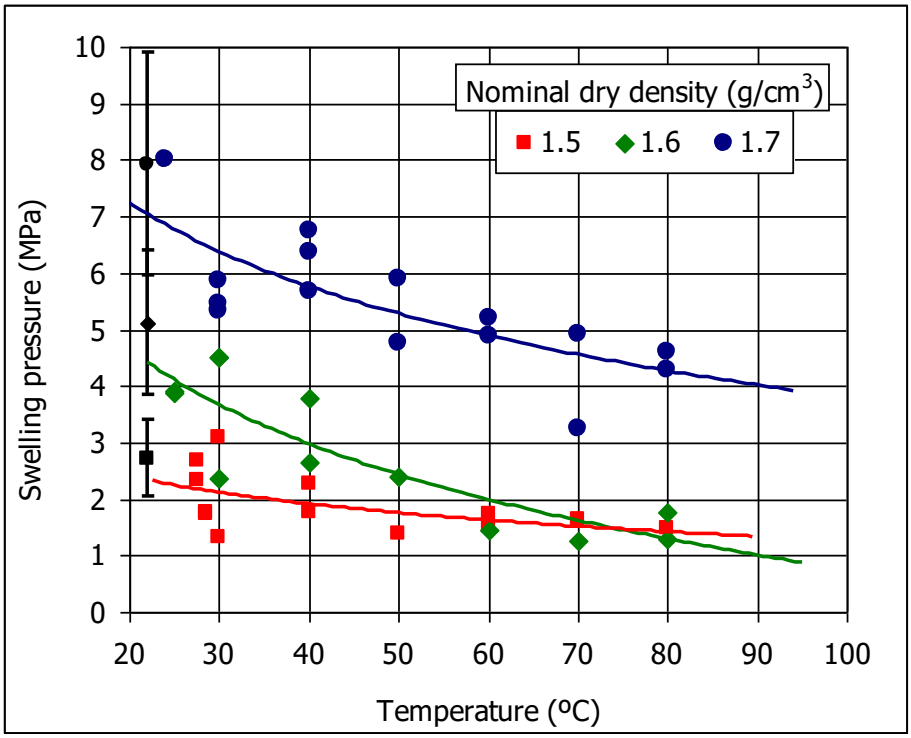

Figure 3-12. Swelling pressure as a function of temperature for saturated FEBEX clay compacted to different nominal dry densities (actual average dry densities were 1.48, 1.57 and 1.65 g/cm³) (Villar & Gómez-Espina 2009)

The thermal conductivity (λ, W/m·K) of the compacted bentonite at laboratory temperature is related to the degree of saturation (S_r) through the following expression:

$$\lambda = \frac{A_1 - A_2}{1 + e^{(S_r - x_0)/dx}} + A_2 \qquad [5]$$

where A_1 represents the value of λ for S_r=0, A_2 the value of λ for S_r=1, x_0 the degree of saturation for which thermal conductivity is the average of the two extreme values and *dx* is a parameter. This equation was chosen because it accurately represents the behaviour of conductivity versus water content (degree of saturation), which are directly related but not in a linear fashion (Villar 2002). The empirical fitting obtained, with r^2 of 0.923, gives the following values for each parameter:

A_1 = 0.57 ± 0.02

A_2 = 1.28 ± 0.03

x_0 = 0.65 ± 0.01

dx = 0.100 ± 0.016

3.1.3 BCV bentonite

Bentonite BCV is a typical Czech bentonite that formed via the in-situ alteration of Fe-rich tuffs and augite-biotite-type tuffites. The contribution of Fe to the system occurred as a consequence of the activity of the Krušnohorsko-ohárecká tectonic zone (Franče 1992). And, since Fe erosion did not take place during the argillisation phase, the smectites in these bentonites remained enriched with iron (especially in the octahedral positions). Moreover, the accessory minerals also contain a significant proportion of Fe, i.e. Fe carbonates and oxohydroxides.

The BCV material was first subjected to testing in 2017, and the various characteristics of the material were subsequently summarised in a report by Červinka et al. (2018). SÚRAO anticipates that this material will be subjected to further extensive testing in a number of upcoming research projects. It is already being tested in the EU BEACON and HotBent experiments and several other Czech projects.

BCV is produced industrially by Keramost Ltd at their Obrnice plant. The bentonite treatment process commences with the sieving of the coarse material employing a sieve with a 20x20 cm mesh. The bentonite is then homogenised in a wheeled mill from where it is transferred to a rotary oven where the material is dried (average temperature of 110°C) for 45 minutes. The drying process ensures a water content of around 10% and results in the preparation of the material for final milling and air sieving. The processing of the BCV material leads to a mixture where 1% of the total weight of the grains can be larger than 0.315 mm and at least 70% of the grains are smaller than 0.063 mm. The material is supplied in 48-kg bags, larger bags or tanks.

The montmorillonite content of BCV bentonite is between 58 and 72 wt.% (Červinka et al. 2018 and unpublished data TA ČR project: TK01030031 Inženýrská bariéra 200°C). In addition, the bentonite contains variable quantities of quartz (11 wt.%), calcite (4 wt.%), kaolinite (4 wt.%), illite (3 wt.%), goethite (3 wt.%), anatase (3 wt.%), ankerite and siderite (determined by means of the Rietveld method) (unpublished data TA ČR project: TK01030031 Inženýrská bariéra 200°C). Moreover, BCV bentonite is rich in amorphous phases, the content of which can be as high as 10 wt.% (Červinka et al. 2018).

The cation exchange capacity of BCV bentonite is 63.7±2.2 meq/100g and the major exchangeable cations are magnesium (42.0±0.6 meq/100g) and calcium (15.1±1.8 meq/100g).

The liquid limit of the bentonite is 140±2% and the density of the solid particles 2.76±0.02 g/cm^3. The total specific surface area of BCV bentonite (employing EGME) is 438±6 m^2/g.

The retention curves of the bentonite were determined for samples compacted to various dry densities employing a method which has been described by e.g. Villar (2007) and Večerník et al. (2014). The volume of the samples remained constant during the whole test due to their being confined in constant-volume cells. The samples were compacted directly into the cells, which had been equipped with relative humidity and temperature sensors. The retention curves for various dry densities (1.4, 1.6 and 1.8 g/cm^3) were evaluated at ambient temperature. No differences of gravimetric water content were observed between the samples compacted to different extents (Figure 3-13).

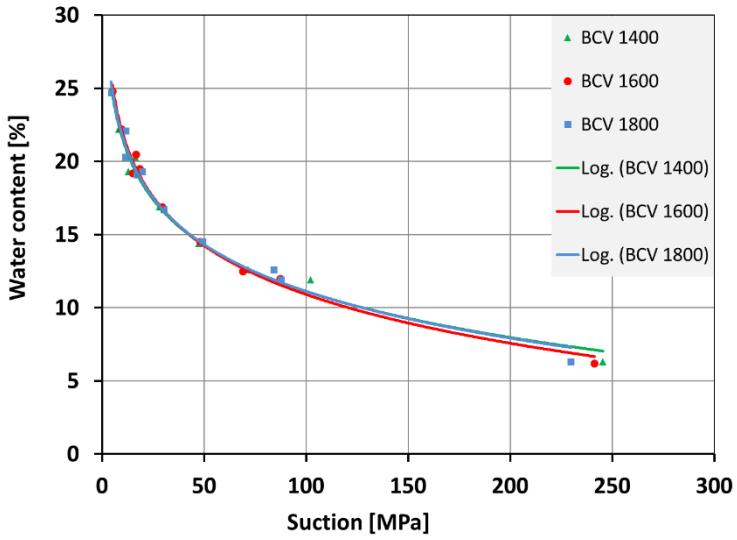

Figure 3-13. Retention curves (gravimetric water content related to suction) of compacted BCV bentonite samples with dry densities of around 1.4, 1.6 and 1.8 g/cm³ (data from Červinka et al. 2018)

The saturated hydraulic conductivity of compacted BCV bentonite samples decreases exponentially with the dry density (Figure 3-14, left). For a dry density of 1.6 g/cm^3, the saturated permeability of the bentonite is approximately $1.14 \cdot 10^{-13}$ m/s at room temperature with deionised water as the percolating fluid.

The swelling pressure of compacted samples is also related exponentially to the dry density of the bentonite (Figure 3-14, right). The material develops a swelling pressure of around 8 MPa when compacted at a dry density of 1.6 g/cm^3 and saturated with deionised water at room temperature.

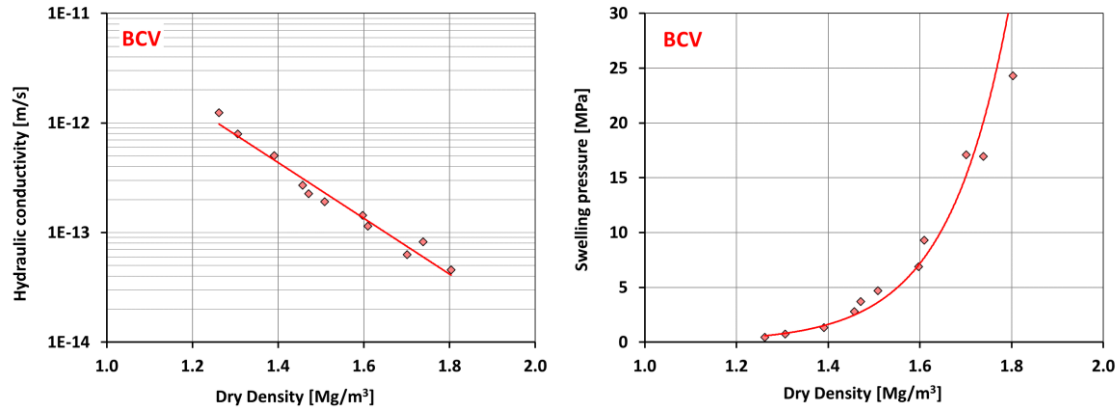

Figure 3-14. Saturated hydraulic conductivity (left) and swelling pressure (right) in relation to dry density - BCV bentonite (Hausmannová et al. 2018)

Figure 3-15 illustrates the thermal conductivity of BCV bentonite related to dry density for two different water contents (12% and 27%). Each point represents an average value for 6 measured values. At a dry density of 1.6 g/cm^3, the thermal conductivity was determined at around 0.6 W/m·K for the dry sample (w = 12%) and 1.4 W/m·K for the almost fully saturated sample.

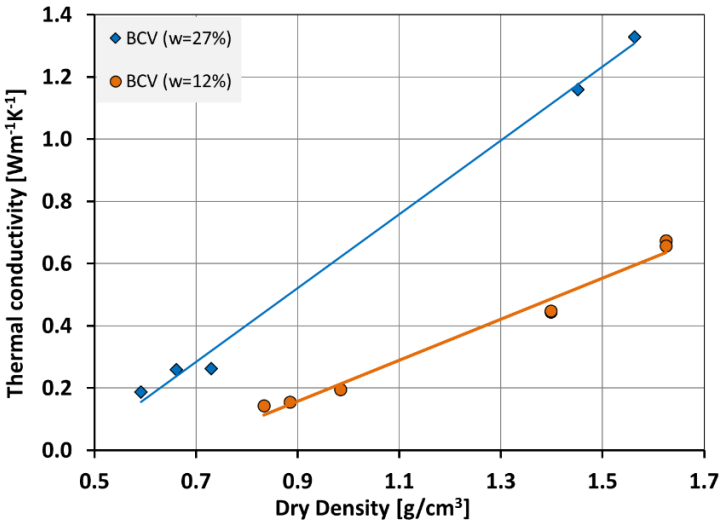

Figure 3-15. Thermal conductivity of BCV bentonite for a water content of 12% and 27% (data from Červinka et al. 2018)

3.1.4 DepCAN, Asha505, Calcigel

DepCAN, Asha505 and Calcigel are commercial names of bentonites included in the ABM (Alternative Buffer Material) experiment conducted by SKB at Äspö Hard Rock Laboratory (described in section 3.2.1). They are all high grade bentonites with smectite content of around 80 wt%, with high swelling pressures at high densities, and regarded as possible buffer or backfill candidates.

DepCAN is from Milos (Greece), and is a calcium dominated bentonite. The smectite is regarded as montmorillonite.

Asha505 is from Kutch (India), is sodium dominated and is high in iron (~13 wt% Fe_2O_3), hence its colour is brown. The smectite is regarded as montmorillonite/beidellite with somewhat higher charge.

Calcigel is a calcium Bavarian bentonite (Germany). The smectite is regarded as montmorillonite. The Calcigel bentonite often changes in colour in experiments, and there are indications that the smectite structural iron is more sensitive to redox reactions than most others of the bentonites studied.

The bentonites are described in further detail in Svensson et al. (2011).

3.1.5 Summary of identification properties

The following tables show summaries of the main properties of the buffer materials considered in HITEC. All of them have a high smectite content (>72%) and CEC (>64 meq/100 g), with sodium as main exchangeable cation in MX-80 and Asha505. The HM properties of bentonites and the effect of temperature on them depend, among others, on the type of cations in the interlayer. The use in the WP of bentonites with different exchangeable cations will allow to check this aspect.

Table 3-2. Mineralogy of the different buffer materials

Bentonite	MX-80[a]	FEBEX	BCV
Liquid limit (%)	450-550 (490)	102±4	140±2
Plastic limit (%)	46-70 (50)	53±3	
Grain density (g/cm^3)	2.76-2.82 (2.78)	2.70±0.04	2.76±0.02
Water content (%)	(12.3±0.1)	13.7±1.3	
Total specific surface area (m^2/g)	(624)	725	438±6

[a] in parenthesis: data for Posiva batches

Table 3-3. Mineralogy of the different buffer materials

Bentonite	MX-80[a]	FEBEX	BCV	DepCAN	Asha505	Calcigel
Smectite	88±3	92±4	72			
K-feldspars	2±2	Tr	-			
Quartz	4±0	2±1	11			
Cristobalite	Tr	2±1	-			
Calcite	Tr	1±1	4			
Pyrite	1±0		-			
Plagioclase	3±1	3±1	-			
Goethite	-	-	3			
Ankerite + siderite	-	-	1			
Illite	-	-	3			
Kaolinite	-	-	4			
Anatase	-	-	3			

[a] data for Posiva batches

Table 3-4. Exchangeable cations and CEC for the different buffer materials

Bentonite	Na^+	K^+	Mg^{2+}	Ca^{2+}	Σ cations	CEC
MX-80[a]	58	2	9	24	93	86
FEBEX	28	3	33	33	98	98
BCV	6.6±0.5	1.5±0.1	42.0±0.6	15.1 ±1.8	68±3	63.7±2.2
DepCAN	21	1.3	21.4	35	79	82
Asha505	62	0.4	12.3	19	94	89
Calcigel	2	1.2	12.1	52	68	66

[a] data for Posiva batches

Table 3-5. Chemical composition of the different buffer materials

Element (wt.%)	MX-80[a]	FEBEX	BCV	DepCAN	Asha505	Calcigel
SiO_2	61.55±0.29	57.89±1.55	47.86±0.68	52.01	46.48	54.67
Al_2O_3	20.55±0.25	17.95±0.71	14.11±0.03	17.54	20.64	17.54
MgO	2.53±0.01	4.21±0.21	2.60±0.03	3.11	2.01	3.37
Fe_2O_3	3.89±0.04	3.12±0.22	10.42±0.05	4.64	12.16	5.05
CaO	1.32±0.05	1.83±0.10	2.58±0.01	5.07	0.84	2.94
Na_2O	2.41±0.01	1.31±0.09	0.30±0.04	0.78	1.97	0.47
K_2O	0.78±0.02	1.04±0.05	0.92±0.02	0.90	0.14	1.16
TiO_2	0.17±0.00	0.23±0.01	2.12±0.01	0.71	1.01	0.41
MnO	2.53±0.01	0.04±0.00	0.18±0.00	0.07	0.05	0.03

Element (wt.%)	MX-80[a]	FEBEX	BCV	DepCAN	Asha505	Calcigel
SO_3	0.15±0.01	0.04	N.D.	N.D.	N.D.	N.D.
P_2O_5		0.03±0.01	0.48±0.01	0.143	0.091	0.096
LoI	6.26±0.01	13.8±2.6	N.D.	14.5	14.4	14.1

[a] data for Posiva batches

3.2 Relevant large-scale tests

Some large-scale tests performed in underground laboratories (Äspö in Sweden, Mont Terri and Grimsel in Switzerland) and also mock-ups are described in the following sections. In all of them a bentonite buffer was used and a heater(s) simulating the waste canister. In the in situ tests hydration was natural and in some cases with an additional artificial contribution. They have been selected because of the relevance of the temperatures on the heater surface (>100°C) or for the long duration, which is the case of the FEBEX in situ test. However, this is not an exhaustive compilation, and only those tests proposed by the contributors have been described in detail. For example, the Temperature Buffer Tests (TBT) ran in Äspö for seven years with a heater temperature of 140°C using MX-80 bentonite as buffer material (Äkesson et al. 2012).

3.2.1 Alternative Buffer Materials (ABM, Äspö)

The ABM test parcels expose different clay materials to conditions similar to a storage place and to adverse conditions with respect to temperature. The first ABM experiments (1-3) were installed in 2006 (Eng et al. 2007), and three additional ones were installed within the ABM45 project in 2012 (Sandén et al. 2018). Each of these parcels is a vertical borehole with a depth of 3.2-3.7 m and a diameter of 0.3 m excavated in the Äspö HRL. For the experiments in general the target temperature was 130°C (the only exception was ABM5), the heater was made of steel and different compacted bentonites were installed in direct contact with each other surrounding the central heater (Figure 3-16). The clays used are Asha 505, Calcigel, Callovo-Oxfordian (COx), IBECO, Deponit CA-N (Dep CAN), FEBEX, Friedland, Ikosorb Ca White, Ibeco Seal M-90, Kunigel VI, Wyoming bentonite MX-80 and Rokle. A water saturation system together with a sand filter allowed rapid water saturation. A summary of the characteristics of the tests performed is shown in Table 3-6.

ABM1 was excavated in 2009 (e.g. Svensson et al. 2011, Svensson and Hansen 2013) and ABM2 was excavated in 2013 (e.g. Svensson 2015). Upon dismantling these tests showed locally precipitates and iron corrosion products. The montmorillonites was typically fairly intact, with a minor formation of saponite. However, no impact on the buffer performance was found (Svensson 2015). The temperature in ABM5 was initially kept low at around 50°C (Figure 3-17), because it was impossible to get the water pressure to the target level. In 2016 the temperature was increased stepwise to very high temperatures of up to 250°C at the heater interface. ABM5 was excavated in 2017, and some blocks looked rather intact while others were highly fractured and very fragile due to the high temperature.

Table 3-6: Characteristics and duration of the ABM tests

Test	Duration	Characteristics
ABM1	28 months (2006-2009)	Artificial wetting
ABM2	6.5 years (2006-2013)	Artificial wetting for 2.5 years, heating to 141°C afterwards

Test	Duration	Characteristics
ABM3	(2006-present)	Artificial wetting
ABM4	(2012-present)	Artificial wetting
ABM5	5 years (2012-2017)	Temperature at 50°C until 2016, then gradually increased up to 250°C, artificial wetting
ABM6	(2012-present)	Artificial wetting

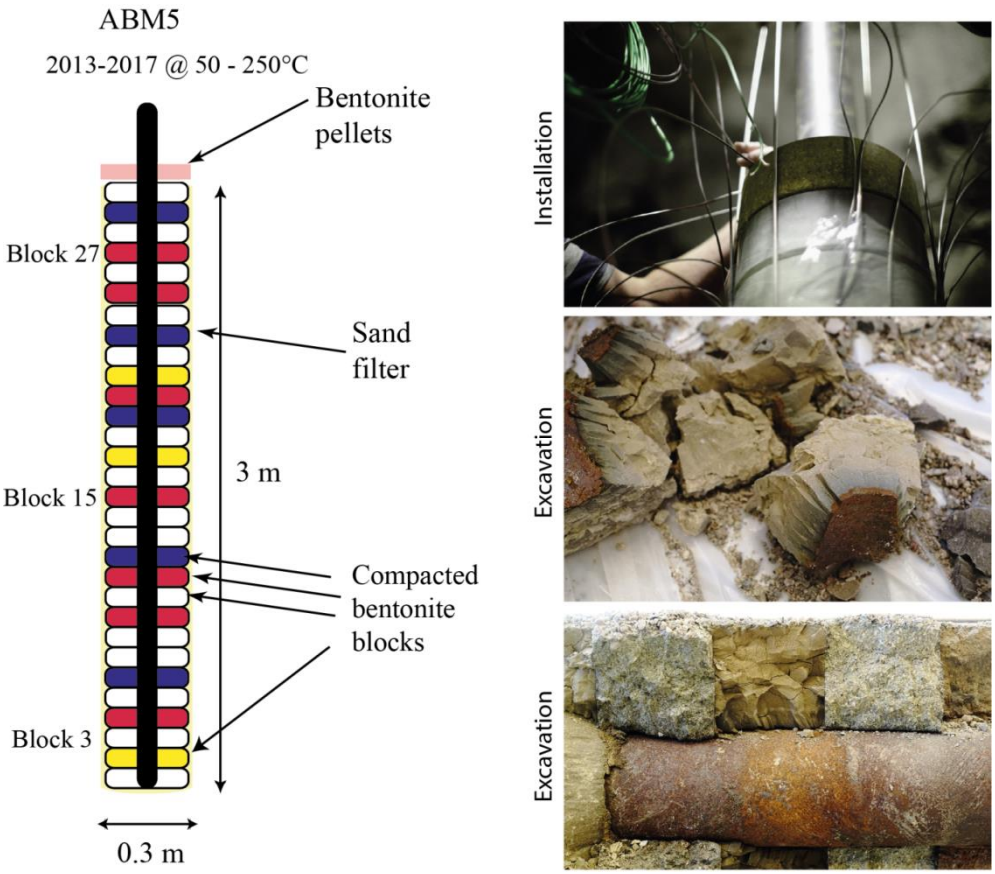

Figure 3-16. Schematic illustration of the ABM5 experiment and pictures from installation and excavation of the ABM5 experiment

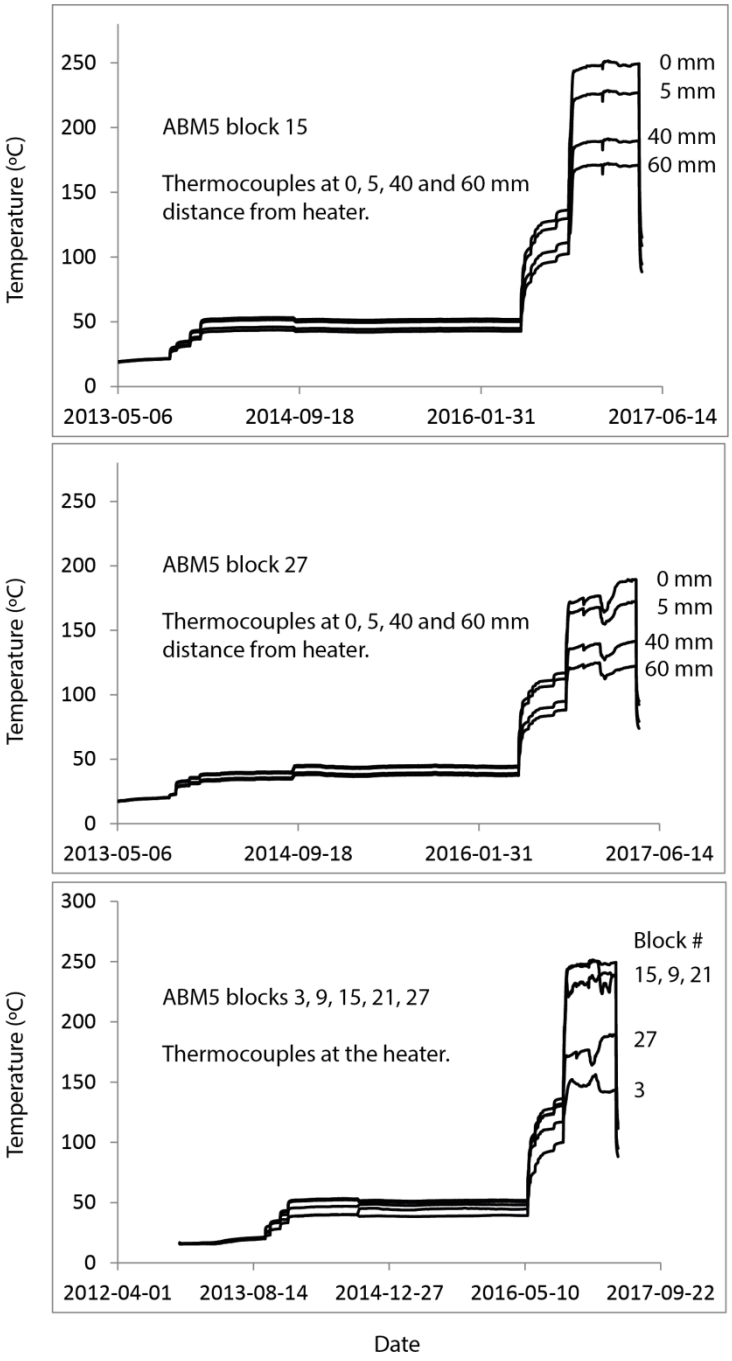

Figure 3-17. Overview of the thermal evolution of the ABM5 experiment

3.2.2 Long term test of buffer material (LOT, Äspö)

The LOT experiments were created mainly to study the long term stability of the bentonite, the mineral composition and the impact on important properties such as swelling pressure and hydraulic conductivity. The overall design of LOT is almost identical to the ABM experiment (Figure 3-16), however ABM uses many different bentonites and steel instead of copper. The LOT experiments (7 installed, 6 retrieved, Table 3-7) use copper heaters and Wyoming bentonite (MX-80) naturally saturated with groundwater, and run at 90°C (S-series) and 130°C (A-series). The copper heaters were not designed for corrosion studies; however, separate copper coupons were installed in the bentonite for that purpose. The LOT experiments are ~4 m high; 0.3 m in diameter and the central copper heaters

are 0.1 m in diameter. The reports of the uptake of the experimental packages A1 (adverse 130°C, 1 year), A2 (adverse 130°C, 6 years) and A0 (adverse 130°C, 1.5 year) are in SKB TR-09-31 and Karnland et al. 2000, 2009 and 2011), respectively. The LOT A2 is perhaps the most interesting of the already reported experiments.

The LOT S2 and A3 were excavated in September 2019, and so far little data are available. XRF data of block 15 in the A3 experiment showed two maxima of Ca and S (at the heater and also at about 20 mm from the heater; Figure 3-18). The elevated levels of Ca and S were attributed to local accumulation of anhydrite, visible in the XRD dataset (Figure 3-19). However, in the neighbour block 16, Ca and S only showed one maximum (Figure 3-18). The reason is currently not understood; however, most likely local variations in e.g. temperature, water saturation history or fractures in the rock possibly may give rise to minor local variations, demonstrating the importance of analysing several different profiles. Anhydrite accumulation was however expected, and has previously been seen in other field experiments. A minor increase in Mg was observed towards the heater (Figure 3-18), which was expected from earlier field experiments, however, no corresponding new phase was observed in the XRD data. Both the S2 and A3 packages are to be analysed in the coming years by SKB (not within HITEC) using geotechnical, chemical and mineralogical methods.

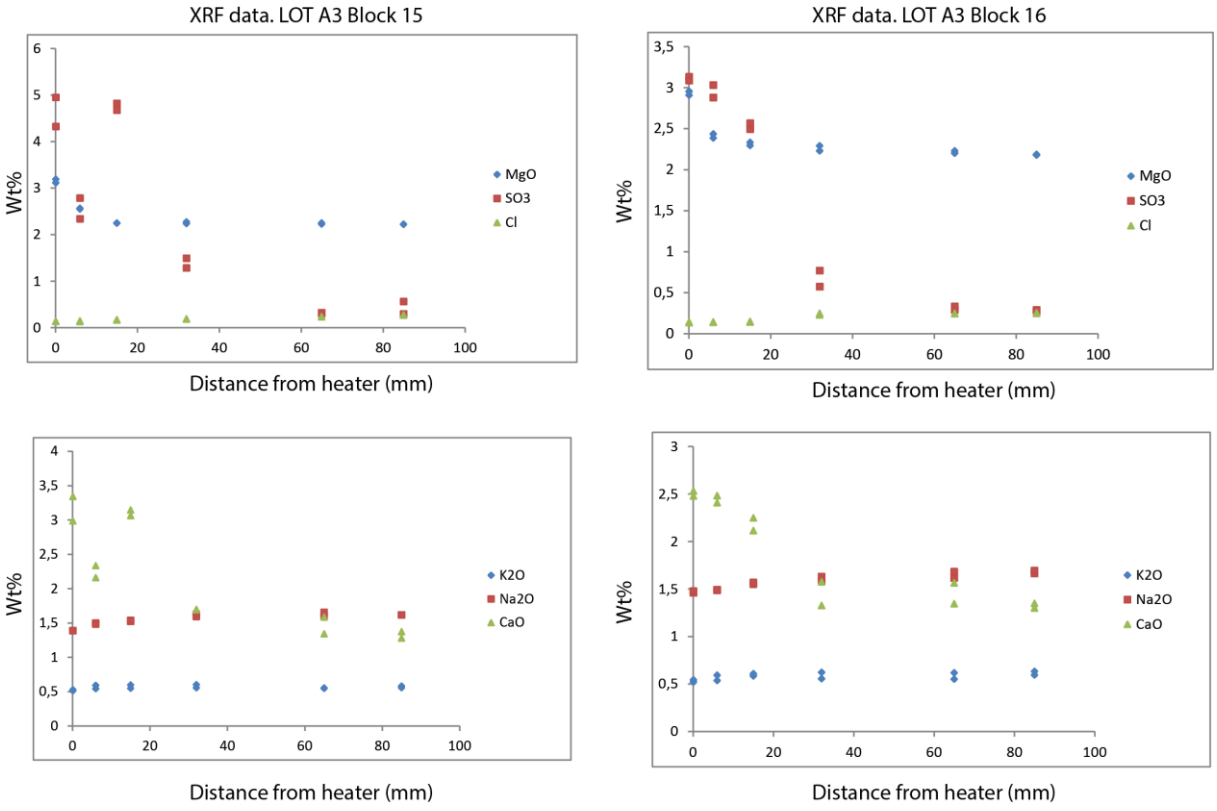

Figure 3-18. XRF data showing the distribution of the main elements in LOT A3 block 15-16

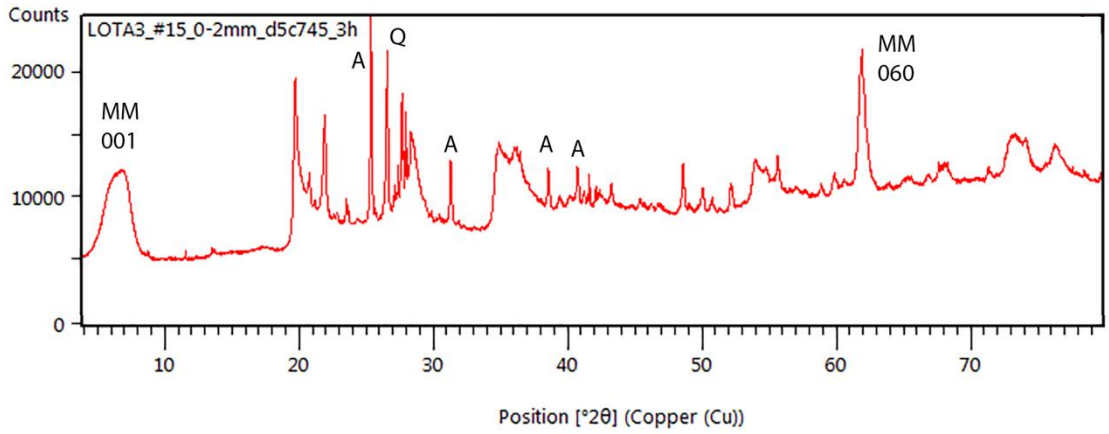

Figure 3-19. XRD data, 0-2 mm sample from the heater (LOT A3, block 15). MM = montmorillonite, A = anhydrite, Q = quartz

Table 3-7: Characteristics and duration of the LOT tests

Test	Duration	Characteristics
A0	1.5 year (1999-2001)	Heater temperature at 130°C
A1	1 year (1996-1998)	Heater temperature at 120 -150°C with a heater of 1000 W
A2	6 years (1999-2006)	Heater temperature at 120 -150°C
A3	~10 years (retrieved in 2019)	Heater temperature at 120 -150°C
S1	1 year (1996-1998)	Heater temperature at 90°C with a heater of 600 W
S2	~9 years (retrieved in 2019)	Heater temperature at 90°C
S3	>10 years (ongoing)	Heater temperature at 90°C

3.2.3 Heating Experiment Series (HE, Mont Terri)

A series of heater experiments, identified by the HE code, have been undertaken in the Mont Terri underground research laboratory (URL) with the broad aim of investigating the THM processes occurring in the Opalinus Clay and the bentonite buffer (NAGRA 2019). Those focused on the buffer are:

- In the HE-B Experiment (Göbel et al. 2007), a heater and bentonite buffer were installed in a vertical borehole. The buffer was artificially saturated, monitored for an 18-month heating period and then recovered.
- In the HE-E Experiment (Gaus (Ed.) 2011, Teodori & Gaus (Eds.) 2012) a 1:2-scale heating experiment was undertaken in a 50-m-long micro tunnel of 1.3-m diameter. The experiment considered the natural re-saturation of the bentonite buffer at a maximum heater surface temperature of 140°C.

3.2.3.1 HE-B Experiment

The HE-B Experiment was performed in a specially excavated niche in the shaly facies of the Opalinus Clay (Figure 3-20). Emplacement commenced in May 1999 and dismantling was complete in December 2003. The Experiment is summarised in Göbel et al. (2007). A central vertical borehole, 300 mm in diameter and 7.5 m long, was drilled in the niche floor. Heat-producing waste was simulated by a

heater element with a diameter of 10 cm. The 2-m-long heater element was placed in the borehole at a depth between 4 and 6 m. It was embedded in a barrier of ring-shaped compacted bentonite blocks (FEBEX bentonite) with an outer diameter of 280 mm and a dry density of 1.8 g/cm^3.

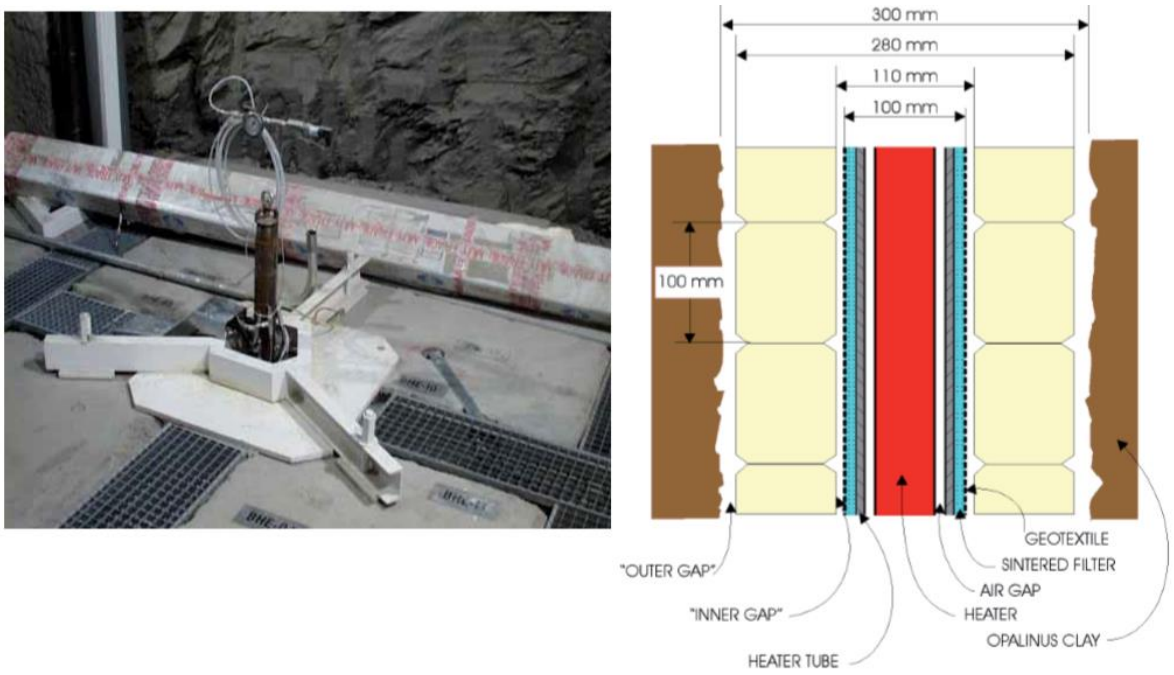

Figure 3-20. Photograph of the HE-B Experiment (left) and cross-section of the components (right) (Göbel et al. 2007)

The HE-B Experiment was artificially saturated over a 35-month period with synthetic water chemically similar to the water in the Opalinus Clay formation. During the 18-month heating period, the heater was automatically regulated to a constant temperature of 100°C at the contact between the heater and the bentonite buffer. During the heating phase, the power required to maintain the heater temperature at 100°C reduced. This was the result of drying in response to the heating, which led to a reduction in the thermal conductivity of the bentonite. Heating also led to release of hydrogen sulphide from the Opalinus Clay host rock (Jockwer et al. 2006).

Monitoring of the HE-B Experiment was complemented by a substantial laboratory programme for determining THM properties of the host rock and providing input data for most of the parameters needed to undertake THM modelling. A post-heating drilling campaign in the HE-niche provided samples for laboratory tests. The associated boreholes were used to acquire mechanical, hydraulic, and seismic data for comparison with the laboratory results. With regard to heat-induced changes in bentonite and Opalinus Clay, no conclusive answers could be found because temperatures were too low to cause any significant impact on the bentonite or Opalinus Clay over the timescale of the experiment. In addition, the temperature of the canister surface in the DGR is expected to exceed 100°C by several tens of degrees centigrade. However, insights into the buffer evolution were gained, providing important input in the planning of subsequent heating experiments:

- The volume increases on saturation ranged between 5 and 9%. A swelling pressure of the bentonite up to 2.8 MPa was reached within 6 days.
- The estimated saturation was slightly above 50% in all samples, indicating that full saturation of the bentonite was not reached.
- Modelling of the hydration phase demonstrated that the high initial suction of bentonite would result in partial desaturation of the surrounding rock, reaching a maximum at a radial distance of

0.7 m. Modelling also showed that the desaturation and subsequent re-saturation of the rock surrounding the borehole would complete within approximately 200 days.
- Modelling of the hydration of the bentonite predicted that swelling of the bentonite would result in elevated stress in the rock, with a maximum value of 14 MPa reached close to the rock-bentonite interface.

3.2.3.2 HE-E Experiment

The HE-E Experiment is a 1:2 scale heating experiment considering natural re-saturation of the EBS at a maximum heater surface temperature of 140°C. The experiment was constructed between December 2010 and June 2011. It was initially planned to operate until 2014, but operation has been extended and is on-going in December 2019. The experiment is conducted in a 50-m-long tunnel of 1.3 m diameter (Gaus et al. 2014). The test section of the micro-tunnel has a length of 10 m and was characterised in detail during a ventilation experiment which took place in the same test section (Mayor et al. 2007). The aims of the HE-E Experiment are focused on the early non-isothermal re-saturation period and its impact on the THM behaviour of the EBS, namely:

- to provide the experimental data required for the calibration and validation of existing THM models of the early re-saturation phase
- to upscale thermal conductivity of the partially saturated EBS from laboratory to field scale for pure bentonite and bentonite-sand mixtures

The experiment consists of two independently heated sections, each with a length of 4 m. The heaters were placed in a steel liner supported by MX-80 bentonite blocks with a dry density of 1.81 g/cm^3 and a water content of 10.3% (Figure 3-21). The dimensions and materials of the two sections were the same apart from the granular filling material: Section One was filled with a 65:35 granular mixture of sand and bentonite (Bentosund WH2), and Section Two was filled with pure MX-80 bentonite pellets. For the sand/bentonite mixture, the grain spectrum was 0.5-1.8 mm, the water content was 13% for the bentonite and 0.05% for the sand (giving a total water content of the mixture of approximately 4%) and a dry density of 1.38 g/cm^3 (and an emplaced dry density of 1.48-1.50 g/cm^3). The pellets were the same as used for the ESDRED emplacement test. Use of two types of granular filling material allowed comparison of the THM behaviour of the two EBS materials under almost identical conditions.

The heating started in June 2011, and the maximum temperature was reached in June 2012. Since then, the temperature has been held constant. The results from the HE-E to date have been consistent with the previous heater experiments conducted in Mont Terri and have allowed further development of the capability to predict the early-stage performance of the EBS and near-field rock. The EBS is characterised by a high temperature gradient owing to its low thermal conductivity in response to drying from the introduction of the heaters. By December 2013 the temperature at the interface of the Opalinus Clay and the EBS was less than 50°C. The highest temperatures measured in the experiment (>100°C) occur where the EBS water content is low (<20% relative humidity). Re-saturation of the Opalinus Clay has been slowly progressing with the hydraulic pressure front (the location where hydraulic pressure is registered) being situated farther than 1 m from the Opalinus Clay/EBS interface. An overpressure of 1 MPa has developed in the Opalinus Clay as a result of differential thermal expansion of the rock and the pore water.

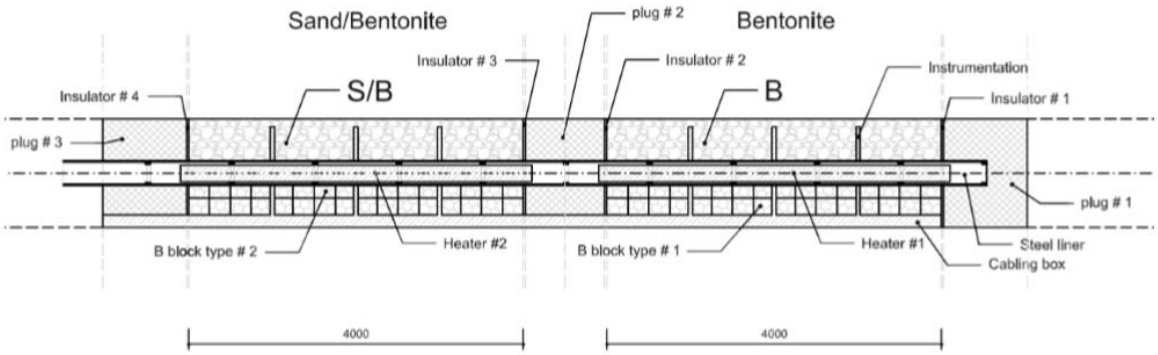

Figure 3-21. Schematic layout of the HE-E experiment showing the section in the back of the tunnel filled with bentonite pellets and the section in the front of the tunnel filled with sand/bentonite

3.2.4 Full-Scale Emplacement experiment (FE, Mont Terri)

The main aim of the FE experiment is the investigation of SF/HLW repository-induced THM coupled effects on the host rock at this scale and the validation of existing coupled THM models (NAGRA 2019). Further experimental aims are 1) the verification of the technical feasibility of constructing a disposal tunnel using standard industrial equipment, 2) the optimisation of the bentonite buffer material production and 3) the investigation of (horizontal) canister and bentonite buffer emplacement procedures for underground conditions.

The layout of the FE experiment was designed to simulate the Swiss repository concept for SF/HLW conditions in one single tunnel at the Mont Terri URL (Müller et al. 2015, Figure 3-22). First, a 50-m long experimental tunnel was constructed. At the deep end of the FE tunnel an ISS (interjacent sealing section) was built using only steel arches for rock support, while the rest of the tunnel is supported by shotcrete. A 'bentonite block wall' was erected manually in a section of the ISS. In the FE tunnel, 3 heaters with dimensions similar to those of waste canisters were emplaced on top of 'bentonite block pedestals'. The first heater emplaced at the deep end of the FE tunnel was named H1, the middle one H2 and the most 'shallow' heater (close to the plug) H3. The remaining space was backfilled with a highly compacted 'granulated bentonite mixture' (GBM). For the purpose of backfilling the GBM as densely and homogeneously into a horizontal tunnel as possible, a prototype 'backfilling machine' with 5 screw conveyors was developed. Finally, the experiment was sealed off (towards the FE cavern) with a concrete plug holding the bentonite buffer in place and reducing air and water fluxes. The heating phase started in December 2014, with the heaters surface temperature at values between 120 and 130°C, although it is expected they eventually reach 130-150°C at the surface of the middle heater and approximately 60-80°C at the rock interface.

Even though in the case of the FE-Experiment the swelling potential of the bentonite does not apply directly to the FE as full saturation is not likely to happen within the 10-15 years planned for the experiments duration, the emplaced material had to comply with the safety related requirements (Leupin & Johnson 2013). The reason for this is that in the FE the focus was set on the THM behaviour of the buffer, which should be as close as possible to the one expected for real disposal conditions.

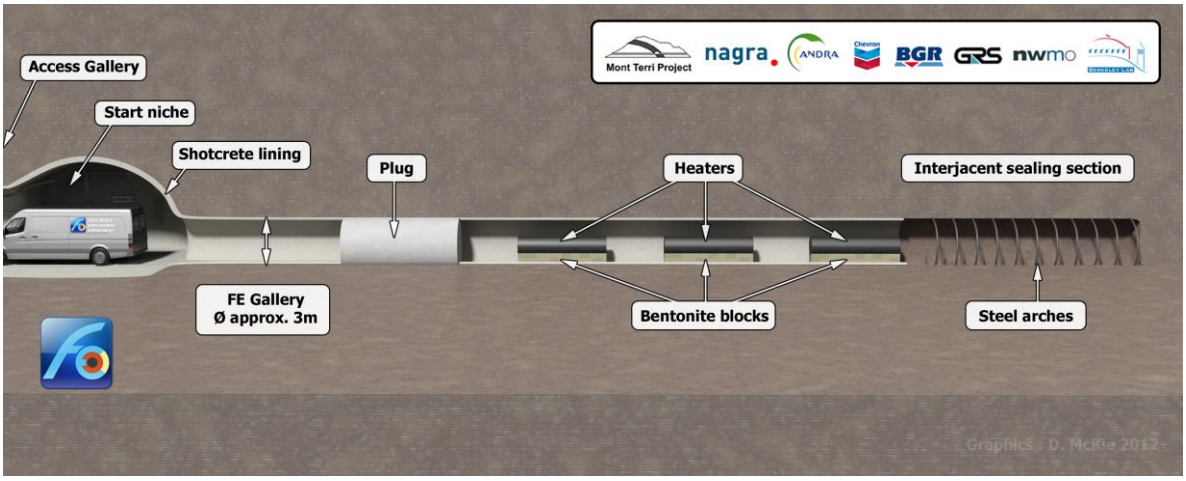

Figure 3-22. Layout of the FE test

A full description and location of the sensors is given in Nagra (2019) and a summary of the instrumentation aspects can be found in 4.2.3.2.

In the context of the FE experiment, several modelling exercises have been carried out (e.g. Ewing & Senger 2011, Senger 2015, Garitte et al. 2014). A set of scoping calculations aimed at bracketing the main parameters and independent variables associated with the FE experiment (e.g. temperature at the different components, pore water pressure and strain in OPA, etc.) was carried out by Ewing & Senger (2011). Such exercise supported the design of the FE experiment and its monitoring system. Second, a calibration and validation exercise, which included uncertainty analysis was carried out by different modelling teams. These modelling exercises are summarized in subchapters 4.4.4.3 and 4.4.4.4.

The experience and data from previous experiments, especially HE-E, were used to develop scoping estimates of key parameters and variables of the FE experiment, including 1) the evolution of temperature on the heater surface, in the bentonite and in the Opalinus Clay, 2) the degree of saturation and relative humidity in the bentonite and Opalinus Clay, 3) the pore water pressure in the Opalinus Clay, and 4) the strain in the Opalinus Clay.

3.2.5 FEBEX in situ test (Grimsel)

The aim of the project was to study the behaviour of near-field components in a repository for high-level radioactive waste in granite formations. The main objectives of the project may be grouped in two areas:

- Demonstration of the feasibility of constructing the engineered barrier system in a horizontal configuration according to the Spanish concept for deep geological storage (AGP), and analysis of the technical problems to be solved for this type of disposal method.
- Better understanding of the thermo-hydro-mechanical (THM) and thermo-hydro-geochemical (THG) processes in the near field, and development and validation of the modelling tools required for interpretation and prediction of the evolution of such processes.

As part of the FEBEX project, an “in situ” test, under natural conditions and at full scale, was performed at the Grimsel Test Site (GTS, Switzerland), an underground laboratory managed by NAGRA (ENRESA 2006). The thermal effect of the wastes was simulated by means of heaters, whereas hydration was natural. The test was monitored, this allowing the evolution of the temperature, total pressure, water content, water pressure, displacements and other parameters to be obtained continuously in different

parts of the barrier and the host rock, this information being used as a contrast to the predictions of the THM and THC models.

The basic components of the test (Figure 3-23) were: the gallery, measuring 70 m in length and 2.3 m in diameter, excavated through the Aare granite; the heating system, made up of two heaters placed inside a liner installed concentrically with the gallery and separated one from the other by a distance of 1.0 m, with dimensions and weights analogous to those of the real canisters; the clay barrier, formed by blocks of compacted bentonite; the instrumentation and the monitoring and control system for data acquisition and supervision and control of the test both autonomously and remotely from Madrid. Up to 632 sensors of very diverse types were initially installed to monitor the different THM processes that occurred in both the clay barrier and the surrounding rock throughout the entire life of the test. The gallery was closed by a concrete plug.

The clay barrier was made of FEBEX bentonite, which was extracted from the Cortijo de Archidona deposit (Almería, Spain). The physico-chemical properties of the FEBEX bentonite, as well as its most relevant thermo-hydro-mechanical and geochemical characteristics are summarised in section 3.1.1. To build the clay barrier, various types of blocks were manufactured from the bentonite in the shape of 12-cm thick circular crown sectors. The blocks were arranged in vertical slices with three concentric rings. In the heater areas the interior ring was in contact with the steel liner, whereas in the non-heater areas a core of bentonite blocks replaced the heaters. The thickness of the bentonite barrier in the heater areas was 65 cm (distance from liner to granite). The blocks were obtained by uniaxial compaction of the FEBEX clay with its hygroscopic water content at pressures of between 40 and 45 MPa, what gave place to dry densities of 1.69-1.70 g/cm^3. The initial dry density of the blocks was selected by taking into account the probable volume of the construction gaps and the need to have a barrier with an average dry density of 1.60 g/cm^3.

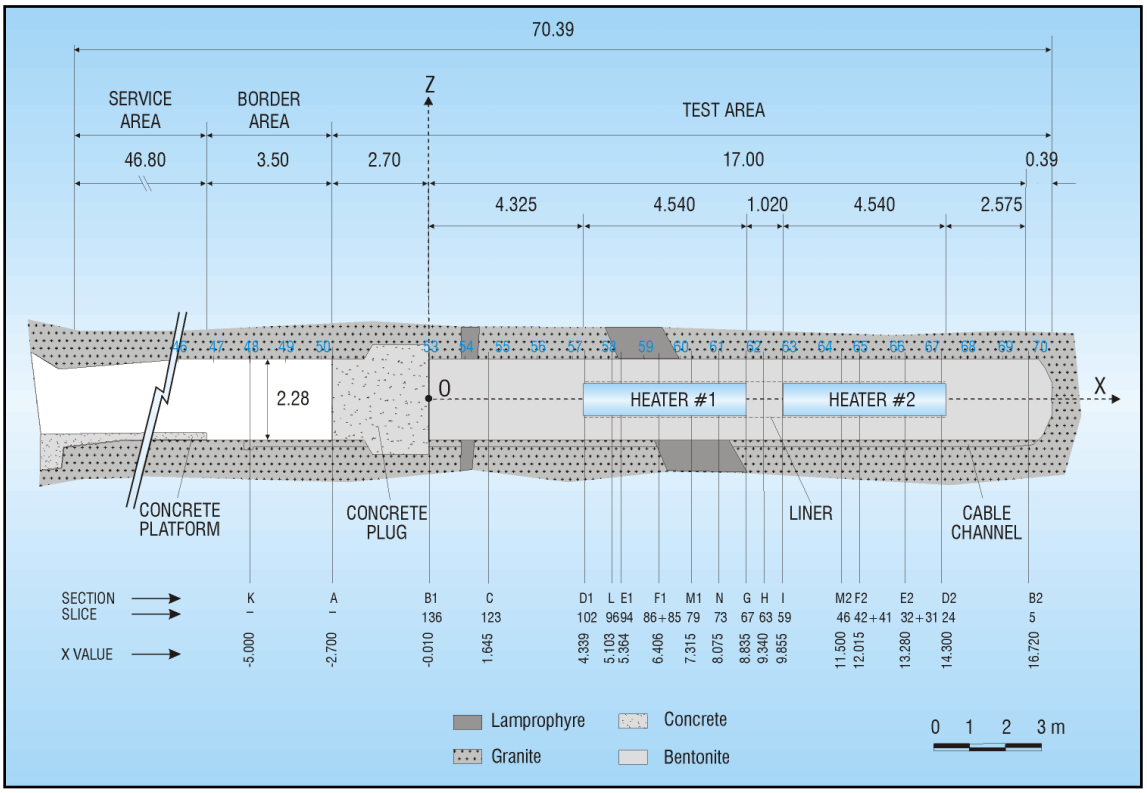

Figure 3-23. General layout of the FEBEX in situ test during phase I, including instrumented sections (ENRESA, 2000)

The heating stage of the in situ test began on February 27th 1997. The power of the heaters was adjusted so that to keep the temperatures at their surfaces at 100°C. After five years of uninterrupted heating at constant temperature, the heater closer to the gallery entrance (heater #1) was switched off (February 2002). In the following months this heater and all the bentonite and instruments preceding and surrounding it were extracted. A large number of bentonite samples were also taken for analysis in different laboratories. The remaining part of the experiment was sealed with a new sprayed concrete plug. New sensors were installed in the buffer through the concrete plug, and a second operational phase started. The test continued running until April 2015, when heater #2 was switched off. The concrete plug started to be demolished some days earlier, and the buffer removal and sampling took place between May and August. A detailed postmortem bentonite sampling program was designed. Clay samples were taken to characterise the solid and liquid phases, in order to confirm predictions and validate existing models of THM and THG processes. In particular, samples were taken to determine on site their water content and dry density, with the aim of assessing the final state of the barrier and supply data to validate and check the capacity of the THM numerical codes to predict the bentonite evolution in an engineered barrier.

The FEBEX-DP investigations undertaken by several laboratories confirmed the good performance and stability of the bentonite barrier over a time period of 18 years (Villar 2018). As it was observed during the partial dismantling in 2002, the swelling capacity of the bentonite was able to fill all the construction gaps after a further 13 years. It provided a continuous barrier, in which, once saturated, the interfaces between blocks did not have any role on the water content and density distribution or fluid transport. The physical state of the barrier after 18 years of operation was very much affected by the processes to which it had been subjected, namely hydration from the granite and/or thermal gradient-induced moisture redistribution.

The water content and dry density in every section followed a radial distribution around the axis of the gallery, with the water content decreasing from the granite towards the axis of the gallery and the dry density following the inverse pattern. The main changes in the period from 2002 to 2015 took place in the internal part of the barrier, its core. This was particularly so around the heaters: the water content and dry density gradients from the granite inwards were steeper in the hot sections than in the cold sections, and despite the overall increase in water content during the further 13 years of operation, the water content gradients did not wane, although they attenuated. The water content at all points in the barrier, even those close to the heater, was higher than the initial one (14%).

Within the accuracy limits of the techniques used no relevant changes were observed in the mineralogy of the bentonite, its physico-chemical and surface properties, water adsorption capacity or montmorillonite crystal-chemistry. Because of the inwards groundwater movement and the thermal gradient caused by the heater, changes in the pore water chemistry and the cation exchange complex were observed. The thermal, hydraulic and mechanical properties analysed were consistent with the range expected for the reference bentonite, although because of the dry density gradients generated in the barrier, these properties were not homogeneous across the barrier.

For further information see Bárcena et al. (2006), ENRESA (2006), Martínez et al. (2016), Villar (2006, 2017), Villar et al. (2016a).

3.2.6 Mock-Up Josef experiment

The description of the Mock-Up Josef is taken from EU BEACON project. The Mock-Up Josef project is the first in-situ experiment to simulate a vertical storage container surrounded by a bentonite barrier in a real natural environment made up of granitoid rocks to be conducted in the Czech Republic. The bentonite barrier in the experiment is exposed to the effects of groundwater and, simultaneously, thermal load is provided by a heating element simulating the emission of heat from spent nuclear fuel contained in a storage cask. The main objective is to study the behaviour of the bentonite barrier under

repository conditions with concern to temperature development, hydration and changes in the various geotechnical and geochemical/mineralogical parameters (by means of sampling).

The Mock-Up Josef experiment was built in the form of a supercontainer (Figure 3-24) and consists of:

- Bentonite barrier: A total of around 280 bentonite segments each with a height of 67 mm in 33 layers. The gap between the blocks and the heater (27.5 mm) was filled with powdered bentonite and crushed blocks. The gap between the blocks and the stainless-steel mesh was filled with powdered bentonite and crushed blocks (10 mm) and the gap between the stainless-steel mesh and the rock (15 mm±10 mm) was filled to approx. 30% with silica sand. The bentonite used in the experiment is called B75 which is a Czech Ca-Mg bentonite (similar properties to BCV bentonite).
- Heater: the heater consists of a hollow high-grade steel cylinder with a diameter of 320 mm and a height of 1300 mm. The heater was covered with copper sheeting and positioned during model construction upon the sixth layer of bentonite blocks. Oil is used as the heat-transferring medium and heat is provided by two 2000 W heating spirals installed inside the cylinder.
- Temperature of the heating medium: 100°C (surface of the heater 90°C)
- Instrumentation: 105 sensors were installed inside the bentonite body (65 thermometers, 37 hydraulic pressure cells and 3 relative humidity sensors) in 5 measuring profiles. Temperature sensors were also installed in the host rock. Data are collected at 10-minute intervals and is accessible online in both raw and graph forms. The data obtained provides immediate information on the behavior of the bentonite layer.
- Permanent construction elements employed to facilitate construction and transport: expanded metal casing, steel base and lid.

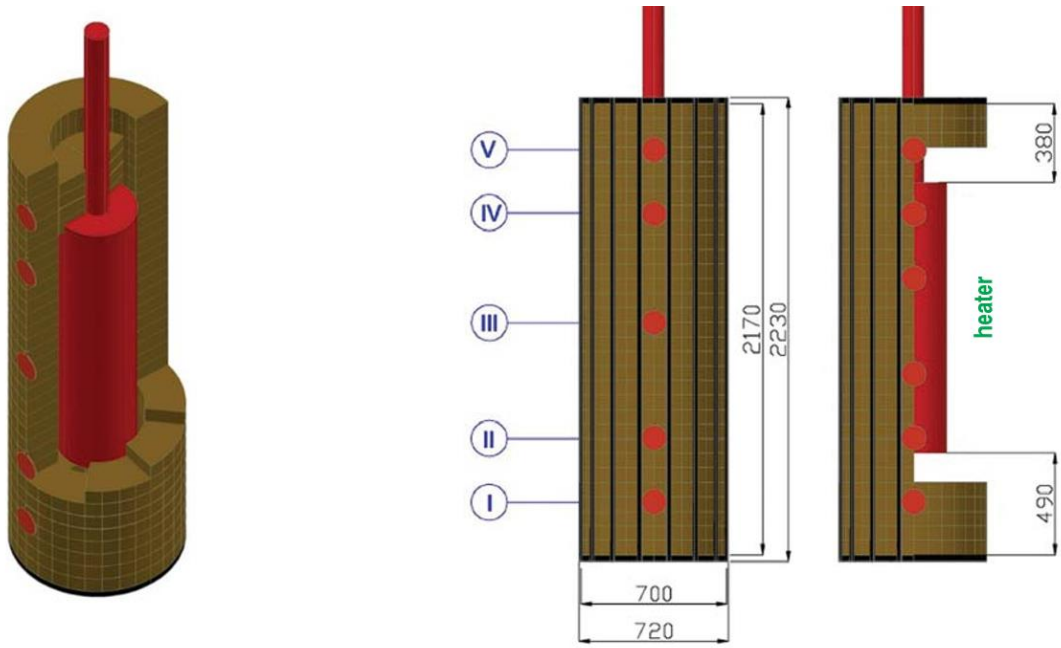

Figure 3-24. Scheme of the Mock-Up Josef experiment indicating the profiles monitored (I - V), adapted from Šťástka (2014)

In addition to the monitoring system, the sampling of the bentonite barrier is performed every half year to provide an indication of changes in the bentonite material and the rate of saturation. The samples are obtained by means of drilling vertically through the steel lid. The samples help to provide

a description of the saturation state of the bentonite via the evaluation of water content and density (Figure 3-25). In addition, the samples are studied for indications of mineralogical, hydraulic conductivity and swelling pressure changes brought about by heating and saturation.

The red circles in Figure 3-25 reveal the results from the first sampling procedure (at 1st location) after 11 months - depth 320 mm (2 mineralogical samples taken from depths of 15 mm and 297 mm). The black squares show the first sampling (2nd location) after 16 months - depth 640 mm (4 mineralogical samples taken from depths of 75 mm, 242 mm, 277 mm and 580 mm). The light red circles represent the second sampling procedure from 1st location after 30 months - depth 660 mm (4 mineralogical samples obtained from depths of 160 mm, 340 mm, 480 mm and 590 mm). The dark grey squares show the results from the second sampling procedure (2nd location) after 43 months - depth 690 mm (3 mineralogical samples were obtained from depths of 15 mm, 270 mm and 680 mm). The light grey squares show the results from the third sampling session (2nd location) after 47 months - depth 960 mm (2 mineralogical samples were taken from depths of 840 mm and 950 mm). The green line shows the level of the top of the heater (480 mm).

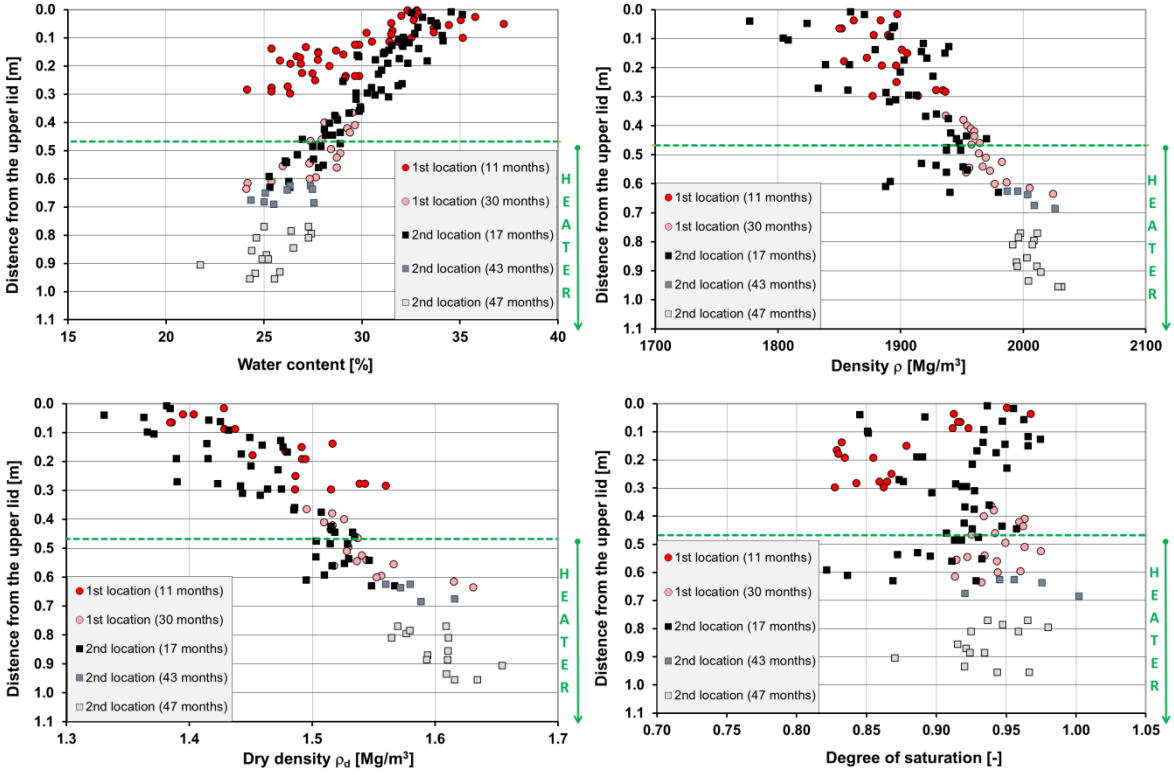

Figure 3-25. Water content, density, dry density and degree of saturation results obtained by sampling

3.2.7 Ophelie mock-up

The OPHELIE mock-up simulated (full-scale with respect to the diameter, and with a length of 5 m) a section of a disposal gallery of the SAFIR-2 reference design (valid in the 90s) as far as the buffer material and the disposal tube were concerned. The initial objective of the mock-up was to verify some practical aspects like the robustness and performance of the sensors in harsh conditions over a period of several years, the specification, manufacture and placement procedures for the buffer material and the hydration process for this material (Van Humbeeck et al. 2009). The mock-up also served as a preliminary investigation into the buffer material's thermo-hydro-mechanical behaviour and an

observation of its evolution, during and after 4.5 years (1997-2002) of hydration and heating, through the monitoring and post-mortem analysis programme.

The mock-up's metallic structure was composed of a main jacket, two covers and the central tube simulating the disposal tube (Figure 3-26). The hydration system was fixed at 1 MPa to saturate the buffer. The buffer material consisted of pre-fabricated blocks of a mixture of 60% FoCa clay, 35% sand and 5% graphite uniaxially compacted at 61 MPa. A complete buffer section consisted of three concentric rings. A concrete ring was installed at the end of the mock-up to test the behaviour of measuring instruments.

The operational stage of the mock-up consisted of the following phases: hydration at ambient temperature, heating with continuing hydration and cooling phase. The heating phase, at 170°C, started six months after the start of hydration (when the buffer was mostly saturated and a high thermal conductivity was measured) and lasted 4.5 years. The mock-up was then cooled down rapidly by switching off all heating elements six weeks before dismantling began.

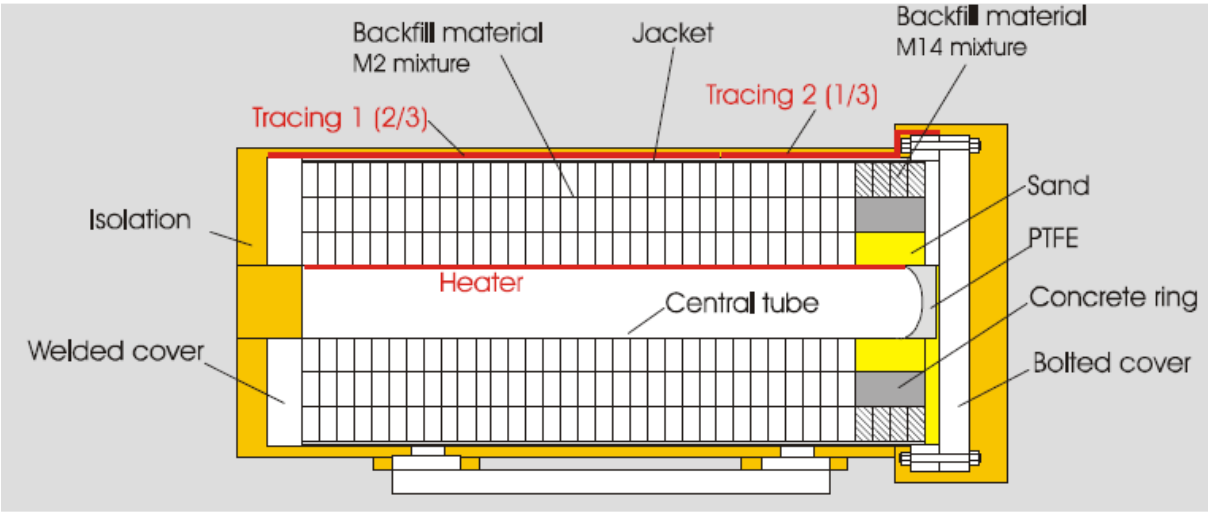

Figure 3-26. Schematic design of the Ophelie mock-up

Mineralogical changes observed on the exposed buffer material after 4.5 years of hydration and heating were very limited. The main modifications concerned the presence of gypsum where the buffer made contact with the central tube, at the interface with the stainless steel liner at the periphery and in the joints between blocks. An enrichment of chemical species towards the central tube (chlorides…) was identified, combined with an impoverishment of chemical species like bicarbonate or sulphate towards the tube.

Overall, from a thermo-hydro-mechanical point of view, the buffer material fulfilled its role: it retained a low hydraulic conductivity/permeability and a high thermal conductivity. However, the hydraulic conductivity of the exposed material was slightly higher that for the initial material. All physical gaps were filled by swelling. However, the swelling process was not homogeneous. The swelling mainly occurred close to the liner and the joints between blocks, although closed, remained visible.

3.2.8 Summary

A summary of the main characteristics of the large-scale tests presented in the previous subchapeters is given in Table 3-8. Different host rocks, buffers, spatial configurations and temperatures are represented. Except for the FEBEX in situ and the JOSEPH mock-up, the temperatures are relevant for HITEC. Some of the tests have already being dismantled (some parcels of the ABM and LOT tests, FEBEX

and OPHELIE), and information on the postmortem state and modification of properties is available. The others are still running and providing online information.

Table 3-8. Summary of relevant large-scale tests characteristics

Test	Host Rock	Duration	Characteristics	Temperature	Buffer
ABM SKB	Granite (Äspö)	1, 3, 5 years	Reduced scale, vertical pit	130°C (250°C)	11 different clays[a]
LOT SKB	Granite (Äspö)	1, 6, (20) years	Reduced scale, vertical pit	Up to 130°C	MX-80 (Na bentonite)
HE-E NAGRA	Opalinus (Mont Terri)	>8 years	Reduced scale, gallery	140°C	Sand/MX80 mixture MX80 pellets
FE NAGRA	Opalinus (Mont Terri)	>5 years	Real scale, gallery	140°C	MX80 blocks MX80 pellets
FEBEX CIEMAT	Granite (Grimsel)	5, 18 years	Real scale, gallery	100°C	FEBEX (Ca-Mg bentonite)
JOSEPH SÚRAO	Mock-up (CZ)	>7 years	Reduced scale, vertical	90-100°C	B75 (Ca-Mg bentonite)
Ophelie	Mock-up (BE)	4.5 years	1:1 scale	170°C	FoCa/sand/graphite (60/35/5)

[a] see section 3.2.1 for details

3.3 Effect of high temperature on buffer: test procedures and results

The study of the effect of temperature on bentonite properties can be tackled either by analysing the change of properties of preheated material or the properties of the bentonite at high temperatures. Both cases are dealt with in Task 3.1 of HITEC because they are complementary. In the first instance the material can be heated in the laboratory (usually in powder form) or come from the dismantling of a TH cell (section 3.3.3) or an in situ test (section 3.2), where samples for postmortem analysis are obtained. The properties of these preheated materials are usually tested at laboratory temperature and compared with those obtained in non-heated material to assess the changes during operation. In contrast, the aim of the THM tests that are performed in non-treated material at high temperature is to determine the parameters that define the behaviour of the buffer while in operation, i.e. under high temperature.

The following subsections summarise results obtained for all the cases mentioned in the previous paragraph. Most of the information has been gathered by the agencies, but some relevant information has also been taken from literature.

Safe Barriers was a project which ran from 2012 until 2016 led by Strathclyde University, and explored several research areas through eight work packages at different UK institutions. The project objectives were to deploy and refine advanced monitoring techniques for THM-C imaging of clay barrier systems, and to integrate these methods into an experimental programme to understand the evolution of clay barriers under strong thermal gradients, at temperatures of up to 150°C. A summary of the outputs of

this research project was provided by RWM (2017), with specific details of outputs relevant to HITEC included in the following subchapters.

3.3.1 Mineralogical/geochemical changes

Montmorillonite mineralogical stability in high temperatures has been studied in Leupin et al. (2014). The report contains literature review of montmorillonite stability in high temperature and reviews several different kinds of high-temperature experimens:

- smectite-to-illite hydrothermal experiments with MX-80 bentonite at temperature of 270°C that reveal no evidence of any illitisation even with variable postassium activity conditions;
- experiments on thermal stability of montmorillonite at 90-150°C, showing montmorillonite dissolving and releasing silica, altering the montmorillonite towads beidellite;
- experiments on the effect of steam on the swelling capacity of bentonite at temperatures up to 200°C showing that high-temperature water vapour and unsaturated conditions do not cause significant reduction of the water uptake capacity of montmorillonite.

The tests by Valter & Plötze (2013), with MX-80 bentonite with different degrees of saturation stored at different temperatures in a closed system, showed a high mineralogical stability but considerable changes in physicochemical properties, particularly above the critical temperature of 120°C. The cation exchange capacity decreased during heating at 150°C by approximately 10%. The specific surface area dropped by more than 50%. The water vapour adsorption ability dropped by 25% already within three months at 120°C. These changes were mostly related to the variations in the interlayer cation composition (a slight conversion from the sodium to an earthalkali form of the bentonite) and to smectite aggregation processes.

An RWM funded research project (PhD) at the University of Bristol between 2015 and 2019 explored alteration of bentonites at the interface between the bentonite and the container surface in mock-up experiments. The research focussed upon in-situ experiments at Grimsel (FEBEX, section 3.2.5) and Äspö (ABM, section 3.2.1) underground research laboratories, in addition to conducting laboratory scale bentonite-metal interface interaction experiments. Leal Olloqui (2019), conducted the study on a sample which was in contact with the container of the FEBEX in situ test (section 3.2.5). Figure 3-27 shows the bulk sample and sub-sampling sections used for analysis. According to the data presented, the clay adjacent to the steel heater presented excess Fe^{2+} either as Fe^{2+} sorbed on the clay or as structural Fe^{2+} inside the clay. No other indications of clay transformation or newly formed clay phases were found. The processes at the bentonite/metal interface are dealt in detail in EURAD-ACED.

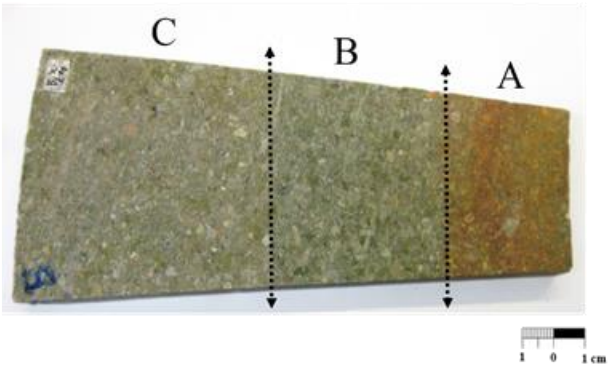

Figure 3-27. FEBEX samples analysed by Leal Olloqui (2019). Note colour change in proximity to container surface on right hand side of sample

The final report of the FEBEX-DP project about the post-mortem analysis of the bentonite submitted to temperatures below 100°C concluded that, within the accuracy limits of the techniques used, no

relevant changes were observed in the mineralogy, physico-chemical and surface properties, water adsorption capacity or montmorillonite crystal-chemistry, although because of the inwards groundwater movement and the thermal gradient caused by the heater, changes in the pore water chemistry and the cation exchange complex were observed (Villar 2017).

In the SKB field experiments at Äspö using various bentonites, at least the following processes were identified:

- Stiffening of the buffer (MX80, LOT, Karnland et al. 2009).
- Accumulation of non exchangeable magnesium towards the heater (LOT, ABM, Prototype, e.g. Karnland et al. 2009, Olsson et al. 2013, Svensson 2015).
- Dissolution of cristobalite close to the heater (e.g. Svensson & Hansen, 2013).
- Formation of oxygen-sensitive Fe(II) phases at steel/bentonite interface (Svensson & Hansen, 2013).
- Formation of ferrosaponite/saponite in ABM2 with FEBEX bentonite (associated with a high increase in Mg, Svensson 2015).
- Accumulation of $CaSO_4$ (gypsum/anhydrite). This has been observed in LOT, Prototype and ABM experiments and is a rather common observation.
- Accumulation of NaCl (halite) was observed locally in the ABM2 experiment (not yet reported).
- Physical disintegration of bentonite blocks was observed in ABM2 (in some parts together with halite accumulation) and ABM5 (in several parts, not yet reported).

3.3.2 THM properties

In the framework of the Safe Barriers project, researchers at Newcastle University explored the impacts of corrosion products, ionic solutions and heating on the behaviour of bentonite (Davies et al. 2017). Experiments were conducted using 1:10 bentonite suspensions in NaCl, CaCl and KCl solutions (up to 1 M) with steel coupons, and in constant volume test cells with compacted bentonite. Data showed an inverse relationship between salinity and swelling and plasticity indices, with greatest reduction in swelling and plasticity observed for CaCl. Data for heated (up to 150°C) samples, and those exposed to iron corrosion products, yielded low reductions in swelling indices, compared to those exposed to saline solutions (Davies et al. 2019). These data do not, however, reflect impacts upon the swelling pressure of highly compacted bentonites, which is arguably a more safety relevant property than free-swelling index. Therefore, further comparative studies exploring the impacts of these variables on swelling pressures would be of interest.

The British Geological Survey undertook research into the hydraulic permeability of bentonite subjected to high thermal loading, to determine whether hydraulic conductivity and self-sealing behaviour were altered as a result of exposure to high temperatures. Experimental work involved isotropic and constant volume tests in custom made cells, at temperatures up to 200°C whilst monitoring the swelling pressure, pore water pressure, total stress and fluid flux. The results of these experiments are presented in Zihms & Harrington (2015) and Daniels et al. (2017a), which showed for all four tests, a trend for decreasing intrinsic permeability of up to an order of magnitude with increasing temperature up to ~150°C. Intrinsic permeability still remained below 10^{-20} m^2 for temperatures up to 150°C. However, whilst the changes in permeability were relatively small, the fluid fluxes increased significantly on heating because of the reduction in viscosity. Above 150°C, large increases in permeability were seen which were attributed to sample thermal contraction, but uncertainties exist in the expected amount of vessel expansion, combined with water entering the vapour phase at the downstream end of the test (steam generation). This meant that it was not possible to confidently interpret the results of the 200°C tests (Daniels et al. 2017a). As part of the HITEC project, the BGS plan to test up to this temperature using a modified constant volume cell that

is constructed from a steel with a lower thermal expansion coefficient. Additionally, by using higher injection and backpressures, the HITEC experiments will avoid entering the water vapour phase.

The BGS has also conducted some preliminary experiments into gas permeability and breakthrough pressure of bentonites at elevated temperature. In the gas experiments, it was not possible to achieve dilatant gas pathways through isotropically confined samples; since gas entry pressures were greater than confining pressures, gas entry was only observed in cells with constant volume boundary conditions where confining pressures were high. Daniels et al. (2017b) presented some preliminary data, suggesting that gas permeability initially increased at elevated temperatures, but dropped for temperatures between 80 and 100°C, which was the highest temperature tested (Daniels et al. 2017b). However, Daniels et al. (2017 a, b) identified limitations with experimental methods for assessing gas flow at high temperatures, which requires further development of apparatus to ensure robust data collection at temperatures above 150°C.

Micro-Electrical Mechanical System (MEMS) sensor development for the monitoring of temperature and relative humidity are presented in Yang et al. (2015), with laboratory scale testing subsequently undertaken as described in Yang et al. (2017). The small size of the sensor design was to reduce their interference with hydro-mechanical responses of the bentonite buffer, thereby improving quality of data. Reliable data were generated at swelling pressures of 2 MPa (Yang et al. 2017) and across a range of temperatures from -20 to +120°C (Yang et al 2015).

The results of the THM analyses performed on the samples retrieved from the FEBEX-DP in situ test after 18 years operation with the heater surface at 100°C (section 3.2.5) showed that the thermal, hydraulic and mechanical properties analysed were consistent with the range expected for the reference bentonite (Villar 2017).

3.3.3 Small-scale simulation experiments

Laboratory tests in thermo-hydraulic cells that simulate the conditions of the sealing material in a radioactive waste repository are very useful to identify and quantify processes taking place in the engineered barrier. This kind of tests have gone on at CIEMAT for the last 30 years, evolving from simple designs in which just temperatures inside the material were measured, to the current designs that involve the measurement of temperature and relative humidity, total pressure and water intake. These tests keep running for different periods of time (up to several years) and the analysis of the material upon dismantling includes mineralogical, geochemical, microstructural, hydro-mechanical and chemical studies, which allows gaining insight into the time evolution of the properties of the barrier.

In the TH cells the sealing material can be subjected simultaneously to heating and hydration (Figure 3-28). They are cylindrical and designed to be hermetic and non-deformable. The heat generated by the radioactive decay of the wastes in the containers is simulated by an electric heater and the simulated groundwater is injected through a porous stone or a stainless steel sinter that assures a uniform distribution of water over the sample surface.

Although most tests have been performed with the heater set at 100°C, two tests were performed to simulate the Äspö field test TBT (Äkesson et al. 2020), in which highly compacted MX-80 bentonite was used and the heater temperature was set to 140°C. The laboratory cell tests lasted 1.4 and 5 years, and the postmortem analyses focused on the mineralogical, microstructural and geochemical changes (Gómez-Espina & Villar 2010, 2015, 2016). Problems to correctly measure the water intake and vapour leakages through the sensors' openings and the bottom of the cell were identified. These technological problems were solved and, in the framework of the PEBS project and to support the HE-E in situ test (section 3.2.3.2), two tests in which the heater was set to 140°C were launched in 2012 (cells CG-50 in Figure 3-28). Two sealing materials were tested: a granulate of MX-80 bentonite pellets (B) and a 65/35

sand/MX-80 bentonite mixture (S/B). The two materials have very different gas and liquid permeabilities, as well as water retention capacity, and this conditioned the water redistribution in the vapour phase triggered by heating as well as the liquid water intake, which were both much more restricted in the bentonite pellets. The S/B cell was dismantled after 2.8 years and evidences of soluble species transport and their precipitation close to the heater were found (Villar et al. 2016b). Cell B is still running and will be dismantled during HITEC.

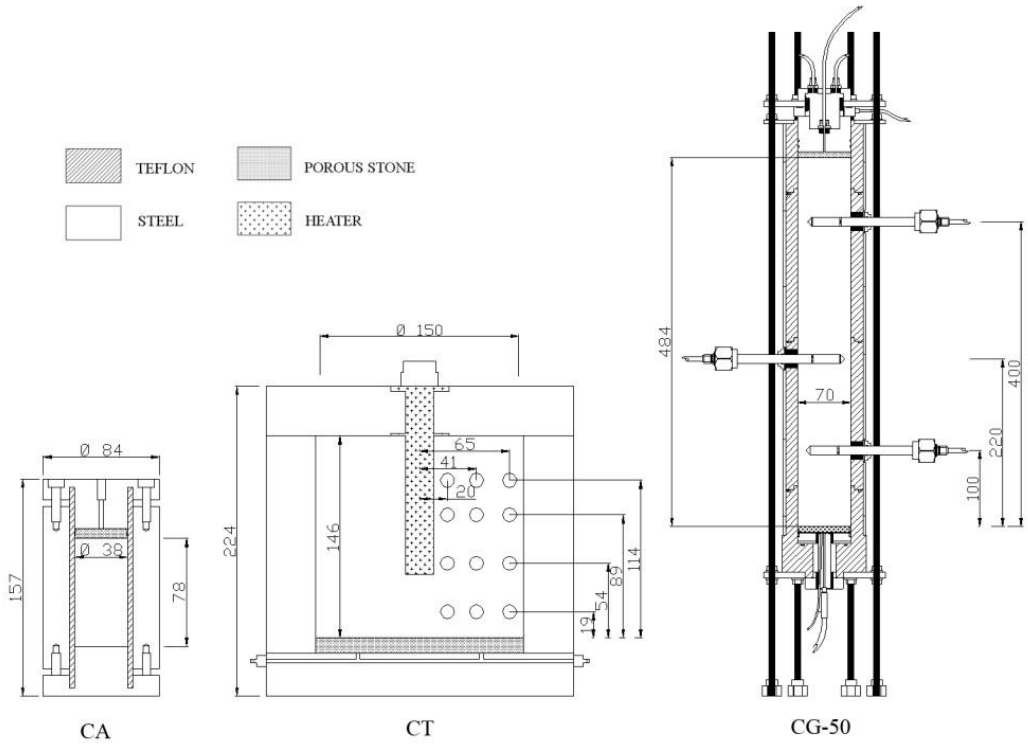

Figure 3-28. Schematic representation of different kinds of TH cells used at CIEMAT (Villar et al. 2012)

CEA performed two THM mock up tests in the laboratory on compacted MX-80 bentonite using two different initial water contents (Gatabin & Billaud 2005). Each test consisted of two phases. In Phase 1 heat was applied to one end of the column while the temperature at the other end was kept at 20°C. A maximum temperature of 150°C was applied. Phase 2 started after thermal equilibrium had been achieved and involved the gradual hydration of the sample. A constant water pressure was applied to the end opposite to the one where the temperature variation was prescribed. Constant volume conditions were ensured in the two phases of the test. During the tests temperatures, relative humidity, pore pressure, total axial stress and total radial stress were measured. The samples had both a diameter and a height of 203 mm (Figure 3-29). The tests provided interesting information about temperature distribution, water movement and pressure development that were modelled as part of the SKB Task Force on Engineered Barrier Systems (Gens 2019). The possible influence of the initial water content and sample length (scale effect) on the water transfer process was pointed out. In addition, conclusions concerning the instrumentation performance and gas tightness of the cell were reached.

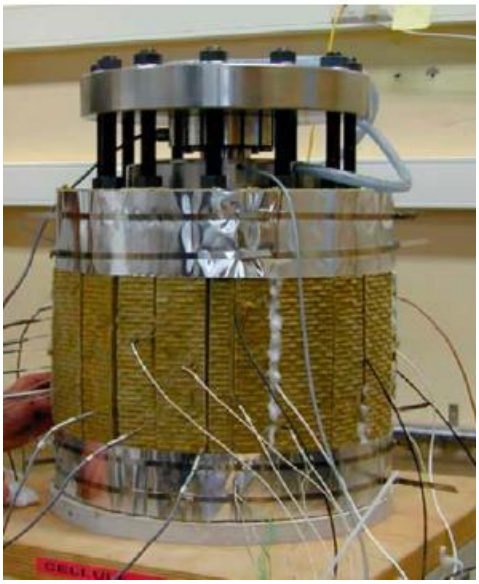

Figure 3-29. Small-scale test by CEA (Gatabin & Billaud 2005)

In the framework of the Safe Barriers project, experimental work by Cardiff University explored THM-C evolution under non-isothermal conditions (Tripathy et al. 2017). Column cells were configured using compacted bentonite cylinders with heater elements at one end to achieve temperatures of 85 and 150°C, whereas the other end was maintained at 25°C. Monitoring of relative humidity, temperature and axial stress was undertaken. In parallel, hydraulic tests were conducted using the same configuration, where water was injected into the cool end of the sample. For the former, non-hydraulic tests, data highlighted moisture re-distribution occurred as a function of temperature, with greater relative humidity measured further from the heater. Increased drying near the heater over time was also observed. Hydraulic tests also showed an increase in water content at the inlet end of the cell. However, difference in temperature between 85°C and 150°C and water injection pressures (5 and 600 kPa) appeared to have little impact upon axial stress over the experimental period.

3.4 State of models' development (modelling tools and approaches)

One of the objectives of HITEC is the development and validation of suitable THM models for clay buffer at temperatures higher than 100°C and the incorporation in them, if necessary, of the processes identified during the WP activities, mostly those in subtask 3.3 "Small-scale experiments".

3.4.1 ENRESA

A good knowledge of the THM performance of the bentonite barrier below 100°C does already exist and THM formulations have been developed and validated for temperatures below 100°C in a number of experiments and projects (FEBEX, HE-B). Within HITEC, the main objective is to develop a conceptual framework and a mathematical model (at element level) for clay buffer materials able to incorporate the effects of high temperature (>100°C) on their predicted thermo-hydro-mechanical behavior.

A crucial element of the planned development is the availability of a double structure framework and constitutive model that distinguishes between the microstructure and macrostructure of the material. The microstructure is the seat of the physico-chemical phenomena that occur at particle level. Therefore, the available conceptual model is readily available to incorporate the mineralogical and physical changes caused by high temperatures in a natural way. Although it is not the main thrust of the project, chemical effects associated to high temperatures can also be considered within the

microstructural model. Other larger scale effects will be assigned to the macrostructure. Different types of clay buffer materials will be considered. Thermo-elastic-plasticity is the theoretical framework where the constitutive developments will take place.

CODE_BRIGHT will be the computer code used for the numerical simulations. It is a general coupled THM (thermo-hydro-mechanical) code that incorporated many features related to thermal effects such as: temperature-dependence of hydraulic laws (retention curve, permeability, diffusion coefficient, vapor equilibrium and migration), mechanical law (thermo-elasto-plastic stress-strain relationships, strength, thermal expansion) and physical properties of the solid, liquid and gas components (density, viscosity, etc…). If, as a result of the calculations, enhancements of the formulation and/or computer code are required, they can be readily implemented because CODE-BRIGHT is an in-house development so there exists the necessary expertise and access to the source code

3.4.2 POSIVA

Posiva is participating to model development in BEACON and through Code_Bright. Lately used Code_Bright THM models are discussed for example in Toprak (2018). Views in montmorillonite transformation are same as SKB's (see 3.4.4). Moreover, there is ongoing work to improve reactive transport modelling and coupling it into THMC model.

3.4.3 RWM

RWM participates in a number of modelling tasks through projects such as DECOVALEX and BEACON, and has been a member of SKB's EBS Task Force since 2011. Through the EBS Task Force, RWM has completed a number of modelling activities related to bentonite THM-C evolution. A summary of key tasks relevant to the thermal evolution of engineered barrier systems is as follows:

Prototype Repository

The Prototype Repository modelling project, undertaken by Amec Foster Wheeler on RWM's behalf, as part of the Engineered Barrier Systems (EBS) Task Force, focused on describing the TH evolution of the Prototype Repository experiment at the Äspö HRL and to provide a better understanding of the interaction between the fractured rock and bentonite (Tsitsopoulos et al. 2018).

Modelling methodology utilised generic site characterisation data, including site statistics for fracture occurrence/properties and employed a discrete fracture network (DFN) approach to statistically represent the fractured host-rock. Through the upscaling process, a selected number of stochastic realisations were used to supply equivalent heterogeneous permeability/porosity fields for the rock, suitable for use in the continuous porous media (CPM) concept. As a result, a coupled integrated TH model for predicting the wetting and temperature of the bentonite and accounting for the heterogeneity of the fractured rock was developed.

DFN and CPM simulations were performed using ConnectFlow. The model was in good agreement with the experimental data. For all sensors, the modelled temperature evolution appears to be largely independent on the discrete fracture network model simply because of the dominance of conduction through the rock. This reinforces the understanding that the temperature evolution, important for determining the appropriate spacing of heat generating containers, is fundamentally dependent on the heat conduction parameters of the rock and EBS. This work contributes to knowledge of the influence of parameters on numerical modelling of bentonite-rock interactions, building upon earlier work undertaken on the Bentonite-Rock Interaction Experiment (Baxter et al. 2018).

FEBEX

A number of FEBEX modelling tasks were funded by RWM, including an iron-bentonite interaction study (Wilson 2017) and THM modelling (Thatcher 2017, Ghiadistri 2019). The work reported in this section uses data from the FEBEX in situ experiment (described in section 3.2.5) and, data from supporting laboratory work, to continue development of coupled numerical models of the thermal, hydraulic, mechanical and chemical processes that control the behaviour of bentonite buffers.

Thatcher (2017) documents coupled THM modelling for the FEBEX experiment. This builds upon previous work for RWM developed an HM model, called the Internal Limit Model (ILM), which was used for an MX-80 bentonite and sand mixture. Thatcher (2017) documents the first application of this model to an alternative bentonite, with the addition of thermal coupling, and tests its transferability to a large scale emplacement experiment. It is concluded that it is possible, after minimal calibration, that the model was effective at describing the THM evolution of the experiment, despite the new addition of thermal parameters and the different materials modelled. It also concludes that under high strains, the bentonite behaviour is more akin to a fluid than an elastic material.

PhD research conducted by Ghiadistri (2019) developed a new constitutive framework for compacted highly expansive clays, which was implemented into the Imperial College Finite Element Program (ICFEP, Potts & Zdravkovic 1999). The model builds upon a single structure model previously developed at Imperial College (Georgiadis et al. 2005, Tsiampousi et al. 2013), and develops a double structure model by extending the formulation to capture the double porosity structure characteristic of highly expansive clays. The model was validated using available experimental data, demonstrating substantial improvements in the numerical predictions of the hydro-mechanically coupled processes in compacted bentonite, compared to those of the single-structure model. In conjunction with the THM formulation of the governing finite element equations in ICFEP, the model has successfully reproduced the behaviour of compacted bentonite clays both at the laboratory scale, in the simulations of a series of swelling pressure tests, and at the field scale, in the simulation of the FEBEX large-scale experiment. A key outstanding knowledge gap identified by this research was a lack of experimental data to enable the quantification of the microstructure of compacted bentonites, which influences the calibration of microstructural parameters of the new constitutive model (Ghiadistri 2019).

Bentonite model development – ongoing research

Ongoing work is being conducted by Wood PLC into the re-saturation of bentonite pellets under thermal gradients, and in collaboration with Clay Technology AB, the development of a prototype model to describe the behaviour of solutes within bentonite. Both approaches adopt the 'homogenous mixture model' for saturated bentonite, which assumes a single porosity relevant to saturated bentonite.

3.4.4 SKB

Handling in safety assessment

The montmorillonite transformation in a KBS-3 repository is assumed to be small based on the following observations and arguments:

1. The time scale for significant montmorillonite transformation at repository temperatures in natural sediments is orders of magnitude longer than the period of elevated temperature in a KBS-3 repository (e.g. Velde & Vasseur (1992).

2. The bentonite material is close to mineralogical equilibrium to start with (e.g. Fritz et al. 1984).

3. Transformation is limited by low transport capacity, principally regarding potassium (Hökmark et al. 1997) and silica (Karnland & Birgersson (2006).

4. All published kinetic models, based both on natural analogues and laboratory experiments indicate that the transformation rate is very slow under repository conditions (e.g. Huang et al. 1993).

The montmorillonite transformation process can also be quantified by modelling, as exemplified above. Based on the above description, no mineral transformation is expected to be faster than illitization as a result of elevated temperature. Consequently, the maximum temperature effect is modelled by the kinetic expression for illitization proposed by Huang et al. and by use of different but realistic potassium concentrations.

As long as the maximum temperature is below 100°C the montmorillonite in the buffer is assumed to be stable for the timescale of the repository.

In the reference evolution, alteration is not expected to proceed to a level where it will affect the properties of the buffer. Alteration is therefore treated as a separate scenario.

Modelling of the LOT A2 experiment

In Sena et al. (2010) a numerical model was developed with the purpose of simulating 1) the thermo-hydraulic, 2) transport and 3) geochemical processes that have been observed in the LOT A2 test parcel (section 3.2.2). The LOT A2 test lasted approximately 6 years, and consisted of a 4 m long vertical borehole drilled in diorite rock, from the ground of the Äspö HRL tunnel. The borehole contained a central heater, maintained at 130°C in the lower 2 m of the borehole, a copper tube surrounding the heater, and a 100-mm thick ring of pre-compacted Wyoming MX-80 bentonite around the copper tube (Karnland et al. 2009).

The numerical model developed was a 1D axisymmetric model that simulates the water saturation of the bentonite under a constant thermal gradient, the transport of solutes and the geochemical reactions observed in the bentonite blocks. Two cases have been modelled, one considering the highest temperature reached by the bentonite (at 3 m depth in the borehole, where temperatures of 130 and 85°C were recorded near the copper tube and near the granitic host rock, respectively) and the other case assuming a constant temperature of 25°C, representing the upper part of borehole, where the bentonite was not heated.

In the LOT A2 test, the initial partially saturated bentonite became progressively water saturated, due to the injection of Äspö granitic groundwater at granite/bentonite interface. The transport of solutes during the bentonite water saturation stage is believed to be controlled by water uptake from the surrounding groundwater to the wetting front and, additionally, in the case of heated bentonite, by a cyclic evaporation/condensation process (Karnland et al. 2009). Once bentonite is water saturated, the transport of solutes is driven by diffusion.

Although Donnan equilibrium (Birgersson & Karnland 2009) and anion exclusion (Muurinen et al. 2004) are able to influence the mobility of chloride in the bentonite buffer, under the high temperature LOT A2 test conditions, measured data seem to indicate a relatively low influence of these processes on the transport of chloride. For this reason, the transport of chloride was modelled taking into account advective, dispersive and diffusive fluxes that are believed to have occurred in the LOT A2 test.

Numerical results were conducted at fixed thermal gradients for both heated and non-heated bentonite based on the temperatures recorded during the experiment for both heated and non-heated bentonite.

The computed evolution of the bentonite saturation indicates that, within approximately one year, the bentonite blocks located at the depth of the heater were completely water saturated which agrees

with measured data. The simulated transport of chloride is also in good agreement with data measured at the end of the LOT A2 test for the two cases considered, reflecting the reliability of the conceptual model defined for the LOT A2 test.

Based on the geochemical data obtained at the end of the LOT A2 test and on previous modelling exercises (Arcos et al. 2006), the main geochemical processes that are believed to have developed during the LOT A2 test are: 1) precipitation/dissolution of carbonate, sulphate and silica minerals and, 2) cation exchange in the montmorillonite interlayer. Numerical results predict the dissolution/precipitation of anhydrite, calcite and silica in the heated bentonite in agreement with data measured at the end of the LOT A2 test.

3.4.5 SURAO (CU & CTU)

In this chapter a summary of the constitutive model for bentonite used by the Czech teams (Charles University, Czech Technical University & SURAO) for simulations within the EURAD project is presented. The model is a coupled thermo-hydro-mechanical model based on hypoplasticity principles combined with the concept of double structure. The model has been developed by Mašín (2017) by a hierarchical enhancement of the earlier model by Mašín (2013), which did not consider the effects of temperature. That model, in turn, was a double structure enhancement of earlier models for unsaturated and saturated soils.

The model has been developed using a double-structure framework originally proposed by Gens & Alonso (1992), who introduced the double structure concept, and Alonso et al. (1999), who developed a complete constitutive model. The model is based on the hydro-mechanical double structure hypoplastic model proposed by Mašín (2013), which has been enhanced by the effects of temperature. Background and basic hypotheses of this model are briefly described in this section.

The hypoplastic double-structure model, and double-structure models in general, are based on the assumption supported by various micro-mechanical studies that in expansive soils one can identify two levels of structure: a macrostructure, which represents an assembly of silt-size aggregates of the clay particles, and a microstructure, which represents the internal structure of these aggregates. A conceptual sketch of these two levels of structure is shown in Figure 3-30.

In Mašín (2013), separate models were considered for the mechanical and hydraulic responses of the microstructure and of the macrostructure. These responses are coupled at each structural level, and the behavior of the two structural levels is linked through the double-structure coupling function.

The model by Mašín (2017), adopted in EURAD simulations, evolved from the Mašín (2013) by including the thermal component. To accomplish this task, additional thermal dependency has been introduced for water retention curves, volumetric behaviour of microstructure and normal compression behaviour of macrostructure. The final model is a comprehensive model capable of predicting complex THM behaviour of bentonites.

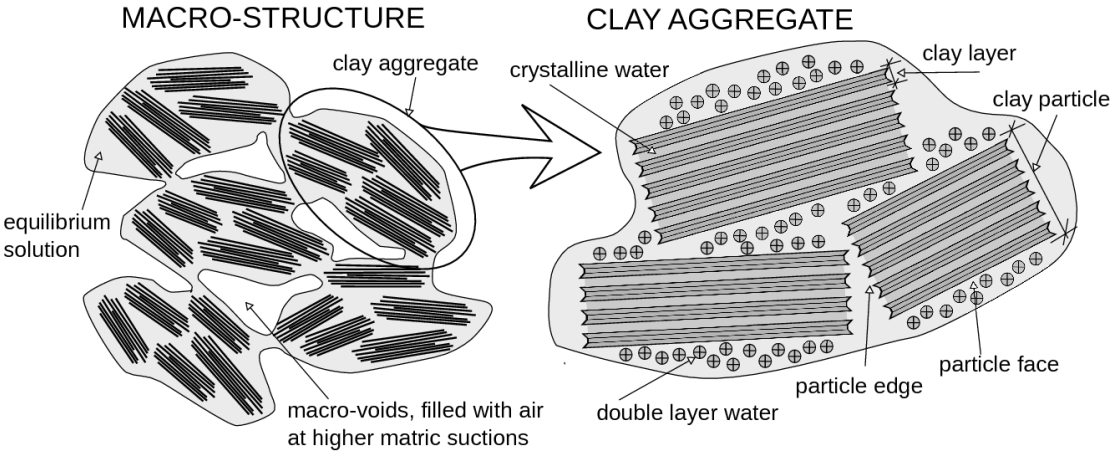

Figure 3-30. Schematic representation of double structure concept (Mašín 2013, 2017)

Input parameters

Model parameters and their description are summarised in Table 3-9. For their detailed explanation, the reader is referred to the original model publications by Mašín (2013, 2017).

Table 3-9 Model parameters and their description (Mašín 2017)

Parameter	Description
φ_c	Critical state friction angle of macrostructure in a standard soil-mechanics context
λ^*	Slope of isotropic normal compression line in $\ln(p^M/p_r)$ versus $\ln(1+e)$ space
κ^*	Macrostructural volume strain in p^M unloading
N	Position of isotropic normal compression line in $\ln(p^M/p_r)$ versus $\ln(1+e)$ space
ν	Stiffness in shear
n_s	Dependency of position of isotropic normal compression line on suction
l_s	Dependency of slope of isotropic normal compression line on suction
n_T	Dependency of position of isotropic normal compression line on temperature
l_T	Dependency of slope of isotropic normal compression line on temperature
m	(1) Control of f_u and thus dependency of wetting-/heating-induced compaction on distance from state boundary surface; (2) control of double-structure coupling function and thus response to wetting-drying and heating-cooling cycles (Mašín 2013b)
α_s	Dependency of microstructural volume strains on temperature
κ_m	Dependency of microstructural volume strains on p^m
e_{r0}^m	Reference microstructural void ratio for reference temperature T_r, reference suction s_r, and zero total stress
c_{sh}	Value of fm for compression
s_{e0}	Air-entry value of suction for reference macrostructural void ratio e_0^M
a	Dependency of macrostructural air-entry value of suction on temperature
b	Dependency of macrostructural air-entry value of suction on temperature
a_e	Ratio of air entry and air expulsion values of suction for macrostructure water retention model
s_r	Reference suction for e^m

Parameter	Description
e_0^M	Reference macrostructural void ratio for air-entry value of suction of macrostructure
T_r	Reference temperature

Model performance

Model performance to simulate THM experiments has been evaluated by Mašín (2017). For example, predicted water retention curves are shown in Figure 3-31. The dependency of water content on suction is predicted correctly. The experiments show a slight decrease in water retention capacity with temperature, which the model predicts in a minor way only.

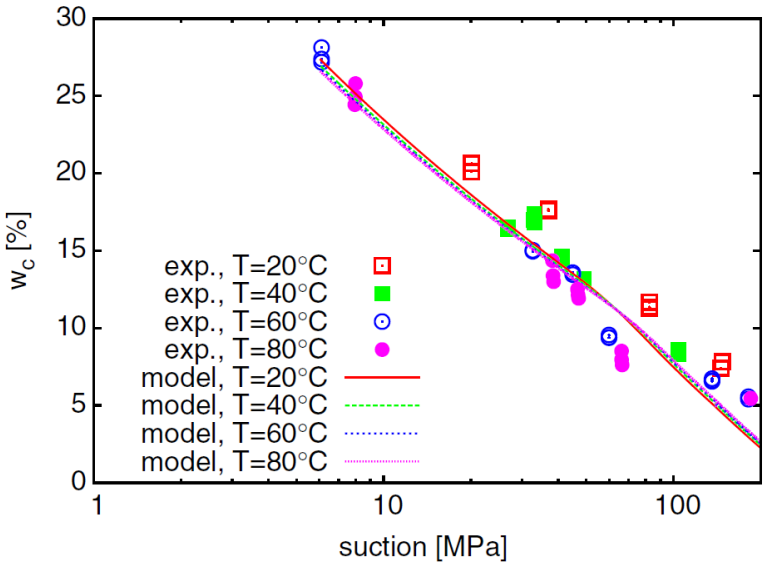

Figure 3-31. Water retention curves at different temperatures: experimental data on MX80 bentonite by Tang & Cui (2007) compared with model predictions

Volume strains because of heating at various values of suction and mean total stress are shown in Figure 3-32. The model accurately predicts the observed complex behavior:

- At high suctions (110 MPa), the model correctly predicts swelling, whose magnitude is controlled by α_s; heating-induced swelling at high suctions is primarily reversible.
- At lower suction (9 MPa for a total stress of 0.1 and 39 MPa for a total stress of 5 MPa), the model predicts heating-induced compaction (collapse), which is irreversible and controlled by the offset of normal compression lines at different temperatures (by the parameters l_T and n_T, see Table 3-9); however, for a stress of 0.1 MPa at a suction of 39 MPa, the state is well within the state boundary surface and heating-induced swelling is predicted in agreement with experimental data; in principle, the model can also be calibrated using negative α_s to predict the heating-induced contraction observed by some authors.
- The model predicts cooling-induced contraction, which depends on suction such that it is most pronounced at 110 MPa and least significant at 39 and 9 MPa; these predictions are governed by the dependency of the double-structure coupling factor f_m on macrostructural degree of saturation.

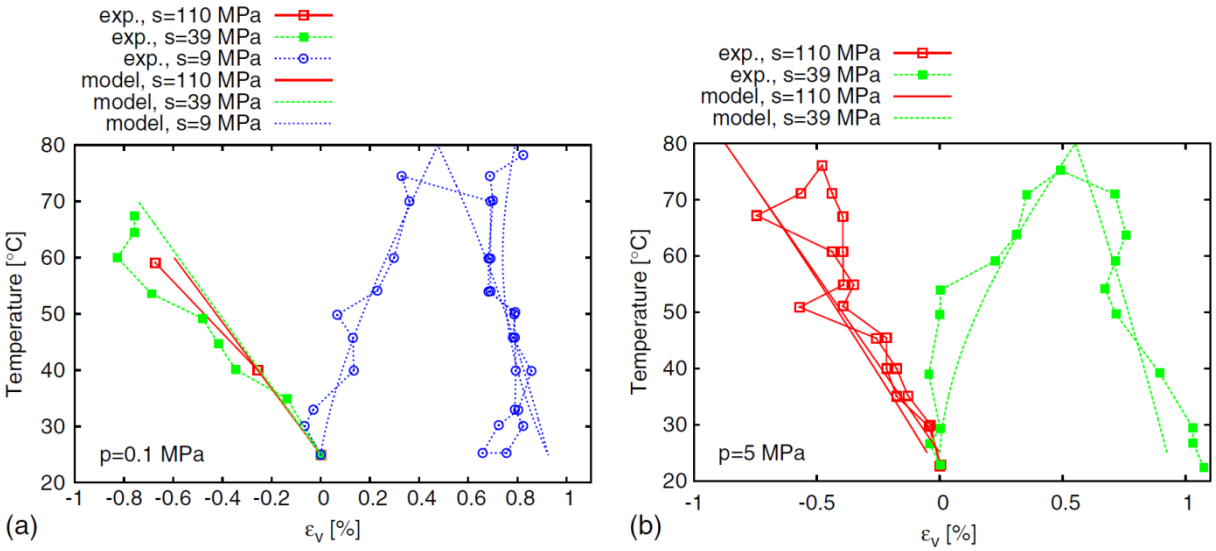

Figure 3-32. Volume change due to heating and cooling at total isotropic stresses of (a) 0.1 MPa and (b) 5 MPa; experimental data on MX80 bentonite from Tang et al. (2008b)

Model limitations and further development

Within EURAD project, we will focus on the following modelling aspects for further development of the model:

- The thermal part of the model model has to date been evaluated using limited experimental data on MX80 bentonite. The model needs to be evaluated using wider range of materials. In particular, we will adopt the model for simulations of the behavior of Czech BCV bentonite.
- Performance of the model has up to date only been checked at maximum temperature of 80°C. For EURAD (HITEC) applications, the model needs to be evaluated at higher temperatures and, if consistent deviations between model predictions and experimental results occur, the model formulation will be updated.
- While the model algorithm is stable at "standard" unsaturated conditions, it becomes less robust at unusual states (low dry densities, in particular). Also, its numerical implementation within SIFEL finite element code is prone to oscillations and numerical divergences at states approaching full saturation. This is partly caused by the constitutive model itself and partly by the coupled THM numerical finite element algorithm. Problematic aspects will have to be resolved to maximise usability of the model at various repository conditions.

3.5 Main conclusions from SotAs of previous related projects/reviews/relevant WMO documents

Within the PEBS project (Long-term Performance of the Engineered Barrier System, 7th European FP 2007-2011) the conclusion was reached that the characterisation of bentonite performance and THM properties below 100°C was largely established (Johnson et al. 2014). Overall, the observed effects of temperature on the hydro-mechanical properties (decrease of swelling pressure, increase of permeability, decrease of water retention capacity) can be qualitatively explained by considering the transfer of high-density interlayer water to the macropores that is triggered by the increase in temperature. The different behaviour of smectites exchanged with monovalent versus divalent ions can be explained by taking into account the different interlayer/diffuse-double-layer water ratio in both.

However, the literature survey performed during the PEBS project confirmed that the information regarding bentonite at higher temperatures was less abundant. Lack of information was identified in particular:

- for granular bentonite material (manufactured bentonite as grains or pellets);
- with respect to the water retention curve;
- concerning the effect of degree of saturation on thermal conductivity (low thermal conductivity would lead to higher temperature) and water permeability; and
- regarding the effect of temperature on swelling capacity depending on exchangeable cations.

Wersin et al. (2007) reviewed work assessing the performance of the bentonite barrier beyond 100°C. No significant changes of hydraulic and mechanical properties had been reported for bentonite materials exposed to temperatures of at least 120°C under wet conditions, but the data suggested significant cementation and perhaps also illitisation at 150°C and beyond. Natural analogue bentonite samples that showed substantial cementation and illitisation effects still displayed rather favourable hydraulic properties. Under dry conditions, bentonite was found to be stable to higher temperatures, maybe as high as 350°C. Hence, the mineralogical transformation of bentonite minerals that are likely to occur at temperatures of relevance (between 100°C and 150°C) seem to be limited even over very long times. The fact that in repository relevant conditions, temperatures above 100°C coincide with low water saturation might further reduce the already slow reaction rates.

An additional aspect of concern is that, because of the slow groundwater inflow towards the engineered barrier and the existence of a thermal gradient across the barrier, the unsaturated bentonite close to the canister will be exposed to elevated temperatures for some decades. Sellin & Leupin (2013) identified as a safety-relevant issue the effects on bentonite of long periods of unsaturated conditions with elevated temperatures, including the stability of bentonite under non-isothermal conditions and different degrees of saturation. In particular, the question of how this may influence the subsequent swelling properties after full saturation was discussed in Johnson et al. (2014) from a literature review perspective. The evidences found were not completely consistent, but nonetheless showed that significant reduction in swelling pressure can occur in some cases above 110-120°C, although in most cases in which swelling pressure was measured, values of more than 50% of initial values were observed. The reasons for inconsistency of results may relate to hysteresis factors and also to rapid cooling of samples to room temperature in experiments prior to measurement of swelling pressures. Because re-saturation would be expected to occur in a repository while the bentonite is still at elevated temperatures, it is not clear that the experiments adequately simulate the evolution of repository conditions. It was noted that if fully saturated samples are exposed to short-term laboratory heating as high as 150°C and swelling pressure and hydraulic conductivity are measured after cool-down, property changes are small compared to reference untreated samples (Dueck 2014). Furthermore no significant changes were found after the six-year duration LOT study, performed at Äspö (section 3.2.2), in which the bentonite experienced temperatures up to 130°C (Karnland et al. 2009). Deviating test results, compared to reference tests, were seen on stresses and strains at failure or hydraulic conductivity determined on samples from large-scale field tests (Dueck et al. 2011, Karnland et al. 2009, Åkesson et al. 2012), i.e. samples that had been submitted to high temperatures for different time periods. It could not be excluded that the deviations were caused by the increased temperature. The impact of the duration of the elevated temperature period on the property change was neither clear but changes could occur already after short heating/cooling cycles.

In relation to the above, some impact of vapour on bentonite properties under repository relevant conditions (120-150°C) can be expected and should be clarified taking into account repository relevant vapour regimes. This impact might be due to minor surface cementation effects, although this needs further confirmation. The possible scale dependence of the vapour movement is also to be assessed.

Concerning modelling, another conclusion from the PEBS project was that the THM formulations developed and validated for temperatures below 100°C can be extended without modifications to temperatures above that value. Variations of retention curve, water permeability and surface tension with temperature can be taken into account without any modification of the basic formulation. In the SKB Task force of Engineered Barrier System reported in Gens (2019), several teams modelled laboratory small-scale THM tests (some of them introduced in section 3.3.3). Some of the conclusions related to the thermal problem are:

- The main difference between the general formulations was their capacity to incorporate or not the air balance equation. Without the gas equation, the usual assumption is that gas pressure is constant. This may lead to non-physical situations if the vapour pressure exceeds 1 atmosphere when temperatures rise above 100°C.
- The only thermal effect considered on mechanical behaviour was the thermal expansion derived form a constant coefficient of thermal dilation.
- The dominant heat transfer mechanism identified was conduction. Hence, a good modelling of the thermal problem requires the consideration of the changes of thermal conductivity with degree of saturation.
- The differences between computed and observed hydraulic results were more apparent in the non-isothermal tests. The reason might be though, the existence of unnoticed vapour leaks from the testing cells not accounted for in the models.

With respect to the application of experimental methods used for temperatures lower than 100°C to higher temperature, the problems with vapour leakage and gas tightness issues were mentioned in section 3.3.3 concerning the small-scale tests. Daniels et al. (2017a, b) identified also limitations for assessing gas flow at high temperatures, which requires further development of apparatus to ensure robust data collection at temperatures above 150°C.

4 Clay host rock

4.1 Materials considered in HITEC: properties and temperature impact

The following sections summarise for the three selected host clays (Boom Clay, Opalinus and Callovo-Oxfordian claystone) aspects of the geology of the formation, mineralogy, pore water composition, parameters at the formation level and, in different subsections, the hydro-mechanical and THM properties derived from laboratory tests and the impact of temperature on some of them. In particular, the following temperature-dependent material properties are considered to be important (Li et al. 2007):

- the temperature induced variation in hydraulic conductivity
- the temperature induced variation in thermal conductivity
- the temperature induced stiffness and strength modification
- the temperature dependence of creep rates
- the thermal sensibility on anisotropy

Most of the information gathered comes from research projects (including thesis) financed by or with participation of the WMOs.

4.1.1 Boom Clay (EURIDICE)

The Boom Clay Formation (Tertiary clay formation) is one of the two potential clay formations studied in relation with the feasibility of the nuclear waste disposal in Belgium. This clay is a detrital marine

deposit from the Oligocene and more specifically from the Rupelian stage, between 33.9 and 28.4 Ma. The Boom Clay dips gently towards the northeast, is located in the north part of Belgium and covers a surface of almost 5000 km² (Figure 4-1). The thickness of the formation increases from a few decametres at outcrop to more than 150 m in the deeper part of the basin. This sedimentary formation has been deposited in layers according to the climate and geological conditions change. The formation is composed of rhythmically alternating clay-rich and silt-rich materials resulting in a gray-tone banding (Vandenberghe et al. 2014)

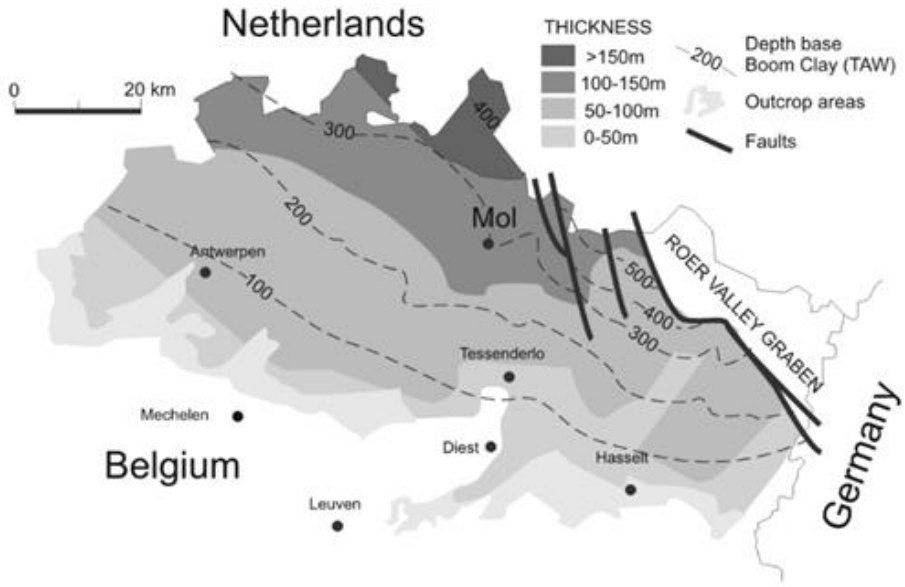

Figure 4-1. Extension of the Boom Clay Formation in the north part of Belgium. The formation dips towards the northeast. The underground research facility is located at Mol (from NIRAS/ ONDRAF, 2001)

At the level of the URL in Mol (Belgium), the Boom Clay has a thickness of about 100 m and is located at depths between 185 and 287 m below the surface with the underground laboratory at a depth of 223 m below the surface (Mertens et al. 2004).

The Boom Clay is an uncemented fine-grained compacted mud with a well-developed particle alignment according to the bedding plane and high porosity. Moreover, the microstructure shows porosity of larger pores caused by the presence of silt particles. The clay can be considered as an open structure with a high porosity (Dehandschutter et al. 2004). Figure 4-2 shows an image of the microstructure of the clay taken with Scanning Electron Microscopy (SEM) technique where it is possible to observe the preferential alignment of the clay particles in relation with the bedding plane. Such observations of the microscopically well-developed arrangement are the results of the geological history of the clay. Indeed, this one has been deposited in a marine environment and has been submitted to different vertical load during its history (Mertens et al. 2003). Consequently, this microstructure results from the post-sedimentation history.

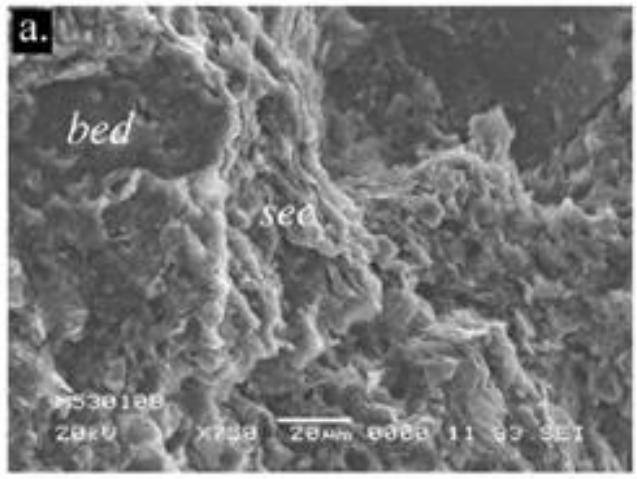

Figure 4-2. Image of the microstructure of the Boom Clay with the preferential alignment according to the bedding plane (bed) (Dehandschutter et al. 2004)

The granulometry of the clay is composed of more than 60% of very fine particles (clay particle) for the more clayey beds while there are 40% of clay particles for the more silty beds. Figure 4-3 presents the results of a compilation of the granulometric curves for the Boom Clay taken from different studies (Lima et al. 2011).

Figure 4-4 (right) presents results of mercury intrusion porosimetry (MIP) tests. The majority of the pores have a radius in the order of 0.01 µm with a unimodal distribution (Lima 2011).

The mineralogical composition of Boom Clay consists of clay minerals (up to 60 wt%), quartz, feldspars, and minor amounts of muscovite, biotite, and some heavy minerals. The clay mineralogy is dominated by illite, smectite, illite/smectite interstratifications, and kaolinite. Chlorite, degraded chlorite and illite/chlorite interstratifications are present. Organic matter can also be found in the clay. Table 4-1 presents the main mineralogical composition of Boom Clay compiled by determined by Frederickx (2019) based on 21 samples.

The pore water composition of Boom Clay is presented in Table 4-2. Pore water sampling was done *in situ* from various piezometers, or by the squeezing or leaching of clay cores in the surface laboratory. Piezometer water is considered to be the most representative for the *in situ* pore water since piezometer water samples experience minimum laboratory manipulations and therefore suffer minimum artefacts. The composition of the synthetic clay water (SCW) which has to be used in laboratory experiments is also given in the Table.

Based on the differences in granulometry and mineralogical content, the Boom Formation is subdivided in three members: the Belsele-Waas Member, the Terhagen Member and the Putte Member. Figure 4-5 presents the distinction between the different members based on the macroscopic description of the cores and the FMI (Fullbore Formation Microimager) log of Schlumberger (Aertsens et al. 2004).

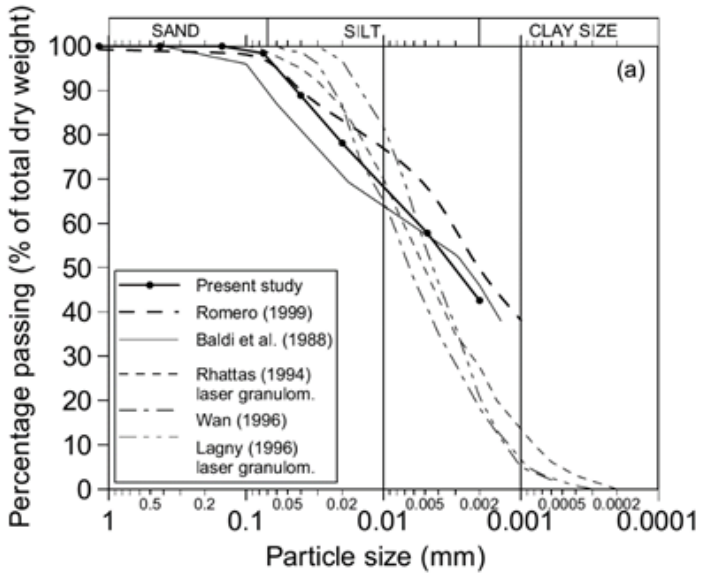

Figure 4-3. Particle size distribution of the Boom Clay, granulometric curves compiled by Lima (2011)

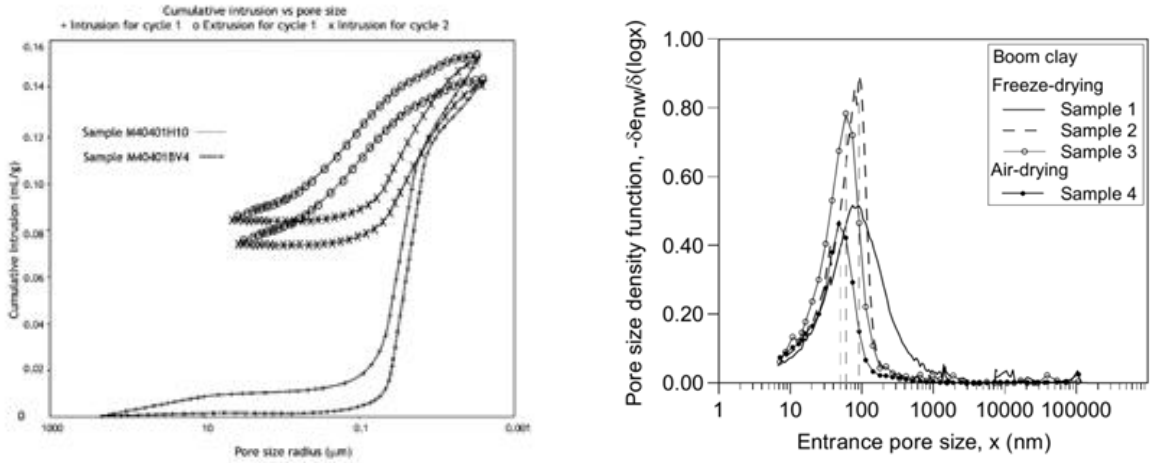

Figure 4-4. Cumulative mercury intrusion versus pore size for undisturbed Boom Clay (left); Pore size density function for Boom Clay for different samples (Lima 2011)

Table 4-1. Compositional range of the Boom Clay sample set, based on the mineralogical analysis of all size fractions. Values in weight percent (Frederickx 2019)

n = 21	Min	Median	Average	Max
Quartz	20	33	34	52
K-feldspar	3	5	6	9
Plagioclase	0.6	1.6	2	5
Calcite	0	0.3	0.7	6
Siderite	0	0	0.2	4
Dolomite	0	0.3	0.3	0.9
Pyrite	0.2	1	1.3	3.9
Gypsum	0	0.2	0.2	0.6
Anatase	0.3	0.7	0.6	1

n = 21	Min	Median	Average	Max
Apatite	0.1	0.1	0.1	0.2
Organic matter	0.4	1.7	1.8	5
Kaolinite	1.4	4	4	6
Interstratified kaolinite-smectite	1.1	4	4	6
Chlorite	1	1.7	1.8	3
Smectite	7	10	11	17
Interstratified illite-smectite	7	18	17	25
Illite	5	9	8	11
Muscovite	5	7	7	9
Glauconite	0	0.2	0.3	1.3

Table 4-2. The reference Boom Clay pore water as compiled by De Craen et al. (2004)

Element	mg/L	mmol/L	SCW (mg/L)
Na	359	15.6	330
K	7.2	0.2	13
Ca	2.0	0.05	saturated
Mg	1.6	0.06	2.6
Fe	0.2	0.003	1.3
Si	3.4	0.1	
Al	$0.6 \cdot 10^{-3}$	$2.4 \cdot 10^{-5}$	
B			7.5
HCO_3^-	878.9	14.4	848
TIC	181.3	15.1	
Alkalinity (meq/L)	15.12		
Cl	26	0.7	27.3
Total S	0.77	0.02	
SO_4^{2-}	2.2	0.02	0.2
F			4.9

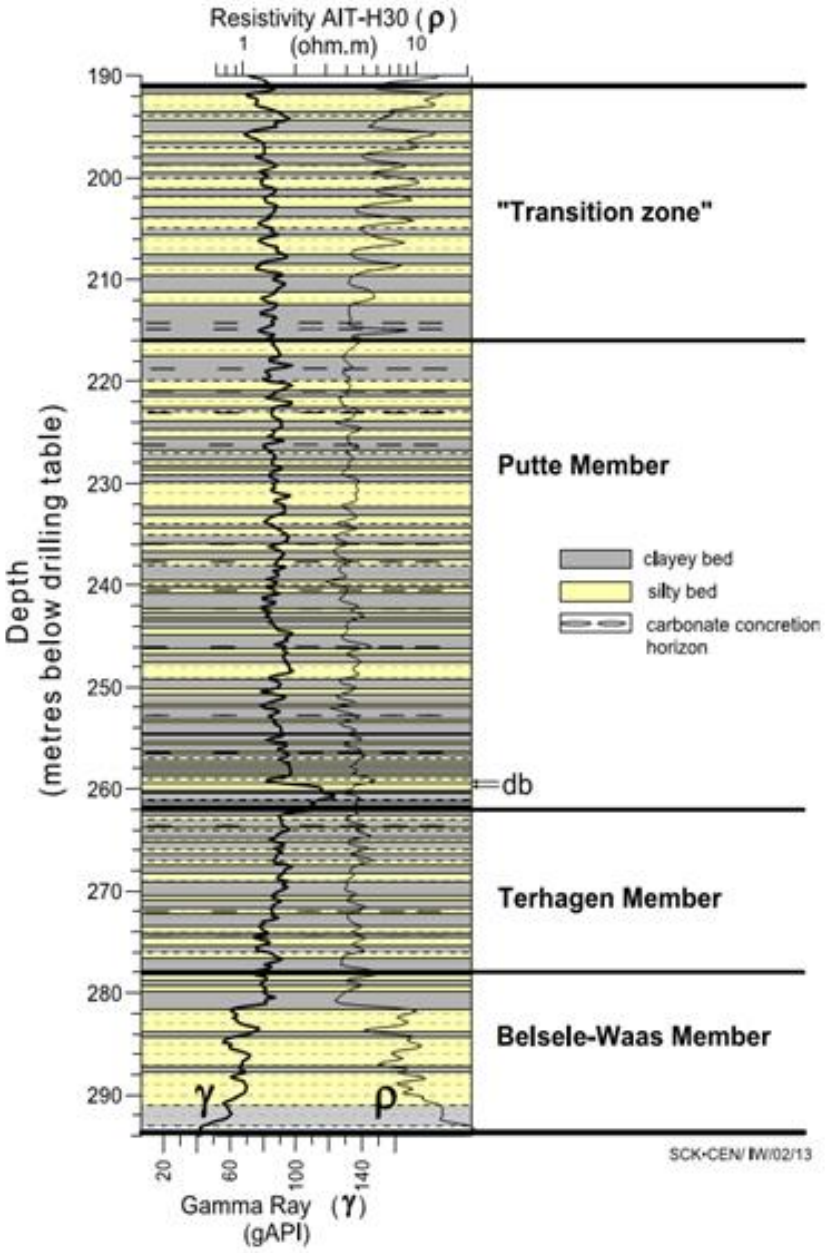

Figure 4-5. Lithostratigraphic log of the Mol-1 borehole interpreted by Mertens & Wouters in 2003 (Aertsens et al. 2004)

The Boom Clay is classified as plastic clay, stiff, overconsolidated with a very low permeability and a relatively high swelling pressure. The total vertical stress and pore water pressure at the level of the URL in Mol are respectively 4.5 MPa and 2.2 MPa. A K_0 value was determined by laboratory methods and *in situ* investigations (pressuremeter, dilatometer, self-boring pressuremeter (SBP), hydrofracturing tests, borehole breakouts and back-analysis of the stresses in the segmental concrete lining) (Bernier et al. 2007). The value of K_0 ranges from 0.7 to 0.8 (ONDRAF/NIRAS 2013).

The Boom Formation is characterized by a very low permeability with limited hydraulic gradient over the formation. As a consequence, the main mechanism of transport is via diffusion, the water flow by advection being negligible. Figure 4-6 presents a hydrogeological cross-section of the Boom Clay layer studied where it can be seen that the formation is surrounded by two sandy aquifers. Aertsens et al. (2004) studied with cores the value of the hydraulic conductivity parallel and perpendicular to the

bedding plane in all the formation. Figure 4-7 presents the results of this study. The vertical and horizontal values are different with a ratio (k_H/k_V) more or less equal to two. Note the different values of the hydraulic conductivity in relation with the granulometry of the studied material. For instance, the values in the Belsele-Waas member are higher than those of the other members of the formation because of its higher sand content. Aertsens et al. (2004) proposed an average value of 2.3 10^{-12} m/s for the vertical hydraulic conductivity.

Table 4-3 gives an overview of the basic geotechnical properties with their ranges. This table was obtained by lumping together several studies.

The total vertical stress and pore water pressure at the level of the URL in Mol are respectively 4.5 MPa and 2.2 MPa. A K_0 value was determined by laboratory methods and *in situ* investigations (pressuremeter, dilatometer, self-boring pressuremeter (SBP), hydrofracturing tests, borehole breakouts and back-analysis of the stresses in the segmental concrete lining) (Bernier et al. 2007). The value of K_0 ranges from 0.7 to 0.8 (ONDRAF/NIRAS 2013).

The Boom Formation is characterized by a very low permeability with limited hydraulic gradient over the formation. As a consequence, the main mechanism of transport is via diffusion, the water flow by advection being negligible. Figure 4-6 presents a hydrogeological cross-section of the Boom Clay layer studied where it can be seen that the formation is surrounded by two sandy aquifers. Aertsens et al. (2004) studied with cores the value of the hydraulic conductivity parallel and perpendicular to the bedding plane in all the formation. Figure 4-7 presents the results of this study. The vertical and horizontal values are different with a ratio (k_H/k_V) more or less equal to two. Note the different values of the hydraulic conductivity in relation with the granulometry of the studied material. For instance, the values in the Belsele-Waas member are higher than those of the other members of the formation because of its higher sand content. Aertsens et al. (2004) proposed an average value of 2.3 10^{-12} m/s for the vertical hydraulic conductivity.

Table 4-3. Basic geotechnical properties of the Boom Clay compiled by a review of several studies (Horseman et al. 1987, Baldi et al. 1988, Sultan 1997, Mertens et al. 2003, 2004, Dehandschutter et al. 2004, Bernier et al. 2007)

Soil density (kg/m³)	1900 - 2100
Grain density(kg/m³)	2682
Dry density (kg/m³)	1490 - 1648
Water content (%)	20 - 30
Porosity (%)	35 - 40
Plastic limit(%)	13-26.5
Liquid limit (%)	55-80
Overconsolidatio ratio (OCR)	2.4

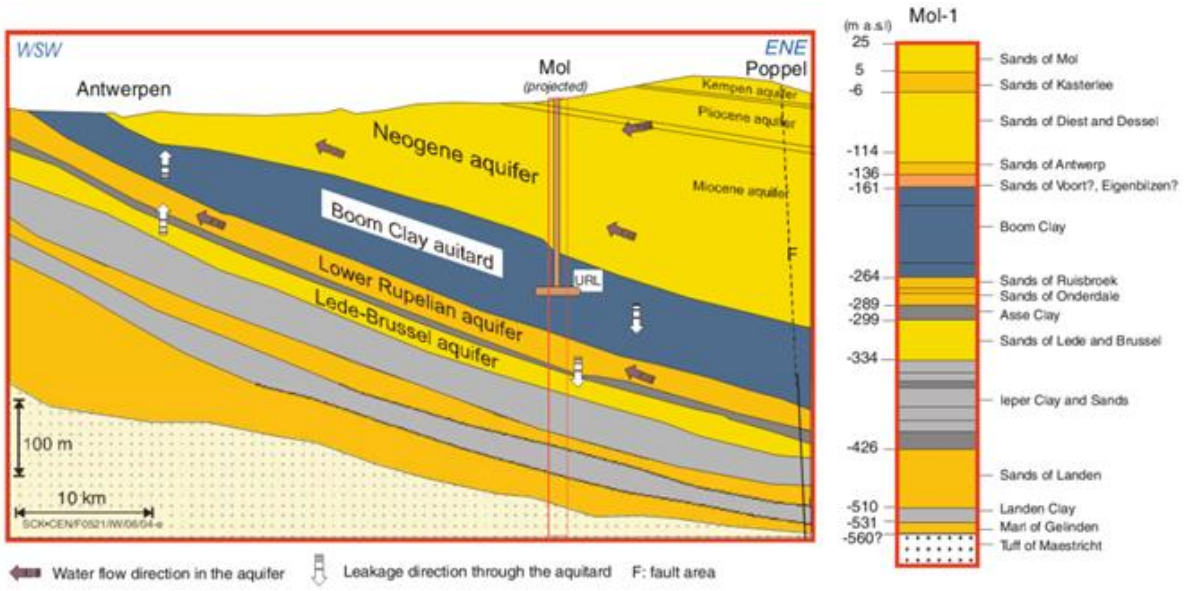

Figure 4-6. Hydrogeological cross-section of the studied area (Wemaere et al. 2008)

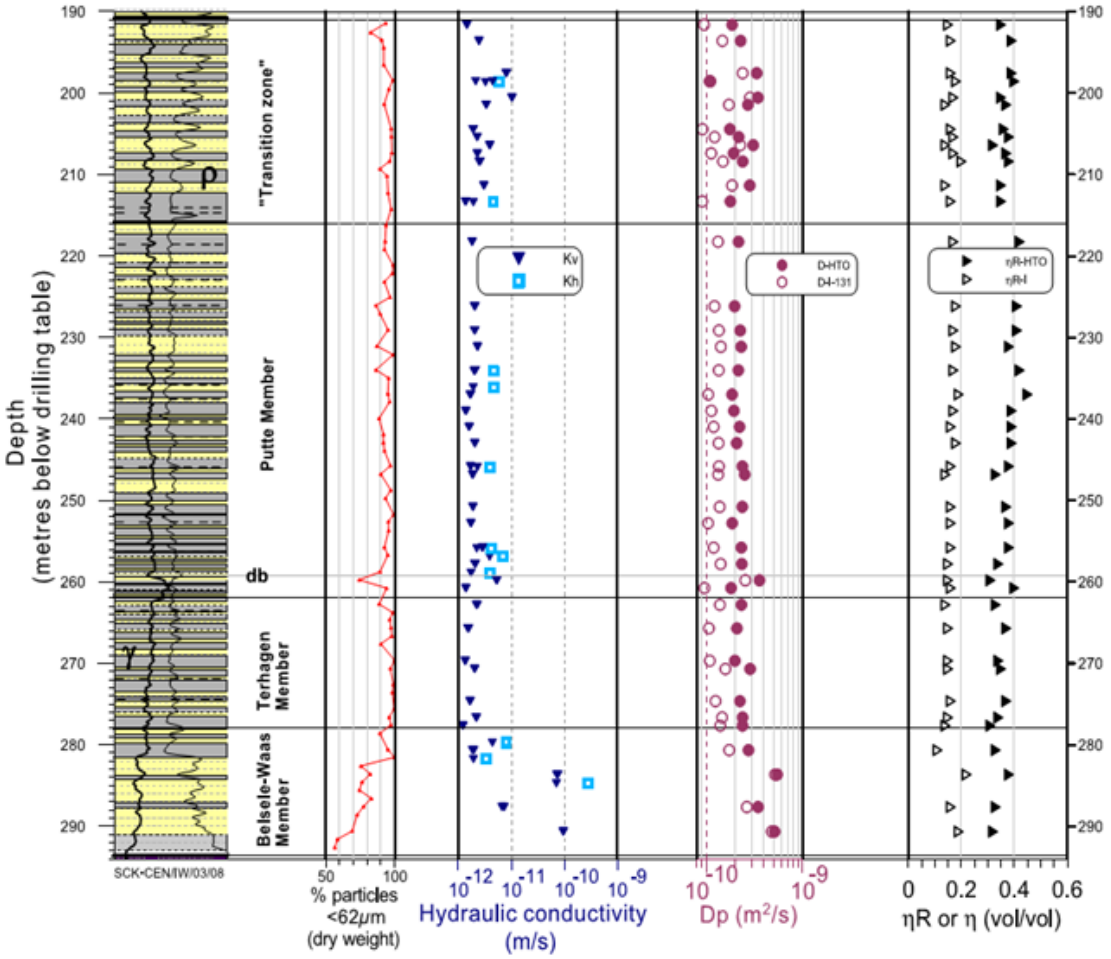

Figure 4-7. Hydraulic conductivity measured in all the formation (Aertsens et al. 2004)

Table 4-4 presents some values of the hydraulic conductivity and their order of magnitude from different scientific publications. It has to be indicated that the measurements done by Aerstens et al. (2004) using the pulse injection method did not involve any mechanical coupling. Indeed, no confining pressure was used to perform these tests whereas the effect of a mechanical load can reduce the value of the permeability due to change in the size of voids and hence in porosity. Knowing the different consolidation parameters obtained by oedometer tests, Horseman et al. (1987) found similar values than observed by the previous authors, considering an effective stress of 2.5 MPa similar to the in-situ stress. Lima (2011) estimated the permeability of the Boom Clay from MIP results by an equation proposed by Garcia-Bengochea (1979) in Romero (1999). The values found by this back-analysis were in the order of magnitude of the previous method. The water permeability was also determined experimentally in this study with the controlled-gradient permeability test and the measurement of vertical and horizontal water permeability in the purpose of verifying the anisotropy at sample scale. Once again, the values found were compatible with values determined in the previous studies.

The storage coefficient is the volume of water that an aquifer releases from or takes into storage per unit surface area per unit change in head. This value was determined by Horseman et al. (1987) from the consolidation parameters. Coll (2005) performed pulse test on Boom Clay samples and found similar values.

A critical review of the laboratory and in situ measurements can be found in Yu et al. (2013).

Table 4-4. Hydraulic properties of Boom Clay

	Bernier et al. 2007a	**Aertsens et al. 2004**	**Wemaere et al. 2008**	**Horseman et al. 1987**	**Lima 2011**
Hydraulic conductivity, k (m/s)	$2 - 4 \cdot 10^{-12}$				$1.5 - 1.8 \cdot 10^{-12}$
Vertical hydraulic conductivity, k_V (m/s)		$2.3 \cdot 10^{-12}$	$3 \cdot 10^{-12}$	$2\text{-}3.5 \cdot 10^{-12}$	$2.3 \cdot 10^{-12}$
Horizontal hydraulic conductivity, k_H (m/s)		$4.6 \cdot 10^{-12}$		$5.5 \cdot 10^{-12}$	$4 - 4.5 \cdot 10^{-12}$
Specific storage coefficient (m^{-1})				$1.2 \cdot 10^{-4}$	

4.1.1.1 Hydro-mechanical behaviour of the host claystone

Since the operational start of HADES URF early in the 80s, many laboratory tests and in situ testing have been performed to understand the Boom Clay THM behaviour, among which triaxial and oedometer tests. Triaxial tests permit to determine deviatoric behaviour and then the strength parameters while oedometer tests are more focused on the volume change behaviour. Clay samples have been studied in conditions as close as possible to their natural state around the HADES URF. As re-saturating Boom Clay samples at low confining pressure induces an important swelling which affects the microstructure and thus modifies clay properties (Rousset 1988, Coll 2005, Sultan 1997), Le (2008) suggested saturating Boom Clay at a confining pressure close to the in situ state of stress to minimise this swelling and disturbance of the clay. These laboratory test protocols are detailed in section 0.

The Boom Clay behaviour is characterised by a non-linear stress–strain response. Although there is some scatter in the results, laboratory tests showed a trend of stiffness variation with strain level as illustrated by Figure 4-8: its tangent stiffness at 0.01% deformation may be one order of magnitude larger than that at 1% deformation.

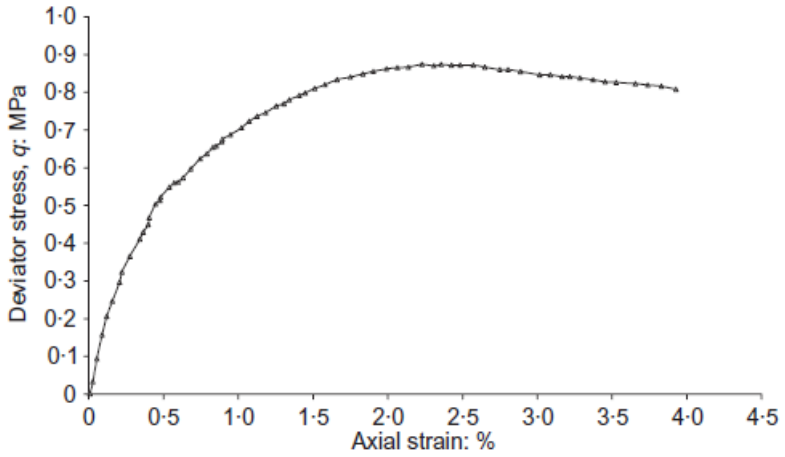

Figure 4-8. Example of the stress–strain data from the drained triaxial compression tests (Bernier et al. 2007a)

The elastic properties which govern the clay behaviour in the reversible domain of deformation have been determined with triaxial tests. Table 4-5 summarises the values found by precedent studies. In general the values are of a few hundred of MPa which is high for a classical soil but low for a rock. All these values come from experimental results except the value by Bernier et al. (2007a) which was deduced by back-analysis of the in-situ measurements during the excavation of the Test-drift obtained by Mair et al. (1992).

Table 4-5. Elastic properties of the Boom Clay in the large deformation domain for different studies

Reference	Tangent elastic modulus (MPa)	Secant elastic modulus (MPa)
Ouvry 1983	322	68
Horseman et al. 1987	152	197
Le 2008	120 -351	
Coll 2005	75 -230	
Bernier et al. 2007	300	

The value of the Poisson's ratio ranges from 0.125 (Bernier et al. 2007) to 0.15 (Horseman et al. 1987).

The uniaxial compressive strength (UCS) is determined with a triaxial cell without any confining pressure. For the Boom Clay, this parameter is not well documented. However, Coll (2005) determined the UCS on Boom Clay samples from a depth of 223 m below the surface and found a value of 2.5 MPa. Bernier et al. (2007a) reported a value of 2 MPa.

As for most of the clay and claystone, the shear strength of the clay is determined through triaxial tests at different confining pressures. Such tests have been performed for four decades starting from De Beer et al. (1977). These results were mostly obtained through undrained tests as a consequence of the very low permeability. The monitoring of the pore water pressure permits to calculate the mean effective stress and to interpret the tests in terms of effective parameters. Figure 4-9 presents classical results of an undrained test performed on Boom Clay sample (Lima 2011). The clay was tested at very low confining pressure representative of an overconsolidated state. As a consequence, the deviatoric behaviour presents a peak before a decrease (strain softening) till a residual strength (Figure 4-9, left). Figure 4-9 (right) presents the stress path in the plane of the mean effective and deviatoric stresses during undrained tests for overconsolidated clay samples. The very low compressibility of the clay-

water mixture implies that the volumetric deformation of the sample can be assumed theoretically as null. The representative stress path for such kind of tests is almost a straight line.

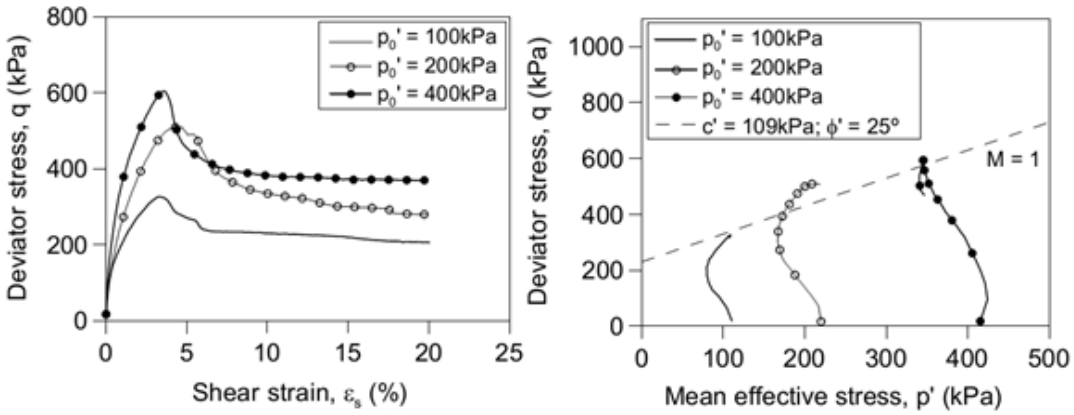

Figure 4-9. Typical response of the Boom Clay during an undrained triaxial tests and determination of the drained parameters (Lima 2011)

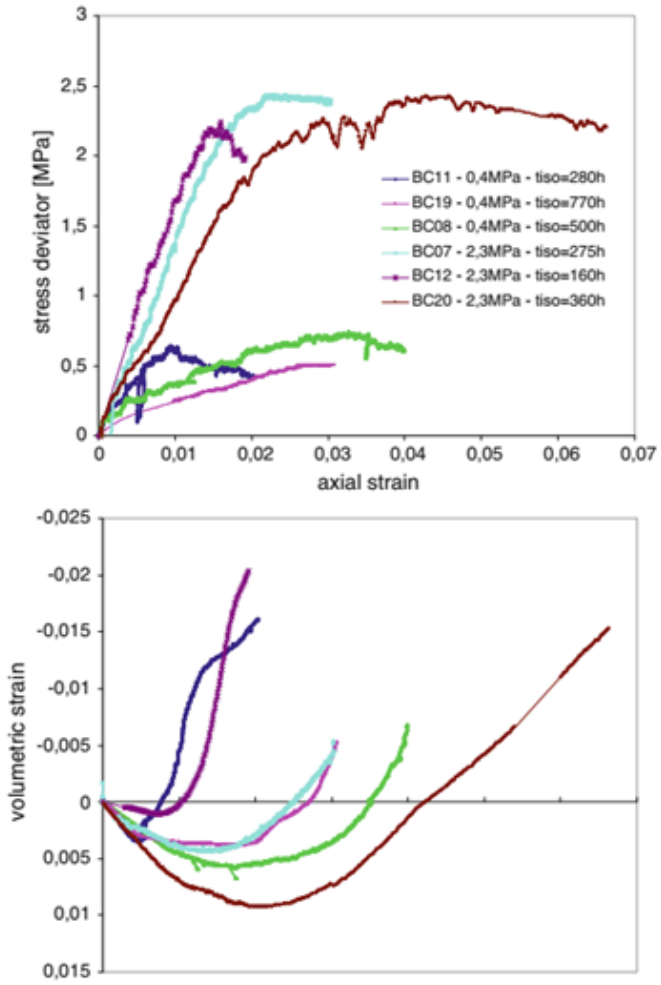

Figure 4-10. Drained triaxial tests performed with different confining pressure on Boom Clay samples (Bésuelle et al. 2014)

Another example of triaxial tests on Boom Clay is presented in Figure 4-10. These results come from triaxial tests performed at several confining pressures and at different shearing rates in drained conditions. They were obtained by Coll (2005) and reinterpreted by Bésuelle et al. (2014). The tests at a confining pressure of 2.3 MPa (BC07 and BC20) were sheared at a constant rate of $\dot{\varepsilon}_a = 1.10^{-7}\mathrm{s}^{-1}$ while BC12 was sheared at a strain rate 100 times higher. It was observed that the difference in results between the two shear rates was not significant in this case.

Figure 4-11 presents all the results in the (*p', q*) plane of the drained and undrained triaxial tests conducted on Boom Clay for decades. The knowledge of the pore water pressure permits to find the value of the mean effective stress for the ones performed in undrained conditions. In this figure, the results are scattered for high confining pressure and a general trend line emerges with difficulty which makes complicated the determination of the strength parameters.

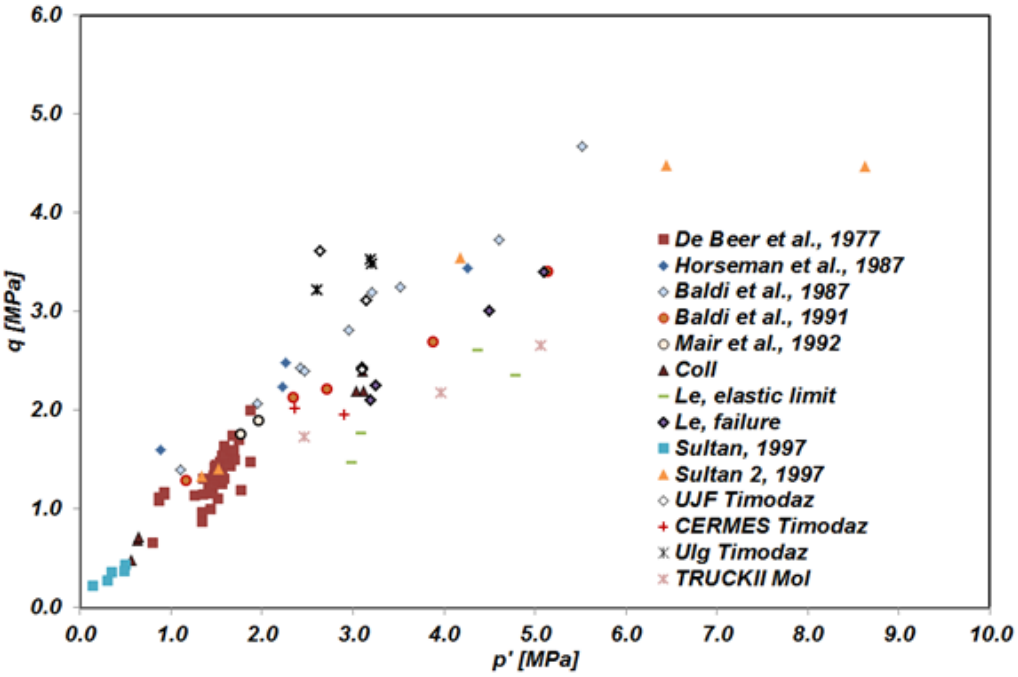

Figure 4-11. Results of almost all triaxial tests performed on the Boom Clay

Table 4-6. Drained strength parameters, drained cohesion and drained friction angle

Reference	Drained cohesion (kPa)	Drained friction angle (°)
De Beer et al. 1977	15	22
Ouvry 1983 (BRGM)	129	16
Coll 2005	130	18
Le 2008	126	16
Lima 2011	109	25
Bernier et al. 2007a	300	18

Table 4-6 gives the values of the drained cohesion and the drained friction angle of the Boom Clay deduced from all the previous studies. Bernier et al. (2007a) estimated the different parameters with an interpretation of the tests of Baldi et al. (1987, 1991) and Mair et al. (1992) based on a Mohr-Coulomb criterion. Figure 4-12 presents the results of the experiments driven by Baldi et al. (1987, 1991). There was a good concordance between the failure point and the yield limit. Baldi et al. (1987)

tested samples at 240 m while in 1991 the depth was 223 m below the surface. There are differences of mineralogy of the clay between both depths and this could explain the variations observed. At a depth of 240 m the content in sand and silt was higher than at 223 m. The higher the sand or silt content, the higher the friction angle. These differences highlight also the inhomogeneity of the clay across the formation and have to be considered for a good interpretation of the results.

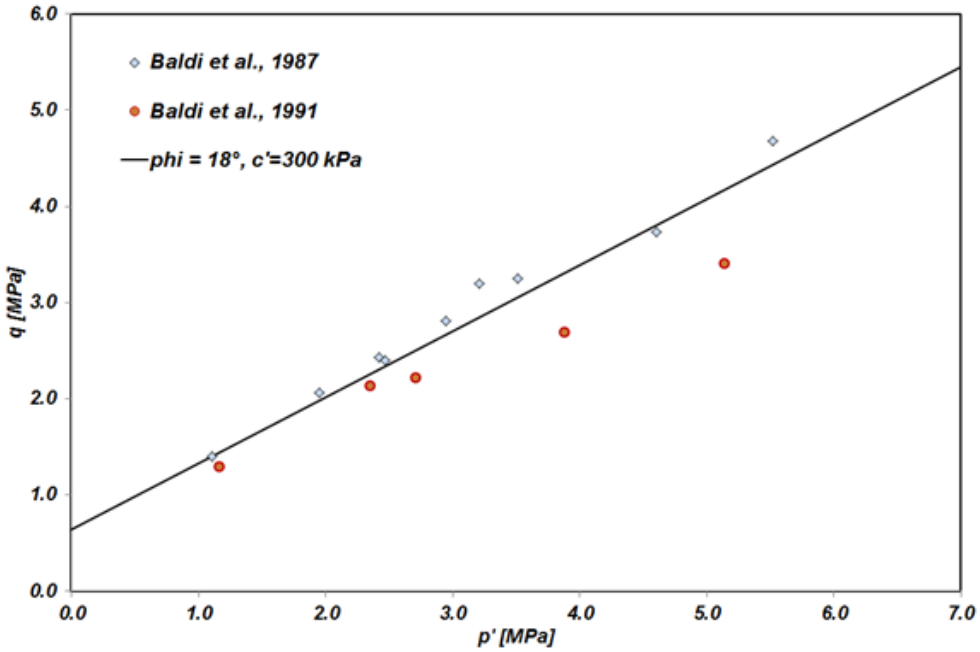

Figure 4-12. Failure point in the (p', q) plane for the triaxial tests of Baldi et al. (1987 and 1991) at 240 m and 223 m respectively

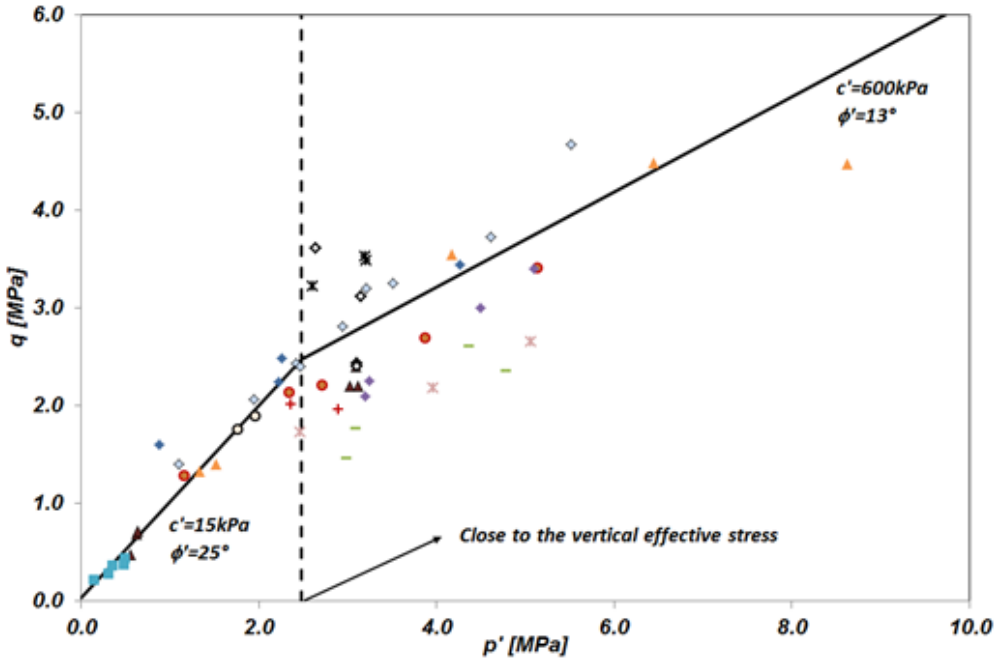

Figure 4-13. Decomposition in two set of the shear strength parameters

Some authors (Petley 1999) proposed for mudrocks and clays to not consider a linear criterion but a non-linear one. Following this idea, a bilinear curve was chosen decomposing the (p', q) domain in two parts; a first one below 2.5 MPa and a second one above this value (Figure 4-13, Table 4-7). This decomposition highlights the nonlinearity of the Boom Clay failure criterion. With this decomposition, the threshold seems to be close to the in-situ state of stress. At this time no clear theories explain this observation which remains an open issue.

Table 4-7. Value of effective cohesion (c') and effective friction angle (ϕ') following the decomposition in two domains of the yield surface

	c' (MPa)	ϕ' (°)
Confining pressure <2.5 MPa	0.015	25
Confining pressure >2.5 MPa	0.6	13

Figure 4-14 presents the comparison between the yield surfaces obtained taken into account the set of parameters above and the set of parameters defined by Bernier et al. (2007a). Near the in-situ stress conditions, it can be noticed that the different yield surfaces are close to each other. Considering low stress or high stress level, the criterion defined by Bernier does not significantly diverge from the observed shear strength.

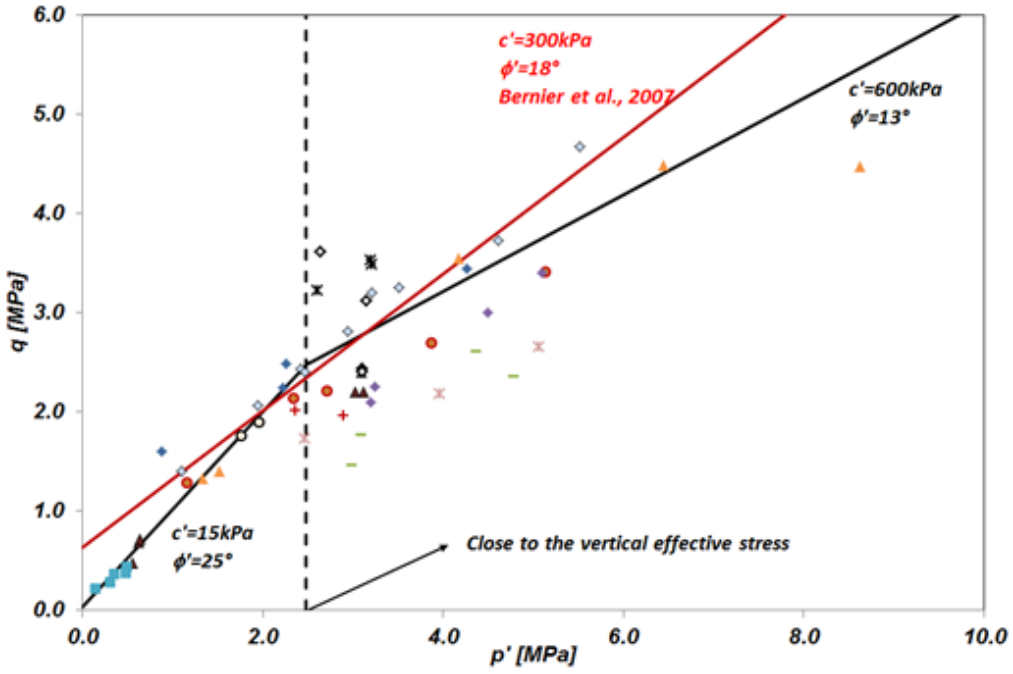

Figure 4-14. Comparisons between different yield surfaces taken into account different set of parameters

In the framework of the critical state soil mechanics, the strength parameter is the slope of the critical state line, M. When the clay is normally consolidated, the critical state parameter is directly proportional to the ratio between the deviatoric stress and the mean effective stress. The values determined by different studies are given in Table 4-8 and show a good homogeneity for the majority of the studies except for the study of Baldi et al. (1991) where a lower value was found. The comparison between the mineralogical content of the Boom Clay at a depth of 223 m and 240 m below the surface shows a higher content in silt particles at a depth of 240 m, which can be the cause of the variation.

Most of these values hold for tests in compression. The mechanical behaviour in extension may be different as it was observed in Mair et al. (1992) who found that the value of the critical state parameter was lower, i.e. *M = 0.65.*

Table 4-8. Summary of the critical state parameter *M*

	Critical state parameter, *M*
Horseman et al. 1987	0.81
Mair et al. 1992	0.85
Baldi et al. 1987 (240 m)	0.87 – 1
Baldi et al. 1991 (223 m)	0.6

Volume change behaviour

Few authors have studied the volume change behaviour of Boom Clay. Figure 4-15 presents the results of an oedometer test with different loading/unloading cycles performed by Horseman et al. (1987) and modified by Burland (1990). The swelling index (C_s or $\kappa = 0.434C_s$) of the clay was determined from the unloading curve, while the plastic slope (C_c or $\lambda = 0.434C_c$) was obtained from the virgin compression curve. The elastic unloading did not present a linear variation but varied during unloading as it is also observed for other clays such as the Ypresian clays which exhibited an important swelling during unloading (Nguyen et al. 2013).

Table 4-9 presents the values of the different volume change parameters according to different studies. The obtained data present a large inhomogeneity which is explained by the variability of the clay. In this case, a unique set of parameters seems difficult to extract. The tests performed by Sultan (1997) showed very different results in comparison with the other studies. Indeed, the tests were realised on old Boom Clay samples where an important swelling was observed prior to the tests due to the re-saturation and the contact with water, these tests results are assumed to not be representative from the real clay behaviour.

Table 4-9. Volume change parameters, preconsolidation pressure and compressibility (elastic and plastic)

Reference	**Preconsolidation pressure (MPa)**	**κ**	**λ**
Horseman et al. 1987	6 MPa	0.046	0.178
Baldi et al. 1987 (240 m)	5.8 MPa	0.031	0.129
Baldi et al. 1991 (223 m)	6.0773 MPa	0.01279	0.1103
Sultan 1997	0.37 MPa	0.0072	0.0728
Coll 2005	5 MPa	0.075	0.218
Le 2008	5 MPa	0.0145-0.0341	0.077-0.1173

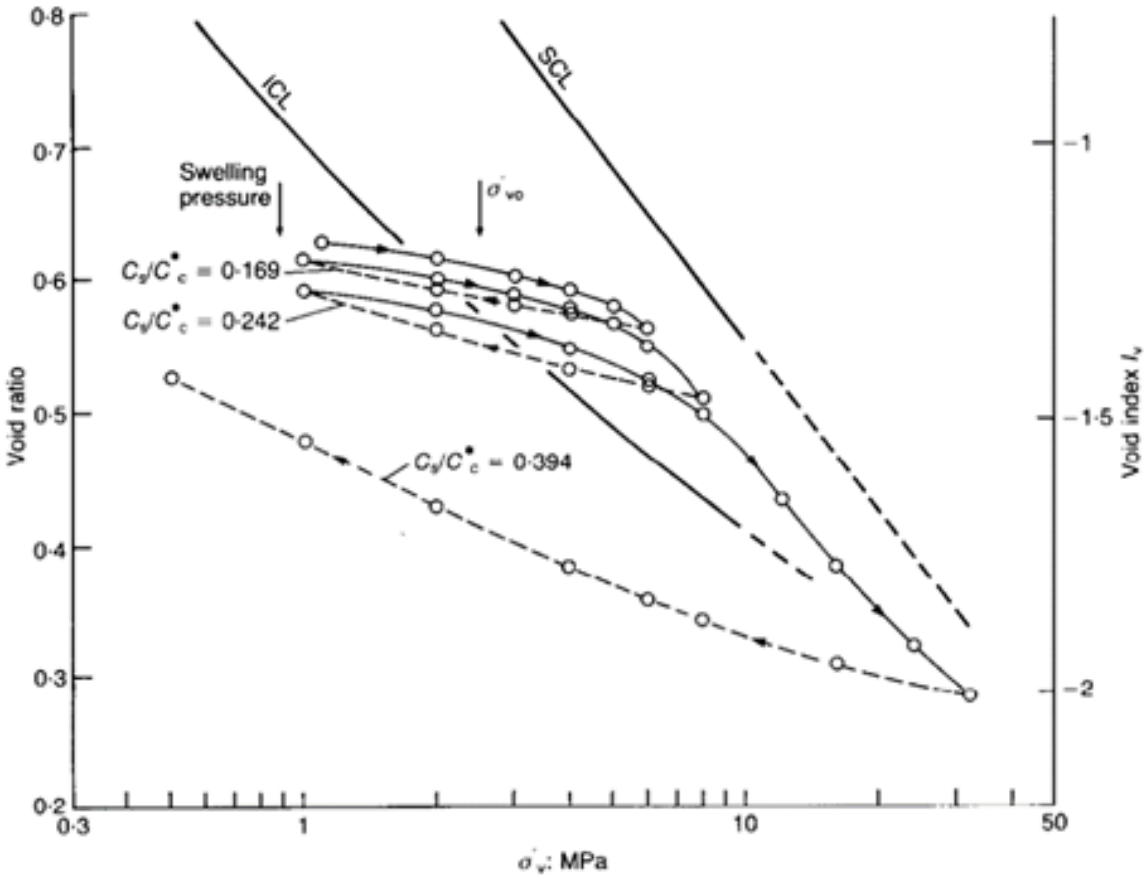

Figure 4-15. Volume change behaviour during an oedometer test on Boom Clay sample. (Burland (1990) from Horseman et al. (1987), SCL: Sedimentation Compression Line, ICL: Intrinsic Compression Line)

Reference mechanical characteristics of Boom Clay

This part presents a short summary of the principal characteristics of the Boom Clay in the purpose of present a useful set of parameters. The elastic properties of the clay may be defined by the following parameters based on Bernier et al. (2007a), keeping in mind that their values depend on the stress levels and on the shear strain. Table 4-10 presents the elastic properties in drained and undrained conditions.

Table 4-10. Elastic properties for the Boom Clay

Drained Poisson's ratio (-)	0.125
Undrained Poisson's ratio (-)	0.4
Drained Young Modulus (MPa)	120-350
Undrained Young Modulus (MPa)	500-900

Concerning the shear strength characteristics, the results of triaxial tests performed over decades show at least two main trends, one related to low confining pressure and the second one to the high pressure, with a threshold about 2.5 MPa. With this decomposition, two sets of parameters have been proposed. Nevertheless, the set proposed by Bernier et al. in (2007a) allows to have a good approximation of the shear strength considering intermediate confining pressure around the in-situ stress. The volume change behaviour presents more scatter in the estimation of the swelling and

plastic indexes defined in the framework of the Cam-Clay model. A range is proposed in Table 4-11, which presents the parameters retained for both shear and volume change behaviour.

Table 4-11. Shear and volume change parameters for the Boom Clay

Drained cohesion (MPa) <2.5 MPa >2.5 MPa	 0.015 0.6
Drained friction angle (-) <2.5 MPa >2.5 MPa	 25 13
Critical state parameter (-)	0.81-0.87
Preconsolidation pressure (MPa)	5-6
Elastic slope, κ (-)	0.0145 – 0.0341
Plastic slope, λ (-)	0.1103 – 0.2558

Long-term volume change behaviour

Deng et al. (2012) performed oedometer tests with the purpose of studying the secondary consolidation behaviour of Boom Clay at Mol and Essen. Figure 4-16 (left) shows the determination of the secondary consolidation coefficient in the Δe–log t (void ratio – logarithm of time) space. Figure 4-16 (right) presents the variation of the secondary consolidation coefficient (C_α) with the applied stress during oedometer tests considering the loading and unloading curves. This coefficient is positive during the loading path and negative during unloading. According to a general classification criterion for clay soils, the Boom Clay has a similar behaviour as shales and mudrocks, with a range from 0.02 to 0.05 (Terzaghi et al. 1996). Deng et al. (2012) studied the secondary compression of the Boom Clay and found an average value of about 0.024.

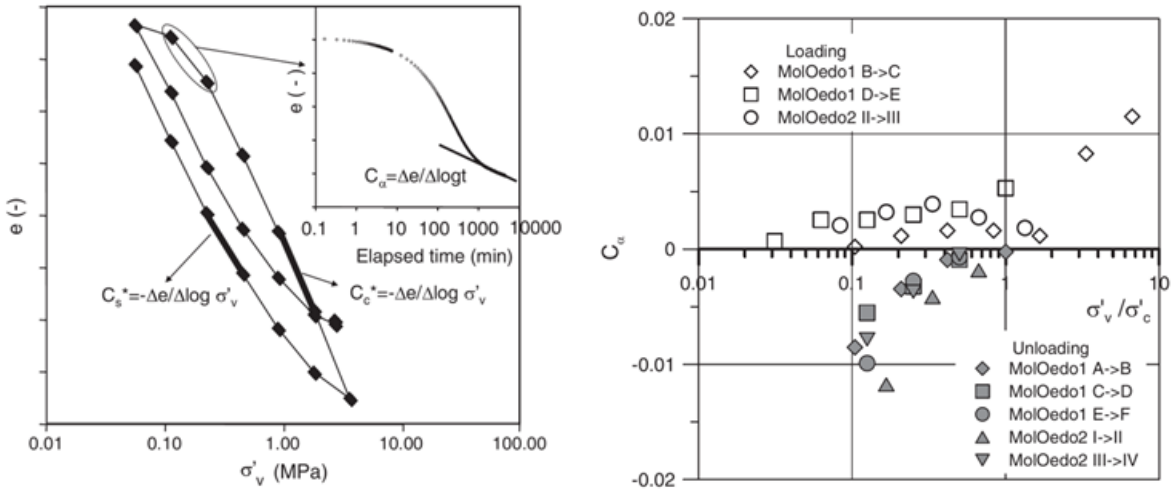

Figure 4-16. Method of determination of the secondary consolidation coefficient (left); Compilation of experimental results determining secondary consolidation coefficient (C_α) for the Boom Clay at Mol as a function of the stresses (right) (Deng et al. 2012)

Long term deviatoric behaviour (creep)

The Boom Clay presents high visco-plastic behaviour, the time related behaviour of the Boom Clay is related to two processes: dissipation of pore water pressure and viscosity of the solid skeleton. A clear

distinction between them by means of laboratory tests is still a challenge issue due to the very low permeability of Boom Clay.

A set of laboratory tests was nevertheless performed under different conditions to investigate the elasto-visco-plastic behaviour of Boom Clay. Besides the long-term oedometer tests as described above, triaxial creep tests under different confining pressure and deviatoric stresses at different temperature, triaxial tests with different shearing rates have been performed during last years. More insight on the creep behaviour of Boom Clay has been gained, however, more systematic test program is still needed to draw a quantitative conclusion.

Figure 4-17 and Figure 4-18 show the triaxial creep tests results performed in two different laboratories at ambient temperature. The creep behaviour has been put in evidence: the steady strain rate increases with the deviatoric stress level as observed for most other clay materials. Under a stress state close to the in-situ one (mean effective stress around 2. 5 MPa, deviatoric stress around 1.5 MPa), the steady strain rate got from these tests for the test duration (about two months for each creep stage) is in order of 10^{-6}/h. This has to be confirmed with more tests results.

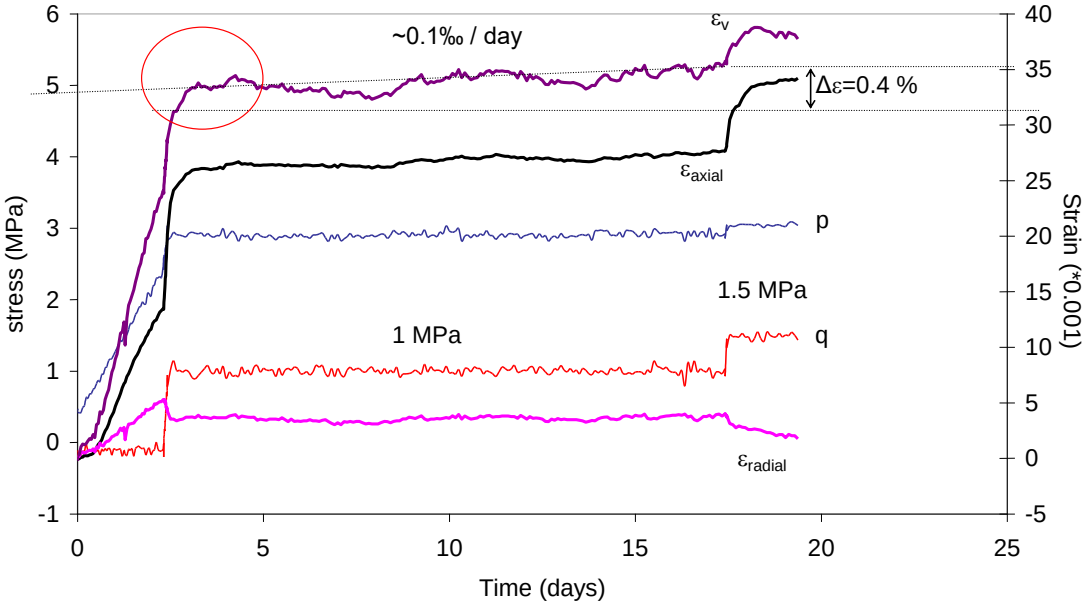

Figure 4-17. Drained creep behaviour of Boom Clay at ambient temperature (σ'_3=2.5 MPa, Test TR03) (Coll et al. 2008)

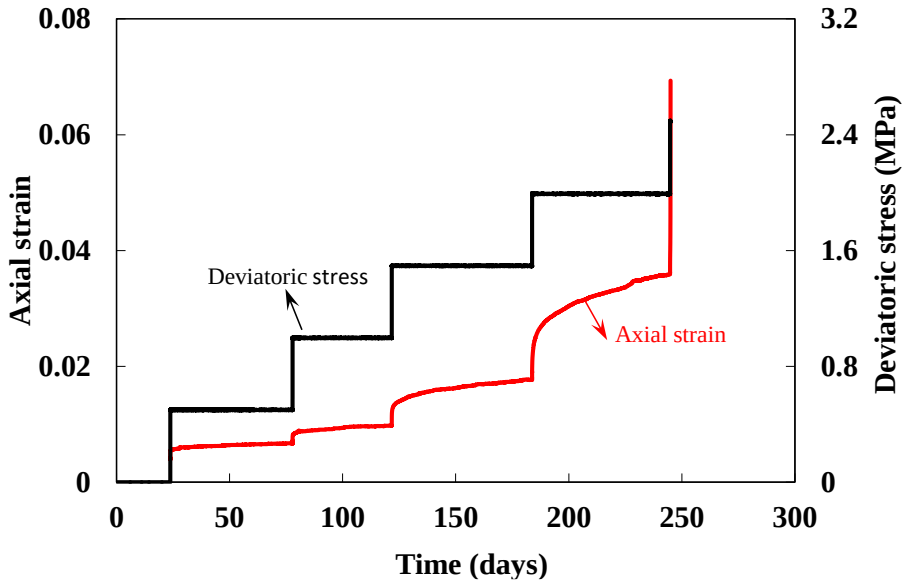

Figure 4-18. Drained creep behaviour of Boom Clay at ambient temperature (σ'_3=2.5 MPa, Test TCP3/LHM45223) (Chen et al. 2017)

Couplings between mechanic and hydraulic properties

Horseman et al. (1987) and Coll (2005) performed series of hydraulic tests on Boom Clay samples at different confining pressures and determined a trend in the evolution of the hydraulic properties with the mean effective stress (Figure 4-19). An increase of the applied load induced a decrease of the hydraulic conductivity.

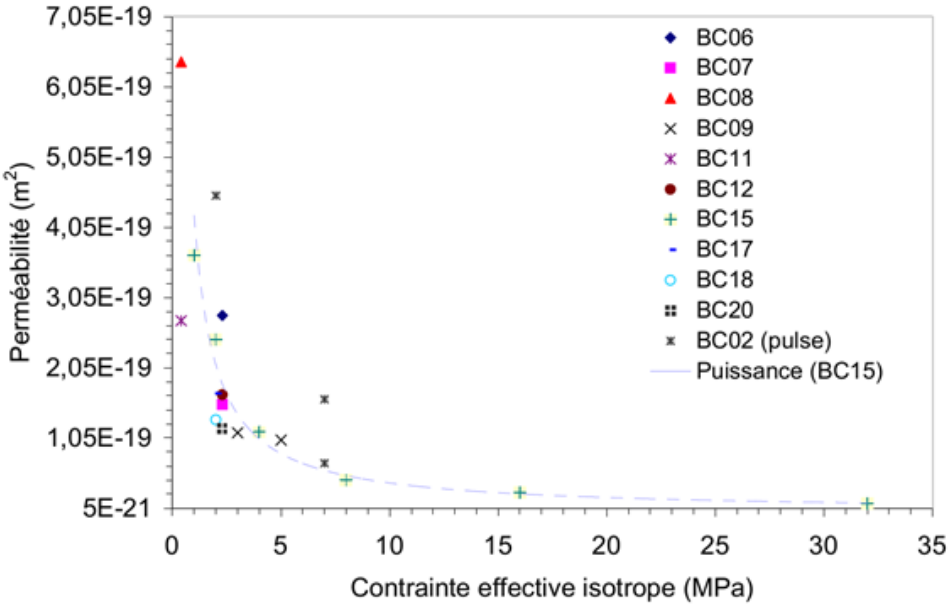

Figure 4-19. Evolution of the hydraulic conductivity with the mean effective stress (Coll 2005)

In addition to the influence of the mean effective stress on the hydraulic conductivity, Coll (2005) studied the effect of the deviatoric stress on this parameter. Even if a discontinuity was initiated in the sample, no clear modification of the hydraulic conductivity was observed. In fact, the permeability was

modified locally around the cracks but this was not observed at the scale of the sample. After shearing, the cracks were characterized by a very thin size which made difficult the description of the porosity along the localised shear band. Monfared (2011) performed also permeability tests before and after shearing and observed that the shear band had no significant effect on the permeability of the sample. Consistently with the results of Coll (2005), very small variations of the permeability were observed. The interpretations given to these results differed in both studies. Coll (2005) assumed that the shear band had a very local and insignificant effect on the global permeability of the sample, while Monfared (2001) made the hypothesis that the absence of permeability variation was a result of the self-sealing behaviour of the clay.

There are not much data dealing with the anisotropic behaviour of Boom Clay. Baldi et al. (1987) compared the calculated and measured volumetric strain during a triaxial test. Later, François et al. (2014) presented the results of a hollow cylinder test on Boom Clay. Different phases of loading and unloading were applied to the sample. Before and after unloading, the sample was submitted to microcomputerized tomography (µCT) and particle tracking to determine the displacement of some specific point. Figure 4-20 presents the convergence of the hole after unloading. It was observed that the convergence of the hole was not homogenous and varied with the direction of the bedding plane, which resulted in anisotropic behaviour and the final eye-shaped of the hole. Figure 4-21 presents the analysis of the radial displacement according to the different directions. It was observed that the radial displacements were not uniform, highlighting the anisotropic response of the clay. The higher displacement was parallel to the bedding plane, while the lowest one was perpendicular to the bedding.

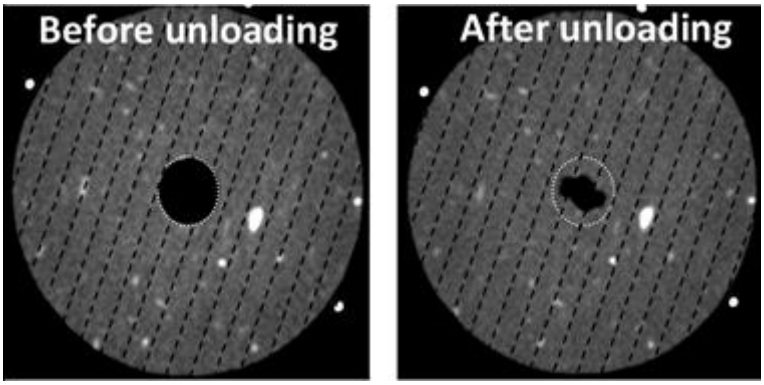

Figure 4-20. Hollow cylinder made in Boom Clay, before the loading and after the unloading (Labiouse et al. 2014)

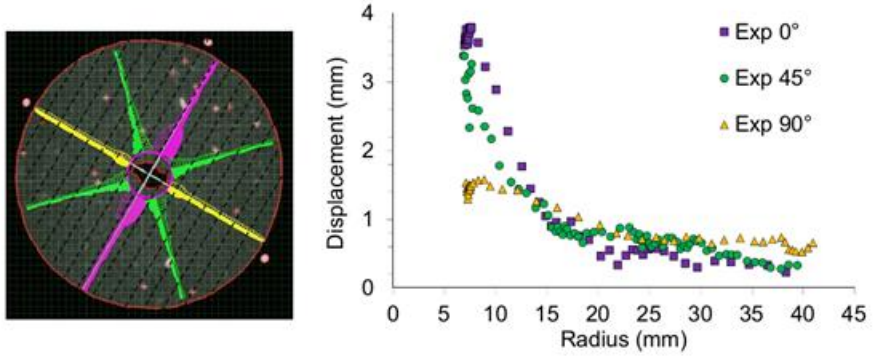

Figure 4-21. Results of the hollow cylinder test performed at EPFL with the observed anisotropy of the radial convergence of the clay (François et al. 2014)

4.1.1.2 Hydro-mechanical behaviour of the fracture/damage claystone

Laboratory tests were performed to study the self-sealing capacity of the Boom Clay. During the SELFRAC project (Bernier et al., 2007b), a fracture was initiated in a Boom Clay sample. The sealing or healing properties were then analysed with different pore water chemistry. The Boom Clay showed very good capacity of self-healing. Figure 4-22 presents the evolution of a fractured Boom Clay sample before and after re-saturation. After a certain time, the fracture was no more visible. The elasto-plasticity/viscosity of the clay skeleton and/or the swelling capacity played a role but this phenomenon is not fully understood yet.

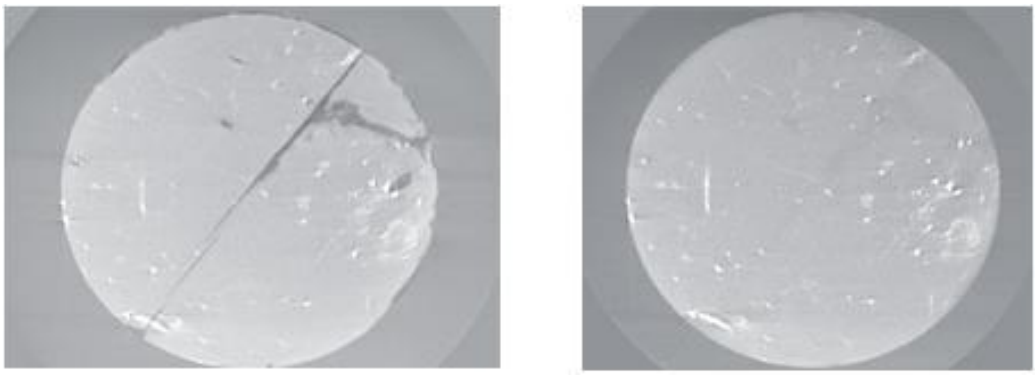

Figure 4-22. Visualisation by µCT technique of the sealing process of a fracture in a Boom Clay sample after saturation (Bernier et al. 2007b)

Another way to study the self-sealing capacity of the clay is to perform permeability tests with damaged clay and to follow with time the evolution of the hydraulic conductivity. Some studies showed that the permeability was not affected by the shear band (see above, Coll 2005, Monfarred 2011). This last author concluded that it was a good sign of self-sealing capacity of the clay. Van Geet et al. (2008) performed permeameter tests on a fractured Boom Clay sample and monitored the evolution of the hydraulic conductivity with time to highlight the sealing process (Figure 4-23). It was observed a decrease of the hydraulic conductivity with time indicating the sealing process from a hydraulic point of view.

Chen et al. (2014) showed with experimental tests that there is no positive or negative impact of the temperature on the sealing/healing properties of the clay by exposing Boom Clay samples (damaged and intact sample) to a heating cycle from 20°C to 80°C under constant volume conditions in a permeameter cell. Figure 4-24 presents the pictures resulting from the hydrostatic test on hollow cylinder of Boom Clay submitted to loading and heating cycle (from room temperature to 60°C). The initial 6-mm diameter hole was closed and sealed indicating that no preferential flow path was anymore possible through it. The hole was not reopened by this loading and heating cycle. In addition, the permeability was not modified under the heating cycle with the same loading condition. A few days after the dismantling of the sample, the hole, which was not visible during the test, reappeared. This confirms the conclusion of the SELFRAC project: the original mechanical properties cannot be fully recovered and only partial healing can be observed.

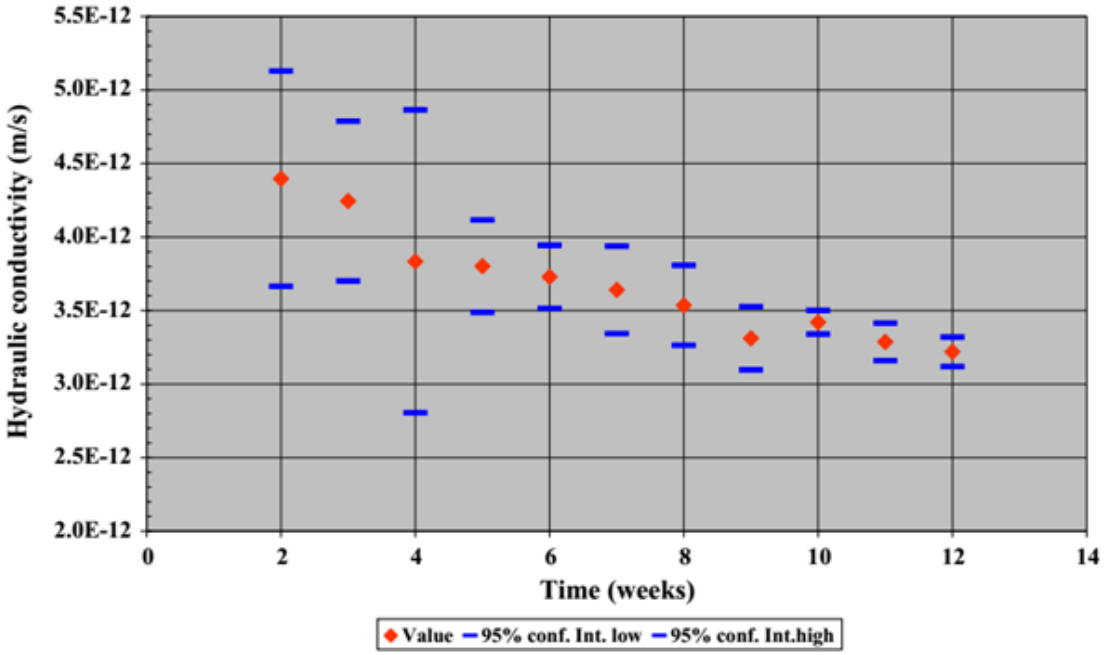

Figure 4-23. Weekly evolution of the hydraulic conductivity in a fractured Boom Clay sample. Permeameter test with synthetic Boom Clay water as pore water solution (Van Geet et al. 2008)

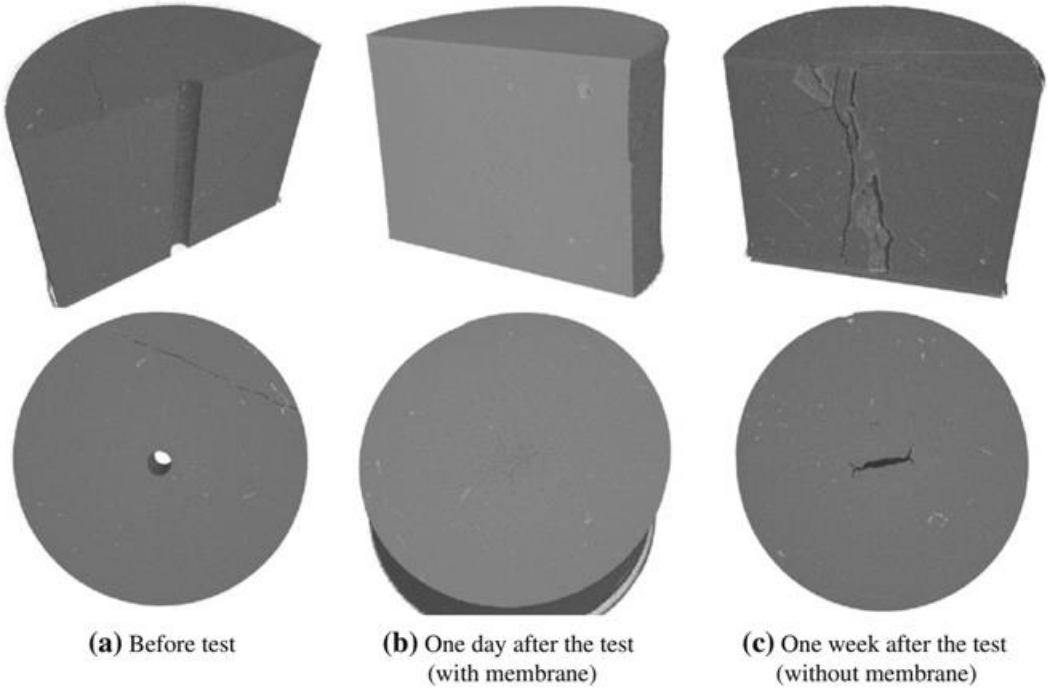

Figure 4-24. µCT pictures of Boom Clay sample in hydrostatic test (Chen et al. 2014)

4.1.1.3 *Thermo-hydro-mechanical behaviour*

The effect of the thermal phase on hydro-mechanical behaviour of the Boom Clay has been studied in order to evaluate the consequences of the temperature increase in the surrounding clay of a disposal

on 1) the clay behaviour around galleries, 2) the extent of the excavation damaged zone (EDZ), and 3) the clay properties within that EDZ. The THM behaviour of clay is characterised by several coupling processes. On the basis of these couplings, the main characteristics of THM behaviour of the Boom Clay are detailed hereafter.

Thermal properties

The thermal dissipation in a medium can be defined by two parameters, the thermal conductivity, which defines the dissipation of heat, and the volumetric heat capacity, a storage parameter. Djéran et al. (1994) performed laboratory experiments with a needle probe to determine the thermal conductivity (λ) and the volumetric heat capacity of the clay. Buyens & Put (1984) estimated the different thermal parameters by back calculation of an in-situ experiment in the quarry of Terhagen. Later, in-situ heater tests, called ATLAS, were conducted in the HADES URF, allowing the determination of the thermal conductivity in different directions. All these values are summarised in Table 4-12.

Table 4-12. Thermal properties of the Boom Clay

	Thermal conductivity (W/m°C)	Volumetric heat capacity (J/m^{3}K)
Buyens & Put (1984)	1.69	$2.83 \cdot 10^6$
Djéran et al. 1990	1.44	$3.27 \cdot 10^6$
Charlier et al. 2010 (TIMODAZ project)	1.25 (horizontal direction) 1.70 (vertical direction)	$2.84 \cdot 10^6$

These results show that depending on the test conditions, different values of the thermal conductivity can be found when comparing the laboratory and the in-situ tests. Djéran et al. (1994) explained these differences by the induced swelling due to the removal of the in-situ stress that can disturb the sample and modify the contact between the clay particles. As a consequence, a possible modification of the density may occur resulting in a change in the thermal conductivity.

Dao (2015) measured the thermal conductivity in clay samples located at different distances from the wall of the connecting gallery. A decrease of the thermal conductivity in the first metres from the wall was observed. The interpretation of this decrease is still under investigation and may be linked to a modification of the fundamental properties of the clay induced by excavation and so by the release of the confining pressure.

Mechanical behaviour of the clay upon heating

The short-term behaviour of clay submitted to heat is mainly governed by the coupling between the solid skeleton, the clay particles and the fluid phase. The volumetric dilation of a solid is much lower than that of the fluid phase filling the pore space. As a consequence, the fluid phase dilates more than the solid phase during heating and occupies more space, generating excess pore water pressure. This excess pressure may lead the sample to failure. Figure 4-25 (left) shows results of an undrained heating test on Boom Clay where the sample was heated under undrained conditions under a deviatoric stress. Figure 4-25 (right) presents the excess pore water pressure induced by the undrained shear test with and without the effect of heating. Two samples were sheared under normally consolidated conditions. At one moment, the load was stopped for one of the two samples and heating at increasingly higher temperature began. Because of the undrained conditions, the generated excess pore pressure conducted the stress path towards the critical state line, characterising the plastic behaviour and the failure of the sample. Monfarred (2011) showed that an undrained heating can be responsible of the reactivation of a pre-existing shear band during thermal pressurisation.

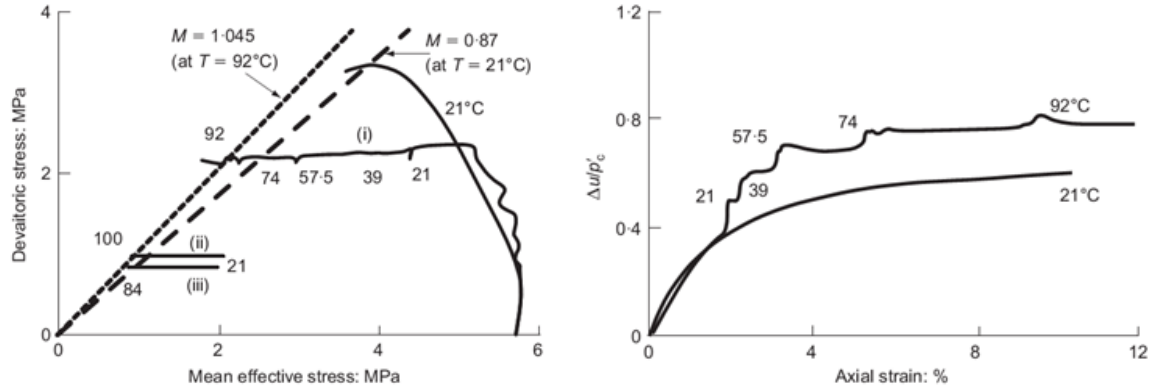

Figure 4-25. Stress path in the (*p'*, q) plane during undrained thermal failure for Boom Clay (left); Excess pore water pressure generation (right) (Hueckel et al. 2009)

The hydro-mechanical behaviour of Boom Clay submitted to heating/cooling phases has been studied for a long time (Baldi et al. 1987, 1988, 1991; Sultan 1997). The main observations of the clay upon heating may be summarised as follows:

- A contractive and irreversible volume change for normally consolidated or slightly overconsolidated clay;
- Dilation followed by an irreversible volumetric deformation in contraction;
- A decrease of the preconsolidation pressure.

This contractive behaviour upon heating is quite unusual for a material. Following different hypothesis, the contractive volume change may be explained by a rearrangement of the forces between the platelets to sustain the stress. Figure 4-26 presents drained heating tests on Boom Clay samples at different confining pressures. The contractive/dilative behaviour may be seen in both cases. For normally consolidated and slightly overconsolidated samples, the behaviour remains contractive during the heating phase.

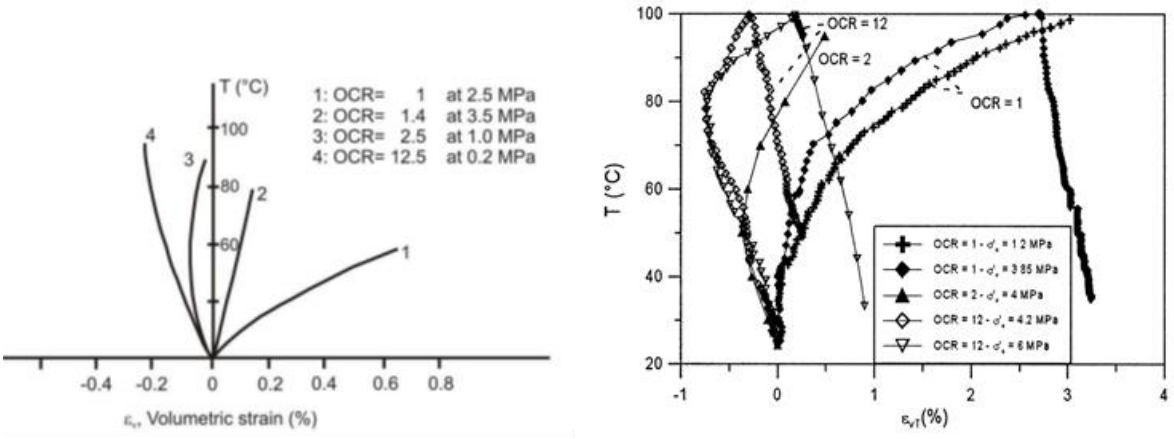

Figure 4-26. Drained heating tests on Boom Clay samples at different confining stresses after Baldi et al. (1991) (left) and Sultan (1997) (right)

In addition of this dilative/contractive behaviour, clayey soils undergo variation of their elastic limit with temperature. In the case of fine grained soils, the preconsolidation pressure decreases with the

increase in temperature. This is shown in Figure 4-27, which shows the evolution of two oedometer tests, at ambient temperature (left) and 80°C (right).

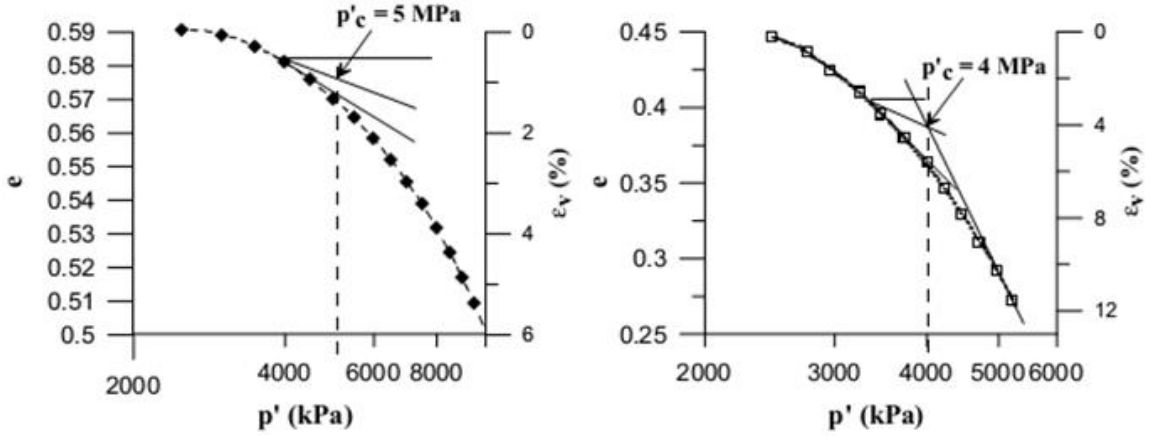

Figure 4-27. Preconsolidation pressure of Boom Clay samples at ambient temperature (left) and 80°C (right) (Le 2008)

Moreover, when a clay sample is submitted to a temperature increase, an overconsolidation effect can occur. Figure 31 presents such kind of effect where it can be seen the evolution of the void ratio as a logarithmic function of the effective stress when the clay is heated at a constant pressure and then reloaded at high temperature. It is observed that the slope of the reloading path (at 70°C) changes before coming back to the previous slope indicating that an overconsolidation process occurs.

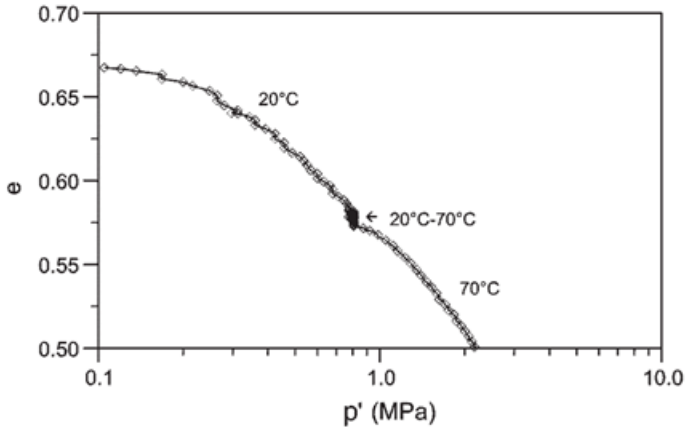

Figure 4-28. Over consolidation effects observed on Boom Clay during isotropic compression (Cui et al. 2000)

Thermo-hydraulic coupling behaviour

When the clay is heated, in the short term excess pore water pressures are generated due to the different thermal dilation coefficients of water and solid and may be dissipated according to the drainage capacity of the clay. The hydraulic conductivity is also affected by temperature, and more specifically, the viscosity of water decreases with the increase of temperature. As a consequence, the hydraulic conductivity will normally increase with temperature (e.g. Delage et al. 2000, Lima 2011). It is important to stress that the change in water viscosity with temperature affects the hydraulic conductivity of the clay, but not its intrinsic permeability.

The temperature may influence the water retention properties as shown during the TIMODAZ project. Salager et al. (2011) presents a comparison between the retention curves obtained at two different temperatures (Figure 4-29). The water retention capacity decreased with temperature: the air entry value determined at ambient temperature (3 MPa) decreased to 1 MPa at 80°C.

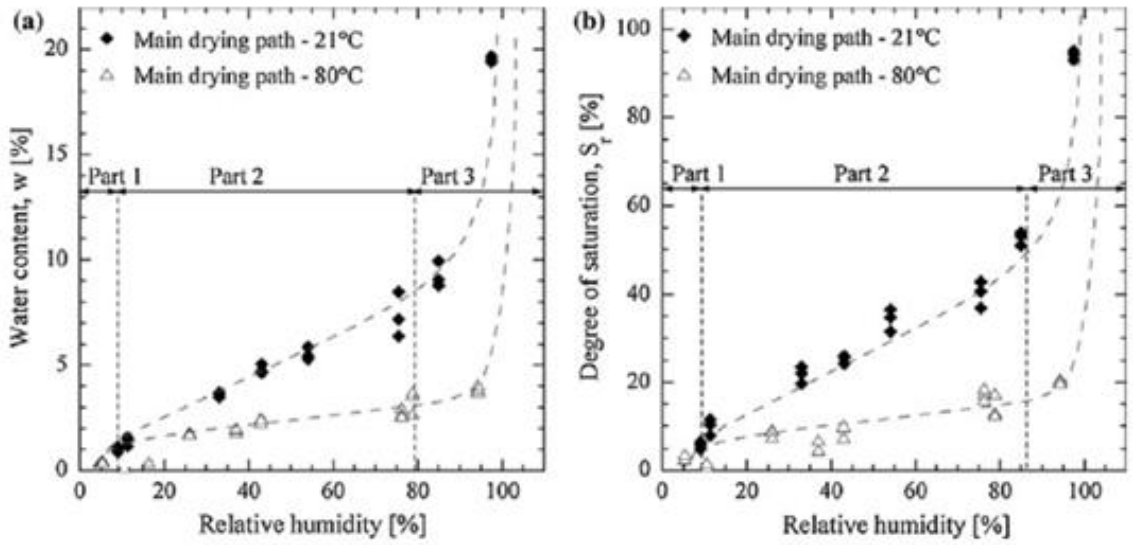

Figure 4-29. Water retention curves at different temperature (21°C and 80°C) for the Boom Clay (Salager et al. 2011)

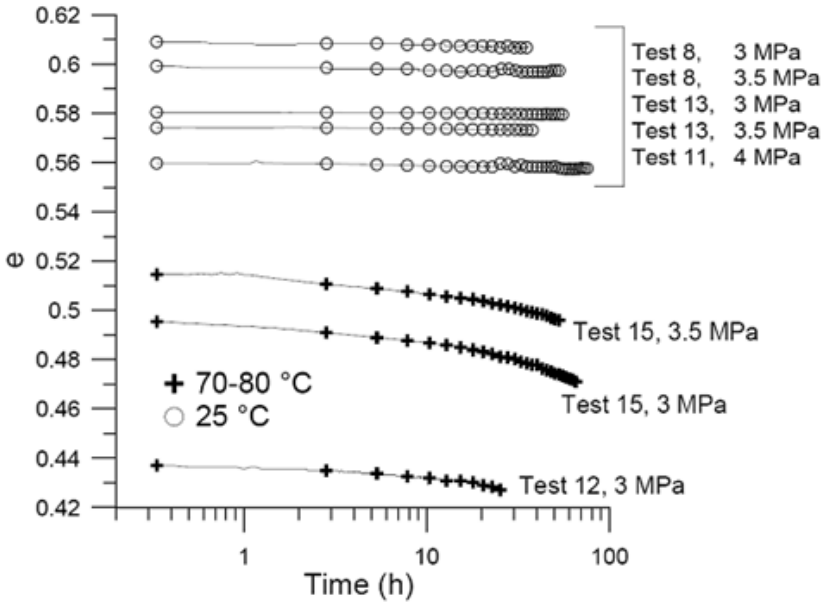

Figure 4-30. Volumetric deformation under constant effective stress at constant temperature as a function of time (Cui et al. 2009)

Triaxial tests were performed to study the influence of the temperature on the creep effect. Djéran et al. (1994) performed these tests and showed that at high temperature the rate of creep seems to increase. The clay became more ductile and viscous with the increase of temperature. The thermal effect on the secondary compression was analysed by Cui et al. (2009). With the increase of

temperature, the strain rate increased more with time than at ambient temperature, i.e. the consolidation rate increased with temperature. Figure 4-30 presents a comparison between the secondary compression at ambient and at high temperature.

4.1.1.4 Open issues on the Boom Clay THM behaviour

The laboratory test programme summarised above mainly investigated the THM behaviour of the Boom Clay as isotropic. However, some few tests and the back-analyses of the observed pore-water pressure variations in the far field of the HADES URF galleries during excavations and around the in-situ heater tests ATLAS and PRACLAY (see section 4.2.1) support the idea that the THM behaviour of the Boom Clay is anisotropic. These last analyses reveal notably that perturbations in the far field – where deformations are small– can be much better represented by models when using different Young's moduli along the vertical and horizontal directions, with values generally larger than those summarised in Table 4-6. Additional laboratory tests are still needed to better characterise this transversely anisotropic behaviour.

Furthermore, this experimental programme mainly deals with Boom Clay samples taken around the HADES URF. Further studies are still needed to characterize the THM behaviour of Boom Clay at other depths and/or other locations in the Boom Clay formation.

4.1.2 COx (ANDRA)

The Callovo-Oxfordian (COx) claystone was deposited 160 million years ago over a period of approximately five million years, in an open and calm marine environment. The formation is surrounded by the Dogger and the Oxfordian limestones. Three major geological units are defined (Figure 4-31):

- the argillaceous unit (UA) at the base is the thickest (thickening from 100 to 120 m from the southwest to the northeast in the zone of interest), the most homogeneous and the richest in argillaceous minerals (more than 40% on average) of the three. It is subdivided into three subunits (UA1, UA2 and UA3) with small and progressive variations. Subunit UA2 corresponds to the stratigraphic level where the clay content is higher and in which the Underground Research Laboratory experiments are carried out
- the transition unit (UT) forms a transition between the mainly argillaceous rocks of the UA and the rocks of the silty-carbonated unit (USC) with the highest carbonate contents (40% to 90%)
- the silty-carbonated unit (USC), 29 m thick, shows considerable vertical petrophysical variability linked with the lithological alternations (marls and calcareous siltstones). It comprises levels with more contrasted and heterogeneous mineralogical composition.

The interval of interest is the UA, that is the level of the URL and the planned repository. Only this unit will therefore be described in detail in this document. The formation dips gently (average 1°) towards the northwest, the bedding plane can therefore be considered horizontal. The main level of the URL is located at a depth of 490 m.

The main mineralogical phases of the COx claystone are shown in Figure 4-32. The clay phase consists mainly of illite and interstratified illite/smectite. The tectosilicates are primarily quartz and feldspar and the carbonates are primarily calcite and dolomite. The RIO (Repere Inférieur Oolithique) layer in the middle of the UA is a 3 to 10-m thick calcareous claystone.

The porosity varies between 14% in the carbonate-rich intervals to 19.5% in the more argillaceous levels; in the UA, the average porosity is 18%. The characterisation of this porosity, performed using several techniques (mercury intrusion porosimetry, helium pycnometer, nitrogen adsorption, water content), indicates that the network of pores mainly comprises meso- and micropores with a predominant pore size of approximately 10 to 30 nm, and that this network has an extremely low

connectivity for pore sizes greater than 40 µm (Figure 4-33). For pores of less than 3-4 nm, the water is influenced by the electrostatic field on the outer surface of the clay minerals, and is therefore relatively immobile. For larger pores, the pore water (free) is not affected by electrostatic interactions and will be mobile for flow.

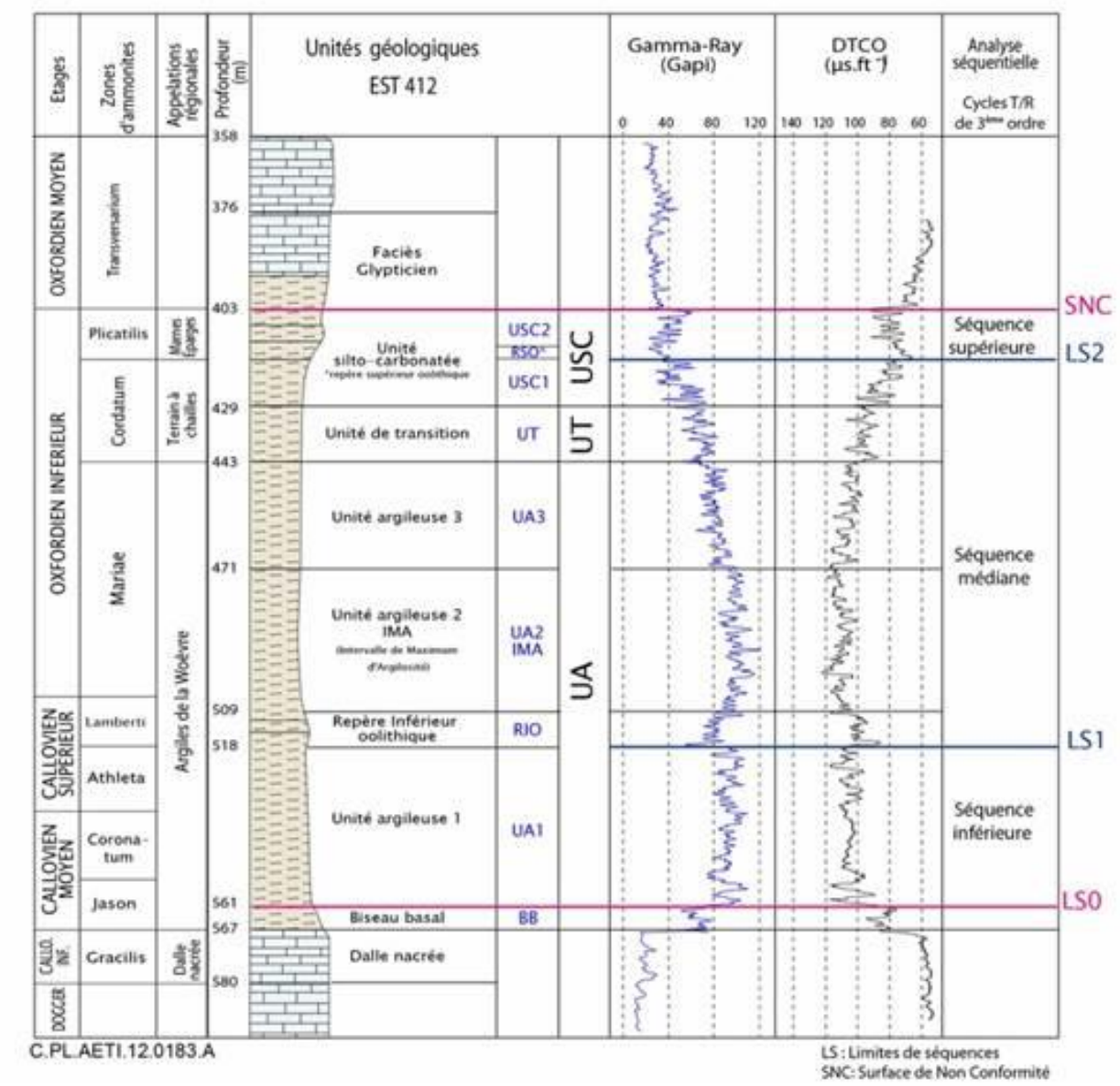

Figure 4-31. Main geological units of the Callovo-Oxfordian claystone: argillaceous unit (UA), transition unit (UT) and silty-carbonated unit (USC)

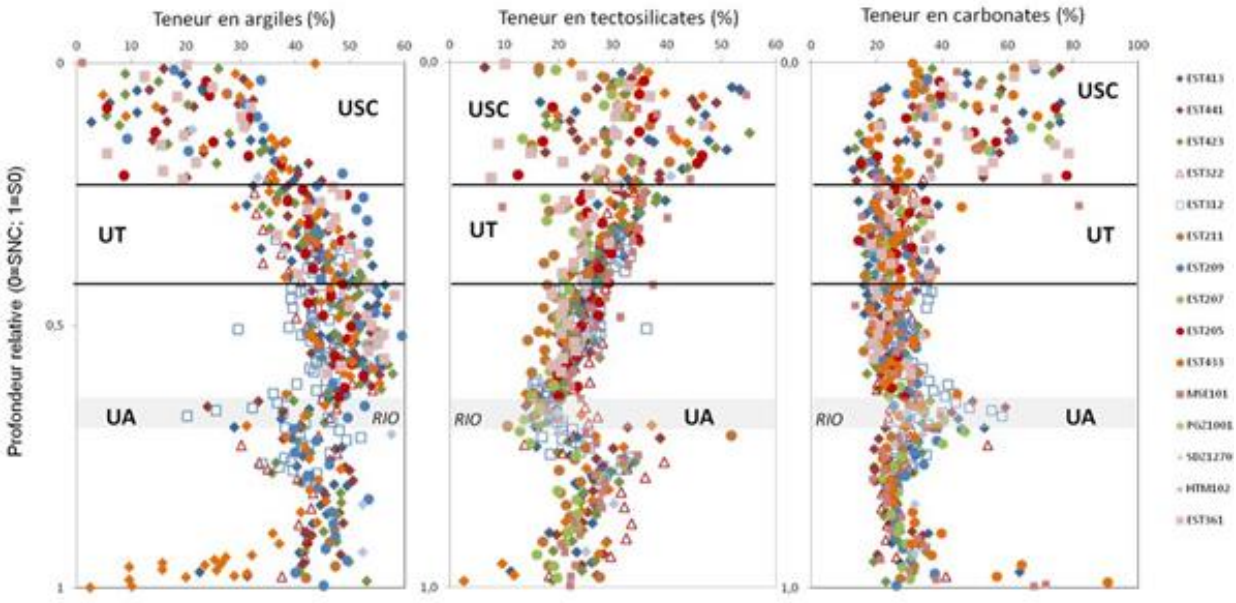

Figure 4-32. Vertical variations in primary mineralogical phases (clays, tectosilicates and carbonates) of the Callovo-Oxfordian claystone in different boreholes

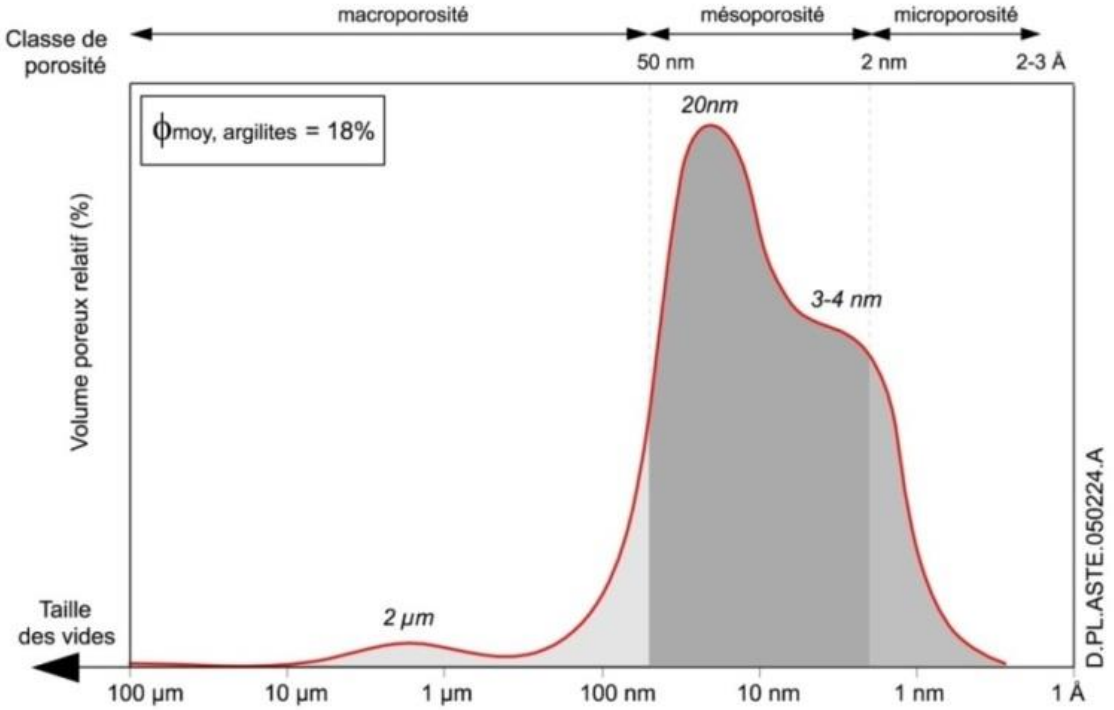

Figure 4-33. Conceptual model of the pore size distribution for the UA2 claystone, based on mercury intrusion porosimetry, NMR and gas adsorption measurements

For levels in which the proportion of clay minerals is greater than 45% (UA), the Callovo-Oxfordian claystone shows a relatively uniform structure beyond a few hundred µm. The texture is finely divided and is an assembly of tectosilicate and carbonate grains, connected by a fine matrix formed of clay minerals and calcite microcrystals (Figure 4-34). Both the tectosilicate and the carbonate grains show a preferential orientation of their long axis parallel to the sedimentation plane. The anisotropy of

magnetic susceptibility (AMS) of the clay minerals shows a magnetic foliation in the sedimentation plane, indicating a similar orientation of the clay minerals. However, the anisotropy is less pronounced than in other undeformed marine claystones.

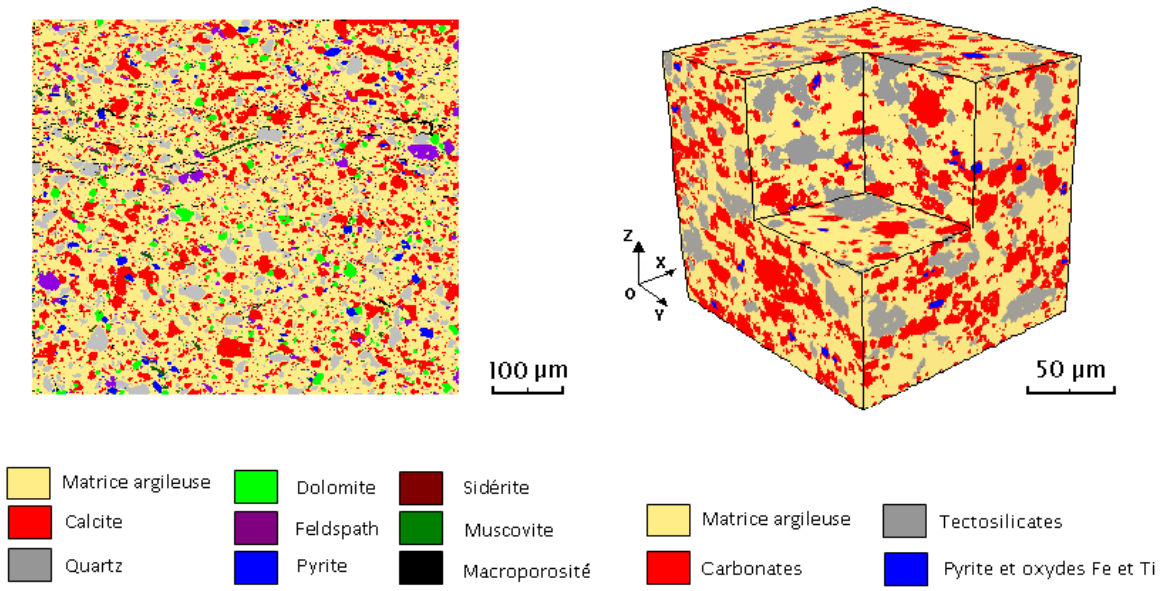

Figure 4-34. Two-dimensional and three-dimensional distribution of minerals in the Callovo-Oxfordian (Robinet et al. 2012)

The water permeability in the UA was measured both in laboratory (over 200 samples) and through in situ testing on a scale of several decimetres to several metres. It is very low and ranges from 10^{-21} m^2 to 10^{-19} m^2, with a relatively low anisotropy (2 to 3 ratio). The reference value of $3 \cdot 10^{-20}$ m^2 corresponds to the geometric mean of the intrinsic permeability.

The stress regime in the area is anisotropic and has the following characteristics (Figure 4-35):

- The major principal stress is horizontal and oriented N155°E (±10°). The vertical stress and the minimum horizontal stress are more or less equal
- The vertical stress is equal to the weight of the overburden formations
- The ratio between the maximum horizontal stress and the minimum horizontal stress (σ_H/σ_h) is at most 1.3.

For the calculations, at the URL level at 490 m, the major horizontal stress σ_H is set at 16.1 MPa, σ_v=12.7 MPa and σ_h=12.4 MPa.

The pore pressure measurements performed for the past 15 years at the level of the URL show that the pressure in the COx is 4.5 bar higher than the pressure in the surrounding carbonates. At 490 m, the pore pressure is 4.7 MPa.

A geothermal gradient of 0.025°C/m is estimated in the area, with a temperature of 22°C at 490 m.

The composition of the COx pore water is given in Table 4-13. The reference chemical composition for the pore water of the COx calculated with the ThermoAr model (Gaucher et al. 2006) and calibrated with all the data acquired in the area is applicable to the URL.

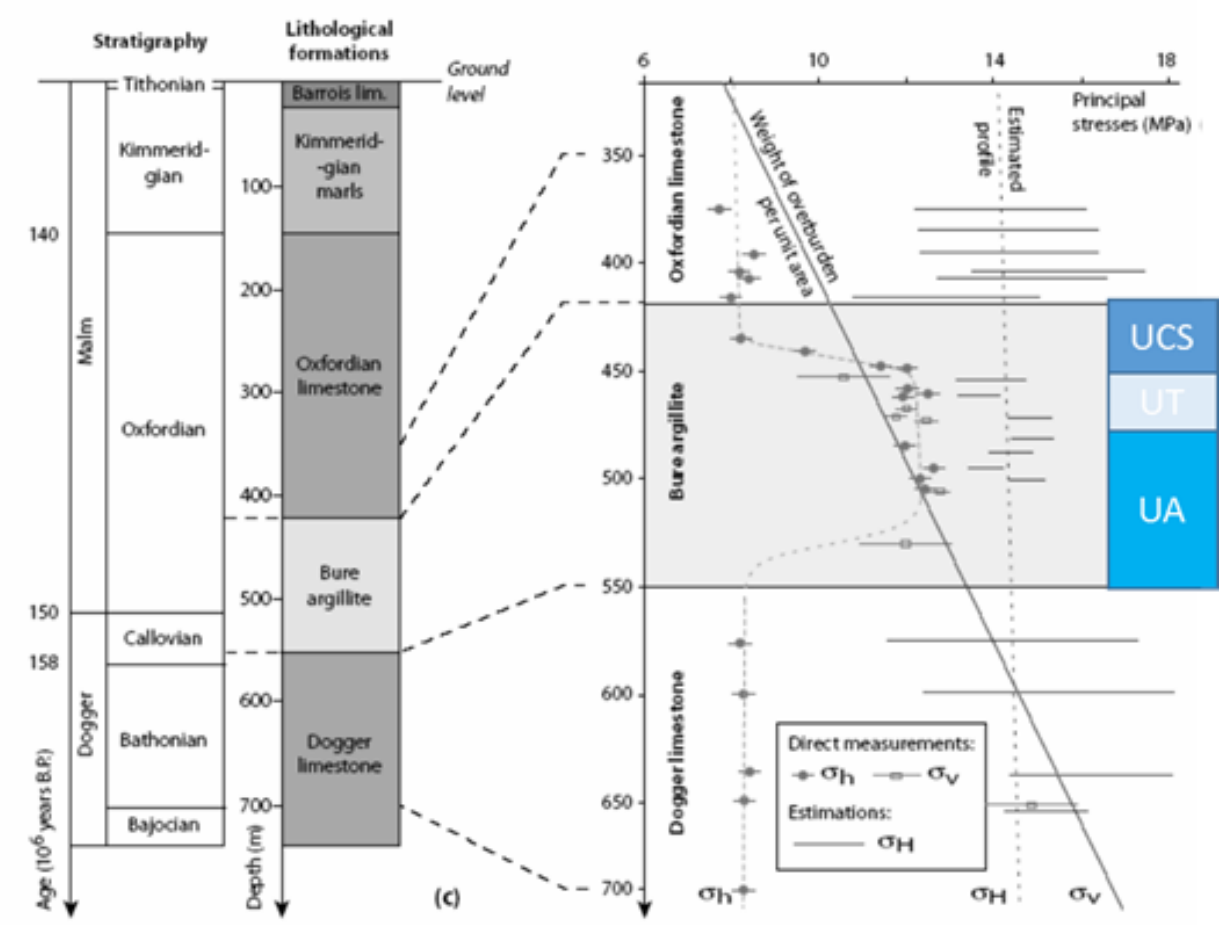

Figure 4-35. Stress profile in the Dogger, Callovo-Oxfordian and Oxfordian in the Bure URL (Gunzburger and Cornet, 2007; Wileveau et al. 2007a)

Table 4-13. Pore water composition predicted from the ThermoAr model and measured in the PAC1002 and POX1201 boreholes

Concentration (mmol/L)	Geochemical model	Experimental data	
	« ThermoAr »	PAC1002	POX1201 (±5%)
pH	7.2	7.1 ± 0.1	7.1± 0.1
Ionic strength (mol/L)	0.08	-	0.08
pE	-3.0	-	-
Chloride	37.0	36.6	38.8
Sulphate	12.8	12.8	12.9
TIC	2.1	2.7	2.4
Sodium	47.0	46.9	46.7
Calcium	8.0	5.0	5.0
Magnesium	5.0	4.2	4.3
Potassium	1.0	0.6	0.5
Strontium	0.2	0.2	0.2
Iron (II+III)	0.002	0.008	0.02
Silica	0.2		0.2

4.1.2.1 Hydro-mechanical behaviour of the host claystone

The COx claystone has a linear non-reversible (pseudo-elastic) behaviour at low levels of deviator stress (below 40-50% of failure) and a non-linear behaviour beyond a level, with significant irreversible strains and slightly lower moduli. Brittle failure is observed at low confining pressures and a more ductile behaviour is seen at high confining pressure (over 21 MPa in the UA). Beyond a certain level of cumulative total strain, some residual strength is shown.

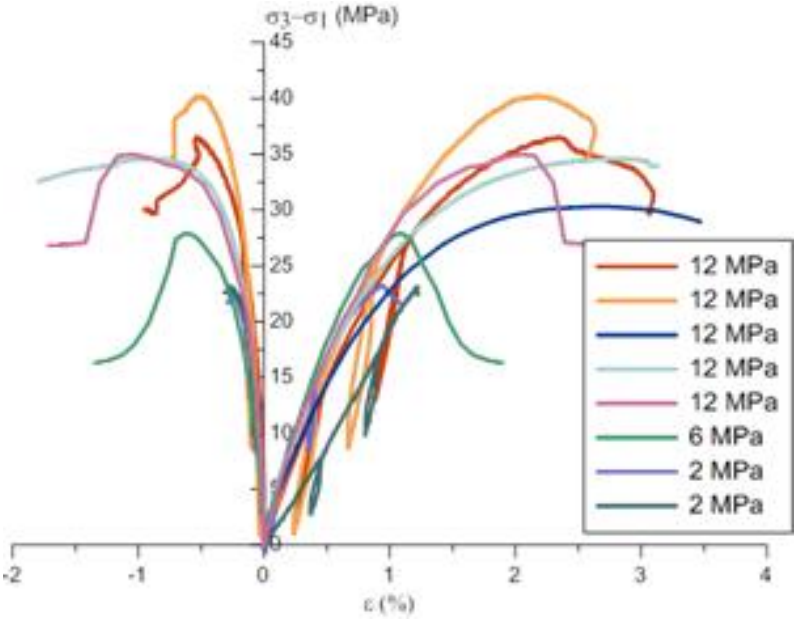

Figure 4-36. Deviator stress *vs.* strain for various confining pressures

The water saturation has a significant effect on the mechanical behaviour of the Callovo-Oxfordian. It was shown that limited desaturation of the Callovo-Oxfordian leads to an increase in the elastic mechanical properties and in the strength of the material, despite some microcracking of the sample due to desaturation (Wang et al. 2013).

Under tensile loading, the Callovo-Oxfordian shows a brittle behaviour. The measured tensile strength shows non-negligible dispersion, increasing with the carbonate content and with a mean value in the UA of 1.4 MPa.

Young modulus

The static Young's modulus results presented here were calculated using the tangent method (taken on the linear part of the strain-axial stress). Triaxial tests performed on samples with various orientations with regard to the bedding showed an anisotropy, the $E_{//}/E_{\perp}$ ratio varying between 1.05 and 1.4. Similar numbers were obtained when calculating dynamic moduli from the compressive and shear wave velocities measured in both directions in parallelepipedic samples.

The average values and standard deviations for the perpendicular and parallel moduli from UCS tests in the UA unit are displayed in Table 4-14. The average values show a ratio of almost 2, however these values are not directly comparable because many more samples were tested in the perpendicular direction (259 vs. 52) and the standard deviations have the same order of magnitude. In addition, the standard deviation for the tests performed on samples parallel to the bedding (≈4 GPa) is related not only to the mineralogical variations, but also to the damage due to the difficulty to cut some plugs parallel to the lamination.

Table 4-14. Young modulus perpendicular and parallel to bedding in UA, from UCS tests

Orientation	UA subunits	Average±standard deviation (MPa)	# samples	Average±standard deviation (MPa)	# samples
$E_{\perp}$	UA3	5724±2484	259	5558±2022	104
	UA2=IMA			5270±2302	112
	RIO			9658±4253	7
	UA1			6854±2894	36
$E_{//}$	UA3	10956±4603	52	8592±4467	13
	UA2=IMA			11457±4487	36
	RIO			x	x
	UA1			15193±761	3

Poisson's ratio

Poisson's ratio (ν) was calculated from the results of all available tests, at room temperature:

$0.18 < \nu < 0.37$ $\nu_{avg} = 0.295$ standard deviation= 0.05

The average value of 0.3 is given for all lithological levels.

Unconfined Compressive Strength

Table 4-15 summarises the average values and standard deviations in the different units of the COx formation. For the most argillaceous part of the UA (UA2=IMA subunit), the dispersion is lower if the number of samples that were tested and the plugs condition are taken into account. The average UCS in the UA unit as a whole is larger than what is measured in the IMA subunit. Depending on the zone of interest it is therefore recommended to use the subunits parameters.

Table 4-15. Statistical variations of UCS in the UA

Subunit	Average±standard deviation (MPa)	# samples	Average±standard deviation (MPa)	# samples
UA3	26.5±6.1	171	28.5±4.9	76
UA2 = IMA			23.3±5.1	80
RIO			43.1±1.7	4
UA1			30.6±3.4	11

Failure criterion

The interpretation of the experimental values is based on a Hoek & Brown failure criterion, defined as:

$$\sigma_1 = \sigma_3 + (\sigma_3 \cdot \sigma_c \cdot m + S \cdot \sigma_c^2)^{1/2} \quad [6]$$

With:

σ_1, σ_3: maximum and minimum principal stresses at failure

m, *S*: fitting parameters (as defined by Hoek & Brown, they characterise the rock)

σ_c: uniaxial compressive strength of the intact rock, without any damage. For the Cox claystone, this parameter is different from the UCS and is considered as a fitting parameter, not a rock property.

In order to manage the uncertainties due to various effects (scale, time effect on the long-term strength, sample preservation, etc.), two criteria are defined:

- An average criterion that goes through the cloud of test results over a range of confining pressure $0<\sigma_3<25$ MPa (red line in Figure 4-37)
- A low criterion that goes through the lower limit of test results over the same range of confining pressures (blue line in Figure 4-37)

The resulting parameters are presented in Table 4-16.

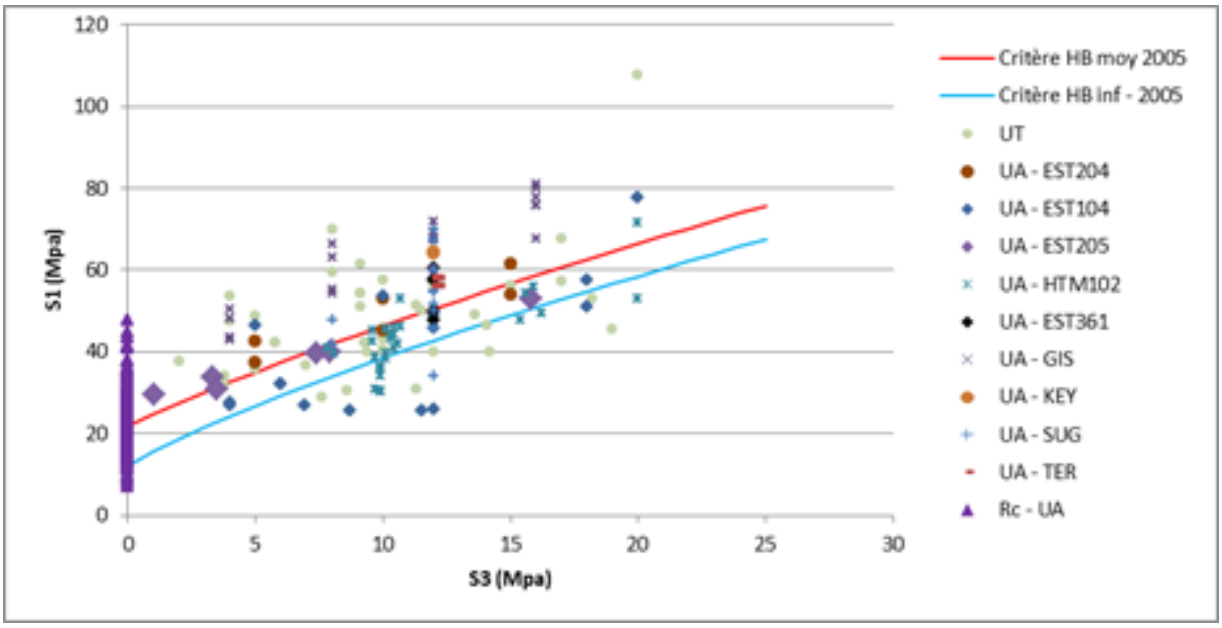

Figure 4-37. Stresses at failure on UT and UA claystone in triaxial tests

Table 4-16. Hoek & Brown fitting parameters for the unit UA of the COx claystone (values from ANDRA 2009)

	S	***m***	**σ_c (MPa)**	**Back-calculated UCS (MPa)**
Low criterion	0.128	2.0	33.5	12.0
Average criterion	0.430	2.5	33.5	22.0

It is possible to derive equivalent Mohr-Coulomb parameters from the Hoek & Brown criteria. The equivalent cohesion and angle of internal friction for three different levels of minor stress are given in Table 4-17:

Table 4-17. Mohr-Coulomb failure criterion parameters for the COx claystone for 0, 5 and 12 MPa minor stress

	σ_3 (MPa)	c (MPa)	ϕ (°)
Average criterion	0	6.4	29
	5	7.4	24
	12	8.8	21
Low criterion	0	3.1	36
	5	4.5	26
	12	6.1	21

Anisotropy

Because of the variability of their microstructure and of their mineralogy, the COx claystones are characterised by an anisotropic behaviour that results in:

- an anisotropy between 1 and 2 on the elastic moduli depending on the methods used for determination (dynamic and quasi-static modulus)
- compressive strengths measured on samples perpendicular to the stratification are similar to or slightly lower than those measured on samples parallel to the stratification. A decrease in strength is observed for test specimens at 45° but the natural variability of samples can give an opposite result. Figure 4-38 shows the effect of the orientation to bedding to the peak strength, only recent samples from well-preserved cores with high water saturations are displayed here.

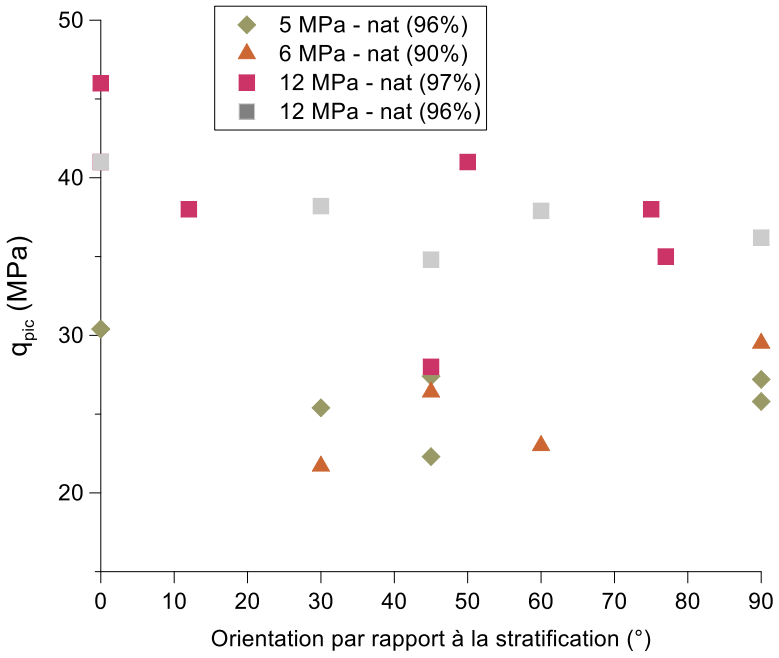

Figure 4-38. Peak strength as a function of the orientation to bedding

For the tests performed by GRS (Zhang 2015), the cores were acquired in six dedicated boreholes drilled from the NER drift at different inclinations from the bedding. Four different loading paths were applied (Figure 4-39):

- TCD: triaxial compression by axial deformation at constant radial stress

- TCS: triaxial compression by axial loading at constant radial stress
- TES: triaxial extension by increasing radial stress at a constant axial stress
- TEM: triaxial extension by keeping the mean stress constant while simultaneously increasing radial stress and decreasing axial stress

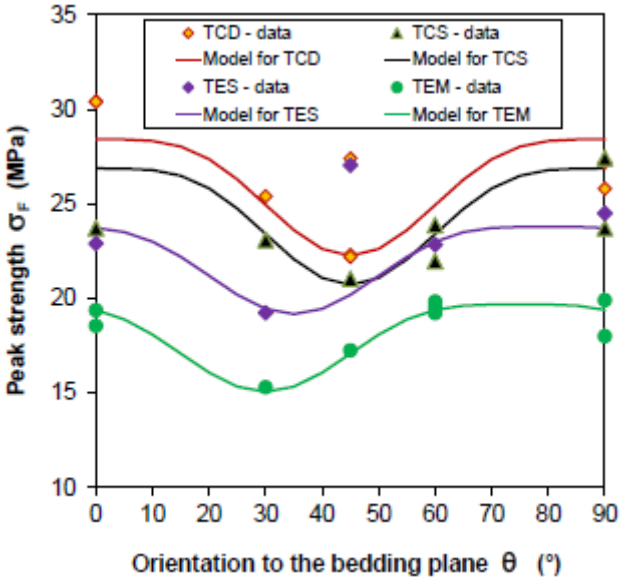

Figure 4-39. Peak failure strength developed along different loading paths as a function of the orientation of the major principal stress with respect to bedding planes (Zhang et al 2015)

These tests confirm that the strength depends both on the loading path and on the direction of the loading compared to the bedding plane. For a given loading orientation, the peak strengths developed during TCD and TCS compression were higher than those reached during TES and TEM extension and the lowest strength was achieved in triaxial extension with constant mean stress. For all loading paths, the maximum strengths were reached parallel and perpendicular to bedding and the lowest strength was obtained at 45° in compression and 30° in extension.

Biot coefficient

The influence of pore pressure on the mechanical behaviour of the COx and of a mechanical load on the pore pressure were tested in laboratory. However, the very low permeability and porosity of the claystone made it difficult to directly measure the pore pressure within a plug and to quantify this coupling. The hydro-mechanical coupling was also revealed in-situ through changes in pore pressure levels around the structures after excavation and through thermal experiments. It is currently described through the concept of effective stress, using Biot's theory.

Several experiments were performed to define the Biot coefficient in the COx claystones. The most recent ones with better test protocols (Braun 2019, Belmokhtar et al. 2017, Yuan et al. 2017), reduced the uncertainty on the value of the Biot coefficient and give higher values than previously, between 0.8 and 1 (Figure 4-40). A value of 0.85 may be retained for the COx claystone.

However, it should be noted that these results strongly depend on the saturation and the mechanical state of the samples. The core processing, the sample preparation and the (re)saturation of the samples may create some damages prior to testing, which may partially explain the dispersion of experimental values obtained over all the studies. Furthermore, all the tests show that the Biot

coefficient seems to decrease with the confining pressure while the drained bulk modulus increases. This could be explained by the closure of microfractures induced when cutting the core and/or preparing the samples.

In addition, the very small pore size of the COx claystone, the presence of both clay-bound and free water, and the possible induced desaturation when acquiring or preparing the samples hinder the characterization of the poro-elastic parameters and the application of a simple behaviour model.

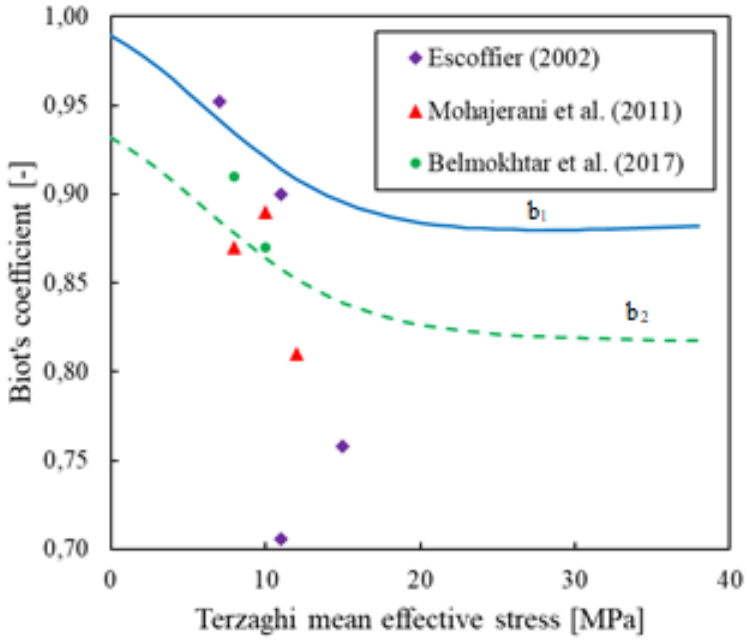

Figure 4-40. Biot coefficient calculated perpendicular to bedding (b_1) and parallel to bedding (b_2) vs. Terzaghi effective stress (Braun 2019)

4.1.2.2 Hydro-mechanical behaviour of the fracture/damage claystone

Drilling underground galleries or boreholes leads to stress redistribution around the hole and some damage in the near-field (Figure 4-41). This Excavation Damage Zone (EDZ) has different mechanical, hydraulic and thermal properties to the sound host rock.

The EDZ can be split between a connected fractured zone (ZFC) where both tensile fractures and shear fractures coexist and a discrete fractured Zone (ZFD) where only the ends of some shear fractures are found.

Because of the strike-slip stress regime in the area, for HLW cells drilled in the direction of the maximum horizontal stress, the EDZ develops mainly on the right and left sides of the borehole. Its maximum extent is approximately one diameter wide on each side (0.8 radius for the ZFC and 2 radii for the ZFD), and there is no "scale effect" between large galleries or thin boreholes (Figure 4-41). The hydraulic conductivity in the ZFC is significant and related to open fractures. Because of this, the pore pressure drops rapidly to atmospheric pressure in the near-field (ZFC), but an increase in pore pressure is observed further away from the hole with some delay.

The apparent stiffness of the ZFC has been evaluated in the CDZ experiment (de la Vaissière 2015); it appears to increase rapidly, reaching already 3 GPa one metre away from the borehole wall.

Several observations in the UA proved that the EDZ has a hydraulic self-healing capacity due to the presence of swelling clay minerals such as smectite. Both laboratory and in-situ experiments showed

that the hydraulic conductivity of the ZFC reduces rapidly when exposed to water and progressively reaches that of the intact claystone. However, water injection does not improve the stiffness of the EDZ that remains a mechanically weak zone.

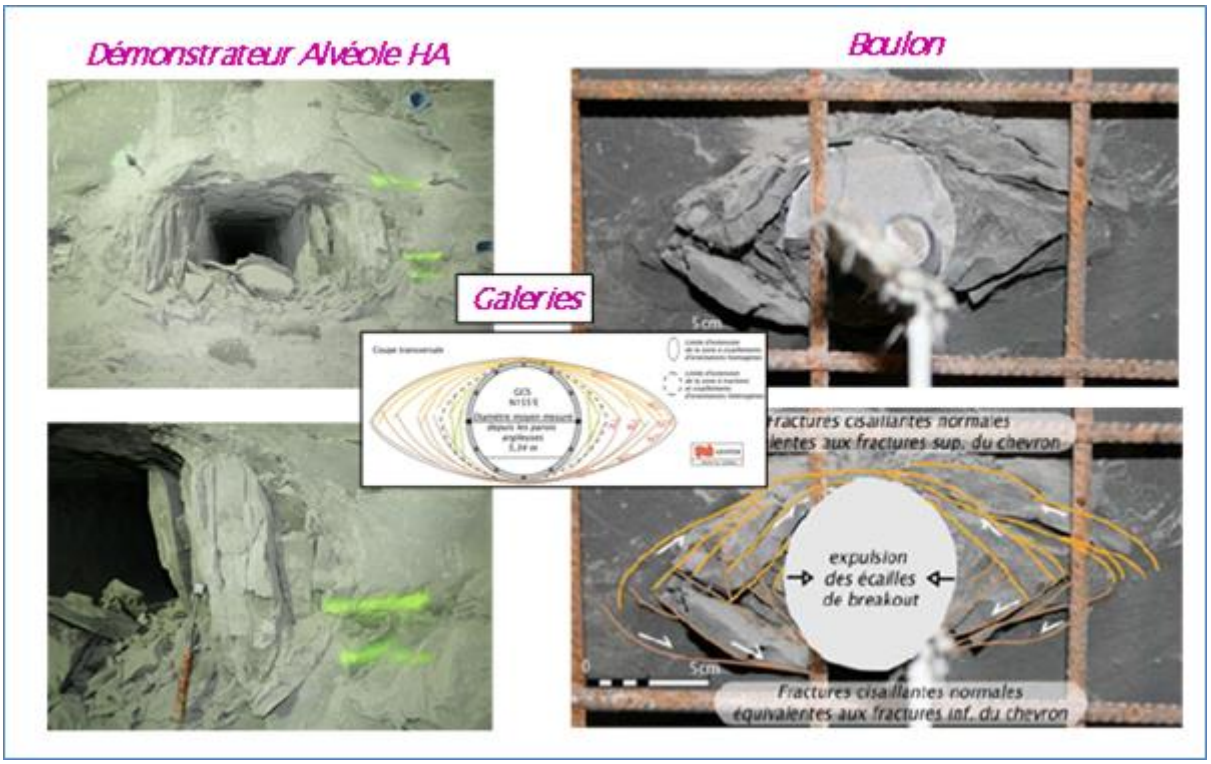

Figure 4-41. Initial damaged zone around a HLW cell (left), drift (center) and a bolt (right) oriented in the direction of the maximum horizontal stress

Creep tests

A creep test consists in applying a load on a specimen and then maintaining it constant over time. The evolution of the strain over time will characterise the long-term mechanical behaviour of the rock. These long tests (up to 3 years) are performed on dedicated rigs, with controlled temperature. All the tests faced important challenges related to the initial state of the samples, the duration of the experiments, the control of temperature and humidity and the precision of the measurements. The measured changes were indeed very low, sometimes of the same order of magnitude as the accuracy of the sensors. However, a general trend was observed, as shown in Figure 4-42.

In most cases, the creeping rate diminished with time; however, in some cases, it appeared to reach an asymptote. The evolution of the creeping rate was very slow and because of the precision of the measurements, it is difficult to say whether a steady state was reached or not. In the first tests, the influence of the following parameters was studied: deviator stress, average stress, saturation and mineralogy (calcite content).

The creeping rate appeared to increase with the deviator stress. The average stress seemed to have very little influence on the delayed deformations. The calcite content had a direct effect on the instantaneous behaviour but no clear trend was observed on the delayed mechanical behaviour; however, when checking the results per study, a slight decrease of the creeping rate with the carbonate content may be seen. A new series of tests is ongoing to study the delayed behaviour of the more calcareous USC unit.

The effect of temperature on the long-term properties is discussed below.

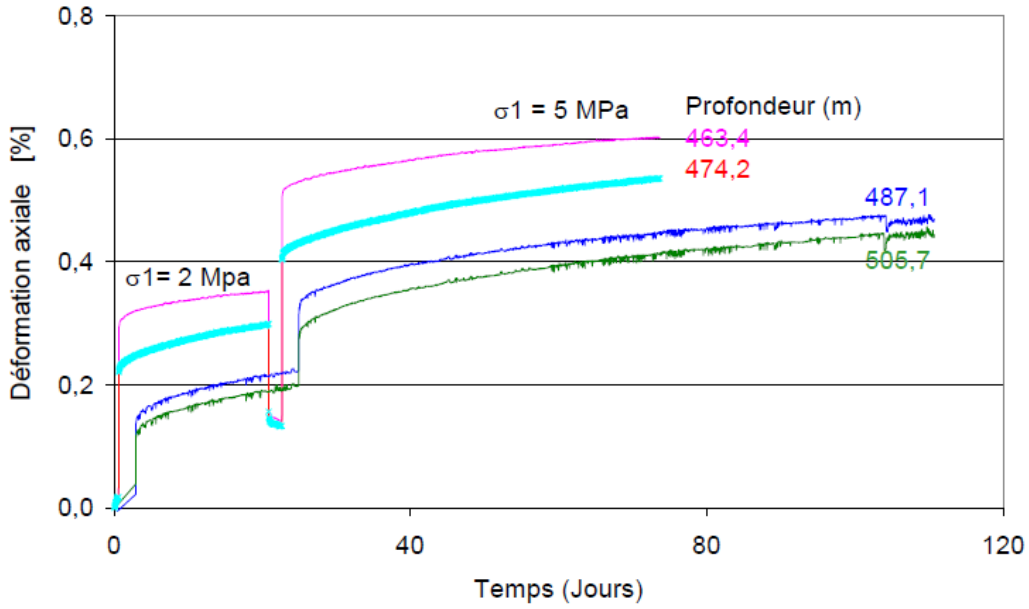

Figure 4-42. Creep tests on samples from UT (463.4m), UA3 (474.2, 487.1m) and UA2 (505.7m) at 2 and 5 MPa deviator (Zhang et al. 2002)

4.1.2.3 Thermo-hydro-mechanical behaviour

Thermal properties of the COx claystone

The thermal conductivity of the UA was both measured on samples taken in boreholes drilled for the TED experiment (see section 4.2.2.2) and determined by inverse analysis during this experiment. The results displayed in Table 4-18 (LAEGO and DBTEC laboratory measurements) and Table 4-19 match very well, which shows that there is no scale effect and that laboratory measurements can be used to characterise the thermal behaviour of the COx claystone.

Table 4-18: Thermal conductivity measured in boreholes drilled for the TED experiment ($W \cdot m^{-1} \cdot K^{-1}$)

	LAEGO	**DBETEC**
λ_h	1.89±0.05	1.96±0.07
λ_v	1.26±0.05	1.28±0.06

Table 4-19: Thermal conductivity ($W \cdot m^{-1} \cdot K^{-1}$) determined by inverse analysis during the TED heating experiment

			λ_h	λ_v	λ_0	λ_h/λ_v
UPC	TED1	Average	1.95	1.30	1.69	1.50
	TED2	Average	1.93	1.26	1.67	1.53
CEA	TED		2.07	1.37	1.80	1.51
DBETEC	TED		2.07	1.32	1.78	1.57

The thermal and THM modelling of the TED experiment using the parameters in Table 4-6 match well the evolution of temperature during the whole heating phase, showing that thermal conductivity does not vary with temperature. This point was also proven by laboratory measurements: for tests performed at temperatures between 20 and 150°C, the horizontal and vertical thermal conductivities are almost independent of temperature (Figure 4-43, left). In contrast, there is a clear increase of the conductivity with the water saturation (Figure 4-43, right).

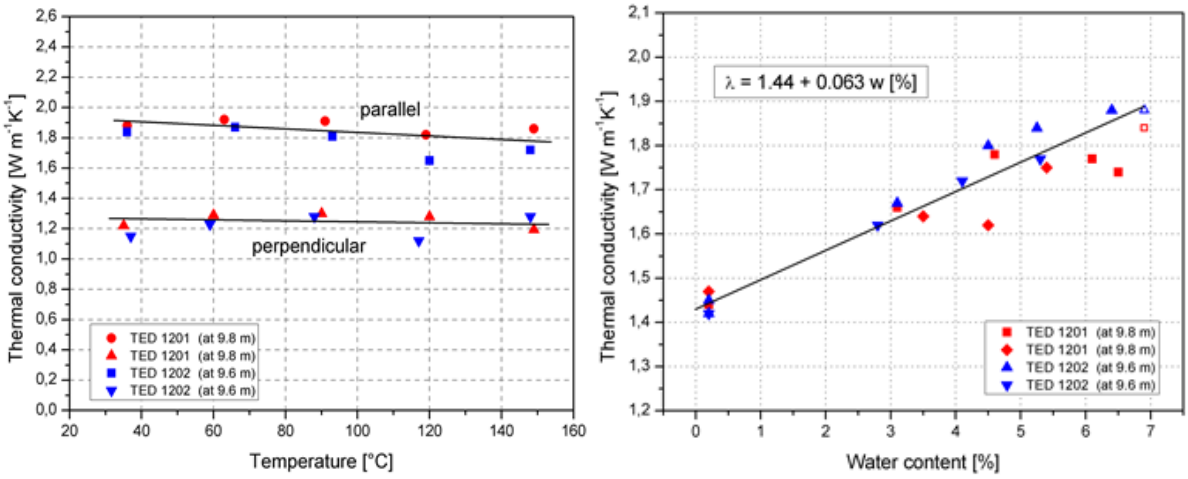

Figure 4-43. Thermal conductivities for various temperatures and water contents (Jobmann et al. 2013)

Specific heat measurements performed on samples from four different boreholes show that it does not vary much with depth. In the UA, the average value at 20°C is 973 $J \cdot kg^{-1} \cdot K^{-1}$. Inverse analyses from the TED experiment gave 971 and 987 $J \cdot kg^{-1} \cdot K^{-1}$.

Thermal properties of the EDZ

There is no direct measurement of the thermal properties of the EDZ. However, they have been estimated by inverse analysis of the temperatures measured during the HLW cell heating test. The 3D modelling of the ALC1604 experiment (see section 4.2.2.4) matched well enough the temperature measurements using the same conductivity in the EDZ and in the intact rock. A sensitivity study was performed in order to better quantify the variations of temperature with the distance to the cell. It showed that the temperature field beyond the EDZ is very weakly influenced by the thermal properties of this zone. It appears therefore justified to use the same conductivity in the EDZ and in the intact COx claystone.

Temperature effects on the HM parameters

The effect of temperature on the hydro-mechanical behaviour was initially studied in laboratory. Based on the results from these tests, coupled THM models were developed and matched with the thermal experiments performed in the underground laboratory (presented in section 4.2.2).

Thermal expansion coefficient

The following undrained thermal expansion coefficients parallel and perpendicular to bedding were found in laboratory tests performed on samples as part of the TED in-situ experiment:

α_u (//) =10.2±1.9·10^{-6} $°C^{-1}$

α_u ($\perp$) = 18.2±4.9·10^{-6} °C^{-1}

The thermal expansion coefficients of the constitutive minerals of the Callovo-Oxfordian from the literature are given in Table 4-20. The mean mineralogical composition in the middle of the UA subunit is 45% clay minerals, 23% quartz, 5% feldspar and 28% calcite. The coefficients of the clay and quartz are similar, but those of calcite and feldspar are almost three times lower. This may trigger some thermal damaging, especially at the interface between calcite and the clay matrix.

Table 4-20. Thermal expansion coefficients and compressibility of the COx constituent minerals and the water

Mineral	Thermal expansion coefficient	Compressibility
Clay (45%)	3.4·10^{-5} °C^{-1} (McTigue 1986)	c_s = 2·10^{-2} GPa^{-1} (Skempton 1960, McTigue 1986)
Quartz (23%)	3.3·10^{-5} °C^{-1} (Fei 1995)	c_s = 2.646·10^{-2} GPa^{-1} (Bass 1995)
Calcite (28%)	1.4·10^{-5} °C^{-1} (Fei 1995)	c_s = 1.36·10^{-2} GPa^{-1} (Bass 1995)
Feldspar (5%)	1.1·10^{-5} °C^{-1} (Fei 1995)	c_s = 1.447·10^{-2} GPa^{-1} (Bass 1995)
Water (at 20°C)	27·10^{-5} °C^{-1} (Spang 2002)	c_w = 44.7·10^{-2} GPa^{-1} (Spang 2002)
Argillite (homogenisation)	2.65·10^{-5} °C^{-1}	c_s = 2·10^{-2} GPa^{-1}

The value of the water expansion coefficient is more than ten times greater than the value for the rock matrix. This large difference is the main cause of thermal pressurisation described below.

Braun (2019) performed several loading tests under controlled temperature. After each heating stage, the deformations were measured and drained linear thermal expansion coefficients were obtained. The following coefficients parallel and perpendicular to bedding were derived (Figure 4-46):

$\alpha_{d,h}$= 0.5·10^{-5} °C^{-1}

$\alpha_{d,v}$= 0.2·10^{-5} °C^{-1}

These values are lower than the ones obtained in undrained conditions and the one used by UPC in their inverse analysis of the TED experiment (1.3·10-5°C^{-1}), but all remain much lower than the coefficient for water. The UPC calculations showed that this parameter does not have much influence on the pressure variations. Additional tests are planned to confirm the results.

Change in mechanical properties as a result of heat

The effect of temperature on the various THM parameters was studied, with particular attention placed on the 25-80°C range. In general, only a very slight change is observed in the elastic modulus, with a tendency to decrease as the temperature increases (Figure 4-44). This reduction is so small that it may also be due to the mineralogical variability between samples. For the strength characteristics, the stress at failure decreases slightly with the increase in temperature (Figure 4-45). and this phenomenon is more pronounced for low confinement values (Zhang et al. 2012).

It should be noted that the influence of the relative humidity of the sample is much stronger than the influence of temperature.

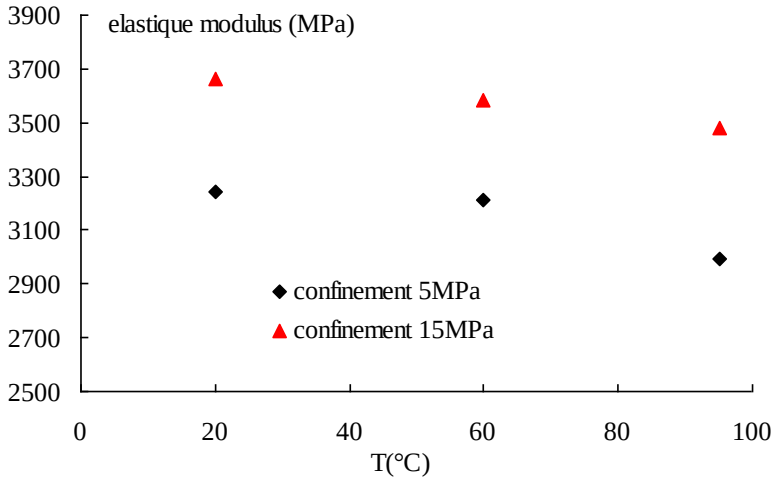

Figure 4-44. Young modulus from triaxial tests for three temperature values (20, 60 and 95°C) and two confining pressures on samples from UA1 (Zhang et al. 2012)

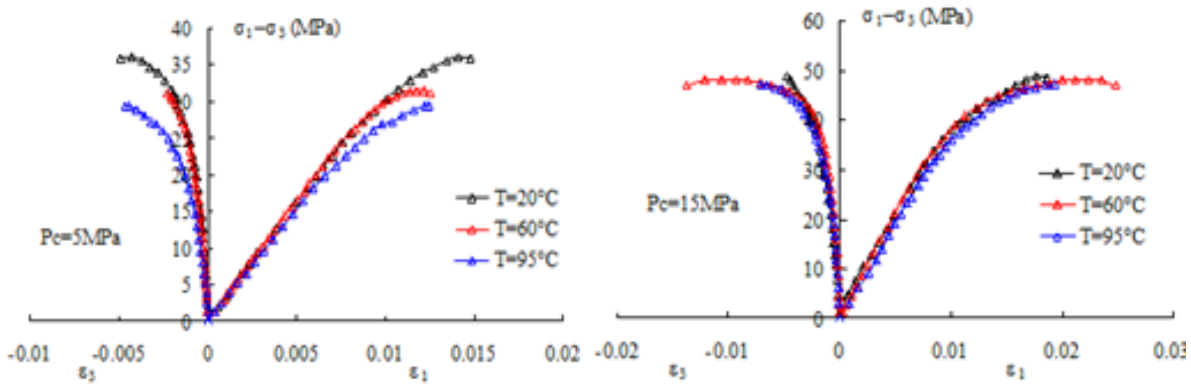

Figure 4-45. Triaxial tests for three temperature values (20, 60 and 95°C) and (P_c = 5 and 15 MPa) on samples from UA (Zhang et al. 2012)

Thermal consolidation

In soil mechanics, several authors (Baldi et al. 1991, Delage et al. 2000) have shown that normally consolidated clays subjected to constant mechanical load and slow temperature increase generally incur an irreversible contraction. Weakly overconsolidated clays experience first a thermal expansion, followed by a contraction. This phenomenon is interpreted by a variation in the elasticity limits with temperature called "thermal hardening". Some thermal experiments on COx samples exhibited a thermo-elastic expansion up to a temperature around 45°C, followed by thermo-plastic contraction at higher temperature (Figure 4-46). In this case, the slight desaturation (S_r=87%) of the samples could have generated some microcracks that could enhance contraction.

Braun (2019) performed a new series of tests under thermal load in drained conditions. The contraction was essentially localised perpendicularly to bedding, whereas the strains parallel to bedding were reversible and linear. In this direction, the samples expanded when heated, and contracted when cooled down, showing that the response to thermal loading is thermo-elastic (Figure 4-47). Perpendicular to bedding, the rock expanded up to 40°C, then contracted for higher temperatures. While cooling, a linear contraction was observed.

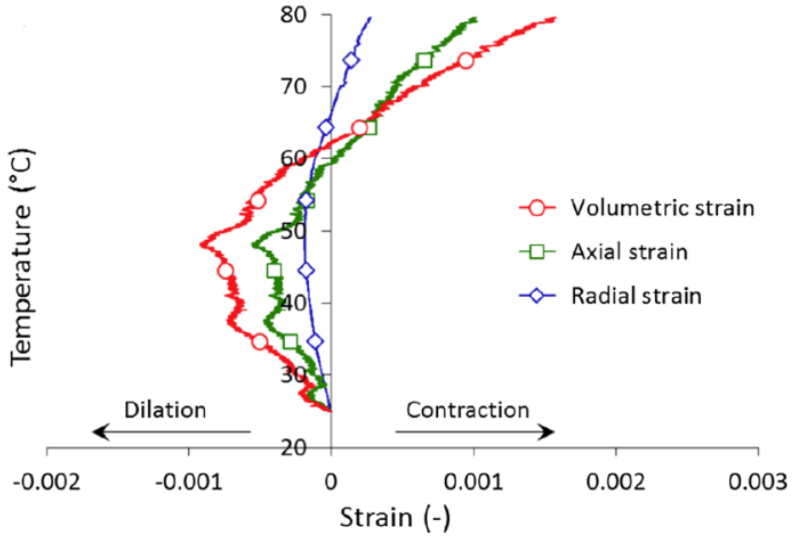

Figure 4-46. Axial, radial and volumetric strain vs. temperature in a drained isotropic compression (Belmokhtar et al. 2017)

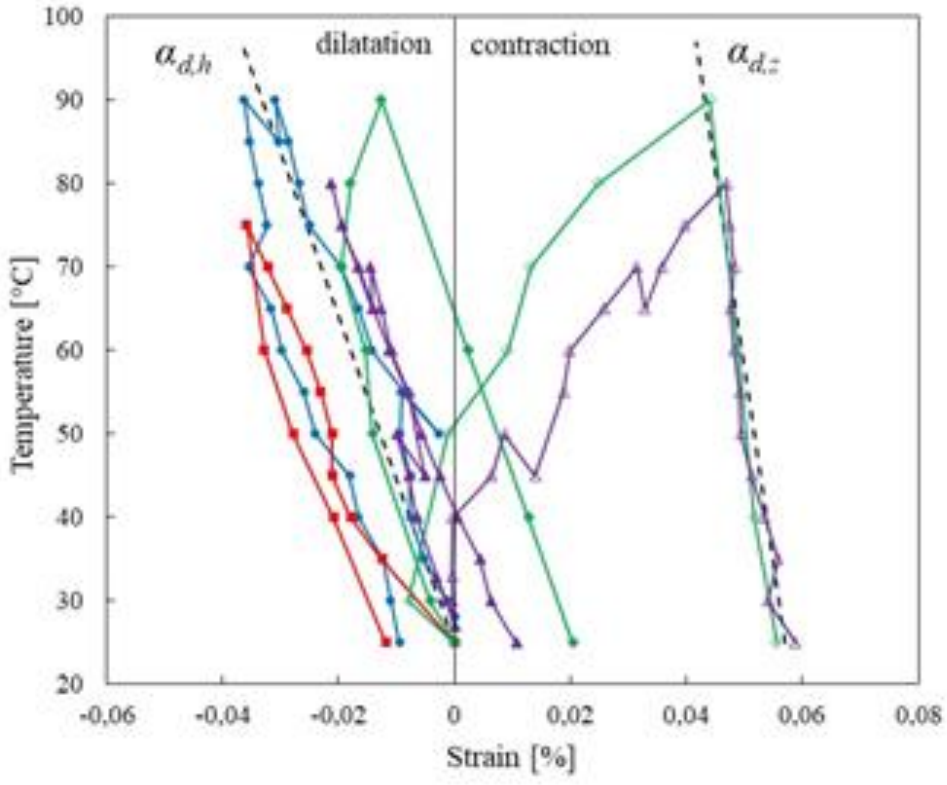

Figure 4-47. Strain measured on samples under drained conditions as a function of temperature – purple and green curves: vertical/perpendicular, blue and red curves: horizontal/parallel to bedding

This phenomenon was not observed in small scale in-situ experiments such as TER or TED (sections 4.2.2.1 and 4.2.2.2), where measurements were performed several diameters away from the heated borehole (i.e. in far field). However, the full-scale ALC1604 experiment (section 4.2.2.4) showed in some cases a "relaxation" of the radial load applied by the rock on the steel casing, that may potentially be a sign of thermal hardening in the EDZ. Investigations are ongoing to better understand the thermal

contraction phenomenon on the COx claystone, and to determine in which conditions it may occur and what consequences may arise.

Thermal pressurisation

An increase in temperature in a porous medium with low permeability, such as the COx claystone, creates an overpressure of the pore fluid, mainly due to the difference between the thermal expansion coefficient of the pore water and of the solid skeleton of the Callovo-Oxfordian. This pore pressure build-up reduces the effective stresses and, in certain cases, may cause shear failures or hydraulic fracturing. Experimental studies show that the change of pore pressure may be related to the applied temperature variations by the thermal pressurisation coefficient, Λ. This coefficient depends on the nature of the rock, the range of temperature variation, the level of damage of the material, and the state of stress.

A special isotropic cell was designed at CERMES (Tang et al. 2008b) to conduct thermal pressurisation tests under stress conditions close to the in-situ state. The experimental setup was used by Mohajerani (2012). With the same device, Braun (2019) performed two heating tests in three phases with application of a thermal load. The resulting thermal pressurisation coefficients shown on Figure 4-48 are consistent with the theoretical values (dashed line), they increased from 0.12 MPa/°C at 25°C to 0.30 MPa/°C at 80°C whereas Mohajerani's values were almost constant (green squares). These differences were explained by the stress conditions during the experiments. Mohajerani did not maintain the effective stresses constant; their reduction led to a decrease in the Biot modulus *M* and a practically constant thermal pressurisation coefficient.

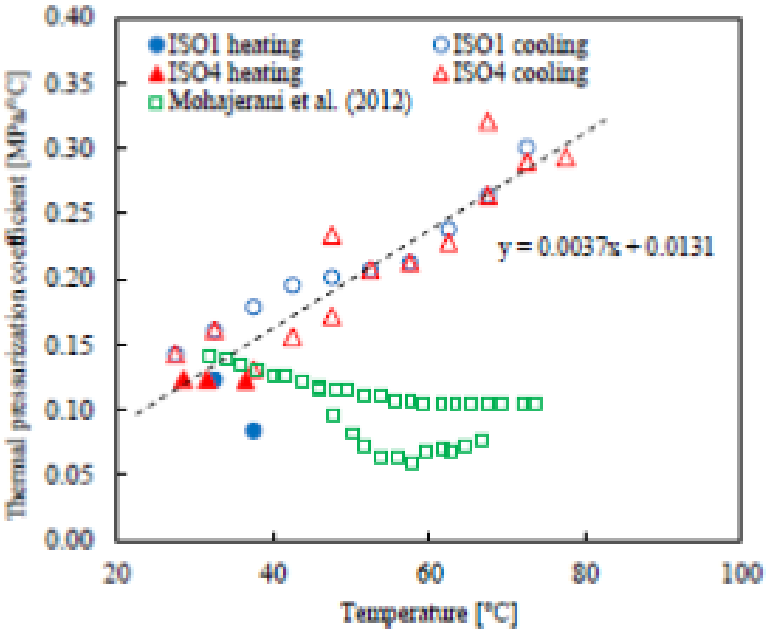

Figure 4-48. Measured/corrected thermal pressurisation coefficients at different temperatures (Braun 2018b) - Comparison with results from Mohajerani et al. (2011)

Temperature effects on the long-term properties

Temperature may play a role in the long-term behaviour of the COx claystone. Pellet (2007) reviewed the studies performed on the time-dependent deformation in 2007. As shown on Figure 4-49, there is

a large dispersion of data; although the deviator stress has a clear influence on the creep rate (right plot), the effect of temperature overall is not obvious (left plot).

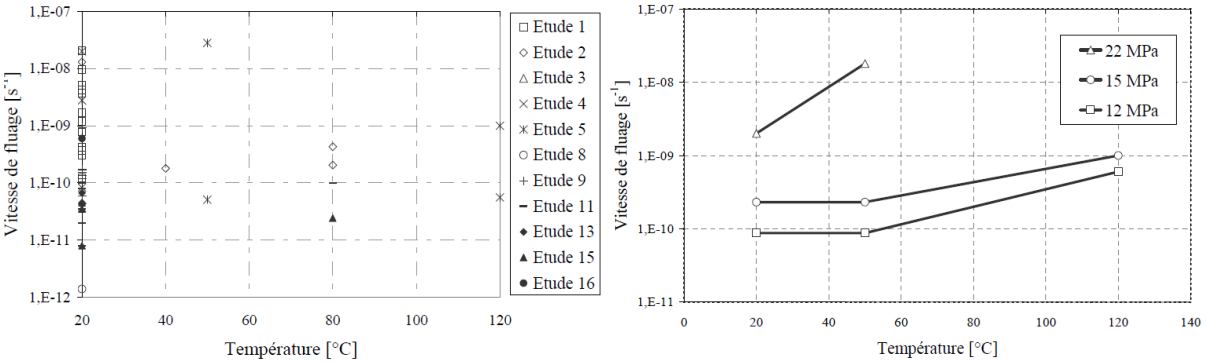

Figure 4-49. Creep rate as a function of temperature – all results (left), and in Study #5 (right) for different deviator stress (Pellet 2007)

Zhang et al. (2010) performed some uniaxial compression tests under two different confining pressures (0.74 and 13.8 MPa) and a series of triaxial tests with a constant axial stress (15 MPa) but different radial stresses, 3.1 and 5 MPa. During these tests, temperature was increased and decreased in steps. The results of these creep tests are shown in Figure 4-50.

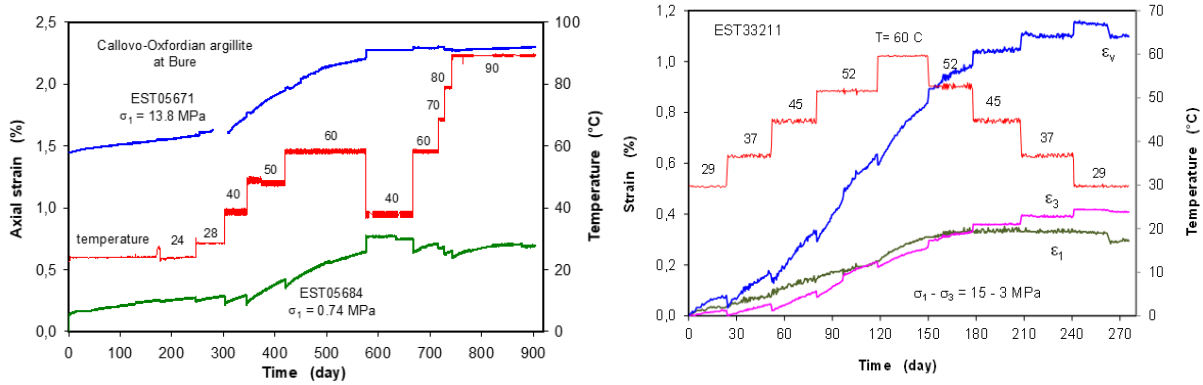

Figure 4-50. Uniaxial (left) and triaxial (right) creep tests under varying temperatures

These tests show that a stepped increase in temperature leads to a slight increase in deformation due to thermal expansion, followed by a resumption of the creeping. The higher temperature in general causes an increase of the deformation rate (up to 5 times larger), which may be related to the fact that water viscosity decreases as temperature increases. Tests are ongoing to understand better this phenomenon. In the uniaxial tests (left on Figure 4-50), a second temperature increase to 90°C after the cooling phase to 40°C did not produce any clear increase of the deformation rate. This difference may be related to the experimental conditions and to a potential loss of water during the test.

4.1.3 Opalinus (NAGRA, BGE)

The Opalinus clay of the Middle Jurassic consists of claystones which show a low variability in facies and lithology (Figure 4-51). The Opalinus Clay is a moderately over-consolidated claystone that has been formed by a complex burial and compaction history with two distinct periods of subsidence during the Cretaceous and late Tertiary, respectively. In the Molasse Basin the greatest burial depth of the Opalinus Clay was about 1000 m below the present depth. From about 10 Ma ago, alpine uplift

and erosion brought the Opalinus Clay progressively up to its present burial depth. Currently it is slightly tilted and the surface of the formation lies between 0 to beyond 1000 m below ground surface. At Mont Terri, the Opalinus Clay reached a maximum depth of about 1000 m and the present burial depth is about 200-300 m. The hydrogeological conditions contain a near-surface groundwater reservoir in unconsolidated Quaternary sediments and several deeper aquifers in the Upper Muschelkalk, Stubensandstein and Upper Jurassic. The model unit of the Upper Jurassic comprises strong dolomitized and karstified limestones. Compared to other Mesozoic formations of Northern Switzerland, it forms a homogeneous thick layer package. There are distinct indications in the Jura region that the Opalinus Clay is less thick than in the other regions. The mineralogical composition of the Opalinus Clay lies in the range of claystones and sandy claystones. For the purpose of the assessing safety of a geological repository, it can be considered as a single lithofacial unit with a clay mineral content >40 wt.%.

The Opalinus clay has been well investigated at northern Switzerland (Figure 4-52). The Mont Terri site and the Benken drilling allow a good understanding of the stratigraphy and substructures inside the formation. Six substructures are defined. The lower part, including the substructures Opalinus clay, claystone with siderite concretions and claystone with less sandstone layer are characterised as a more clay rich part. This part is present in Switzerland. The upper part, including claystones with more sandstone layers, claystone with sandstone layers and siderite concretions and so-called Murchisonae-Layers are characterised by a higher sand and limestone content. At the Mont Terri URL the substructures are called clay rich and sandy facies. The variability of the facies is expected to be low and the same structures can be found in southern Germany as well (Jahn et al. 2016). Within the frame of the ANSICHT project (Reinhold et al. 2016) a generic geological model, called Type SOUTH was developed. The model is situated in the north Alpine Molasse Basin. The region is structured in a crystalline basement, a cover of Mesozoic sedimentary rock, molasses sediments and Quaternary sediments. The generic 3D model contains 16 units from the basis Muschelkalk until the Quaternary (Figure 4-53). Active fault zones are excluded from the model. The model regards an area of about 140 km².

In Switzerland, the Opalinus Clay formation has been selected as the first-priority host rock for a deep geological repository for both low- and intermediate-level and high-level radioactive waste. The properties of the Opalinus Clay that are relevant from the viewpoint of long-term safety can be summarized as follows (Gautschi 2017):

- Below a near-surface decompaction zone with high hydraulic conductivity (up to 10^{-4} m/s), the hydraulic conductivity is very low (~10^{-13}m/s) and diffusion is the dominant transport mechanism, with advection playing a secondary role at best; clay-rich confining units over- and underlying the Opalinus Clay host rock act as a supplementary barrier to migrating radionuclides.
- Faults in the Opalinus Clay do not represent preferential flow paths, which is attributed to an efficient self-sealing mechanism.
- The self-sealing capacity of the Opalinus Clay minimizes the effects of perturbations caused by the repository (excavation damaged zone around underground structures) or by potentially induced or reactivated fractures in the far future.
- Stable, reducing geochemical conditions prevail and, due to its high clay mineral content, the host rock has favourable sorption properties.

The main conclusions are supported by multiple lines of evidence demonstrating consistency among hydraulic properties (tests and observations at various scales, comparisons with data from other clay rocks), pore water geochemistry, laboratory and in situ diffusion experiments, the distribution of

natural tracers across the Opalinus Clay as well as small and large-scale diffusion models and the derived conceptual understanding of solute transport.

For the lithologically relatively homogeneous Opalinus Clay, the good agreement between the very low hydraulic conductivities determined in laboratory experiments and in situ tests in boreholes (taking into account small faults and differing lithofacial subunits) indicates that it is appropriate to model it as a homogeneous-porous medium with diffusion dominated transport. The diffusion properties are based on measurements in the laboratory and on data acquired in field experiments in the Mont Terri Rock Laboratory. There is also an empirical correlation between the porosity and the diffusion coefficient (extended Archies law). This approach is based on an extensive international database and allows a robust estimate to be made solely on the basis of porosity. Pore water tracer profiles allow validation on the formation scale and over long timescales.

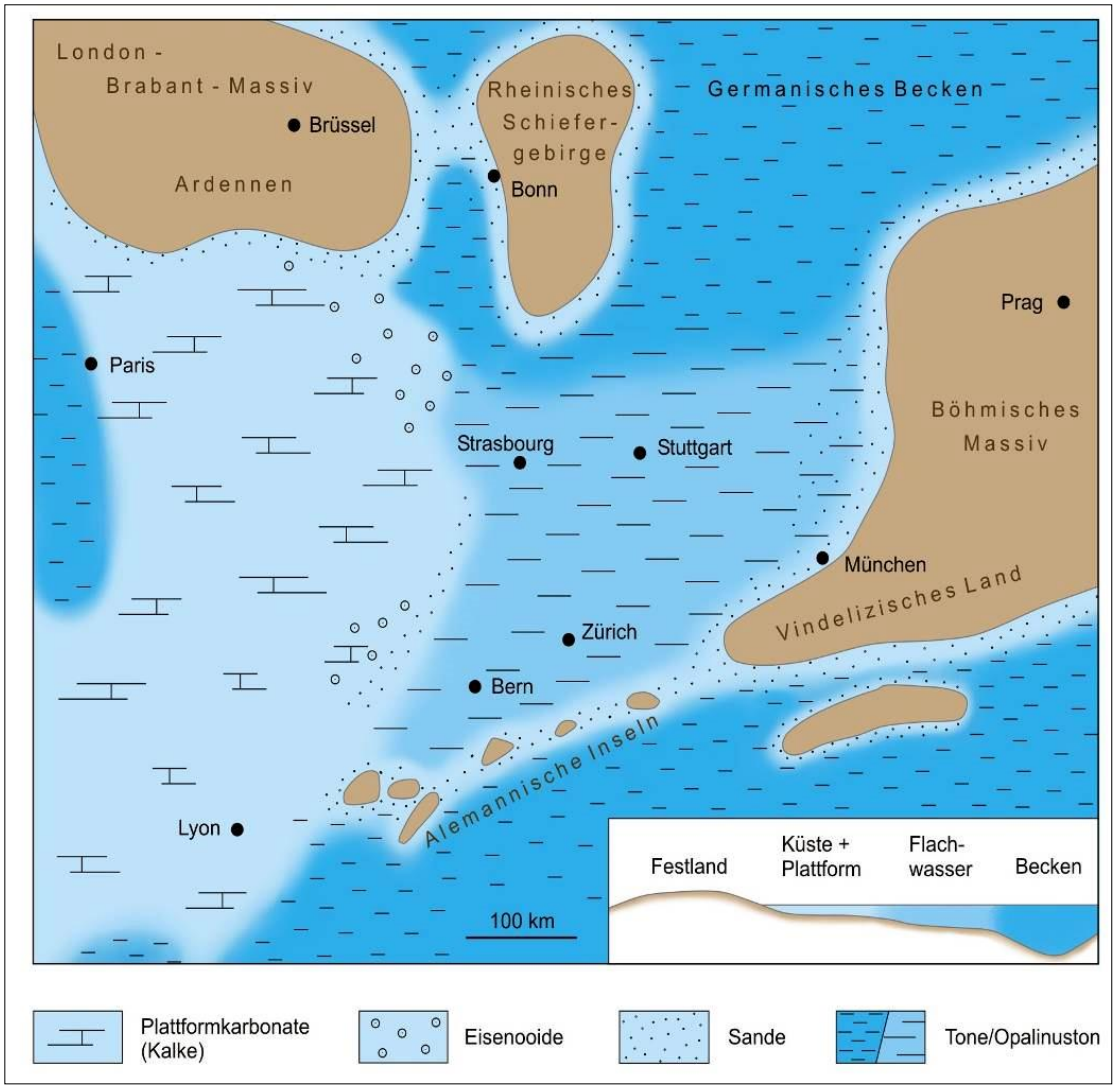

Figure 4-51. Sedimentary basin of Opalinus clay

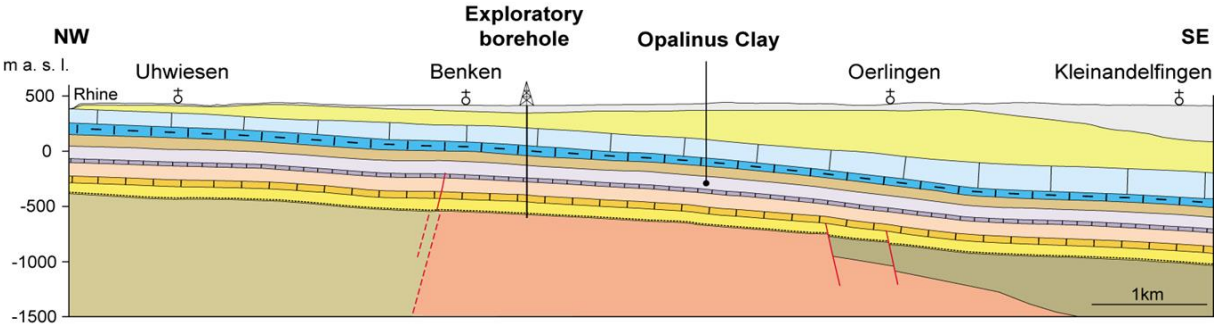

Figure 4-52. Geological profile across northern Switzerland

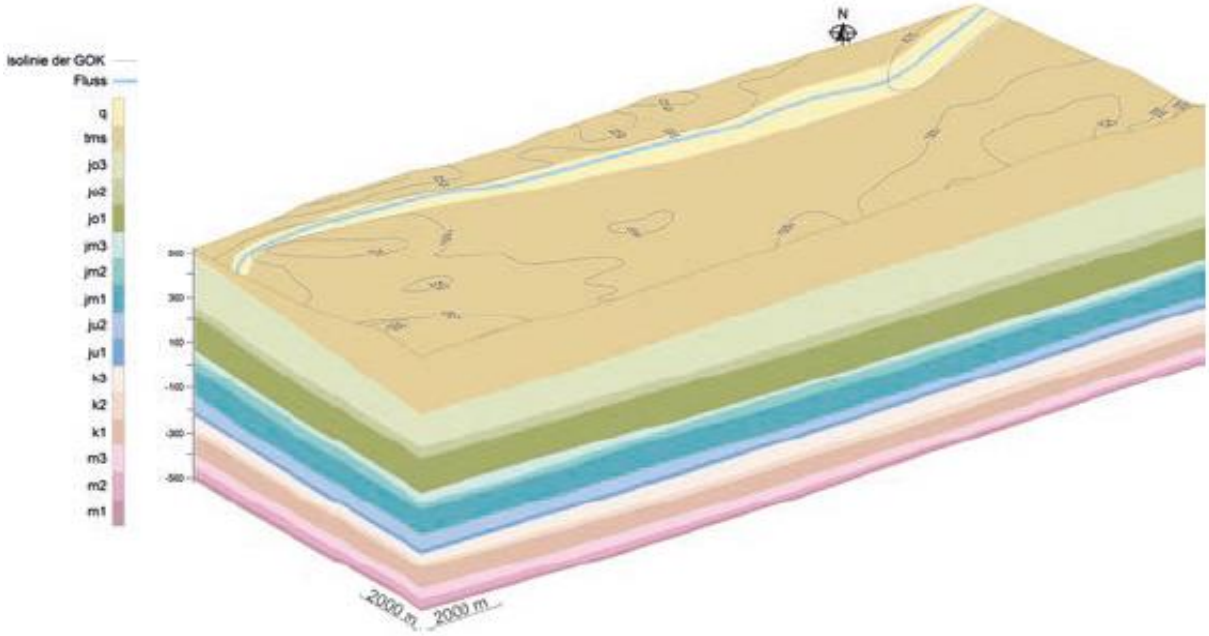

Figure 4-53 Geological reference model with Opalinus clay (jm1) for Southern Germany based on Reinhold et al. (2016)

Independent evidence such as tracer profiles or anomalous hydraulic potentials in the host rock confirm the effective containment function of the host rocks over very long time periods and underpin – for example in the case of the Opalinus Clay – the dominance of diffusive over advective solute transport, as well as the fact that the hydraulic barrier function results in a marked groundwater storey structure.

Opalinus Clay is considered to be challenging in terms of construction due to its low tensile strength and its moderate swelling capacity. On the other hand, it represents an excellent transport barrier for radionuclides due to its self-sealing capacity. The extended geomechanical database was used to derive constitutive laws and associated parameter sets for the Opalinus Clay (NAGRA 2014); this ensures the transferability of the findings on the deformation behaviour of the rock to the different geological situations in the proposed siting regions in Switzerland.

Mineralogy

On a regional scale, the mineralogical composition of the Opalinus Clay exhibits moderate lateral variability and a slight increase in clay content with depth. Quantitative laboratory analyses of core

samples from Benken, Schlattingen and Mont Terri provide a total mass fraction of clay minerals of 40-80%, a quartz content of 15-35% and 5-25% calcite. The fraction of swelling clay minerals contains 10-15% illite/smectite mixed layers. Further minerals are siderite, pyrite and feldspar. The mass fraction of organic carbon is <1%. A reference mineralogy is given in Table 4-21.

Table 4-21. "Initial state" Opalinus Clay reference mineralogy (Traber & Blaser 2013)

Minerals	Content (wt. %)
Illite	24
Ill/Sm mixed layer	9
Smectite	0
Kaolinite	18
Chlorite	9
Chl/Sm mixed layer	0
Quartz	20
Calcite	13
K-feldspar	2
Plagioclase	0.9
Dolomite/ankerite	0.4
Siderite	4
Anhydrite	0
Gypsum	0
Pyrite	1

Figure 4-54 illustrates the mineralogical and structural features of the Opalinus Clay in northeastern Switzerland on various scales. Petrophysical logs in the Benken borehole indicate moderate variability and a slight increase of clay content with depth, suggesting a division of the Opalinus Clay into 5 lithostratigraphic subunits (facies). Core inspection reveals a distinct anisotropy, made up of siderite concretions and silt and sandstone lenses, which are embedded in the clay-rich strata. The anisotropy due to bedding is largely a result of microscopic heterogeneity as seen in the thin sections, where diagenetic cementation of the pore space has been observed in the silty and sandy layers. Scanning electron microscope (SEM) images reveal that the size of the mineralogical components (10^{-7}-10^{-3} m) determines the microstructure of the rock. Quartz minerals may exhibit grain sizes in the range 0.01-1 mm, whereas the clay minerals form flake-like packages with typical sizes in the order of 100 nm to 10 µm.

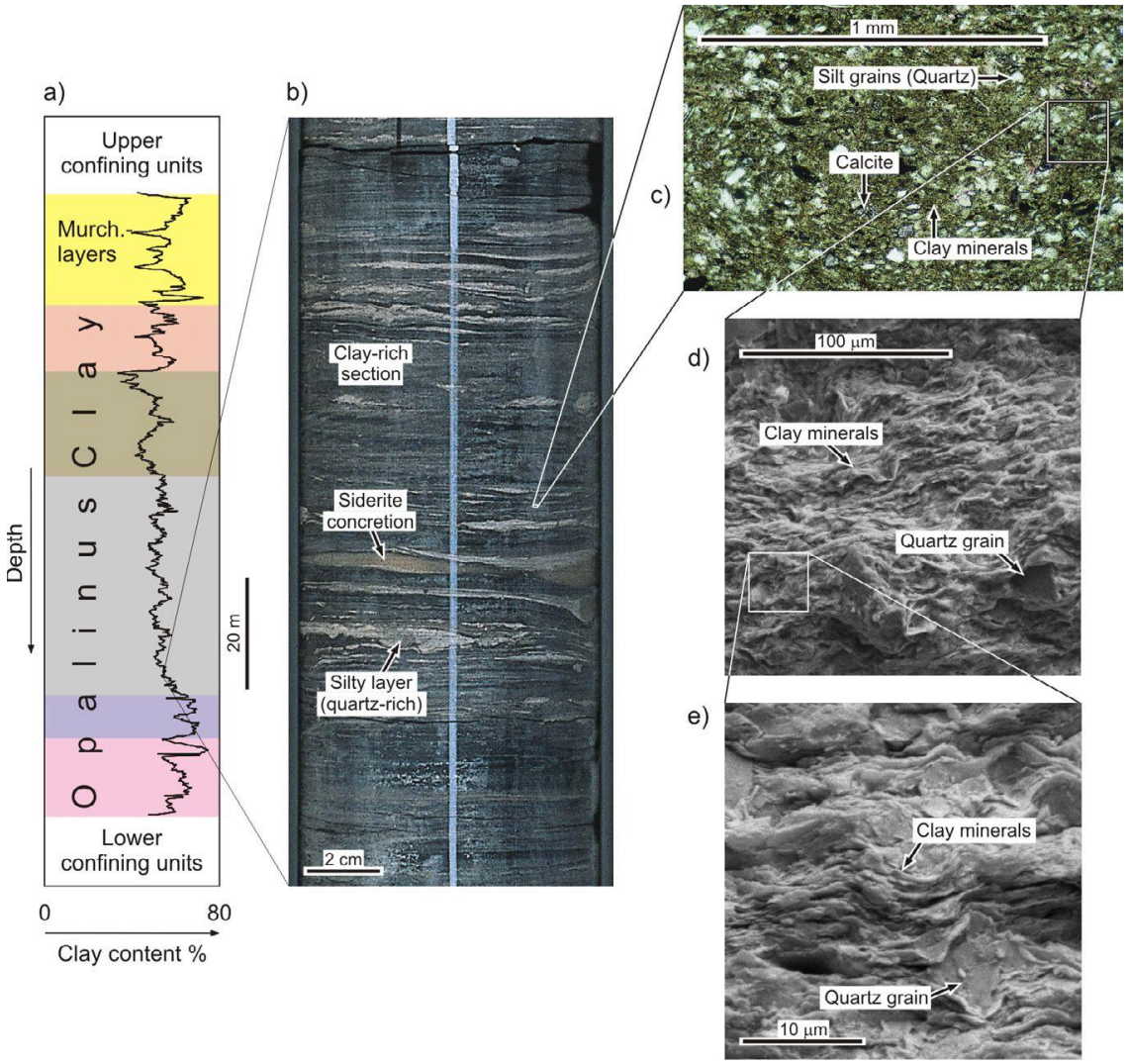

Figure 4-54. Illustration of the mineralogy and structure of the Opalinus Clay at different scales based on data from the Benken borehole in the ZNO siting area: (a) vertical profile of clay content determined by petrophysical logging, (b) core sample, (c) thin sections and (d+e) SEM images (NAGRA 2002a)

Porosity

Porosity depends on clay content and burial depth. Average values of 10, 12 and 16% are reported for Schlattingen, Benken and Mont Terri Rock laboratory, respectively. Figure 4-55 depicts a compilation of porosity measurements from various locations in Northern Switzerland as a function of the burial depth; a clear decrease of porosity with depth is observed.

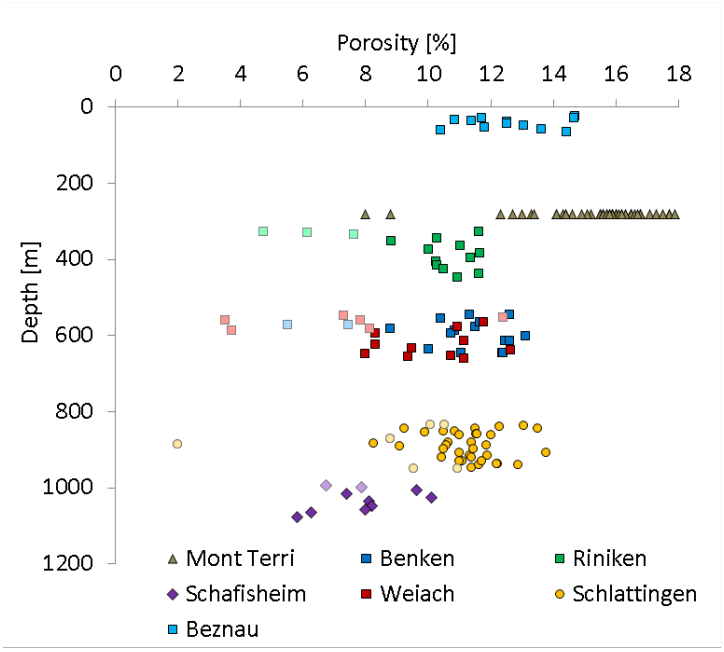

Figure 4-55. Depth dependency of porosity measured in Opalinus Clay core samples recovered from different depths, from Mazurek (2011, 2013b), Ferrari et al. (2013) and Sarout et al (2013). Light colours denote core samples with exceptionally low clay content and/or high carbonates content

The pore space of the rock is formed by a network of micro/meso and macropores, which is too small (in the order 1-100 nm) to be shown by conventional SEM methods. This network of pores actually dominates the flow and transport properties of the rock. Complementary methods were used to characterize the pore space of the Opalinus Clay, such as the measurement of the adsorption/desorption isotherms and mercury intrusion porosimetry (NAGRA 2002a). To obtain nitrogen and water isotherms, the powder samples were dried at temperatures of at least 120°C and degassed under vacuum. Nitrogen isotherms were measured at 77 K, water isotherms at 303 K by gravimetry in quasi-equilibrium mode, where water vapour was introduced at a constant, low flow rate. The pore size distributions were obtained by incremental saturation of the sample. Table 4-22 depicts the volume fractions of the different pore classes (definition according to IUPAC 1997), indicating that the majority of pores can be classified as mesopores (1-25 nm).

Table 4-22. Volume fractions (%) of the different pore classes, determined by adsorption and desorption isotherms (H_2O, N_2) after NAGRA (2002). Complementary experimental evidence suggests that at least 20% of the total pore water can be attributed to the interlayer water

Equivalent radius (nm)	Micropores <1	Mesopores 1-25	Macropores >25
Assumption: fraction of micropores is 20% (interlayers)			
N_2-Isotherm	20	46-56	24-3
H_2O-Isotherm	20	54-63	17-26

For mercury porosimetry, Hg was injected at increasing pressures into crushed, dried and degassed samples. In the context of the Project Entsorgungsnachweis (NAGRA 2002b) the maximum injection pressure was 200 MPa, and thus only pores with a radius larger than 3.7 nm could be detected. As part of NAGRA's collaboration with the oil & gas industry, new mercury intrusion experiments were conducted in 2004 at the geotechnical laboratories of Chevron in Houston by Philip Mariotti using

injection pressures up to 420 MPa. Two core samples from Benken and Mont Terri were tested - the equivalent pore size distributions are shown in Figure 4-56. The general distributions are consistent with the results of the adsorption/desorption measurements, indicating that the majority of pores in the Opalinus Clay can be classified as mesopores. The more detailed comparison of the cores from Benken and Mont Terri reveals that the pore size distributions of the core samples from Benken are shifted towards the lower pore radii. This is a clear indication for the higher degree compaction of the samples from Benken, corresponding to the higher burial depth.

	HA4 - horiz.	HA4 - vert.
Porosity (%)	9.9	10.8
Bulk density (Mg/m^3)	2.45	2.43
Grain density (Mg/m^3)	2.72	2.73

	Benken - horiz.	Benken - vert.
Porosity (%)	8.5	7.6 %
Bulk density (Mg/m^3)	2.52	2.46
Grain density (Mg/m^3)	2.75	2.66

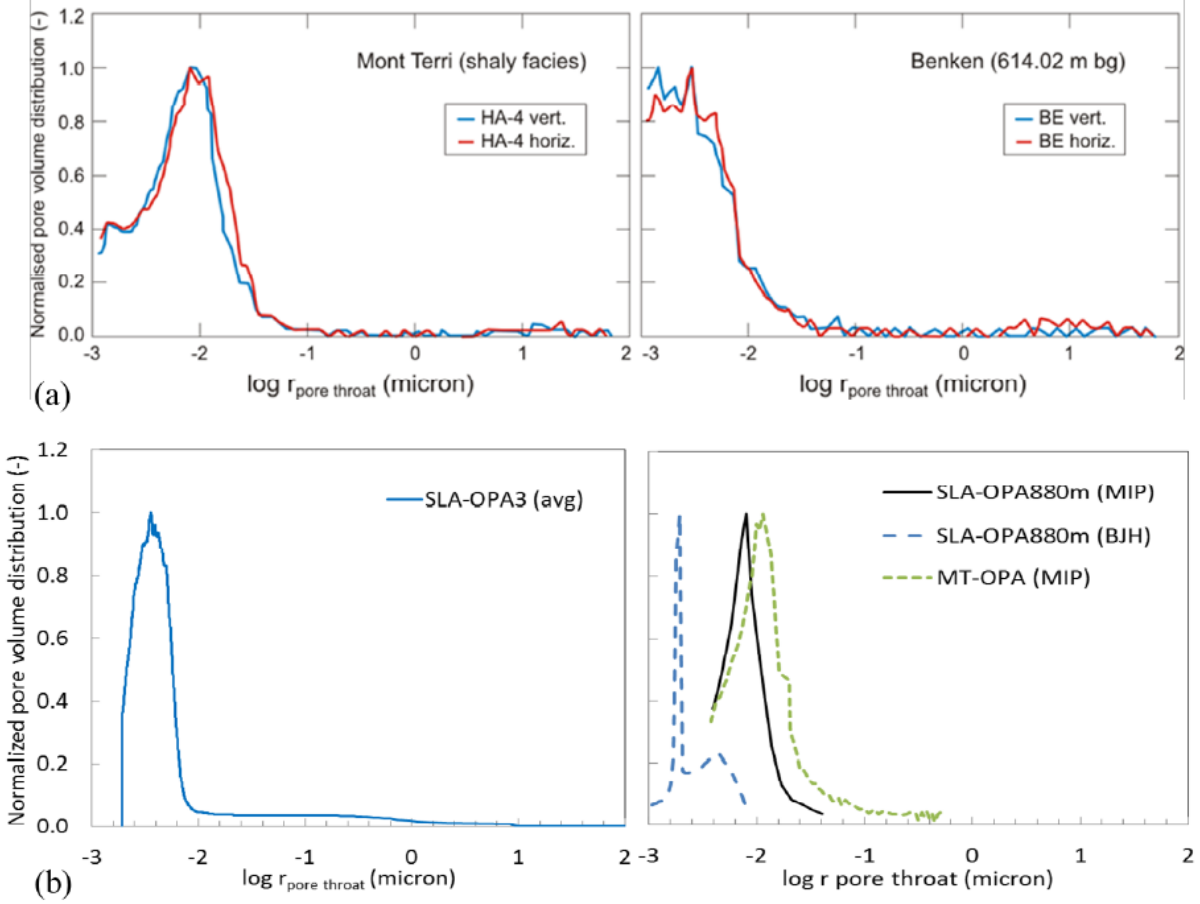

Figure 4-56. Equivalent pore size distributions of drillcore samples: (a) from Benken (sampling depth 614.82 m below ground) and Mont Terri (shaly facies), determined by mercury intrusion methods at Chevron's laboratories in Houston (by courtesy of Philip Mariotti); (b) from Schlattingen (sampling depth 880 m below ground), determined by mercury intrusion methods at EPFL (left) and UPC (right), that was complemented by BJH method

Pore water chemistry

The Opalinus Clay pore water chemistry is given in Table 4-23 (Mäder 2009) and is defined in NAGRA (2012). In addition to the "initial state" case, two further compositions representing the bandwidth of partial pressures of carbon dioxide in the Opalinus Clay were calculated. The reference composition for the Opalinus Clay pore water was derived based on a large body of experimental data on aqueous extracts from the underground laboratory (Mt. Terri) or deep boreholes (Benken), combined with

supplemental chemical constraints. For instance, the Ca and Mg concentrations were fixed by imposing calcite and dolomite saturation, respectively. Si, Fe(II) and S(-II) were constrained via quartz, siderite and pyrite saturation. Chloride concentrations were determined based on squeezed aqueous extracts and Na, K, Sr were controlled by measured occupancies in the exchangeable cationic complex combined with selectivity coefficients. Finally, the carbonate system and pH were constrained by fixing the pCO_2 ($10^{-2.2}$ bar in the reference case) and applying charge balance. An overview of the assumptions and constraints can be found in Mäder (2009).

Table 4-23. "Initial state" and range of Opalinus Clay pore water chemistry, concentrations are given in mol L^{-1}

	Opalinus Clay "Initial state"	**Opalinus Clay HIGH P-CO_2**	**Opalinus Clay LOW P-CO_2**
Temperature (°C)	25	25	25
pH log P-CO_2 (bar) Ionic strength (mol kg^{-1}) pe	7.203 -2.20 0.2299 -2.781	7.001 -1.80 0.231 -2.550	7.505 -2.80 0.229 -3.126
Dissolved constituents			
Na	1.644×10^{-1}	1.650×10^{-1}	1.638×10^{-1}
K	2.604×10^{-3}	2.616×10^{-3}	2.594×10^{-3}
Mg	9.625×10^{-3}	9.748×10^{-3}	9.519×10^{-3}
Ca	1.251×10^{-2}	1.268×10^{-2}	1.237×10^{-2}
Sr	2.106×10^{-4}	2.124×10^{-4}	2.091×10^{-4}
Ba	--	--	--
Al	--	--	--
Fe^{II}	5.24×10^{-5}	5.42×10^{-5}	5.09×10^{-5}
Fe^{III}	3.31×10^{-9}	1.73×10^{-9}	9.72×10^{-9}
Si	1.779×10^{-4}	1.78×10^{-4}	1.79×10^{-4}
Cl	1.600×10^{-1}	1.600×10^{-1}	1.600×10^{-1}
S^{IV}	2.472×10^{-2}	2.470×10^{-2}	2.474×10^{-2}
S^{-II}	1.24×10^{-8}	1.37×10^{-8}	1.16×10^{-8}
C^{IV}	2.506×10^{-3}	4.148×10^{-3}	1.214×10^{-3}

In order to perform reactive transport calculations including clay and cementitious materials, the Opalinus Clay pore water from Mäder (2009) had to be adapted. In essence, the modified model includes the additional equilibrium phases barite, kaolinite, illite and an ideal montmorillonite solid solution. This montmorillonite solid solution controls the cation exchange. Further, the modified model includes the elements Ba and Al. The resulting Opalinus Clay pore water is identical to that defined by Mäder (2009). The differences concern the number and nature of the constraints. The adapted Opalinus Clay pore water is constrained by ionic strength, the dominance of Na in solution, the SO_4/Cl-ratio in solution and the occupancies of exchangeable cations on the montmorillonite solid solution.

The main difference to the model of Mäder (2009) is that the system pCO_2 becomes a calculated entity ($10^{-2.32}$ bar in the adapted model), in accordance with the requirements formulated in Pearson et al. (2011). The adapted model involves 90% of the Opalinus Clay mass.

Hydraulic properties

Hydraulic tests have been performed in the Opalinus Clay in the Riniken, Schafisheim and Benken boreholes. Beauheim (2013) carried out a detailed review of the packer test data, applied methods and associated uncertainty providing an evaluation of the test interpretations quality. Field investigations suggest a hydraulic conductivity of the Opalinus Clay in the order of 10^{-13} to 10^{-14} m/s.

Over the course of the Mont Terri research programme, a comprehensive hydrogeological investigation programme has been conducted. Some of the key achievements on pore water flow in the Opalinus Clay were summarized in Bossart & Thury (2008):

- The highest packer tests transmissivities recorded for the Opalinus Clay at Mont Terri, which cannot be explained by EDZ phenomena are $<1\cdot10^{-10}$ m^2/s. Hydraulic packer testing in boreholes and permeameter testing with drillcore specimen exhibit consistently low values for hydraulic conductivity, typically in the range between $5\cdot10^{-12}$ and $1\cdot10^{-14}$ m/s (see also Mettier et al. 2012). No significant variations in hydraulic conductivity are seen among the different facies. A reference value of $5\cdot10^{-13}$ m/s has been reported for the Opalinus Clay at Mont Terri.
- No marked enhancement of hydraulic conductivity has been measured in the vicinity of tectonic features, indicating that fractures in the Opalinus Clay are tight. Extensive packer testing in the main fault did not reveal any correlation between hydraulic conductivity and fracture frequency along the boreholes.

Water retention functions describe the capacity of a porous medium to retain water at a given suction head. Thus, the water retention function is in principle identical to the water adsorption isotherm. The main differences are the experimental procedure and the preparation of the samples. Water retention curves of the Opalinus Clay were determined at the geotechnical laboratories of UPC (Universitat Politècnica de Catalunya) by stepwise desaturation and re-saturation of core samples under controlled humidity (NAGRA 2002a, Muñoz et al. 2003). A comprehensive experimental programme was accomplished by the laboratories of GRS (Braunschweig), aimed at comparing the capillary pressure – saturation relationships of different clay formations. More recently, the Laboratory for Soil Mechanics at EPFL (École Polytechnique Fédérale de Lausanne) and the Department of Geotechnical Engineering and Geosciences at UPC determined water retention curves as well as hydraulic and geomechanical properties of core samples from Mont Terri and from a deep borehole (Ferrari & Laloui 2012, Ferrari et al. 2013, Romero & Gomez 2013). Figure 4-57 depicts a compilation of water retention curves of Opalinus Clay samples from Mont Terri, determined by GRS, UPC and EPFL. Water retention curves of deep Opalinus core samples (880 m depth in Schlattingen borehole) obtained using the FDT (Fluid Displacement Technique with Kerdane) for the volumetric determination of the specimen are shown in Figure 4-58. The water retention curves in Figure 4-59 were based on the progressive method (Ferrari et al. 2013), where the wetting and drying paths of the retention curve are obtained on a single specimen from a core. This method better reproduces the hysteretic behaviour compared to the FDT method where the data points are from different specimens, resulting in greater scatter. The water rentention measurements were fitted with the van Genuchten model, and the curves obtained are also shown in the Figures.

Characteristic features of the Opalinus Clay are the high capillary pressures in the order of 10 MPa even at high water saturation >90% and the marked hysteresis between wetting and drying path.

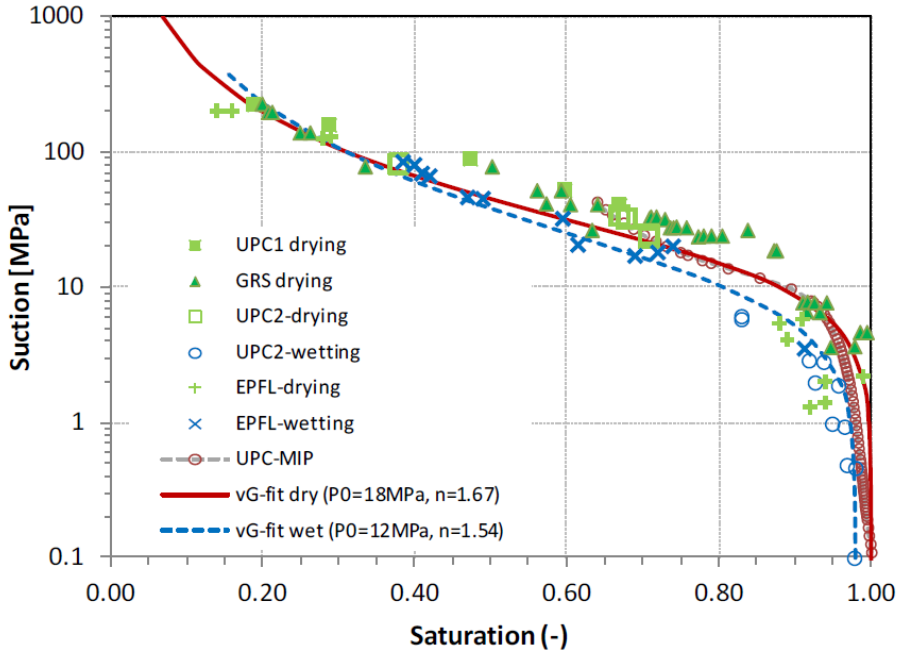

Figure 4-57 Capillary pressure measurements (water retention curves) by stepwise desaturation and re-saturation in a desiccator. The experiments were conducted by GRS (Zhang & Rothfuchs 2007) and UPC (Muñoz et al. 2003, Romero & Gomez 2013) and by EPFL (Ferrari & Laloui 2012)

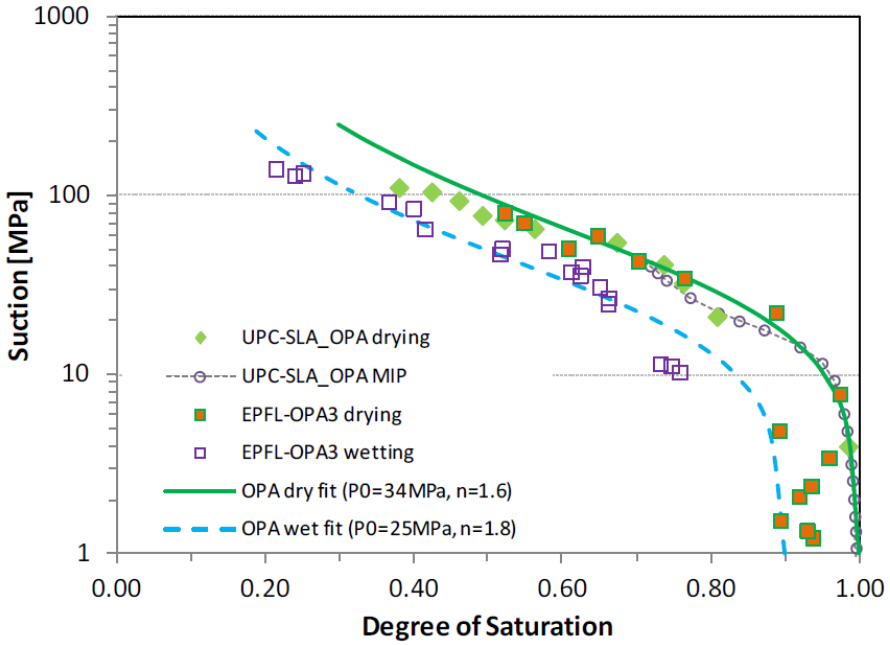

Figure 4-58. Capillary pressure measurements (water retention curves) by stepwise desaturation and re-saturation using a WP4c dew-point psychrometer and volumetric measurements using the Kerdane method on deep core samples from the Schlattingen borehole (Ferrari et al. 2013, Romero & Gomez 2013)

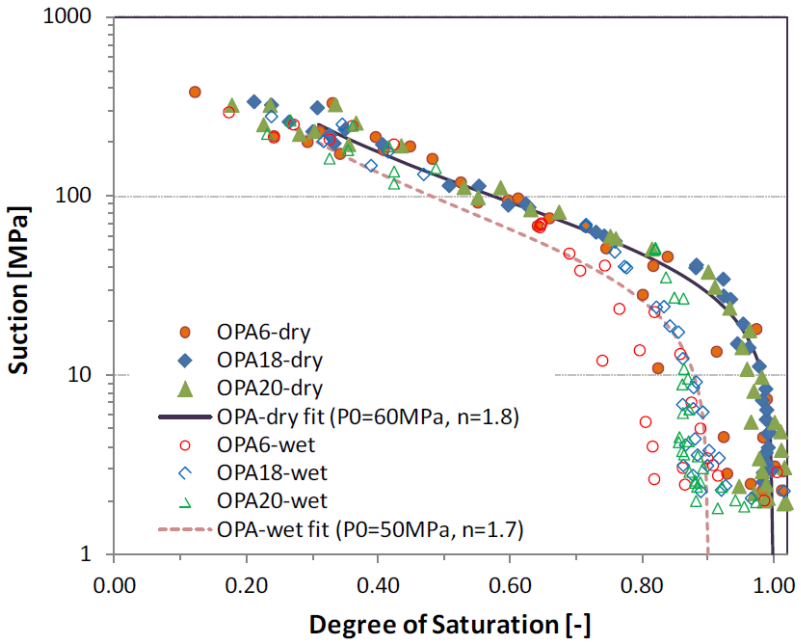

Figure 4-59. Capillary pressure measurements (water retention curves) by stepwise desaturation and re-saturation using a WP4c dew-point psychrometer and volumetric measurements using the progressive method on a deep core sample from the Schlattingen borehole (Ferrari et al. 2013)

The mobility of the gas in the intact Opalinus Clay (expressed in terms of a relative permeability relationship) can be determined by water and gas permeameter experiments in the laboratory and by in-situ gas injection tests in boreholes. An experimental data base for the derivation of relative permeabilities of the intact Opalinus Clay was elaborated in the context of the Project Entsorgungsnachweis. The key references of previous experiments are given in NAGRA (2002a) and in Marschall et al. (2005). Further experiments and data analyses have been conducted since then as part of the Mont Terri Project (Poller et al. 2007, Croisé et al. 2006) and in the context of the EU-funded integrated project NF-PRO. In the context of SGT/Stage 2, a complementary test programme was initiated, drawing on Opalinus Clay core samples from Mont Terri ("shallow samples") and from the Schlattingen borehole ("deep samples"). The tests were conducted in a triaxial cell with flow direction parallel (shallow samples only) and perpendicular to bedding at isotropic stress levels of 15 and 19 MPa, respectively (Romero & Gomez 2013). The corresponding gas injection pressures (14 and 18 MPa, respectively) remained below the confining stress.

The water/air permeability experiments on the Opalinus Clay sample show clear evidence for the dependency of water permeability on void ratio and thus on constitutive stress (estimated as the isotropic stress minus the air pressure at the injection point). Furthermore, a marked dependency of gas dissipation was observed on the direction of gas flow with respect to bedding orientation. Significantly higher gas flow rates were observed for the flow direction parallel to bedding. Another important observation is the marked dependency of volumetric strain on the constitutive stress changes during air injection/dissipation tests. The samples displayed expansion at the early fast air injection stage in response to constitutive stress decrease, and dominant compression on air pressure dissipation.

4.1.3.1 Hydro-mechanical behaviour of the host claystone

Geotechnical characteristics of the Opalinus Clay have been determined as part of comprehensive laboratory programmes, revealing moderate stiffness (Young's modulus in the range 5–15 GPa),

moderate strength (UCS values of the intact rock matrix between 10 and 35 MPa), distinct swelling pressures (0.5–2 MPa) and OCR of between 1.5 and 2.5 (NAGRA 2002b).

Parameters of the Opalinus Clay as defined for the FE Experiment in Alcolea et al. (2019) are shown in Table 4-24.

Table 4-24. Parameters of the Opalinus Clay used for the scoping calculations of the FE Experiment

Group	Parameter	Symbol	Units	Value
Elasticity	Young modulus parallel to bedding	$E_{\parallel}$	MPa	8000
	Young modulus perpendicular to bedding	$E_{\perp}$	MPa	4000
	Poisson ratio parallel to bedding	$n_{\parallel}$	-	0.35
	Poisson ratio perpendicular to bedding	$n_{\perp}$	-	0.25
	Thermal expansion	α_T	1/K	$1.7 \cdot 10^{-5}$
Retention curve	Type of curve	Van Genuchten		
	Entry pressure	p_0	MPa	20
	Shape parameter	n	-	1.67
	Res. liqu. sat.	$S_{r,l}$	-	0.3
Darcy	Intrinsic permeability parallel to bedding	$k_{\parallel}$	m^2	$5.0 \cdot 10^{-20}$
	Intrinsic permeability perp. to bedding	$k_{\perp}$	m^2	$1.0 \cdot 10^{-20}$
	Shape factor (rel-perm)	ε, γ	-	0.5, 0.33
Fick	Tortuosity for vapour	τ	-	0.8
Fourier	Sat. thermal conductivity parallel to bedding	$\lambda_{sat,\parallel}$	W/mK	2.4
	Saturated thermal conductivity perp. to bedding	$\lambda_{sat,\perp}$	W/mK	1.3
General	Solid density	ρ_s	kg/m^3	2340
	Solid specific heat	c_s	J/kgK	995
	Initial porosity	ϕ	-	0.13
	Initial degree of saturation	S_l	-	1

4.1.3.2 Hydro-mechanical behaviour of the fracture/damage claystone

The values for the scoping calculations of the FE experiments used in Senger (2015) are given in Table 4-25.

Table 4-25. Parameters of the Excavation Damage Zone as defined for the FE Experiment in Alcolea et al. (2019)

Group	Parameter	Symbol	Units	Value
Elasticity	Young modulus	E	MPa	6000
	Poisson ratio	n	-	0.3
	Thermal expansion	α_T	1/K	$1.7 \cdot 10^{-5}$
	Type of curve	Van Genuchten		

Group	Parameter	Symbol	Units	Value
Retention curve	Entry pressure	p_0	MPa	9
	Shape parameter	n	-	1.67
	Res. liqu. sat.	$S_{r,l}$	-	0.3
Darcy	Intrinsic permeability parallel to bedding	$k_{\parallel}$	m^2	$5.0 \cdot 10^{-20}$
	Intrinsic permeability perp. to bedding	$k_{\perp}$	m^2	$1.0 \cdot 10^{-20}$
	Shape factor (rel-perm)	ε, γ	-	0.5, 0.33
Fick	Tortuosity for vapour	τ	-	0.8
Fourier	Sat. thermal conductivity parallel to bedding	$\lambda_{sat,\parallel}$	W/mK	2.4
	Saturated thermal conductivity perp. to bedding	$\lambda_{sat,\perp}$	W/mK	1.3
General	Solid density	ρ_s	kg/m^3	2340
	Solid specific heat	c_s	J/kgK	1086
	Initial porosity	ϕ	-	0.13
	Initial degree of saturation	S_l	-	1

4.1.4 Summary

The present chapter aims at summarizing the relevant properties of the three claystone formations proposed to host radioactive waste.

The Boom Clay Formation is a detrital marine deposit from the Oligocene (Tertiary) and more specifically from the Rupelian stage, between 33.9 and 28.4 Ma. The formation is composed of rhythmically alternating clay-rich and silt-rich materials resulting in a gray-tone banding. The Boom Clay is a poorly indurated clay with a well-developed particle alignment according to the bedding plane and high porosity.

The Callovo-Oxfordian (COx) claystone was deposited 160 Ma ago (Middle-Upper Jurasic) over a period of approximately five million years, in an open and calm marine environment. It consists of three major geological units, the relevant one being the argillaceous unit (UA) at the base, the most homogeneous and the richest in argillaceous minerals (more than 40% on average) of the three.

Opalinus Clay occurs extensively in northern Switzerland and neighbouring countries. The layer package is around 110 metres thick and has a uniform structure. It originated from shallow marine sedimentation in the Jurassic period (Aleanian) some 173 million years ago.

Hence, all of them were deposited in a marine environment. As a consequence of their geologic histories (burial, subsidence, uplift, erosion) and particular mineralogy and grain size, the resulting porosity and mechanical characteristics are considerably different. Thus, the Boom clay, which is the youngest and subjected to less burial, has a porosity of 35-40%, consequently with higher hydraulic conductivity (Table 4-28) and lower thermal conductivity (Table 4-29) than the other clays. It can be considered a plastic material (OCR = 2.4 at the level of the URL). In contrast, the COx claystone has a porosity of 14-20% and the Opalinus clay of 10-16%, having been subjected to large extent of diagenesis and tectonic activity (in the case of Opalinus). The two are much stiffer than the Boom clay, can be considered as moderately over-consolidated claystones and are brittle materials at low confining pressure and more ductile at high confining pressure.

To make easier the comparison of the three clays properties at a glance, the following Tables summarise some of them.

Table 4-26. Mineralogical composition of the clay host rocks

Mineral (%)	Boom Clay[a]	COx[b] (UA2)	Opalinus[c]
Clay minerals		24 – 52 (52)	>40
Illite	5 – 11	8 – 20 (17)	23
Smectite + Interstratified illite/smectite	7+7 – 17+25	15 – 30 (28)	12
Kaolinite	1 – 6	0 – 4 (4)	18
Chlorite	1 – 3	1 – 3 (3)	8
Interstratified chlorite/smectite	0 – 5		0
Interstratified kaolinite/smectite	1 -- 6		
Quartz	20 – 52	15 – 26 (17)	20
K-Feldspars	3 – 9	1 (1)	2
Plagioclase	1 – 5	1 (1)	1
Carbonates		24 – 46 (26)	
Calcite	0 – 6	20 – 40 (22)	14
Siderite	0 -- 4	Present	3
Dolomite	0 -- 1	3 – 8 (4)	<1
Ankerite			
Muscovite	5 -- 9		
Pyrite	0 -- 4	1 – 3 (1)	<1
Organic Carbon	0 – 5	0.5 – 1	1
Others			
Gypsum	0 -- 1	Present	
Glauconite, apatite, rutile, anatase, ilmenite	Present	Present	
Zircon, monazite, xenotime			

[a] Frederickx (2019), [b] Rebours et al. 2005: [c] NAGRA 2014c

Table 4-27. Pore water composition of the clay host rocks

Element (mmol/L)	Boom Clay	COx	Opalinus[a]
pH		7.1	7.2
Ionic strength (mol/L)		0.1	0.23
Na	15.6	47	164
K	0.2	0.5	2.6
Ca	0.05	5	12.5
Mg	0.06	4.3	9.6
Fe	0.003	0.02	0.05
Si	0.1	0.2	0.18
Al	$2.4 \cdot 10^{-5}$		-
Sr		0.2	0.2
HCO_3^-	14.4		2.04
TIC		2.5	1.5 – 4.0
Cl	0.7	37	160

Element (mmol/L)	Boom Clay	COx	Opalinus[a]
Total S	0.02		25
SO_4^{2-}	0.02	12.9	75

[a] NAGRA 2014c, Courdouan Merz 2008

Table 4-28. Hydraulic properties of the clay host rocks

	Boom Clay	COx	Opalinus[a]
Hydraulic conductivity, k (m/s)	$1.5 - 4 \cdot 10^{-12}$	$\sim 10^{-13}$	$10^{-13} - 10^{-15}$
Vertical hydraulic conductivity, k_V (m/s)	$2 - 3.5 \cdot 10^{-12}$	$1 - 2 \cdot 10^{-13}$	$1.4 - 9.4 \cdot 10^{-14}$
Horizontal hydraulic conductivity, k_H (m/s)	$4 - 5.5 \cdot 10^{-12}$	$3 - 6 \cdot 10^{-13}$	$2.9 \cdot 10^{-14} - 1.1 \cdot 10^{-15}$

[a] Horseman & Harrington 2002

Table 4-29. Thermal conductivity of the clay host rocks (on site)

	Boom Clay	COx	Opalinus
λ_h	1.25 - 1.35	2.0±0.1	2.4
λ_v	1.61 - 1.70	1.30±0.05	1.3

Table 4-30. Mechanical properties of the clay host rocks

Property		Boom	COx	Opalinus
Solid phase density (kg/m^3)	ρ_s	2639	2690	2340
Bulk density (kg/m^3)	ρ'	2000	2450	
Porosity	n	0.39	0.18	0.13
Isotropic intrinsic permeability (m^2)	k	$2.8 \cdot 10^{-19}$	$2.3 \cdot 10^{-20}$	
Vertical intrinsic permeability (m^2)	k_v	$2 \cdot 10^{-19}$	$1.3 \cdot 10^{-20}$	$1 \cdot 10^{-20}$
Horizontal intrinsic permeability (m^2)	k_h	$4 \cdot 10^{-19}$	$3.9 \cdot 10^{-20}$	$5 \cdot 10^{-20}$
Isotropic Young's modulus (MPa)	ρ_s	300	6000	
Young's modulus parallel to bedding (MPa)	$E_{//}$		10000	8000
Young's modulus perpendicular to bedding (MPa)	$E_\perp$		6200	4000
Poisson's ratio (-)	ρ'	0.125	0.3	0.3
Poisson's ratio parallel to bedding (-)	$\nu_{//}$		0.21	0.35
Poisson's ratio perpendicular to bedding (-)	$\nu_\perp$		0.35	0.25
Linear thermal expansion coefficient (°C^{-1})	α_s	$1 \cdot 10^{-5}$	$1.25 \cdot 10^{-5}$	$1.7 \cdot 10^{-5}$
Solid phase specific heat (J/kg/K)	c_p	769	978	995

4.2 Relevant large-scale tests

4.2.1 Boom Clay

The geological disposal of HLW in Boom clay has been investigated for more than 40 years (ONDRAF/NIRAS 2013). In 1974, the Belgian nuclear research centre (SCK•CEN) initiated the R&D programme on this topic. As the preliminary laboratory research yielded to promising results, the construction of the underground research laboratory (URL) facility HADES (High-Activity Disposal Experimental Site) in the Boom Clay started at the beginning of the 1980s. At the HADES URL site in Mol, the Boom Clay Formation lies at a depth between 185 m and 287 m. The HADES URL was constructed at 223 m below ground surface, which is almost at the middle of the clay formation. Figure 4-60 summarizes its construction history from the commencement with the first shaft and the first gallery to the last construction with the excavation of the PRACLAY gallery in 2007. The 45-m long PRACLAY gallery, perpendicular to the Connecting gallery, was built to demonstrate the feasibility to construct galleries and T-crossings in the deep Boom Clay with industrial techniques (Van Marcke et al. 2013). This gallery hosts now the large-scale PRACLAY heater test.

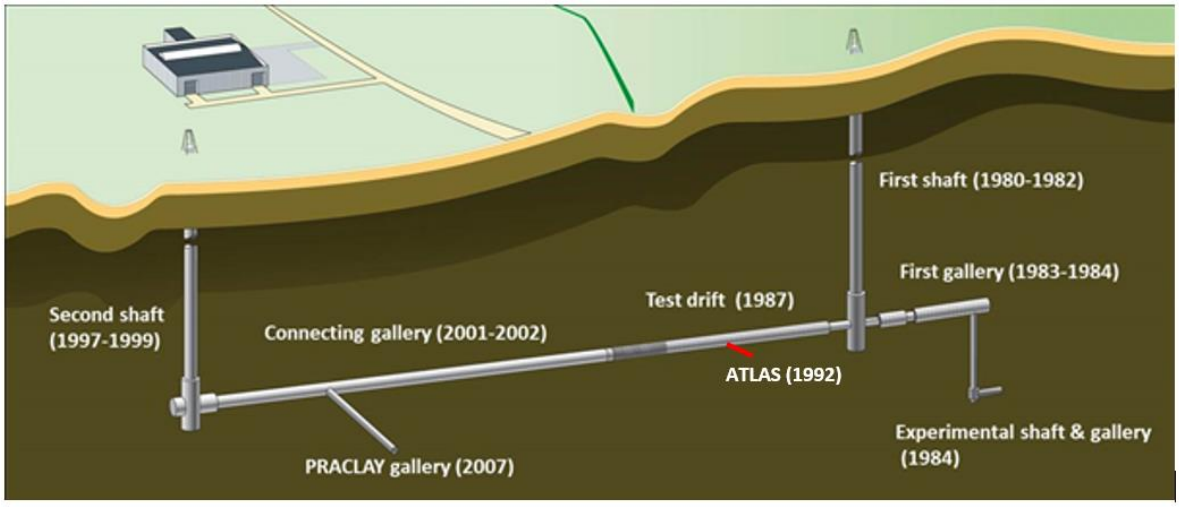

Figure 4-60. Layout of the HADES URL at Mol, Belgium (EURIDICE website, 2018)

The large-scale PRACLAY heater test has been running since November 2014. Before the switching-on of the PRACLAY heater, a small-scale ATLAS heater test ran in a small diameter ATLAS borehole (Figure 4-61) in three phases (ATLAS I to ATLAS III) between 1993 and 2008. These tests were performed to examine at different scales the THM responses to heating of Boom Clay in configurations mimicking disposal galleries for heat-emitting waste, and to confirm and/or refine the THM properties values obtained from the laboratory characterisation programme, especially the transversely anisotropic THM properties of the Boom Clay.

4.2.1.1 Small-scale ATLAS heater test

The small-scale ATLAS heater test was performed to:

- assess the integrated thermo-hydro-mechanical responses to the heating of Boom Clay;
- confirm and/or refine the THM properties representative of the far-field Boom Clay around the disposal gallery, especially the transversely anisotropic properties.

To focus on the THM characterization of Boom Clay and to facilitate the interpretation of the test results, the test setup was designed to have well-defined boundary conditions and a simple geometry

with which the test responses depend only on the Boom Clay properties. Figure 4-61 presents a schematic horizontal view of the ATLAS heater test setup.

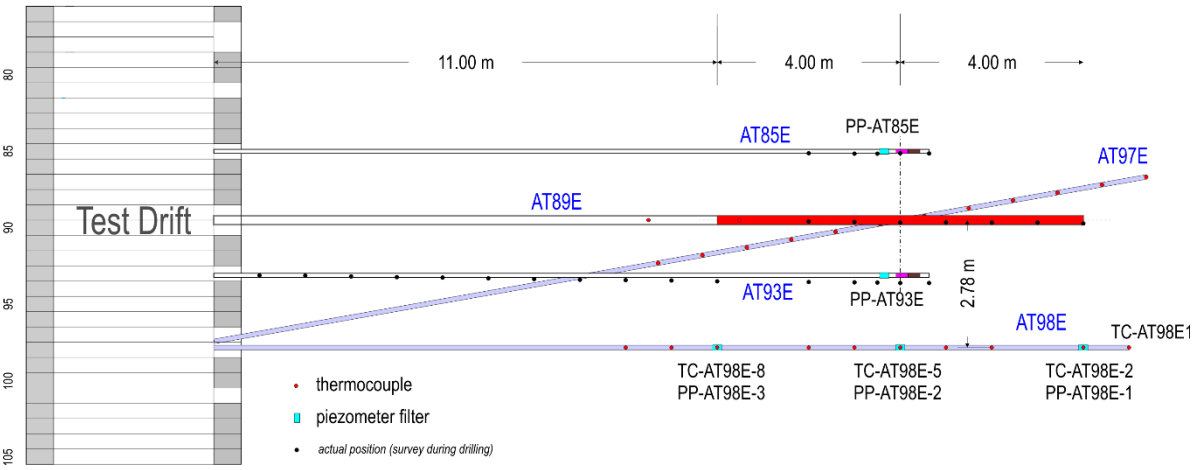

Figure 4-61. Schematic horizontal view of the ATLAS heater test set-up

The original test set-up was established in 1992 by SCK•CEN within the framework of the European project Interclay II (1990–1994). An 8-meter long heater was installed in a small diameter (190 mm) horizontal borehole (AT89E) at a depth of 11 m from the Test Drift. Two horizontal observation boreholes (AT85E and AT93E) were installed at a parallel distance of 1.5 m and 1.3 m to the heater borehole (AT89E) respectively. The ends of two observation boreholes (with similar depth from the Test Drift to the heater centre) were instrumented with piezometer filters and flat-jacks to measure the pore water pressure, temperature and stresses. During the ATLAS I, a constant heater power of 900 W was applied from July 1993 to June 1996 (De Bruyn & Labat 2002). During the ATLAS II, the power was increased to 1800 W and maintained at that level from June 1996 until an instantaneous shutdown in June 1997 (De Bruyn & Labat 2002). The test set-up was extended in 2006 by drilling one downward inclined observation borehole AT97E and one horizontal borehole AT98E (also shown in Figure 4-61) to enlarge the observation extent and investigate the thermo-hydro-mechanical anisotropic behaviour of the Boom Clay. The heater was switched on again from April 2007 with a stepwise power increase from 400 W to 900 W and then 1400 W, followed by an instantaneous shutdown in April 2008. This heating phase is called ATLAS III (Chen et al. 2011).

The test provided a large amount of good-quality data on the temperature and pore water pressure, based on which some noteworthy observations were made. The extended measurements of the temperature field provided clear evidence of thermal anisotropy. The instantaneous but temporary pore water pressure decrease after increasing power and the temporary pore water pressure increase after cooling are observed from the measurements in the horizontal boreholes (AT85E, AT93E & AT98E, Figure 4-62). Since the impact on the Boom Clay thermo-hydro-mechanical behaviour resulting from the drilling of the small-diameter heater borehole and installation of steel casing should be very limited, the ATLAS test responses are more representative of the THM behaviour of far-field Boom Clay around the disposal gallery.

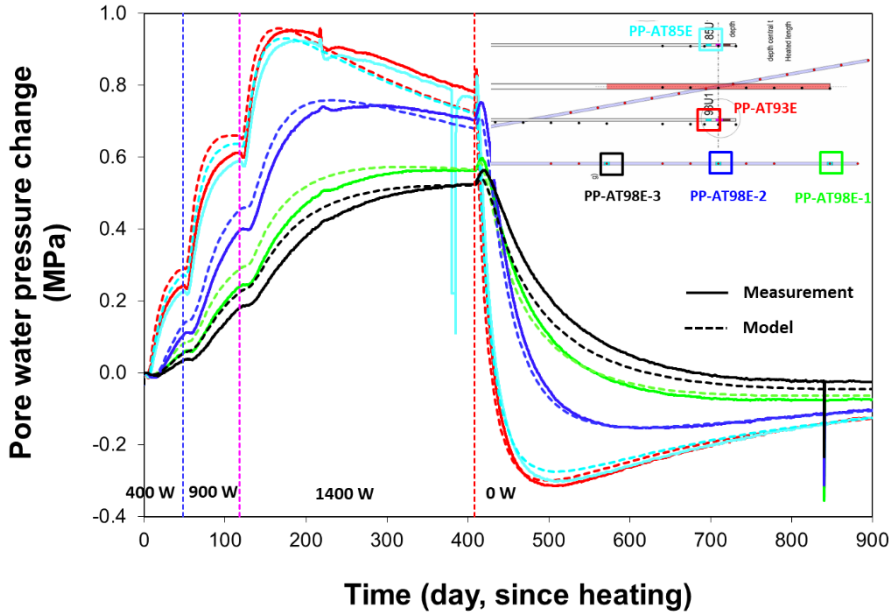

Figure 4-62. Comparison of pore water pressure at some points between measurements and modelling

To enhance the understanding of the THM responses in the Boom Clay to heating, coupled THM numerical analyses were carried out for the ATLAS heater test (François et al. 2009, Chen et al. 2011). For the ATLAS III heater test, a three-dimensional coupled THM model was established incorporating constitutive laws with consideration of the transverse THM anisotropy. A set of transversely anisotropic parameters (Table 4-31) were obtained with which the modelling could well reproduce the measured pore water pressure (Figure 4-62) and temperature from the ATLAS III heater test. Besides, the numerical interpretation indicated that the instantaneous but temporary pore water pressure variations after increasing power and cooling were due to the mechanical anisotropy.

Table 4-31. A set of Boom Clay THM parameters obtained from the numerical interpretation of ATLAS III heater test

Direction to the bedding plane	Thermal conductivity (W/m·K)	Intrinsic permeability (m^2)	Young modulus (MPa)	Thermal expansion coefficient of pore water (1/°C)
Parallel	λ_{par}= 1.65	$k_{i\,par}$= $4.0\cdot10^{-19}$	E_{par}= 1400	$3.4\cdot10^{-4}$
Perpendicular	λ_{per}= 1.31	$k_{i\,per}$= $2.0\cdot10^{-19}$	E_{par}= 700	

4.2.1.2 Large-scale PRACLAY heater test

The main goal of the PRACLAY heater test is to determine the combined impact of mechanical disturbance caused by gallery construction and a large-scale thermal load on the Boom Clay due to heat-emitting high-level waste. This combined impact leads to THM perturbations in the clay. It is important to check whether the perturbation can affect the performance of the Boom Clay as a host rock for the geological disposal of heat-emitting radioactive waste.

More specifically, the goals of the heater test (Van Geet et al. 2007) are to:

– confirm the thermal properties of the Boom Clay on a large scale and refine the models that describe the thermal evolution of the Boom Clay surrounding a disposal gallery containing heat-emitting radioactive waste;

- estimate the major consequences of the thermo-hydro-mechanical impact on the Boom Clay, particularly within the EDZ, focusing primarily on the mechanical damage and hydraulic conductivity;
- assess the long-term stability of the concrete lining under thermal loading;
- increase knowledge of the performance and reliability of monitoring devices under thermal stress and heat;
- assess the thermally and excavation-induced geochemical perturbations and their possible impact on radionuclide transport-related parameters; this is not a priority, however, and should not jeopardise achievement of the other goals.

To cope with possible future changes in the repository design, the test was designed to be as design-independent as possible.

Since it is not possible to fully reproduce the timescale (hundreds or thousands of years, Sillen & Marivoet 2007), the spatial scale and the boundary conditions of a real repository, the heater test is being conducted under a well-controlled and reasonably conservative combination of thermal, hydraulic and mechanical boundary conditions. For the heater test, a 34 m-long PRACLAY gallery will be heated for 10 years at a constant temperature of 80°C at the interface between the concrete lining of the gallery and the clay (before heating, the Boom Clay has a temperature of 16°C at 225 m depth). The temperature of 80°C is higher than expected in a high-level waste repository and, in this respect, the test is on the conservative side compared with the temperature conditions in a real repository. Also to be on the conservative side, the test is designed so that the liquid overpressures in the clay resulting from thermal expansion of the pore water cannot easily dissipate towards the gallery (quasi-undrained hydraulic boundary conditions), which maximises the liquid pressure increase resulting from thermal expansion of the pore water. In fact, an increase in pore liquid pressure within the natural barrier reduces the contact forces between the clay particles making up this barrier, reducing its strength and diminishing the mechanical stability of the repository. The quasi-undrained hydraulic boundary condition required the installation of a hydraulic seal, with bentonite-based material, at the intersection between the heated and non-heated sections of the gallery and backfilling of the heated section with saturated sand. The installation of a hydraulic seal constituted the Seal Test, the main goal of which is to hydraulically seal the heated section of the gallery and its surrounding excavation-disturbed zone from the non-heated section. The hydraulic seal is purpose-built for the PRACLAY experiment and is not representative of seals in a geological disposal repository.

The construction of the PRACLAY gallery and its crossing with the Connecting gallery constituted the Gallery and Crossing Test. The feasibility of excavating a gallery in the Boom Clay at a depth of 225 m using an industrial excavation technique had already been demonstrated in constructing the Connecting gallery. During the construction of the PRACLAY gallery, it was possible to optimise the excavation technique and further investigate the hydro-mechanical response of the Boom Clay to the excavation work.

The Gallery and Crossing Test, the Seal Test and the Heater Test together make up the PRACLAY In-Situ Experiment. A detailed description of all aspects of the design and installation of the experiment can be found in Van Marcke et al. (2013) and Dizier et al (2016).

Experimental set-up

An overview of the main components of the PRACLAY heater test is given in this section. The PRACLAY gallery was excavated in 2007 and has a length of 45 m. The heated part of the gallery is 34 m long and is separated from non-heated part by a hydraulic seal. The heated section of the gallery was backfilled

with sand, saturated and pressurised with water after the installation of the seal in 2010. The main role of the seal is to hydraulically cut off the heated part from the non-heated part (Figure 4-63). Bentonite clay, which has a high swelling potential under hydration, was chosen to achieve this goal. In this way, the interface between the Boom Clay and the bentonite is sealed and permeability in the contact zone surrounding the seal is reduced. The high pressure inside the PRACLAY gallery is thus maintained.

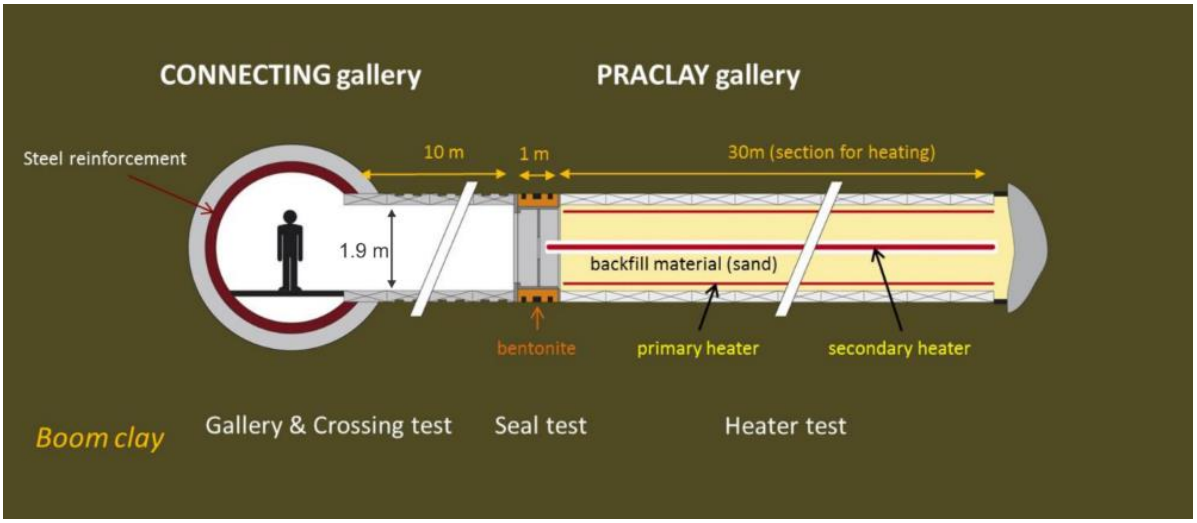

Figure 4-63. An overview of the PRACLAY In-Situ Experiment, including the component of heater test. The PRACLAY gallery has an inner radius of 0.95 m and the thickness of the lining is 30 cm

The heating system consists of a primary heater, attached to the gallery lining, and a secondary heater, which is placed in a central tube that rests on a support structure. Both of these are electrical heaters. Since the primary heater is inaccessible during the heater test, twice as many primary heater cables than necessary have been installed (100% redundancy). The secondary heater is a back-up and remains accessible and replaceable at all times during the test. A control system regulating the heating power as a function of measured and target temperatures is also part of the heating system. During the start-up phase, the power was increased in a controlled manner to limit the thermal gradient over the gallery lining.

The heated part of the PRACLAY gallery is divided into three zones as described in Figure 4-64:

- Zone 1: front-end zone, 2.26 m long, close to the PRACLAY seal,

- Zone 2: middle zone, 28.48 m long, in the middle of the experimental part of the gallery,

- Zone 3: far-end zone, 3.29 m long, at the end of the gallery.

The power input can be controlled independently in each of the three zones. In this way, the end effects can be minimised and a temperature field that is as uniform as possible can be created along the heated section. This also provides the opportunity to study the long-term effects of high temperature on three lining rings made of UHPC (ultra-high performance concrete) installed in zone 3. Each zone comprises four heating sectors (sectors 1 to 4).

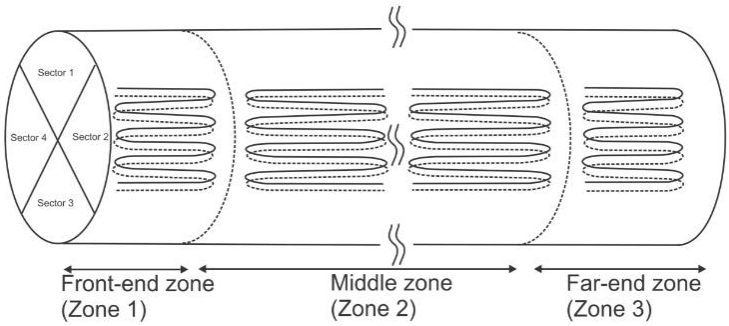

Figure 4-64. The heater layout is divided into three longitudinal zones (front-end, middle and far-end) and into four sectors. In this Figure, only the heater cables in sector 2 are shown

As described in the report on the design and installation of the PRACLAY In-situ Experiment (Van Marcke et al., 2013), the seal has to hydraulically cut off the heated part of the PRACLAY gallery from the non-heated part (Figure 4-65). This is achieved by physically closing off the heated part of the gallery and by lowering the hydraulic conductivity of the clay around the seal. To this end, a bentonite ring was installed around a central steel cylinder and in direct contact with the Boom Clay. This bentonite ring has swelled with the absorption of water causing contact with the surrounding clay and allowing the closure of the Boom Clay/bentonite interface. Moreover, recompression of the Boom Clay is expected due to the swelling of the bentonite, which locally reduces the effect of the excavation of the gallery (EDZ).

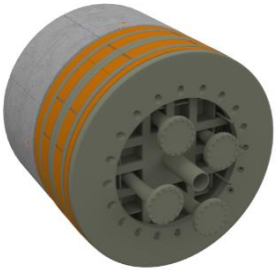

Figure 4-65. 3D view of the seal with a central steel cylinder and an annular ring of bentonite (orange) against the clay

An insulated door was installed on 2 March 2015 in front of the seal to minimize the heat loss from the seal into the accessible PRACLAY gallery.

The part of the PRACLAY gallery that is heated is filled with water-saturated sand in order to:

- create quasi-undrained hydraulic boundary conditions at the clay/lining interface;
- efficiently transfer heat from the heater elements to the lining.

The sand (Mol M34) was put in place by blowing it in a dry state into the gallery before September 2011. Subsequently, a total volume of about 43 m^3 of tap water was injected into this part of the gallery between January and May 2012 (Figure 4-66). Saturation of the backfilled gallery was then naturally completed with the water flowing from the host Boom Clay into the gallery. The pore water pressure in the gallery has gradually increased since then. On 3 November 2014 it reached 1 MPa, and the backfilled PRACLAY gallery was estimated to be fully saturated. During the heating phase of the experiment, the pressure in the backfilled gallery evolves naturally without any human intervention (adding or subtracting an amount of water).

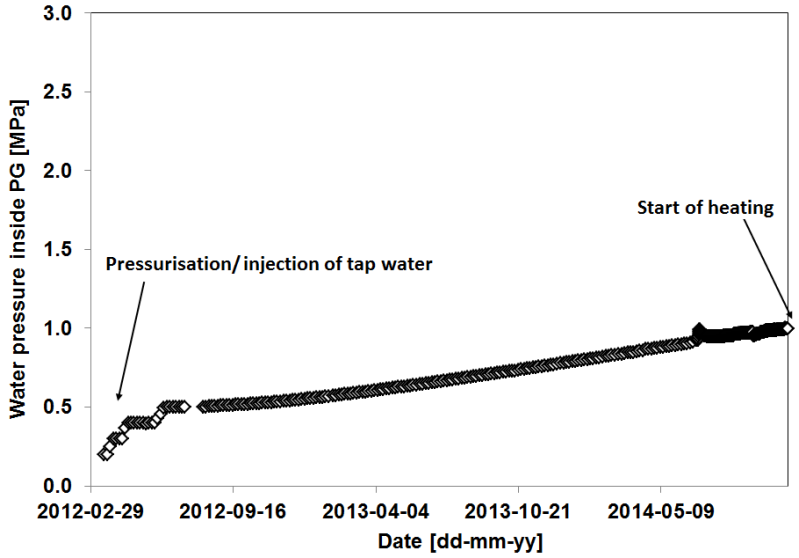

Figure 4-66. Evolution of the pore water pressure inside the backfilled part of PG before switch-on of the heater

The PRACLAY In-Situ Experiment has been intensively instrumented with about 1,100 sensors (piezometers, thermocouples, flat-jacks, strain gauges, etc.), as shown in Table 4-32.

Table 4-32. Inventory of the sensors involved in the PRACLAY experiment

Measurements	Boom Clay	Concrete lining	Seal
Pore water pressure sensors (piezometer filters)	187	14	21
Temperature (thermocouples)	196	144	46
Total pressure (flat-jacks, biaxial stress-meters and piezoresistive sensors)	28	21	21
Strain gauge (vibrating strain wires)	-	176	-
Topographic survey (total station with prisms)	-	43	5
Displacements (inclinometer/fibre optics)	21	23	2
Relative humidity sensors	-	3	11

Instrumented boreholes were drilled from both the Connecting gallery (CG) and the PRACLAY gallery (PG) (Figure 4-67). Most boreholes are so-called multi-filter piezometers, which, in addition to the piezometer filters to monitor pore water pressures, also contain thermocouples (same position as the filters) and, optionally, total pressure sensors (flat-jack or biaxial stress meter) at the deep end of the instrumented casing. Some boreholes were also drilled for displacement measurements (inclinometer and borehole extensometers). In total, the instrumented boreholes contain more than 400 sensors around the PRACLAY gallery.

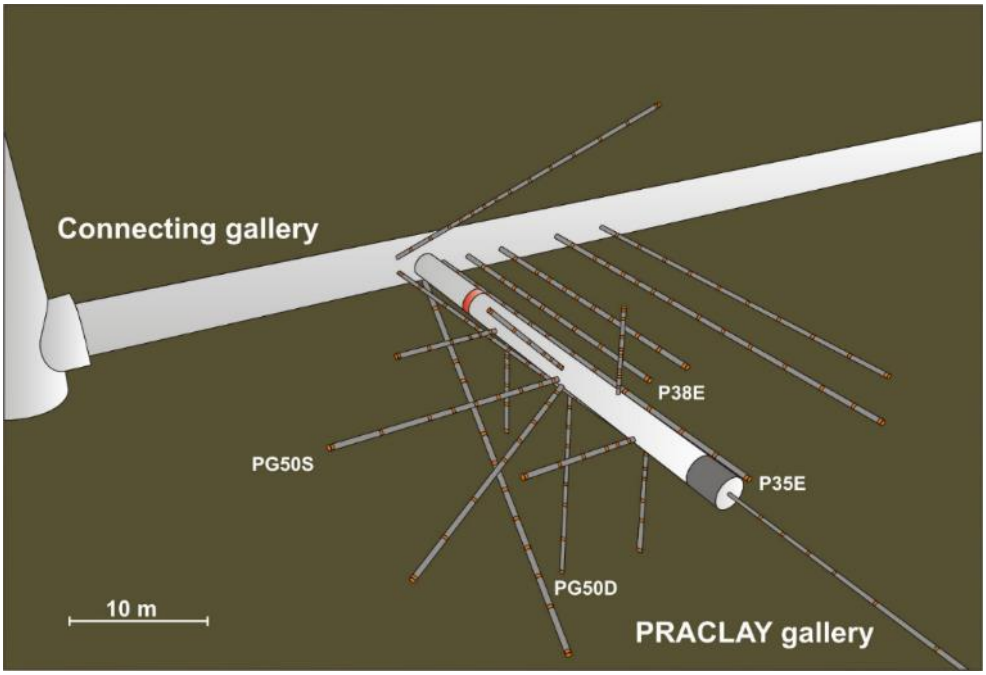

Figure 4-67. 3D view of the instrumented boreholes surrounding the PRACLAY gallery

Several segmental concrete lining rings of the PRACLAY gallery have been constructed with instrumented segments to monitor external radial total pressure on the ring, the normal stresses between the segments (circumferential or hoop stress), the strains and the temperature inside the segments. Moreover, the pore water pressure is measured at different locations inside the gallery. Many thermocouples also monitor the heater cable temperatures. About 600 sensors have been installed in the gallery and in its lining. The instrumentation of the PRACLAY seal is mainly clustered in three sections: one located at the upper level ("section A"), one on the right ("section B"), and one on the bottom left ("section C") (Figure 4-68). Each zone contains total pressure sensors (flat-jacks and piezoresistive types), piezometer filters and thermocouples. The sensors are spread on the radial range from the inner steel cylinder up to the Boom Clay/bentonite interface. In addition, thermocouples have also been installed on the accessible side of the seal. An automated total station, located at the crossing between the Connecting and PRACLAY galleries, is also monitoring the movement of the seal structure. The seal instrumentation contains more than 100 sensors.

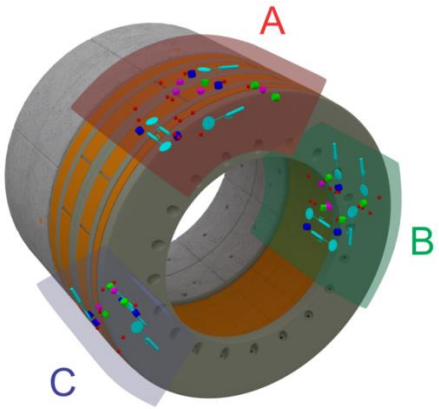

Figure 4-68. Instrumented sections of the seal, with total pressure sensors (turquoise and green), piezometer filters (blue) and thermocouples (red)

Test evolution

The heater was switched-on on the 3rd November 2014 with a constant power of 250 W/m for the three zones of the primary heating system. Two months later (on the 7th January 2015), the power was increased from 250 W/m to 350 W/m. On the 3rd March, the power was again increased to 450 W/m and maintained until the temperature at the extrados of the concrete lining reached 80°C (19 August 2015). This temperature was kept constant by gradually reducing the power in Zone 1 and Zone 2 while the power in Zone 3 was kept constant. Once the temperature reached about 80°C on average for Ring 81, the power in zone 3 was also gradually reduced. Table 4-33 summarises the history of the applied heating power during the start-up phase until the target temperature of 80°C was reached.

Table 4-33. Applied power in the three zones during the start-up phase of the heating experiment

	Zone 1 Front-end Zone	**Zone 2 Middle Zone**	**Zone 3 Far-end Zone**
Axial length (m)	2.26	28.48	3.29
Linear power (3 November 2014) (W/m)	250	250	250
Linear power (7 January 2015) (W/m)	350	350	350
Linear power (3 March 2015) (W/m)	450	450	450

Figure 4-69 shows the measured heating power in one of the heater sectors of each zone during the start-up phase and the stationary phase. The power was gradually reduced in Zone 1 and Zone 2 to maintain the target temperature after the start-up phase, while in Zone 3, the power was only reduced gradually from June 2016 when the temperature also reached 80°C on average in this latter zone.

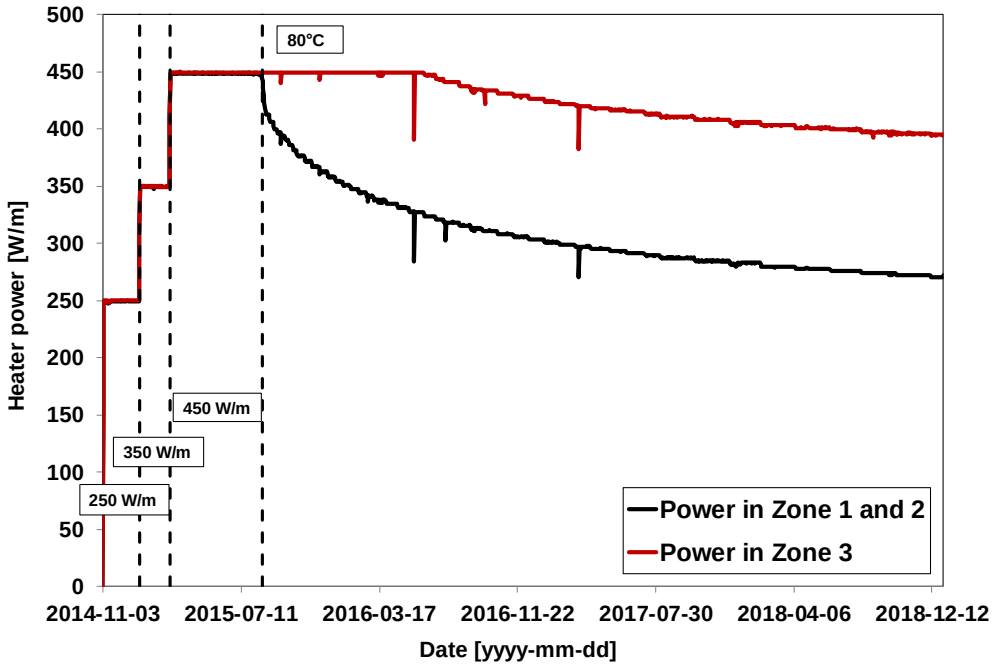

Figure 4-69. Evolution of the heating power in W/m

In order to correctly identify the beginning of the stationary phase, it was necessary to define an indicator for the target temperature of 80°C. For this, the average temperature over the

thermocouples at the outer surface of rings 37, 50 and 55 in Zone 2 is used. In Zone 3, a separate thermal indicator was defined by averaging the extrados thermocouples of Ring 81 inside Zone 3. In this way, the power can be controlled in Zone 3 independently of Zone 2 to also reach 80°C in Zone 3, despite the increased dissipation at the end of the gallery. The reason for doing this is to test the performance of the high-performance concrete segments in that zone under high thermal load. If one of the thermocouples used in a thermal indicator fails or shows abnormal measurements, the indicator is adjusted (e.g. by removing the failed sensor data from the average). Figure 4-70 shows the evolution of these average temperatures. The different heating phases are clearly visible on the graph. It can also be seen that 80°C was reached in mid-August 2015 in Zone 2, indicating the start of the stationary phase. The evolution of the average temperature in Ring 81 showed that the target temperature was reached almost one year after the beginning of the stationary phase.

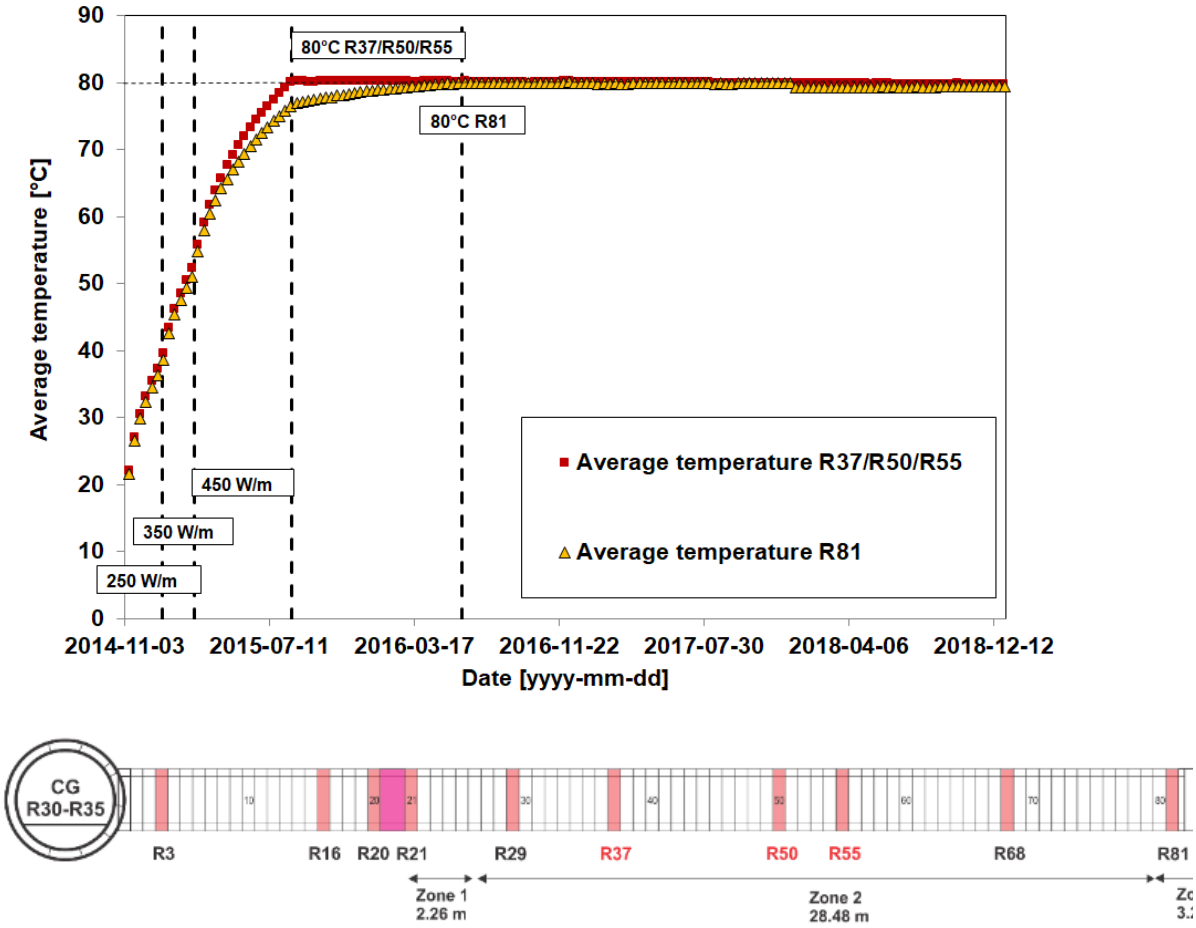

Figure 4-70. Average temperature evolution over the three rings (R37/R50/R55) for Zone 2 and on R81 for Zone 3. The average temperature is calculated based on the extrados thermocouples in the concrete lining

A number of filters are installed inside the backfilled part of the gallery with the goal of monitoring the pore water pressure inside. As already explained, this backfilled part was pressurised by injecting water before the start of the heating phase. Once the pressure reached 0.5 MPa, it was allowed to evolve without any additional injection of water. Because of Boom Clay water inflow, the pressure rose to a value of about 1 MPa just before the start of heating.

Heating generates an excess pore water pressure inside the gallery due to a higher thermal dilation coefficient of water compared with the solid phase (sand, concrete). The evolution of the pressure inside the backfilled part of the PRACLAY gallery can be seen in Figure 4-71. The effect of heating was instantaneous. This confirmed an initial water saturation of the system. The different heating steps can be clearly seen in this Figure. A sudden pressure drop and a quick recovery occurred during the first heating step (at 250 W/m). This can be attributed to a small displacement of a segment or the sudden ingress of a limited volume of pore water into a borehole casing that may have been initially plugged. A value of 2.9 MPa was reached when the temperature measured 80°C at the extrados of the concrete lining. At the beginning of the stationary phase, a small drop in pore water pressure caused by the power decrease was observed. Afterwards, the pore water pressure remained more or less constant at around 2.8 MPa, as expected from the nearly constant temperature evolution in the gallery and at the Boom Clay/lining interface.

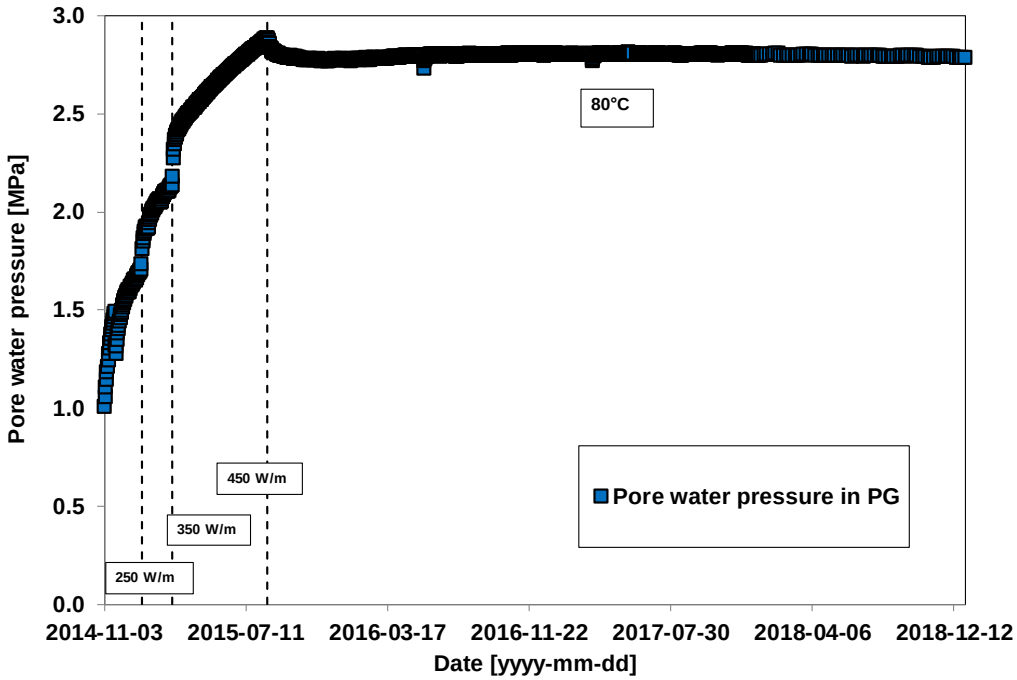

Figure 4-71. Pore water pressure inside the PG

Boom Clay response

Porous media with low permeability, like the Boom Clay, can experience a substantial increase in pore water pressure as a consequence of a temperature rise due to the differential thermal dilatation coefficient between the solid (skeleton) and the liquid phase (water) in the clay. The variation in the temperature and pore water pressure inside the Boom Clay is monitored using instrumented boreholes extending in different directions from the PRACLAY gallery and from the Connecting gallery. The evolution of the temperature and pore water pressure profiles in the vertical direction (monitored from the downward borehole PG50D in the middle section of the heated gallery) is shown in Figure 4-72.

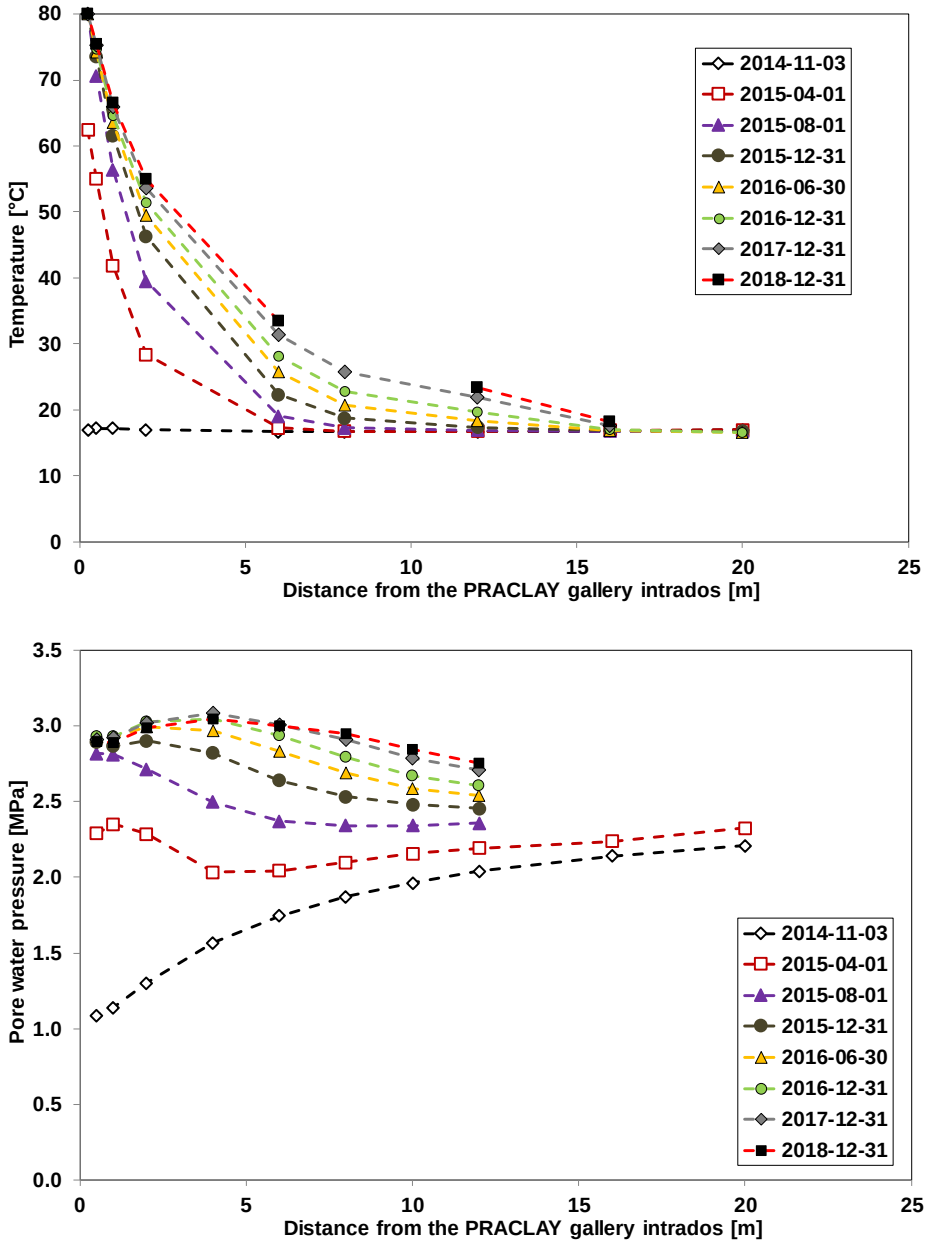

Figure 4-72. Temperature and pore water pressure profiles in the vertical direction at the middle section of the heated part of the PRACLAY gallery (along borehole PG50D)

The evolution of the temperature and pore water pressure profiles in the horizontal direction (measured from the boreholes, drilled from the Connecting gallery and parallel to the PRACLAY gallery, with the sensors located at the middle section of the heated gallery, as shown in Figure 4-65) is shown in Figure 4-73. It was observed that, at the end of 2018, the thermally affected zone had extended to a depth superior to 15 m into the Boom Clay in both directions. At a given time and at the same distance from the heater, the temperature rise in the horizontal direction is larger than that in the vertical direction. These observations clearly indicate an anisotropic heat transfer conduction mechanism through the Boom Clay, as already observed in small-scale in situ ATLAS heater test. Concerning the evolution of the pore water pressure, close to the concrete lining, the pore water pressure increased as expected from its initial value of 1 MPa before heating to a value close to 3 MPa at the end of the start-up phase (August 2015). Since the beginning of the stationary phase, the pore

water pressure has remained nearly constant close to the lining but continues to increase in the clay. Over time the peak in pore water pressure has gradually shifted away from the gallery into the Boom Clay. By comparing the pore water pressure profiles at a distance around 5 m from the gallery intrados in 2017 and 2018, it can be observed that the peak of maximum excess pore water pressure in the Boom Clay was reached in 2017. Since that time, the excess pore water pressure has been dissipating in the surrounding environment.

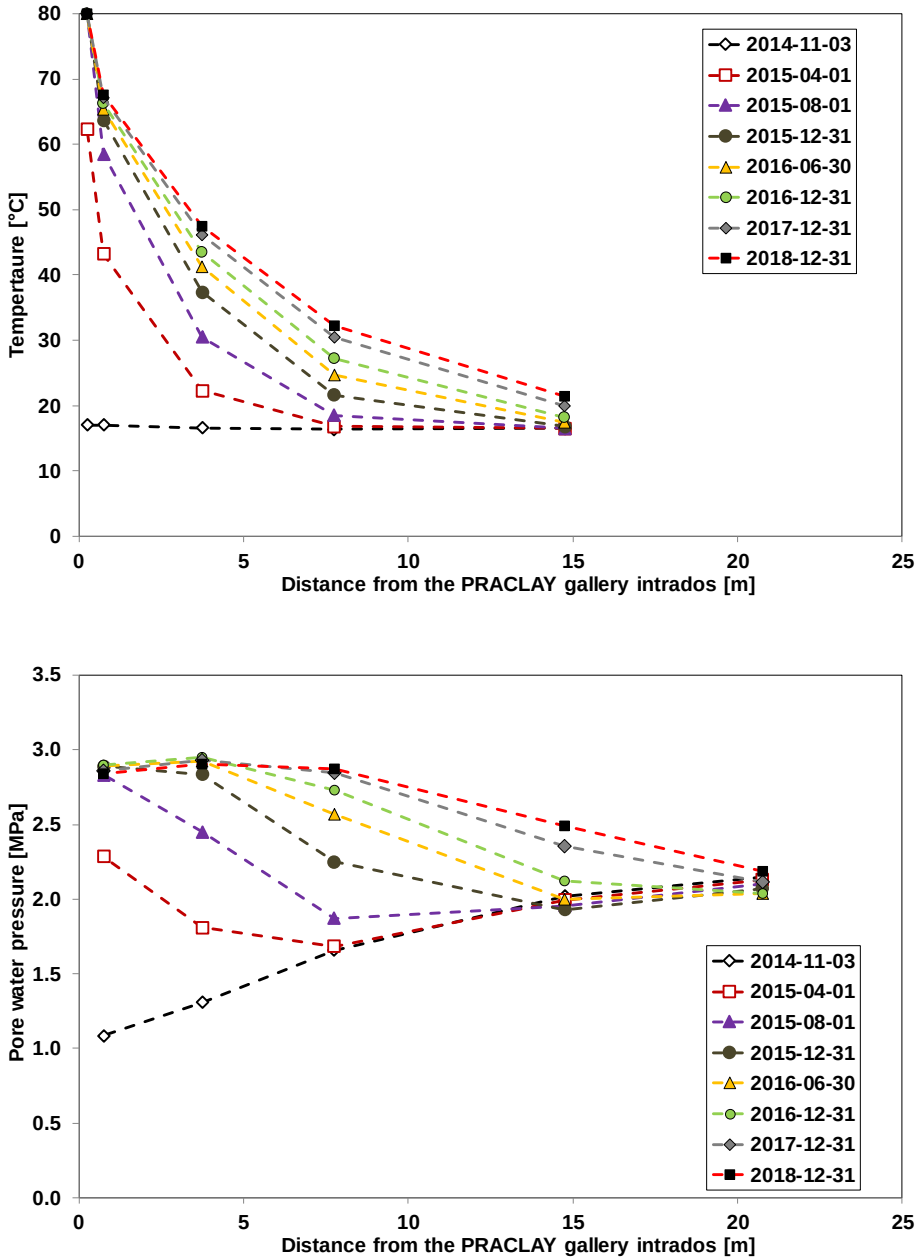

Figure 4-73. Temperature and pore water pressure profiles in the horizontal direction at the middle section of the heated part of the PRACLAY gallery (measured from boreholes drilled from the Connecting gallery)

The spatial distribution of the temperature and pore water pressure around the PRACLAY gallery is illustrated in Figure 4-74, which shows the temperature and pore water pressure profiles along P35E, located approximately 0.75 m from the extrados of the gallery lining. The pore water pressure profile

is almost uniform along P35E, while the temperature profile shows a slight gradient from the seal to the end part of the PRACLAY gallery. The pore water pressure profile clearly shows the hydraulic cut-off by the seal.

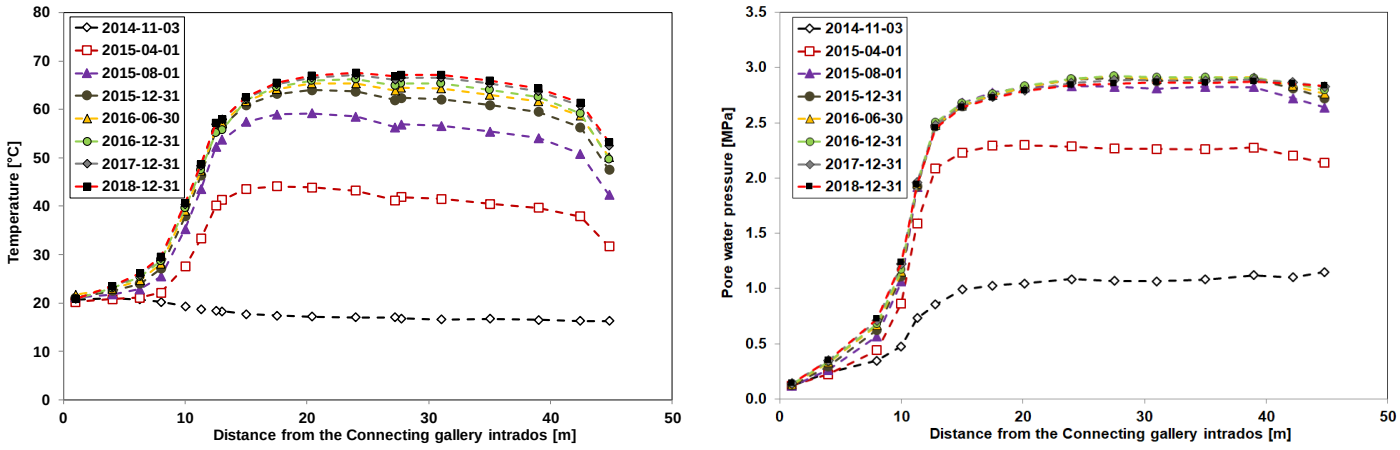

(a) Temperature **(b) Pore water pressure**

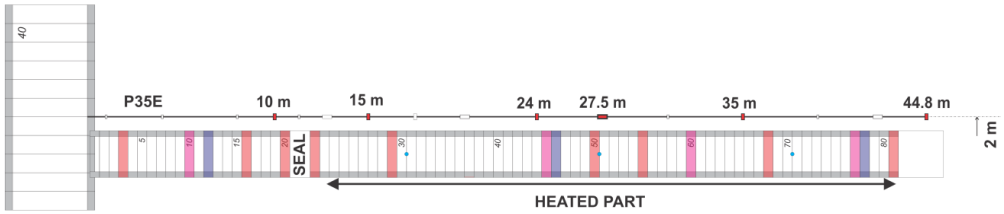

(c) Borehole P35E

Figure 4-74. Temperature and pore water pressure profiles in P35E

Evolution of the hydraulic seal

The hydration of the bentonite and the associated pore water pressure and total pressure evolution were continuously monitored during the heating phase. Figure 4-75, for example, shows the evolution of the pore water pressure at the Boom Clay/bentonite interface with the different heating steps. It can be observed that the pore water pressure at the Boom Clay/bentonite interface evolves in the same way for the three sections A, B and C. One of the main purposes of the seal structure is to provide a hydraulic cut-off between the heated and the non-heated part of the experiment. The effect can be observed in the different evolution of the pore water pressure in sensors Seal-PP-A1 and Seal-PP-A3 in section A. The first is located close to the heated part, while the second is close to the accessible, non-heated part of the PRACLAY gallery. A high difference over a distance of only 34 cm between both sensors can be observed, indicating that the bentonite ring/ Boom Clay interface is well closed and impervious. Moreover, the pore water pressure inside the PRACLAY gallery is maintained as expected due to the seal performing well.

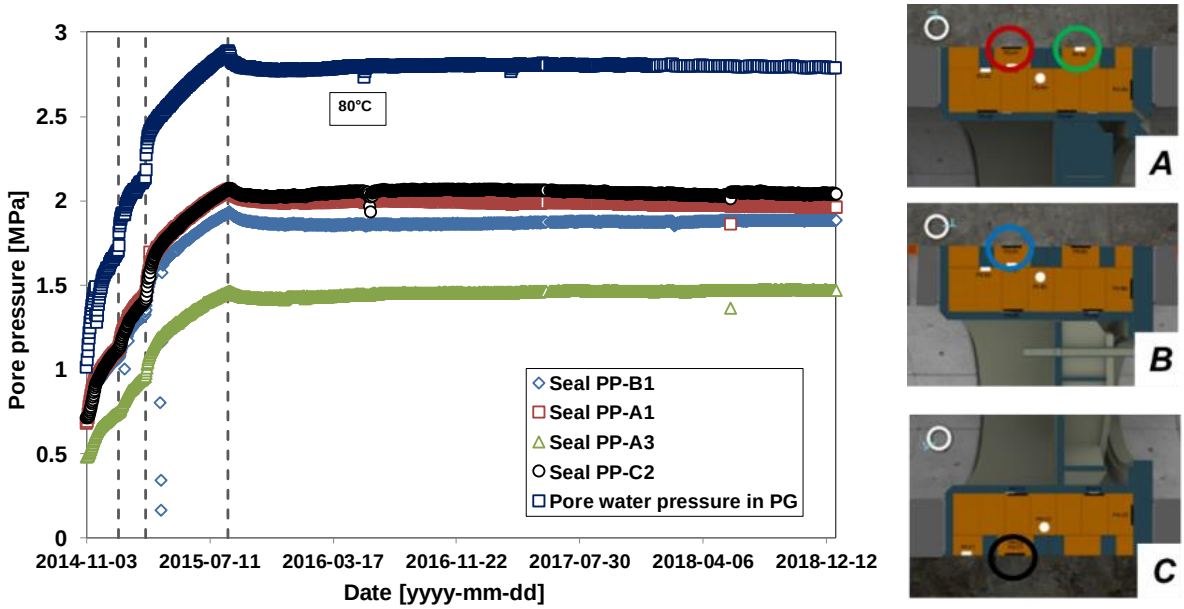

Figure 4-75. Evolution of the pore water pressure at the Boom clay/bentonite interface

In order to highlight the effect of the seal, Figure 4-76 shows the evolution of the pore water pressure at the Boom Clay/bentonite interface for different positions in section A, and at the Boom Clay/concrete lining interface close to section A. It is worth noting that between the non-heated and heated parts of the gallery, a big difference in pore water pressure of almost 2 MPa occurs over a distance of 1.5 m. This significant gradient is clear proof of the good hydraulic cut-off created by the seal: the high pressure inside the backfilled part of the gallery was maintained.

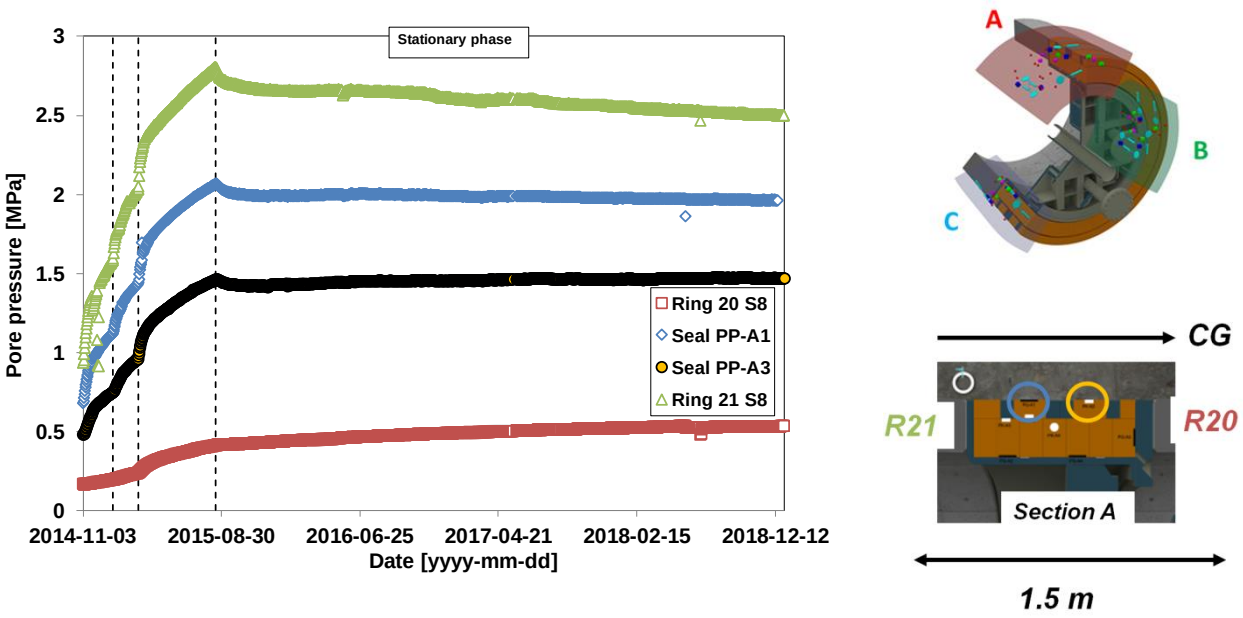

Figure 4-76. Pore water pressure evolution at the Boom Clay/concrete lining and Boom Clay/bentonite interfaces

The movement of the seal structure towards the Connecting gallery was monitored by a total station and prisms attached to this structure, as can be seen in Figure 4-77. A significant increase in

displacement during the start-up phase can be observed, but this has tended to be steady since the beginning of the stationary phase. The measured displacement remained quite constant and an average value of 12 mm over the three monitored prisms was observed at the end of 2018, without any impact on the stability and the functioning of this seal structure.

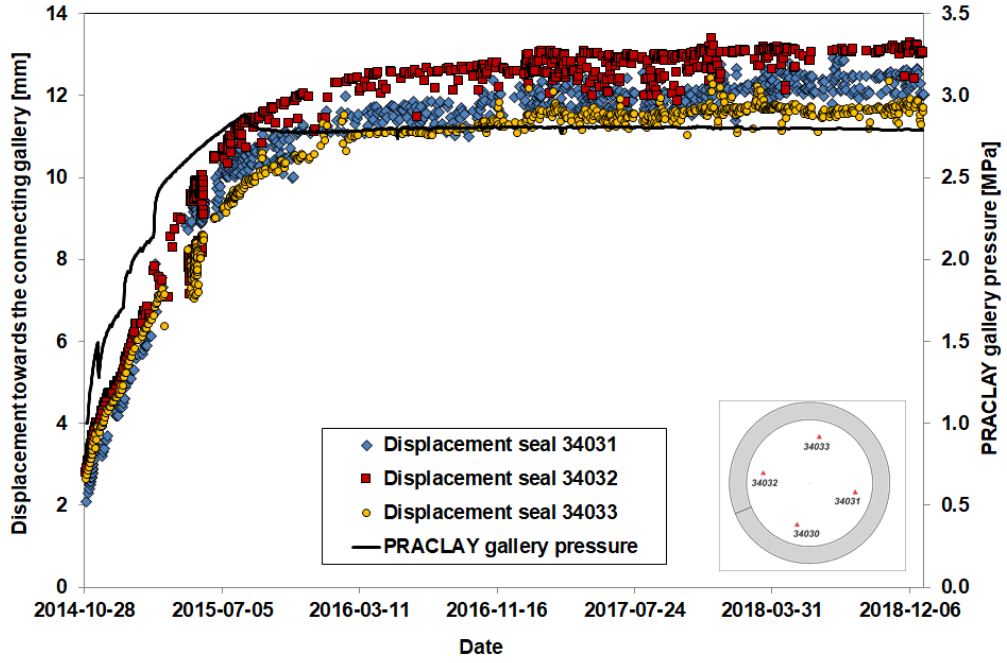

Figure 4-77. Evolution of the movement of the seal structure towards the Connecting gallery since the beginning of the heating phase

4.2.2 COx

Several large-scale heating tests on the COx claystone have been performed in the Bure underground laboratory (URL) since 2006. They are briefly described here; reference is made to the relevant reports for more details. The ALC1605 full-scale experiment, that will be used for the benchmark exercise, should start in February 2020.

4.2.2.1 TER

The TER experiment was conducted between 2006 and 2009. Its main objective was to determine the thermal properties of the intact COx claystone. Another goal was to provide some elements on the hydraulic and mechanical responses to a thermal load. The effect of temperature on the damaged zone is based on permeability measurements.

A borehole was drilled in the direction of the maximum horizontal stress and equipped with a 3 m long heater. Three holes were drilled in its vicinity for temperature measurements (orange in Figure 4-78) and pressure measurements are performed in four holes (in blue in Figure 4-78). Strain measurements were made in two boreholes drilled perpendicularly from the GKE drift. Eight temperatures gauges were later installed (in 2008) in the GKE and GEX drifts.

A complex heating cycle was applied, especially at the beginning of the experiment because of technical issues, and then to improve the back analysis of the thermal parameters. The heater was changed in July 2007 and no more unexpected breaks were observed until the end of the heating phase on 25 March, 2009 (Figure 4-79).

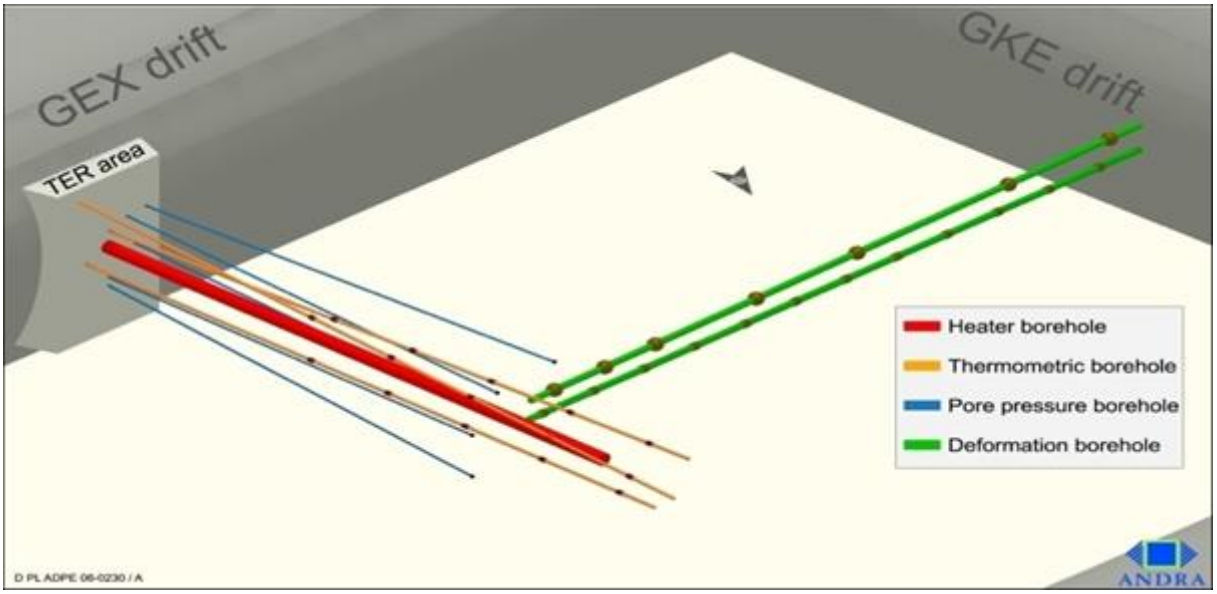

Figure 4-78. General layout of the TER in-situ test (Wileveau et al. 2007b)

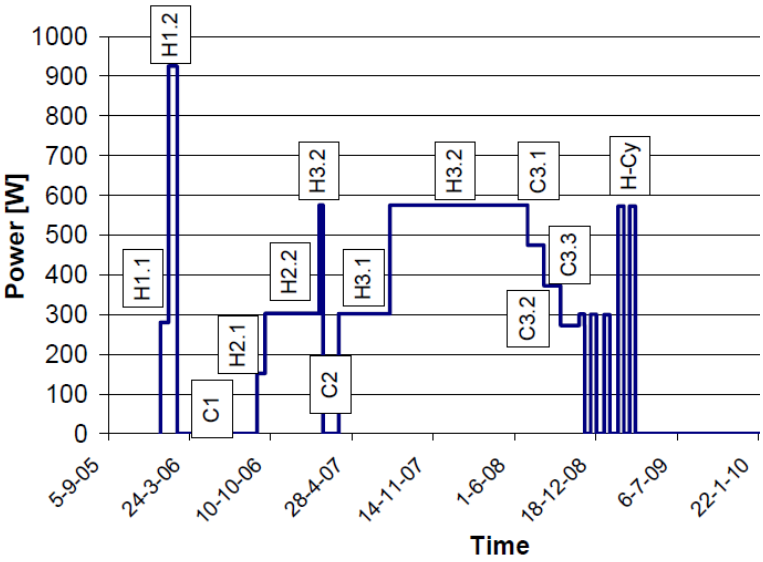

Figure 4-79. Heating stages during the TER in-situ test

Figure 4-80 shows some raw temperature and pore pressure measurements during the TER experiment. A similar phenomenon was highlighted in all the heating experiments: when the heating started, the temperature of the claystone around the borehole increased. The difference of thermal expansion between the water and the rock caused an increase in pore pressure, as the clay permeability is low and the drainage could not dissipate this pressure build-up. The initiation of the pressure build-up and the amount of overpressure depended on the rate of temperature increase and on the distance to the heater. When the heating rate decreased, the generated overpressure dissipated by diffusion. When the heating stopped, the reverse phenomenon happened: the decrease in water volume resulted in a drop of pore pressure.

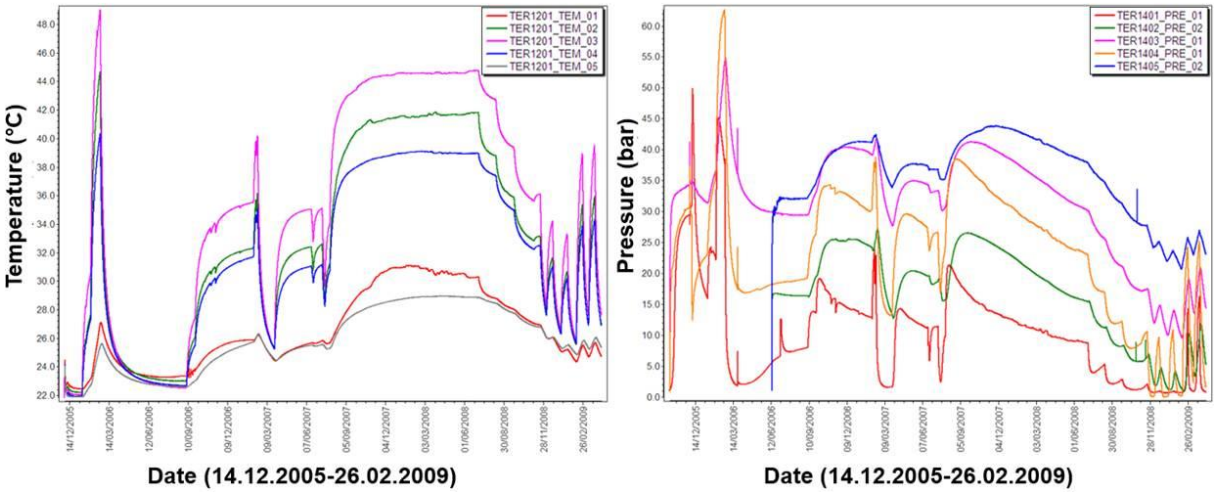

Figure 4-80. Temperature and pore pressure evolution during the TER experiment

Figure 4-81 shows the evolution of temperature measured by sensors at equal distance from the heater in planes parallel and perpendicular to bedding. The temperature measured at the same distance perpendicular to bedding was lower than that measured parallel to bedding. The difference was larger as the distance to the heater increased.

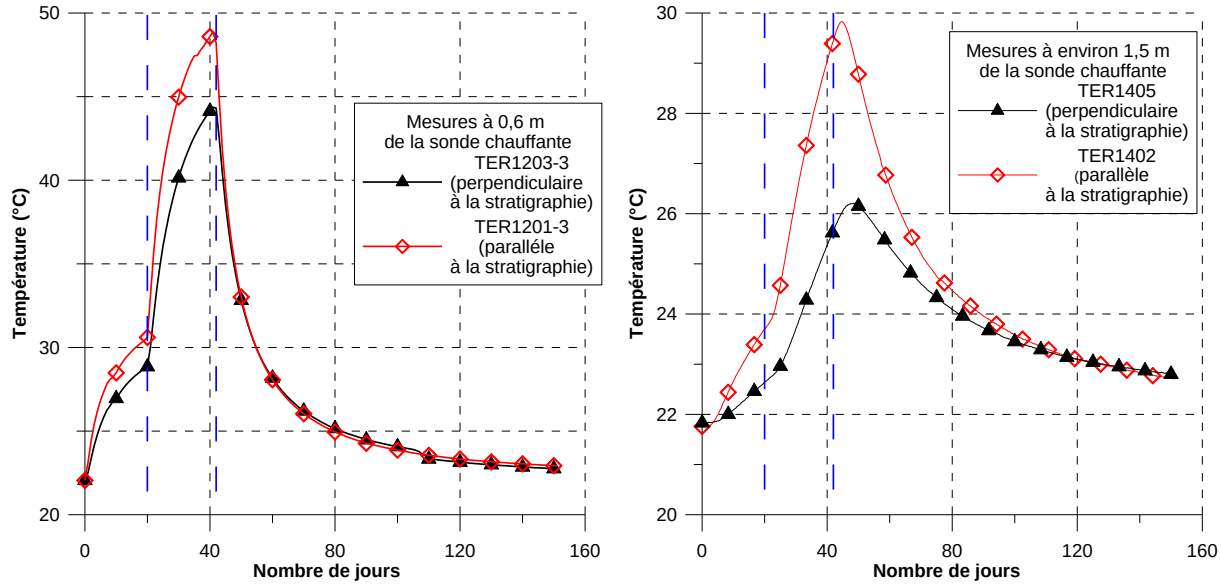

Figure 4-81. Temperature evolution at 0.6m (left) and 1.5m (right) from the heater, measured parallel to bedding (TER1201-3 and TER1402, red curves) and perpendicular to bedding (TR1203-3 and TER1405, black curves)

The higher temperature parallel to bedding shows that the thermal conductivity was not isotropic, and was larger parallel to bedding than perpendicular to bedding. When heating stopped, this trend was confirmed, as the thermal response was slower perpendicular to bedding.

This experiment and the subsequent modelling helped determine the specific heat of the saturated COx claystone and the thermal conductivity parallel and perpendicular to bedding. The pore pressure measurements were also matched using a permeability of $3 \cdot 10^{-13}$ m/s and a liner thermal expansion coefficient of $5 \cdot 10^{-6}$ C^{-1}.

When dismantling the experiment, two boreholes (TER1901 and TER1902) were drilled to acquire some samples and investigate the impact of the heating on the claystone. These analyses did not show any particular influence on the THM properties. However, in-situ hydraulic tests performed 6 months after the end of the heating phase showed an increase of permeability, in particular parallel to bedding.

4.2.2.2 TED

The TED experiment was performed between 2009 and 2013. Its main objectives were to:

- Characterise the thermal properties of the intact COx claystone
- Complete the understanding of the THM behaviour of the claystone and quantify the THM parameters based on in-situ tests
- Check the relevance of the THM coupling parameters derived from lab tests on core samples.

A major challenge for the testing programme in the URL is the evolution of the EDZ during the thermal phase. In this experiment, the creation and potential growth of the damaged zone resulting from the thermal load were studied. Finally, this experiment was designed to be more representative for HLW cells, respecting the "no-flow" boundary conditions near these cells. As in TER, lab experiments on core samples were performed in parallel.

The experiment consisted in three parallel heating boreholes drilled in the direction of the maximum horizontal stress from the GED drift, 10 pressure measurement boreholes, 9 temperature measurements, 2 strain measurement boreholes and 8 temperature gauges installed on the GED drift wall. Compared to the TER experiment (section 4.2.2.1), the heat sources were located further away from the drift (12 m *vs*. 6 m in TER) to avoid any thermal impact from it.

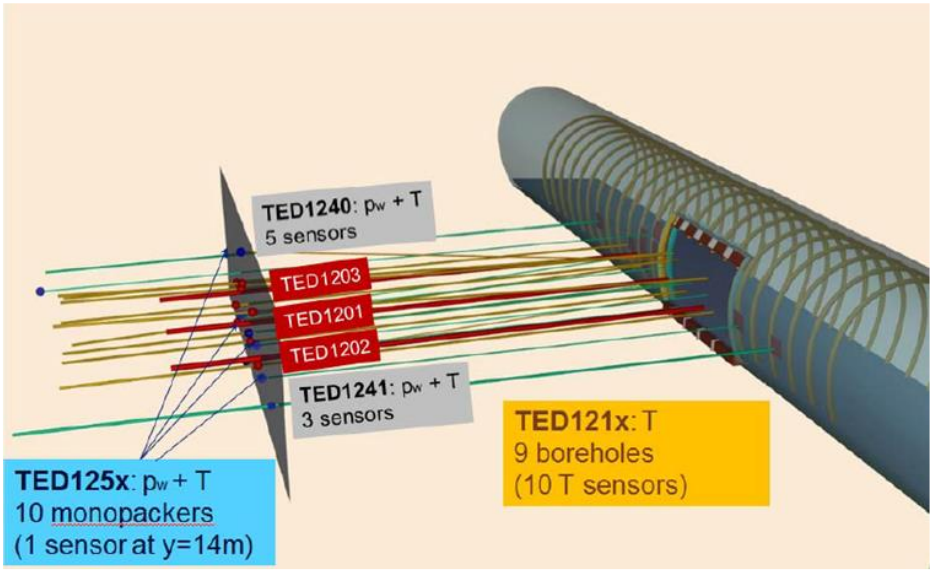

Figure 4-82. Three-dimensional layout of the TED experiment, where the plane at 14 m from the gallery is indicated. Many of the sensors are located on this plane, which coincides with the midsection plane of the heaters

Preliminary calculation showed that 600 W in each heater were necessary to reach 90°C at the wall of the central hole. Heating started in January 2010 in the central heater and a year later in the other two (Figure 4-83). The cooling phase started progressively in October 2012.

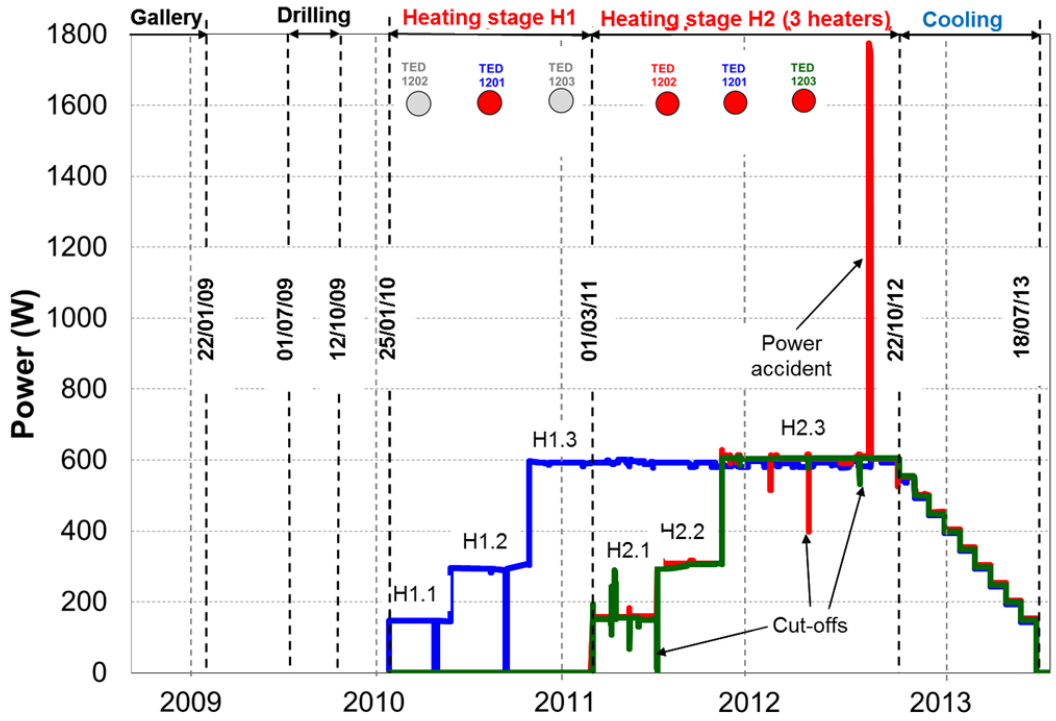

Figure 4-83. Timeline of the TED experiment with the different heating stages applied

The measurements of the temperature field provided again a clear evidence of thermal anisotropy. The pore pressure measurements also confirmed the anisotropy of permeability and stiffness. No variation of the permeability was observed while heating. However, these measurements were made in the far-field in the pressure-measuring boreholes. They do not provide any information on the evolution of permeability in the near-field, but show that if any damage was induced by heating, its extent was limited.

The correlation between the measured temperature and pore pressure and the results obtained by modelling was very good. The thermal conductivity and heat capacity values were determined based on the back-analysis of the in-situ measurements. They are very similar to the values obtained from lab tests, which increases the confidence in those parameters (see also chapter 4.1.2.3). The successful reproduction by numerical modelling of the short instantaneous pressure drop after increasing power in the parallel plane although no temperature change was yet registered (Figure 4-84, up) confirms the mechanical anisotropy in the COx claystone. This phenomenon was also observed in the Opalinus Clay in Mont Terri and in the Boom Clay in Mol (Garitte & Vaunat 2008).

The TED experiment results show the capability of current models to satisfactorily predict the evolution of temperature and pore pressure in the far-field of disposal cells.

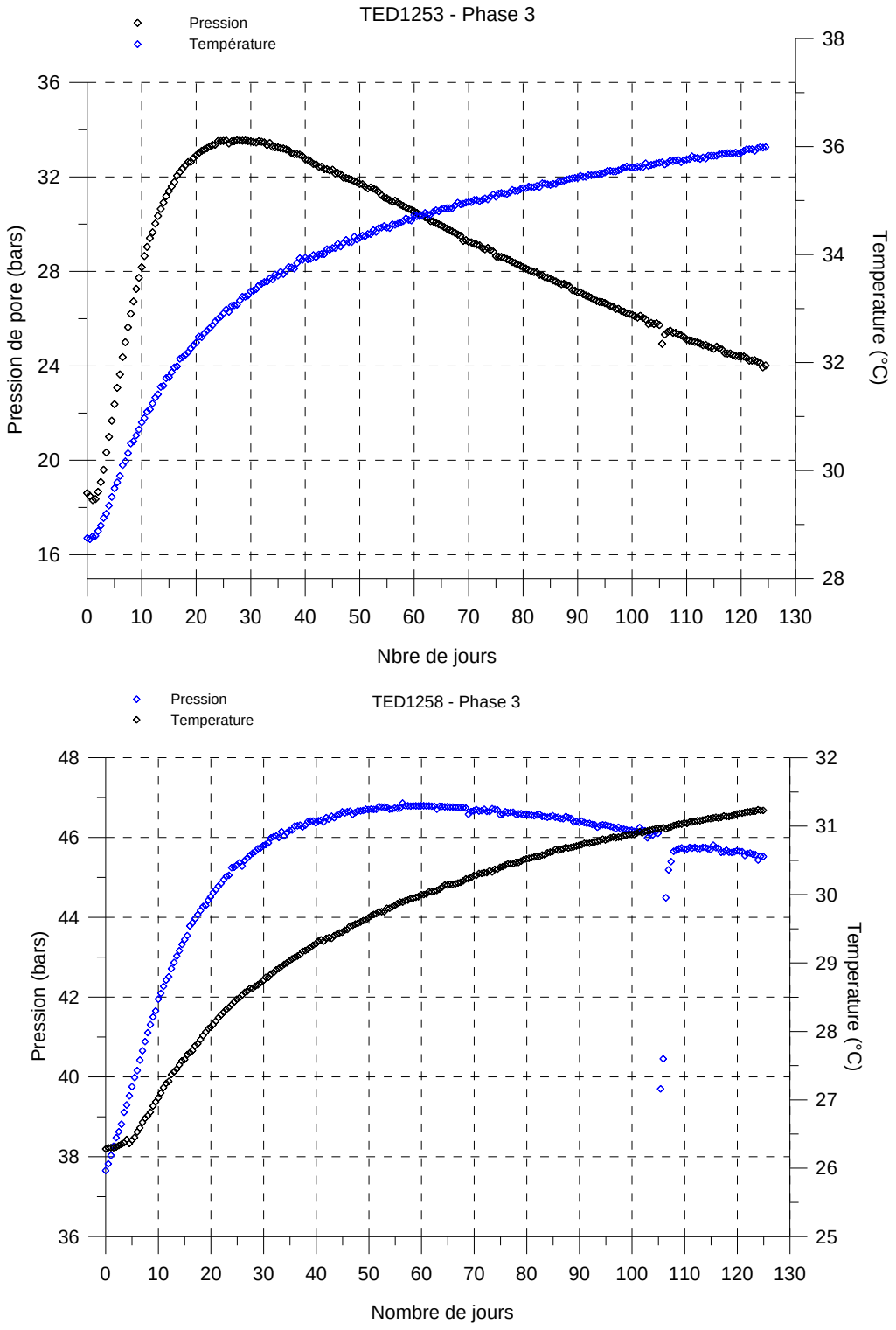

Figure 4-84. Evolution of pore pressure and temperature during the 3rd heating stage in the TED1253 borehole (1.1m away from the heater, parallel to bedding, up) and in the TED1258 borehole (1.3m away from the heater, perpendicular to bedding, down)

4.2.2.3 TFW

The objective of this experiment was to assess the effect of a fast heating episode on an uncased borehole wall, and check if this setup would induce any further fracturing.

A 10-meter long borehole was drilled from the GEX drift and in the direction of the maximum horizontal stress (Figure 4-85); the last 3 metres were heated, re-using the heater from the TER experiment. The borehole shape was filmed and logged before and after heating to identify any potential damage. Two boreholes were also drilled to measure the variations of temperature and pressure parallel and perpendicular to the layering.

Heating started in January 2011 and was planned to last three months. However, because of technical issues, the experiment was stopped after only 57 days (Figure 4-86).

Although testing conditions differed significantly, the observations were similar to those made in the previous experiments. In particular, despite the rapid temperature increase, the induced pressure variations were similar.

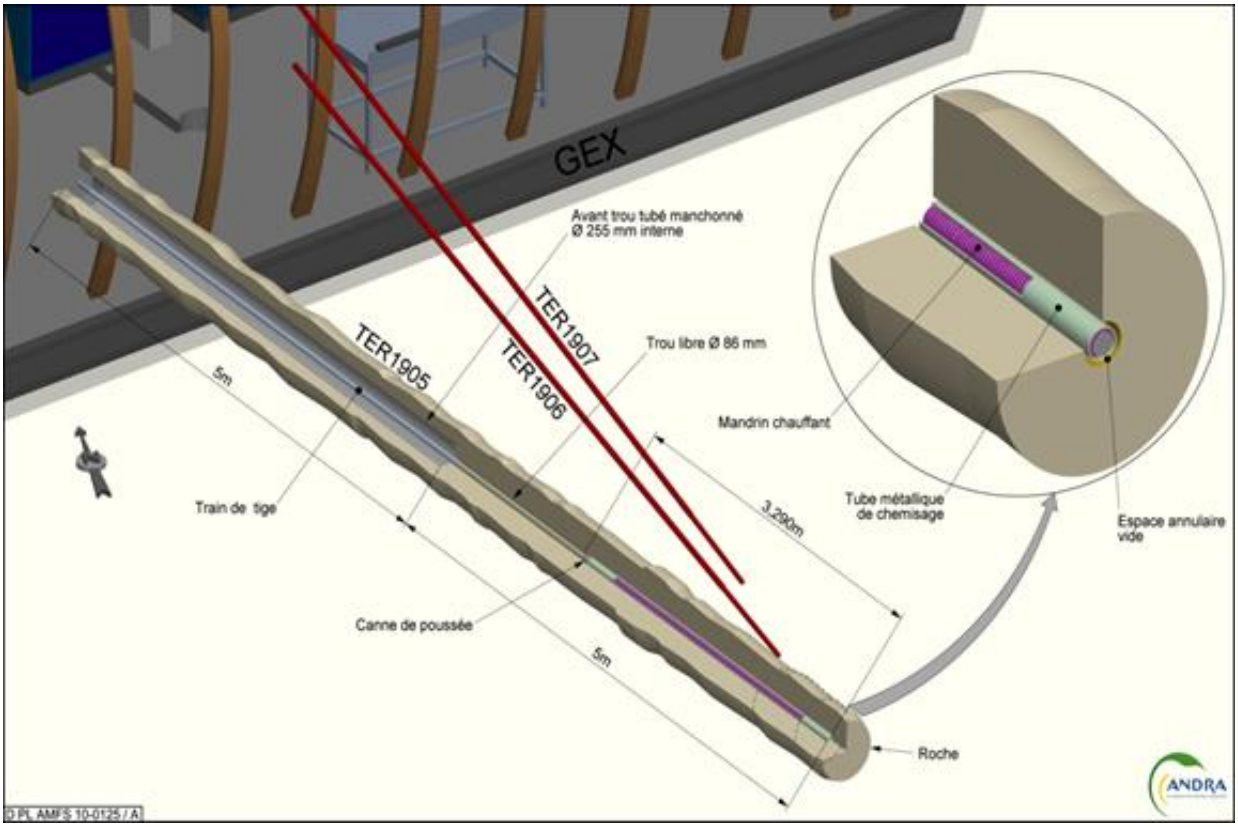

Figure 4-85. General layout of the TFW in-situ test

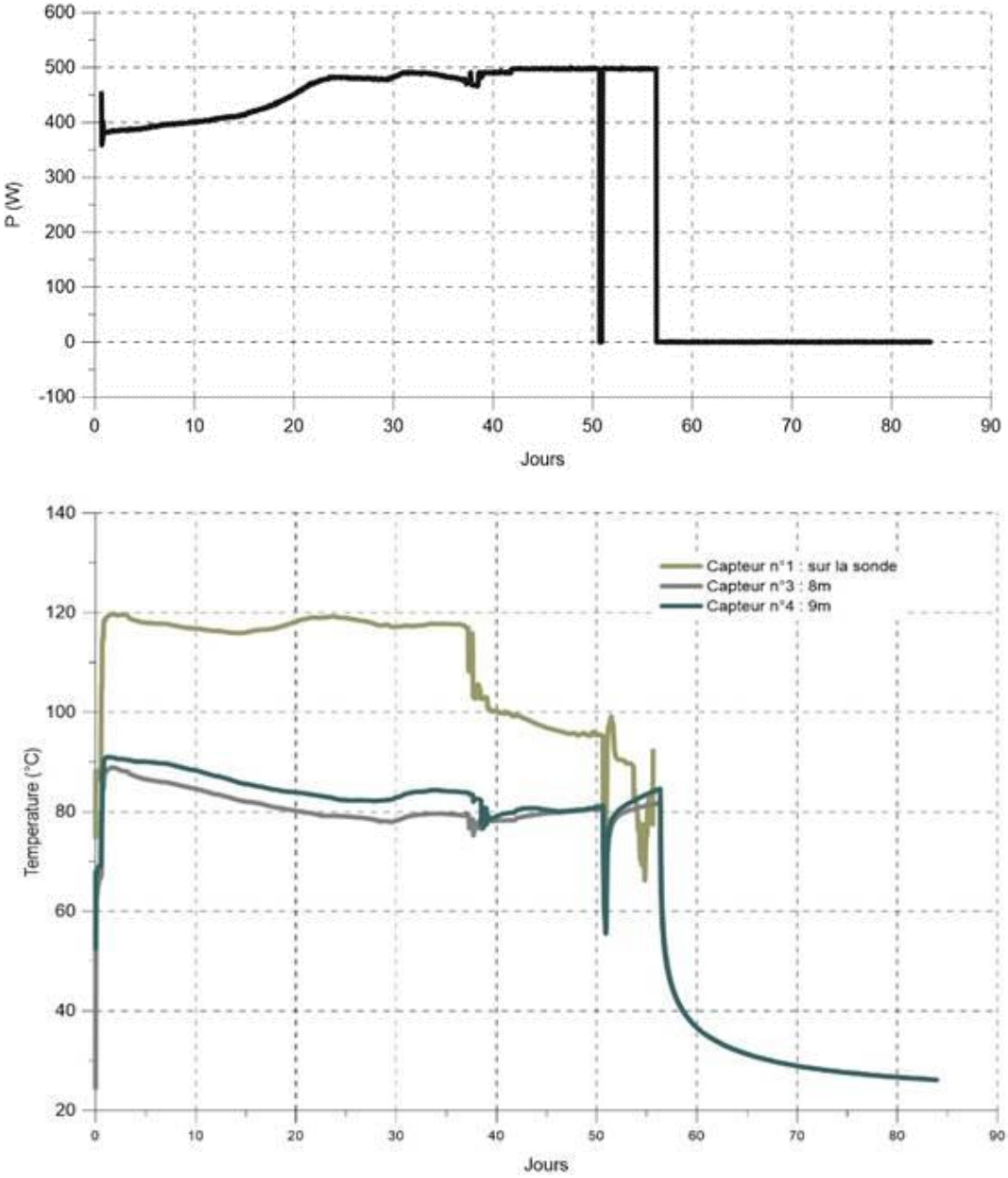

Figure 4-86. Heating power and measured temperature in the TER1905 borehole

4.2.2.4 ALC 1604 HLW cell experiment

A full-scale 25-meter long HLW cell was drilled from the GAN4 drift, and completed following the 2009 concept, without filling between the casing and the formation. The objectives of this experiment were to demonstrate the feasibility of the construction and operation of an HLW cell (as part of the European LUCOEX project) and to study the effect of a thermal load on the THM behaviour of the host rock in the near-field and on the thermo-mechanical behaviour of the casing. The cell was heated by five elements located between 10 and 25 metres from the drift. The modelling of this experiment was included in the DECOVALEX-2019 benchamarking exercise.

Nine observation boreholes were drilled from the GAN drift and the perpendicular NRD drift (6 for pressure measurements, two for temperature measurements and one for strain measurements, Figure 4-87)

After a short heating test in February 2013, the main heating phase started in April 2013 with constant power in order to reach 85°C on the casing. The cooling phase started in February 2019 and was completed in June 2019 (Figure 4-88).

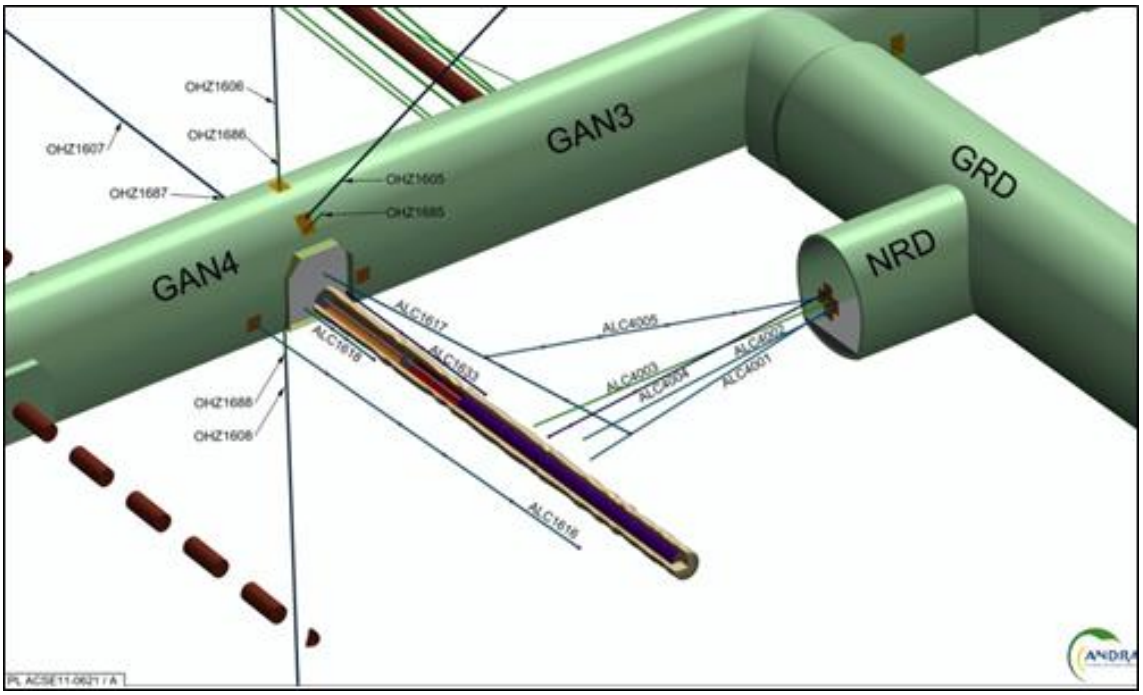

Figure 4-87. General layout of the ALC 1604 in-situ test

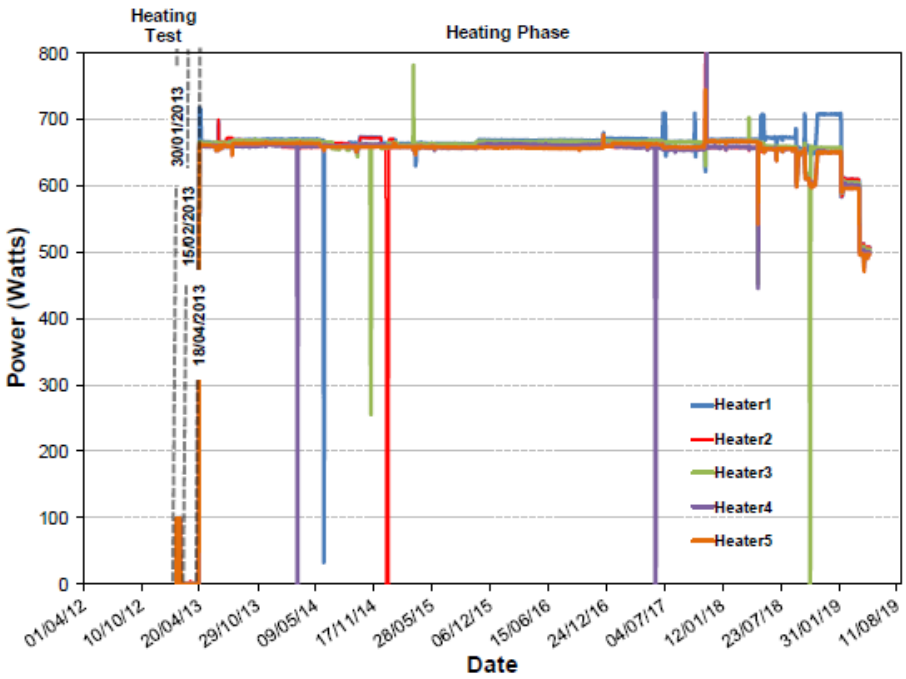

Figure 4-88. Timeline of the ALC 1604 experiment (Tourchi et al. 2019)

The evolution of pore pressure with temperature was similar to that observed in small-scale tests. The pressurisation coefficients ($\Delta P/\Delta T$) at the beginning of the heating phase were of the same order as

those previously observed in the other in-situ experiments. The temperature evolution was better reproduced by the 3D model than in 2D, indicating that heat dissipation along the cell direction has a major effect on the temperature field in the rock. Figure 4-89 shows a comparison of pore pressure measurements and the results from the 2D and 3D modelling at sensors between 1 and 2.3 m from the cell wall (17.5 m away from the GAN drift). It is apparent that pore pressure increase was reasonably well captured by the models for both the excavation and heating phases, although the measured pressure increase in the ALC1616_PRE_02 sensor was much sharper than in the model. This discrepancy was not observed for the two other sensors of the same section and may be due to spatial discretization issues.

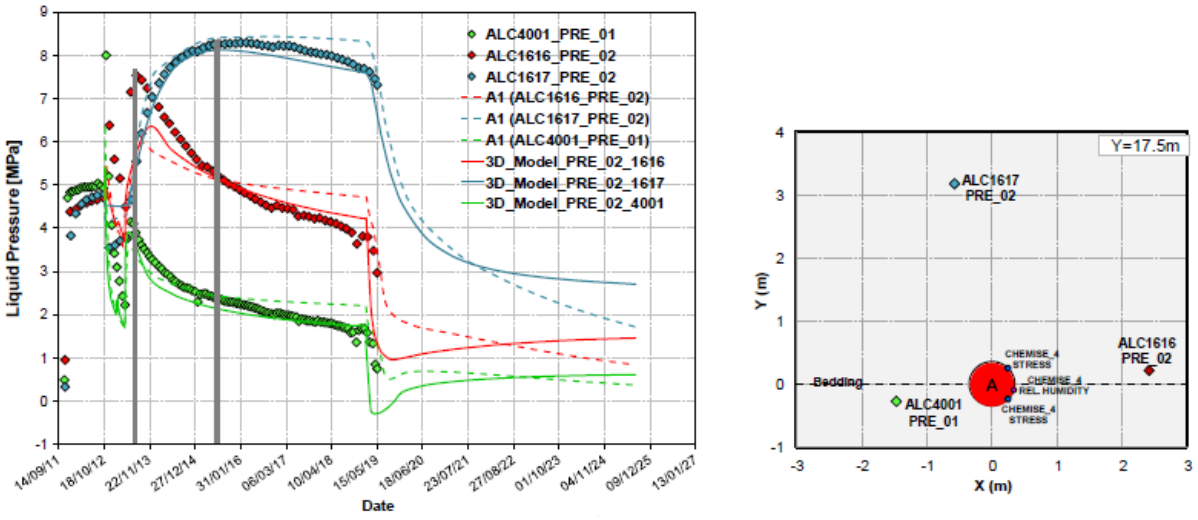

Figure 4-89. Evolution of pore pressure increments in the clay at 17.5m from the drift: observed and computed results (Tourchi et al. 2019)

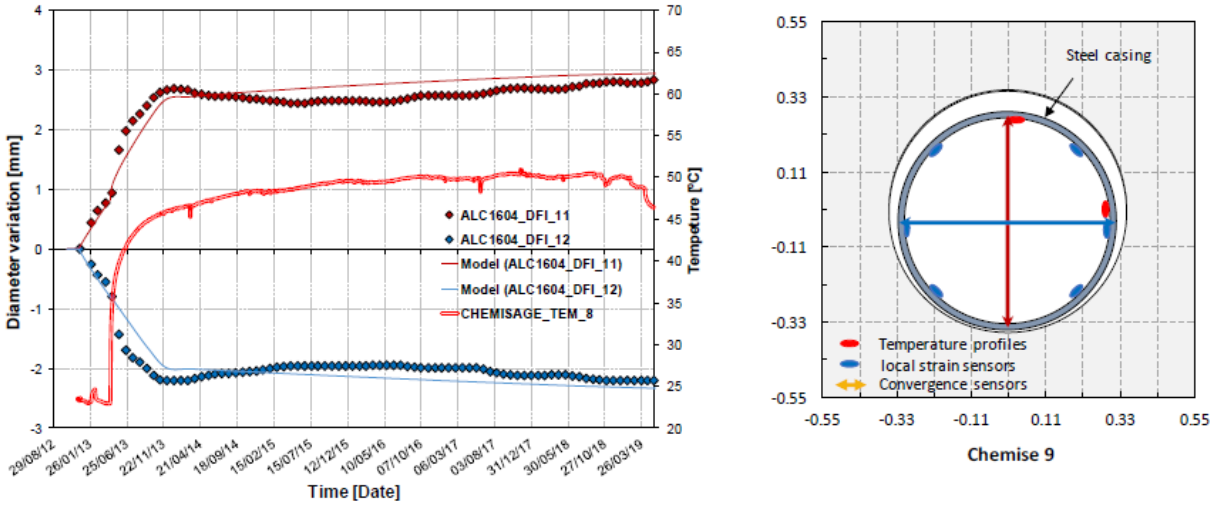

Figure 4-90. Casing diameter variation and temperature evolution at 7-m depth (Touchi 2019)

The evolution of the mechanical behaviour of the casing and the insert was monitored by convergence and local strain measurements on the inner face. Before the heating phase, this behaviour was consistent with previous experiments, i.e. the casing was subjected to radial bending with a maximum loading applied along the horizontal direction. The heating phase strongly increased the cell wall

convergence rate and thus the casing deformation, until a contact with the cell vault occurred (Figure 4-90). The loading anisotropy of the casing tended then to decrease slightly with the evolution of the contact surface between the casing and the cell wall.

Overall, this 3D anisotropic visco-elasto-plastic model with creep reproduced well the temperature, pressure and convergence measurements. On the other hand, the general trends were predicted by a simple poro-elastic model, although drainage seemed to be greater and pore pressures were overpredicted (Armand 2017).

4.2.2.5 CRQ experiment

The objectives of the CRQ (Comportement THM Représentatif d'un Quartier HA) experiment are to:

- Reach an effective stress leading to hydraulic fracturing
- Study how the initiation of the hydraulic fracture affects the evolution of the formation pressure
- Characterise the changes of the mechanical properties in the zone where fracturing occurred

Ten heating boreholes and several observation holes were drilled, perpendicular to the direction of the maximum horizontal stress from the GCS drift (Figure 4-91). The boreholes are 20-meter long and the last 10 m are heated.

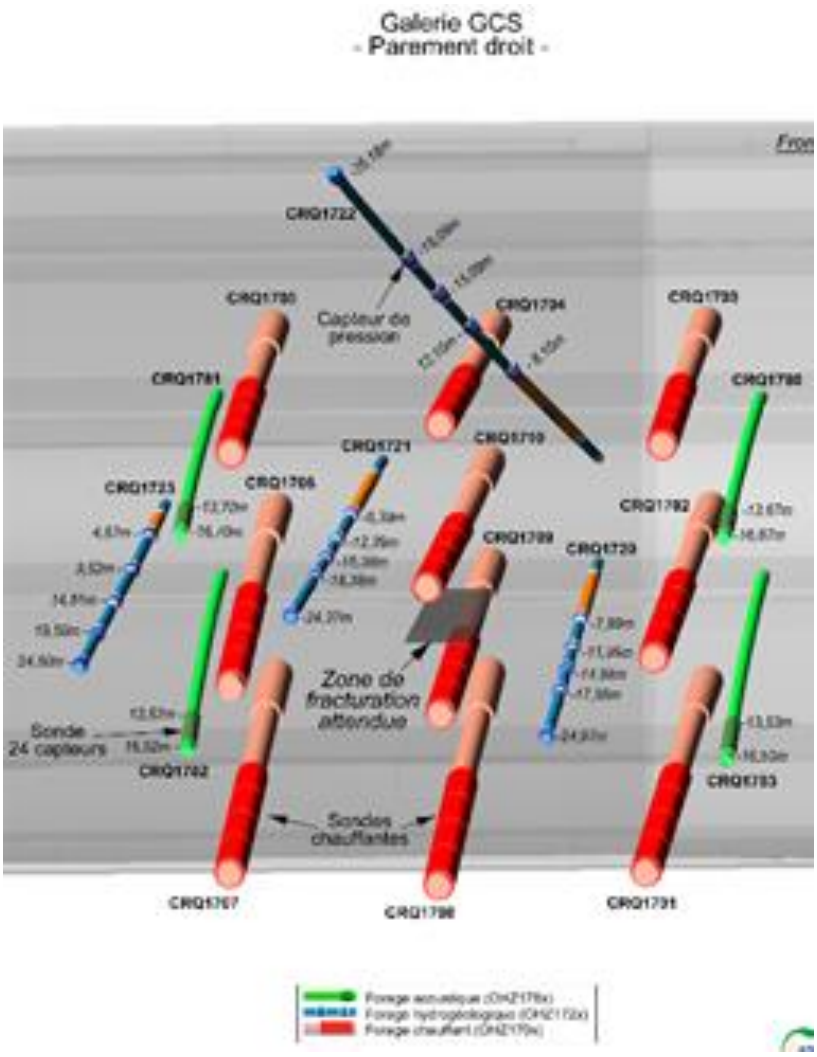

Figure 4-91. Layout of the CRQ in-situ test

A first heating phase was performed between June and July 2019 (Figure 4-92). A maximum pressure of 16.1 MPa was reached, but fracturing was not achieved. A faster heating phase was performed in February 2020, the results are now being analysed.

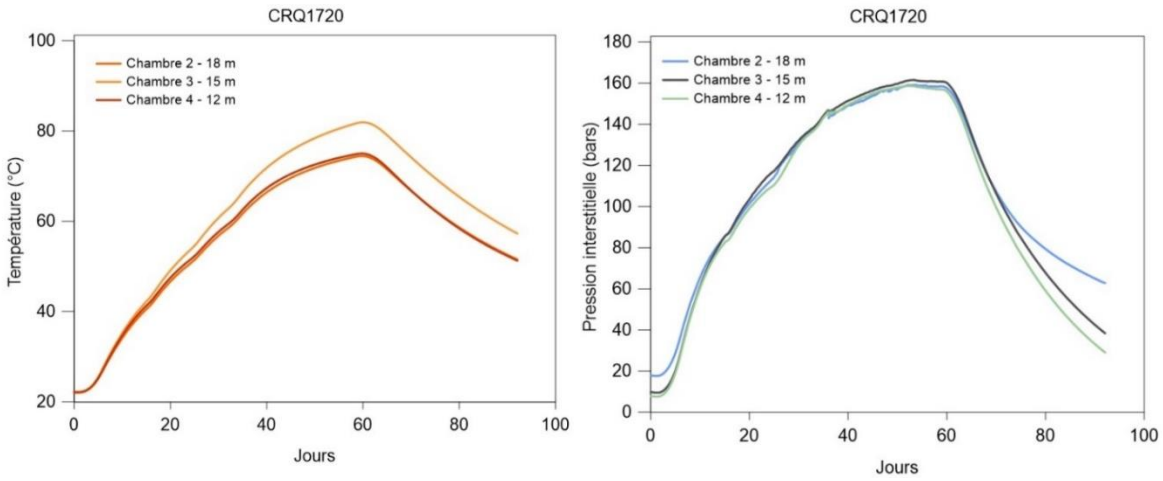

Figure 4-92. Temperature (left) and pressure (right) measurements

4.2.2.6 ALC 1605 HLW cell test

Compared to the ALC 1604 test, this full-scale test is performed on a HLW cell where the annulus between the casing and the formation is filled with a mix of cement and bentonite. The main objectives of this experiment are to study:

- the impact of heating on the casing with a filled annulus
- the impact of heating on the THM behaviour of the claystone in the near-field (beyond the EDZ) and far-field when the annulus is filled.

The 25-m long cell was drilled in the direction of the maximum horizontal stress from the GAN drift. Several casing joints are equipped with strain gauges (to monitor both radial and tangential deformations) and 2 joints are equipped with external fiber optic for strain and temperature measurements. In addition, eight boreholes were drilled around the cell for pressure, temperature and permeability measurements (Figure 4-93). The heating phase is planned to start in January 2020.

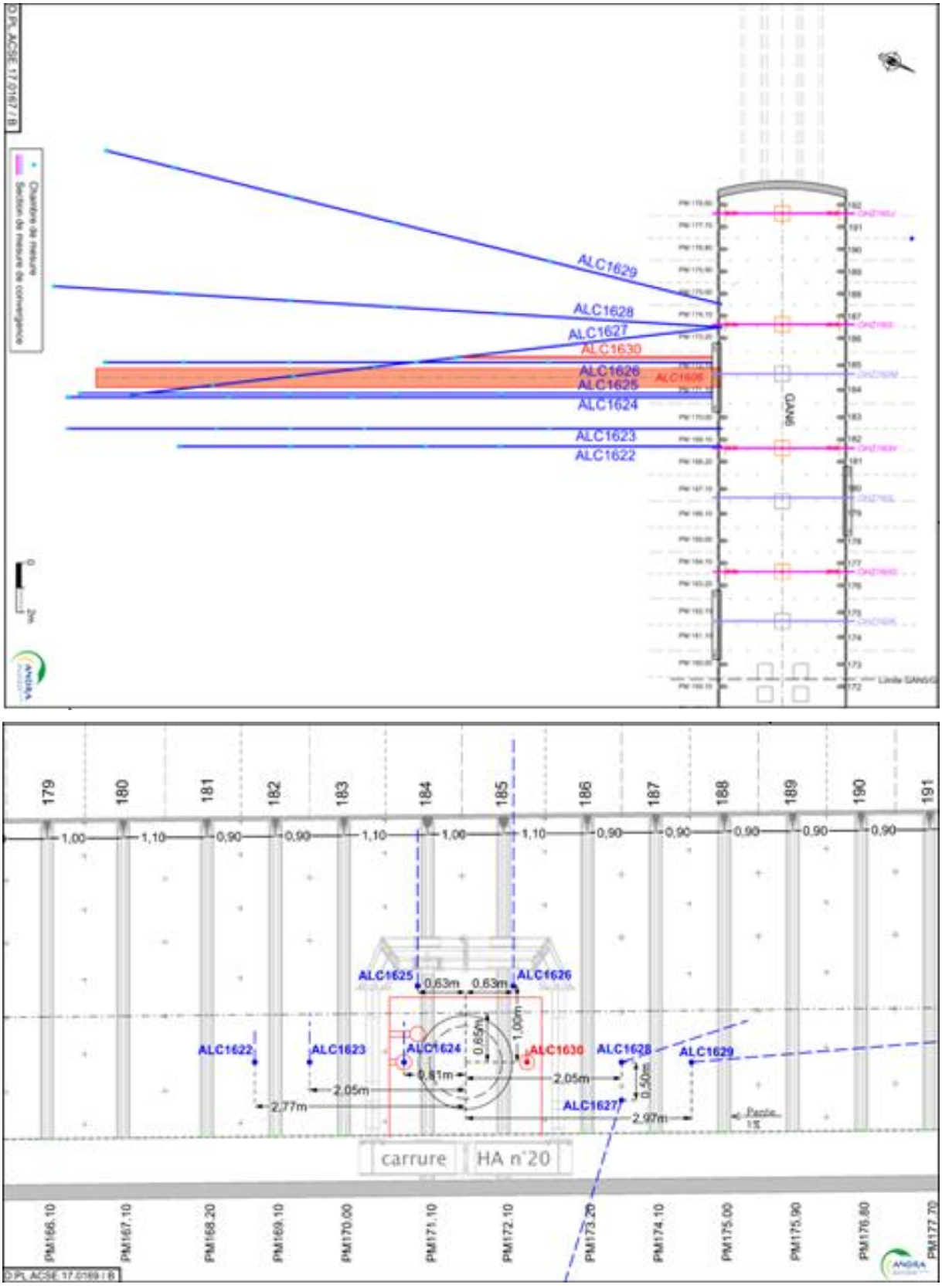

Figure 4-93. Layout of the ALC 1605 in-situ test (up: top view, and down: view from the GAN drift)

4.2.3 Opalinus

The HE-E and FE experiments are described above in sections 3.2.3 and 3.2.4. Test HE-D and a detail of the rock instrumentation in test FE are given below. Details of the modelling of some of these tests are given in section 4.4.4.

4.2.3.1 Test HE-D

In the HE-D Experiment (Wileveau 2005, Zhang et al. 2007), two heater elements were emplaced directly in the Opalinus Clay in a horizontal borehole of 300 mm diameter and 14 m length (Figure 4-94). The heaters were installed in the borehole without the addition of a bentonite buffer. The Opalinus Clay was heated up to 100°C in two heating phases using power output of 650 and 1950 W respectively, followed by a cooling phase. Responses of the clay rock to the thermal loading were investigated by monitoring the temperature, pore-water pressure, gas migration, and deformation in the surrounding rock with 110 instruments installed in 24 boreholes. The HE-D Experiment was conducted between October 2003 and December 2005. The THM evolution of the rock was monitored over a period of approximately 17 months. The set-up and measurements of the HE-D experiment are described in detail in Wileveau & Rothfuchs (2007).

The main technical and scientific goals (Wileveau 2005) of the HE-D experiment were:

- To test new sensor technologies, such as pore-water-pressure sensors suitable for clay formations with very low permeability and a heated environment, or optic-fibre sensors for measuring temperature and deformations;
- To determine the thermal and thermomechanical properties of Opalinus clay on the basis of in-situ observations and tests on samples;
- To determine the impact of temperature on the hydromechanical behaviour of Opalinus clay on the basis of the in-situ test and test on samples;
- To study the scale effect.

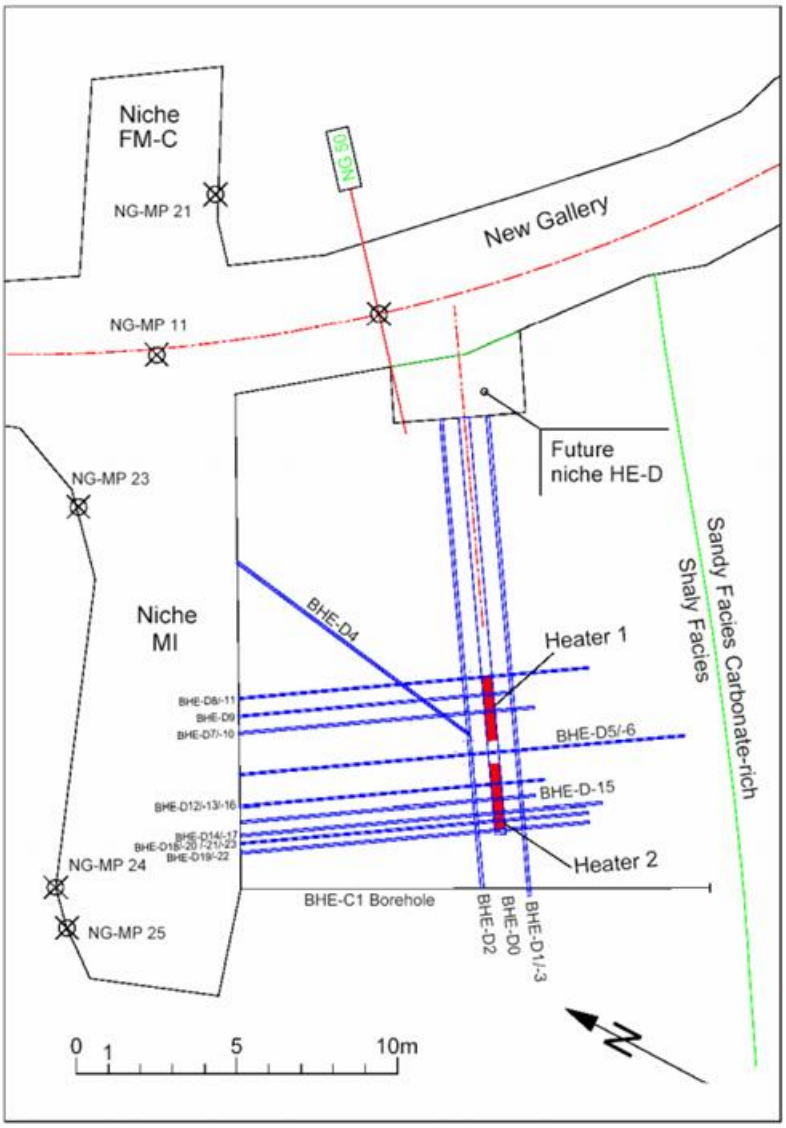

Figure 4-94. Top view of the HE-D test showing the overall borehole layout

4.2.3.2 Instrumentation of the FE test

The general layout of the FE test is described above in 3.2.4, but a summary of the instrumentation aspects is given below.

Instrumentation of the EDZ

The monitoring programme was focused on long-term monitoring of the near-field and far-field rock in response to operation of the heaters. 55 boreholes were instrumented with a range of sensors for monitoring of:

- temperature, monitored at borehole depths of 0 – 8 m. Most boreholes were equipped with conventional temperature sensors (thermocouples and PT1000 sensors) at different depths;
- water pressure, monitored at borehole depths of 1.5 – 3 m using piezoresistive pressure transducers in eight boreholes;
- deformation, monitored at borehole depths of 0 – 8 m in six boreholes using extensometers placed at four locations in each borehole;

- coupled displacement and temperature, monitored in seven boreholes between the heaters using SMARTEC SOFO sensors and thermocouples;
- water content and suction, monitored at borehole depths of 0 – 1.1 m. Rock mass water content is being monitored with a commercial dielectric profile probe originally developed for agricultural applications. This dielectric tool has six measurement sections within its 1 m length. Five of these probes were permanently installed in 28 mm diameter boreholes drilled in the cooler sections of the FE tunnel, i.e. in the Access Section, the Test Section end of the Concrete Plug, and in the ISS. In addition, 17 radial boreholes were equipped with standard and monolithic capacitive relative humidity sensors.

Instrumentation of tunnel wall and heater

The instrumentation installation comprised instrumentation of the tunnel wall, bentonite, and heater surface to monitor THM evolution, installation of fibre-optic cables, geophysical monitoring, monitoring of gas concentration and monitoring of heater corrosion

Instrumentation for monitoring of THM processes, gas concentration and metal corrosion

The tunnel wall, bentonite and heater surface were instrumented with a system for monitoring temperature, relative humidity/water content, total pressure, deformation/displacement and thermal conductivity.

The spatial distribution and temporal evolution of temperature in the bentonite and at the tunnel wall is monitored by a total of 115 conventional temperature sensors (thermocouples and PT1000). Additional temperature sensors are integrated into relative humidity and total pressure sensors (described below). In addition, each heater was equipped with six internal thermocouples, 18 external thermocouples (fixed to the heater surface), and 24 fibre-optical point sensors (fibre Bragg gratings) placed on the heater surface.

A total of 99 relative humidity sensors were installed on the tunnel wall and within the bentonite buffer. Additionally, a total of six prototype TDR probes were installed around heater H2 and heater H3 to monitor volumetric water content, and a further nine combined water content and temperature probes were installed in the ISS and concrete plug.

Twenty-four total pressure cells were installed on the tunnel wall in order to monitor any potential swelling pressure of the bentonite buffer, 18 of these pressure cells incorporated temperature sensors. A further six combined pressure and temperature probes were placed on the surface of each heater for the same purpose.

Two types of displacement sensors were installed to track any potential heater movement after backfilling and during heating. Nineteen linear variable differential transformer (LVDT) sensors were placed at the ends the heaters, and four potentiometric displacement sensors were placed in a cross-like configuration at the ISS end of the Test Section (monitoring cross-section G0 at GM 43.0) and between heaters H1 and H2.

Fiber-optic cables on tunnel wall

Approximately 400 m of fibre-optical cables (excluding the smart rods and acoustic FO cables) were also installed at different positions along the tunnel for distributed strain and temperature sensing, this included:

- 400 m of fibre-optical cables installed at different positions on the tunnel wall for distributed temperature sensing.

– Two 12-sensor arrays placed on each heater for distributed temperature sensing. These consisted of Fibre Bragg Grating (FBG) Smartfibers on Heater H2 and Heater H3, and Draw Tower Grating (DTG) Smartfibers on Heater H1.

Geophysical methods

Geophysical methods were selected with the aim of monitoring changes in the GBM buffer in a quantitative manner with minimal adverse effects on the backfilling procedure or the THM evolution. One monitoring component consists of two gas-tight pipes installed approximately 1.7 m apart in the roof of the FE tunnel at a distance of a few centimetres from the shotcrete liner. These pipes facilitate long-term access through the concrete plug and into the bentonite buffer in front of and above Heater H3 for a variety of geophysical borehole tools.

Measurement campaigns, with the focus on bentonite properties in the near-field around the pipes, include repeated density and porosity logging as well as single-hole georadar surveys. Tomographic georadar and acoustic surveys are performed to better capture and image the changes in the area between the two pipes. An acoustic 'borehole' sensor system (with one source and eight receivers) is typically kept at a fixed position in the pipes for quasi-continuous monitoring of changes to the bentonite properties between different measurement campaigns.

The second monitoring component includes two acoustic sensor arrays that were permanently installed before backfilling, one close to the floor and one in the roof of the tunnel. These permanent installations allow subtle changes in acoustic waveforms to be captured either within the individual arrays or across the arrays when sensor coupling is sufficient. In combination with the acoustic 'borehole' sensor system temporarily installed in the pipes, additional ray paths and imaging capabilities can be tested during the ongoing operation of the FE Experiment.

Gas monitoring

Fourteen prototype in situ hydrogen and six in situ oxygen concentration sensors were installed at different locations along the FE tunnel. Two oxygen sensors were located on the GBM buffer side of the plug retaining wall, one was placed close to Heater 3, two were placed close to Heater 2 and one was placed in the ISS. The other oxygen sensors were located close to Heater 2 and Heater 3. Additionally, ten gas sampling lines were installed to allow continuous gas monitoring by mass spectrometry as well as periodic gas sampling. The sampling lines were chosen to be PEEK with an inside diameter of 1.5 mm. The backfilled sampling points consist of a polyvinylidene fluoride (PVDF) housing with either a stainless-steel filter or a silver-coated nylon mesh. The silver coating is used to hinder the development of biofilms, which could lead to clogging of the filters.

Corrosion monitoring

In order to investigate in situ corrosion phenomena in the case of potential future dismantling of the FE Experiment, sample holders with different metals were installed on heaters H2 and H3 as well as at two different locations on the tunnel wall in close proximity to the gas sensors and sampling ports. The metals used in the sample holders were carbon steel, wrought copper, electrodeposited copper and cold-sprayed copper. Five corrosion coupons from each metal were installed at each position. The corrosion coupons were polished and their surface roughness characterised prior to emplacement.

4.3 Requirement for planning, executing and documenting THM lab tests

The characterisation of the THM behaviour of clay-based materials is commonly done through testing in the laboratory. However, whereas buffer materials such as bentonite are readily available,

representative clay host rock samples need to be extracted at large depths as the planned repositories are 200 to 600 m deep. As the claystone cores are cut and brought to surface, they undergo some alterations due to changes in pressure and temperature and exposure to air or water (Ewy 2015, Basu 2020). The initial stress relief, the core handling and its preservation, the variations of water saturation, the sampling, etc. are all disturbing elements. They can lead to the generation of large fractures that are easy to detect or to a diffuse microcracking that cannot be seen without sophisticated tools such as micro-CT (Lenoir et al. 2007, Chen et al. 2014). These initial perturbations of the material can have a great effect on the measurements, their impact depending on the type of data that is measured. When dealing with rocks, the natural variability of the material that could influence the results of experimental tests has to be also considered. Quantification of the effect of this natural variability through laboratory tests requires systematic laboratory tests on large number of samples with a proper defined test protocol.

Moreover, as clay/claystone, such as Boom Clay, COx and OPA, have very low permeability, the laboratory tests often demand very long duration for certain steps of the testing process, such as the re-saturation and the consolidation phase for example. In addition, all these studied clay/claystones present an elasto-visco-plastic behavior and their THM behaviour depends highly on the stress paths, loading rates and the coupling between all these processes. Consequently, there need to be some requirements/precautions for all the different processes of the laboratory tests to ensure that the test is properly performed and thus allow to delineate the influence of each process on the test results and, at the end, enable to make a proper interpretation of the results and provide relevant input parameters for the modelling development. Consequently, some recommendation/suggestions or requirements are made by the WMOs to ensure each step to be properly performed.

In the current state of the art report, the corresponding WMO for each kind of host rock to be studied in the HITEC, has provided some recommendations/requirements on the protocols for certain test processes based on their experience (laboratory and numerical investigation) gained through years of research.

4.3.1 ANDRA

Coring with non-aqueous drilling fluids is the best way to minimise exposure to water or air (Ewy 2015). This technique was used to acquire the first COx samples in deep boreholes drilled from the surface, but most samples are now extracted from a large number of air-drilled boreholes at the main level (–490 m) of the LMHM underground laboratory. In order to minimise the exposure to air, the cores are rapidly (less than one hour) brought to surface and conditioned in special confining T1 cells (Figure 4-95, Conil et al. 2018).

In order to get measurements that are as reliable as possible, all the preparation chain should be well controlled and all the steps from core extraction to the laboratory test traced. To be able to interpret in a rigorous way the results of tests, this has to be completed by some basic characterization before and after the tests. Knowing the history of the sample and how it is placed with relation to its geological environment are unavoidable stages to improve the quality of the results and deal with the natural dispersion inherent to this type of material.

Andra wrote a guideline (Conil & Talandrier 2019) that defines some rules:

- to preserve as much as possible the samples, their physical and mechanical characteristics;
- to characterise the material before and after testing;
- to standardise test protocols as much as possible in order to facilitate comparisons between results coming from several laboratories.

This experimental guideline results from discussions between Andra and its partners. It is based on the practices used currently when tests are performed on Callovo-Oxfordian samples. Based on these discussions, two types of practices are proposed: 1) Recommendations (noted Rn) which constitute a guide to "good practice", 2) Imposed protocols (noted Pn) which are the rules to be systematically followed during test campaigns. The imposed protocols and the recommendations are summarized in Table 4-34 and Table 4-35.

Figure 4-95. Clay preservation packages. As soon as a clay core is brought to surface, it is sealed and confined in these cells in order to try and keep the clay properties as close as possible to its virgin state

Table 4-34: Summary of the imposed protocols

	Sample machining
P1	Protocol to preserve samples before use: 1) wrap the sample in food film and aluminum foil (preservation of the water content), 2) put under a non-pushed vacuum (food preservation type) in order to remove oxygen, 3) put in an enclosure under a pressure of at least 2 bar under inert atmosphere N_2 or Ar (no CO_2) or under water, 4) label with the date of manufacture of the sample, the identification of the core, the orientation of the sample in the core to know the direction of bedding.
P2	Always include in the reports the date of sample preparation and the date of use.
	Characterization of the initial state
P3	Initial water content will be measured by weighing a sample taken just after cell opening and then drying it at 105°C. The mass of the sample is considered as stabilized when the mass variation between two successive weighings at 24 h intervals is less than 0.1%.
P4	A water content measurement before each test must be performed, if the storage time of the samples is more than 1 month. For this purpose, control samples (samples missed during preparation, scraps, etc.) are kept under the same conditions as the samples used for the tests.
P5	A porosity estimation will be made for each core used in a test campaign and the method used for this estimation will be described in the final report.
	Loading rate
P6	The loading rate during the confining phase when the sample is partially saturated should not exceed 0.1 MPa/min.
P7	The loading rate during a mechanical test in a triaxial cell, even when the sample is partially saturated, ahould not exceed 10^{-6} s^{-1}.
P8	For triaxial cell tests and for all THM tests if it is possible a deformation measurement must be performed. The calibration of the measurement must be indicated in the final report.
	Water saturation

P9	To resaturate a sample, the confining pressure (in triaxial cell) must be increased first to 14 MPa with a maximum loading rate of 0.1 MPa per minute. Then water is supplied to the sample, increasing progressively the water pressure to 4 MPa.
P10	Two criteria are used to verify the total water saturation of the samples: 1) 24-h water pressure variation in the upstream and downstream reservoirs after their insulation, 2) Evaluation of the Skempton coefficient for variations in confinement pressure under non-drained conditions. This phase of saturation should not exceed between 20 to 30 days depending on the size of the sample.
	Composition of the water for the saturation
P11	The water used in the tests must be prepared by the laboratories according to the protocol provided by Andra. The water thus reconstituted must be kept in a cool and dark place for a maximum of 1 year. Salts must be kept away from moisture.
	Resaturation with controlled RH
P12	It is noted that the use of a saline solution is the best way to go back to a given saturation point. A nitrogen or argon sweep of the enclosure is necessary to avoid oxidation of the pyrites which systematically leads to cracking of the sample.
	Postmortem characterization
P13	In order to assist in the analysis of the results, certain measurements must be taken after testing. These measurements can be compared to the one initially measured. At a minimum, it is recommended to carry out a water content measurement on the tested sample and take a photo of the sample.

Table 4-35: Summary of the recommendations

	Sample machining
R1	To avoid desiccation after machining the sample to the proper diameter, it is recommended to wrap it. A food grade film and an aluminum foil are sufficient at this stage.
R2	Prepare as many samples as possible after the opening of cell T1 (Figure 4-95).
R3	The storage period for samples and for the T1 cell must not exceed 1 year. It is recommended to prepare new samples at the beginning of each test campaign.
R4	If it is necessary to know precisely the orientation of the core in relation to the bedding, it is advisable to cut a slice of material from the cell and immerse it in water to cause cracking. The cracks appear in the direction parallel to the bedding.
	Characterization of the initial state
R5	If the laboratory has suitable equipment, for example, Bernard calcimeter, helium pycnometer or dew point hygrometer, a measurement of grain density, carbonate level or suction after cell opening is recommended in order to have additional elements in the analysis of the results.
	Initial damage
R6	It is recommended when it is possible, to use micro-CT to determine the initial state of the sample. This technic can also be used to select the sample and remove damaged samples before testing. The report should provide information on: – The precision of the technics implemented for the detection of heterogeneities and analysis (what is the size of the cracks/inclusions detected?) – How are the "defects" detected in the sample (mainly cracks and inclusions) taken into account in the analysis of THM measurement results? – The choices made upstream in the selection of samples.
	Pore pressure measurement

R7	if the laboratory has the appropriate equipment, a pore pressure measurement is recommended in order to have additional elements in the analysis of the results
	Water saturation
R8	Andra recommends to use the samples without artificial resaturation but the "natural" water saturations of the sample must exceed 90%. This for test when resaturation is not necessary (for strength measurement for example). On this point, a reflection will have to be launched with Andra for each study on the most appropriate choice in function of the objectives.
	Post-mortem characterization
R9	When it is possible, a tomography is also recommended

4.3.2 EURIDICE

The value of the hydraulic conductivity may be determined in laboratory using the Darcy's law. The test can be realised in an oedeometer, in a triaxial cell or in a permeameter. Different techniques can be used: the pulse injection test (Aertsens et al. 2004), the constant pressure measurement (Wemaere et al. 2006) and the value can be determined by back analysis from oedometer tests (Horseman et al. 1986).

Core samples to be used for the laboratory tests

The Boom clay cores for the laboratory tests were taken from the URL HADES by borehole drilling (mostly in the horizontal direction) with an inner diameter of 98 mm and different lengths (ranging from several centimeters to several 10 centimeters). They are all vacuum packed using reinforced aluminium foil. The direction of the core drilling is indicated on the cores. The picture of the core taken before package will be provided to the experimenters, which may help to check the state of the core before trimming and eventually, to identify the bedding.

Characterisation of the initial state of the samples

Even though the Boom Clay cores were conserved in a relative stable condition, the state of the cores can be still modified to some extent, because of the long duration of the cores storage or during the transport of the cores. It is thus strongly suggested, prior to any tests, to determine the fundamental geotechnical properties of the Boom Clay such as water content, porosity, saturation degree, suction, dry density, microstructure. X-ray high-resolution tomography of the specimens before testing would be helpful for the interpretation of the tests results (any pre-inclusions that were not observable by the naked eye? any pre-existing fissures ? both can affect the mechanical response) (Bésuelle et al. 2014).

Specimens preparation technique

The test specimen itself must firstly be prepared from a core sample of soil before placing into the testing cell. This may involve trimming undisturbed specimens extruded from core tube. Note that there is no yet a standard procedure for the specimens trimming. This depends highly on the available equipment of each laboratory and people experience gained by best practice. The basic requirements are the following ones:

– The mechanical disturbance to the specimen should be kept to a minimum during preparation (trimming, shaping, placing into the cell…);

- Before testing, the specimens have to be carefully stored/protected to maintain the initial water content.

In addition, for all tests, it is important to know clearly the orientation of the specimen with respect to the bedding of Boom Clay formation.

For the core samples taken from the horizontal borehole, the bedding (stratification) can be identified usually through naked – eye. The conjugated macro-fractures frequently observed in the cores will help also to determine the stratification of the core samples.

Sample re-saturation process (pre-conditioning phase)

For the tests under saturated condition, the re-saturation process has to be designed to ensure all voids within the test specimen are filled with water and that the pore pressure transducer and drainage lines are properly de-aired. For the Boom Clay sample, a suction was generated during the core drilling due to the stress releasing and, an additional suction may be induced by possible drying during cores storage and the transport. Consequently, careful pre-conditioning (re-saturation) protocols prior to any tests on the Boom Clay samples taken at a large depth like at the level of URL HADES is necessary.

The protocols described below allow to release in an efficient way the suction and thus minimize the damage induced by swelling during the re-saturation process. This protocol implies that any laboratory tests (any stress paths with controlled/measured water pressure) always start at a stress state close to *in situ* conditions.

This protocol has to be followed for all laboratory tests. The re-saturation process consists of mainly four steps as illustrated in Figure 4-96 which includes:

1. To apply of a cell pressure of 100 kPa at a ambient temperature until the stabilisation of the whole test system (cell, hydraulic circles) is reached (about one day);
2. To increase of the cell pressure till 2500 kPa with a constant stress rate (<05 kPa/min is suggested) whilst keeping the specimen in contact with dry porous disks (so without contact with any water). In such conditions, the specimen is subjected to a mean effective stress close to that in-situ, estimated at 2500 kPa by Horseman et al. (1993);
3. To put the SCW in contact with the specimen by injection of SCW under a weak back pressure of 100 kPa (meanwhile, increase equally 100 KPa of cell pressure) and follow up the possible swelling. This phase can last one week to 10 days to be stabilized (volume change) depending on the size of the specimen.
4. To increase the cell pressure and the back pressure simultaneously, during which a constant effective stress of 2500 kPa close to the in situ condition should be maintained. By experience, a back pressure of about 1000 kPa for the Boom Clay specimen is needed, this implies a cell pressure of 3500 kPa. This procedure can be performed in two ways:
   - Increasing step by step (150-200 kPa/step is suggested) (as seen in Figure 4-96). At last two steps, B-Check tests have to be performed.
   - Increasing linearly the cell and back pressure with a constant pressure rate (0.2- 0.5 kPa/min is suggested) till the target cell pressure (usually 3500 kPa) and back pressure (usually 1000 kPa) and keeping them then constant until the stabilization of water exchange between the injection system and specimen (as shown in Figure 4-97). During this later waiting stage, it is suggested to perform the B-check tests.

To check the degree of specimen saturation is sufficiently high before moving to the next stage of the laboratory test, it is suggested to perform a *B*-check test to determine Skempton's *B*-value at last stage. For Boom Clay, when $B \geq 0.90$, we can consider that the specimen reaches to full specimen saturation.

The total duration for the re-saturation phase requires usually about one month depending mainly on the size of the specimen and drainage paths of the specimen.

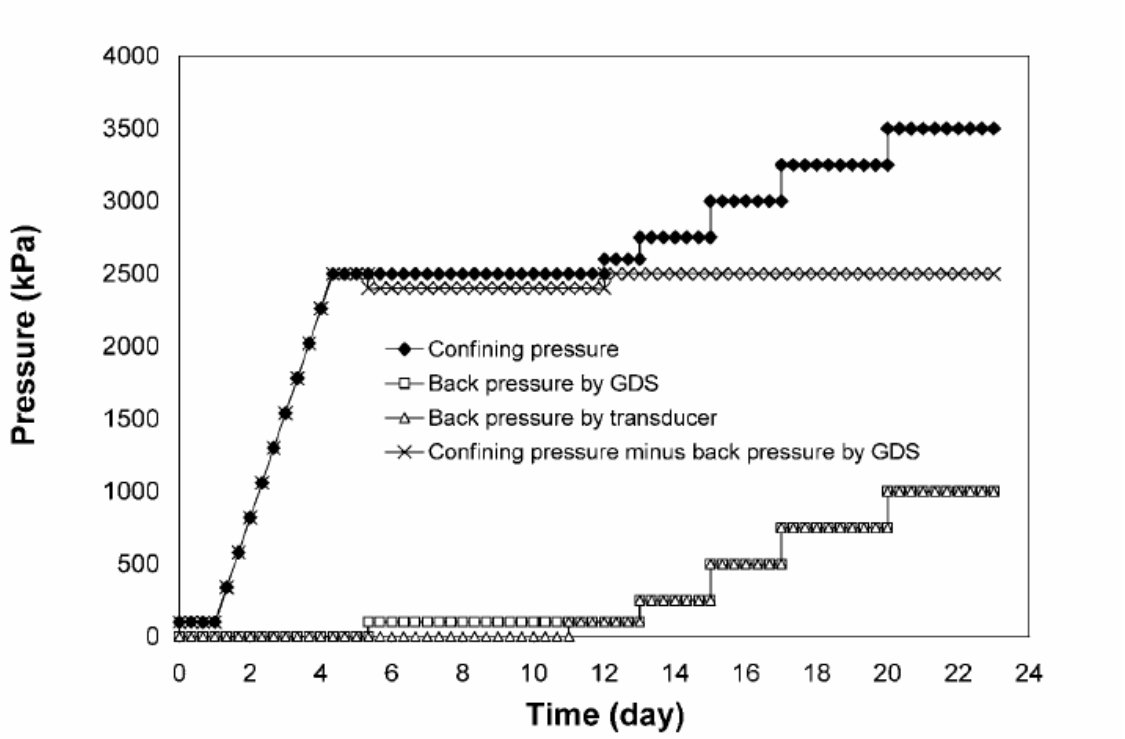

Figure 4-96. Stress paths followed during the saturation phase (Cui et al. 2009)

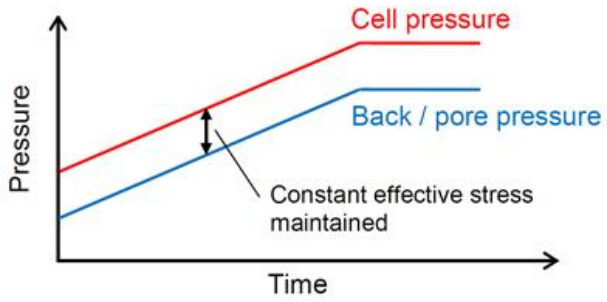

Figure 4-97. Specimen saturation by linear increasing cell and back pressure

Loading rate for the consolidation phase

The consolidation stage is used to bring the specimen to an effective stress state required for shearing, for heating, or for other kind of stress paths. It is typically conducted by increasing the cell pressure whilst maintaining a constant back pressure (often equal to the pore pressure reached during the final saturation B-check). This process is continued until the volume change of the specimen is no longer significant, and at least 95% of the excess pore pressure has dissipated.

For Boom Clay specimen, at ambient temperature, a loading rate of 0.2 kPa/min is suggested. This recommended loading rate can be applied also for the unloading phase if relevant. Higher than 0.2

kPa/min is probably too fast to ensure a complete dissipation of the excess pore pressure, while a slower rate will not increase significantly the efficiency. In any case, it is suggested that the loading rate should not faster than 0.5 kPa/min.

If the tests requires an unloading phase, it is important to keep in mind that the volumetric deformation of the Boom Clay during unloading depends highly on the hydraulic conditions. Drained unloading will induce significantly the swelling and thus modification of the microstructure, while undrained unloading will limit significantly the volumetric deformation. Consequently, the unloading phase has to be carefully designed to meet the objectives of the study.

Loading rate for the shearing phase

For the mechanical triaxial test, the soil is sheared by applying an axial strain to the test specimen at a constant rate. This rate, along with the specimen drainage condition, is dependent on the type of triaxial test :

- For the CU (Consolidated Undrained test), the axial strain rate should to be slow enough to allow adequate equalisation of excess pore pressures. A strain rate between 2-4 10^{-6}/s is suggested.
- For the CD (Consolidated Drained test), the axial strain rate should to be slow enough to result in negligible pore pressure variation. A strain rate between 2-4 10^{-7}/s is suggested.

If the shearing is performed by applying a constant stress rate, for Boom Clay, up to now, limited test results allow us to make a suggestion/recommendation on the stress rate. Further investigations are still needed. By experience, it is suggested to apply the following stress rate:

- For the CU tests, a constant stress rate between 0.45-18 kPa/min have been considered slow enough (Horseman et al., 1987) .
- For the CD tests, a constant stress rate between 0.3-2.5 kPa/min have been considered slow enough (Cui et al. 2009)

Heating rate

The heating rate for the lab tests on Boom Clay specimen is still open issue, since the volumetric change of Boom Clay upon heating depends on the stress state of the specimen prior to heating (mainly the over-consolidation ratio). By experience till today, it is suggested that the heating rate should not be larger than 0.3°C/h to perform a drained heating test (Sultan 1997, Sultan et al. 2000).

Post-dismantling analysis

In order to investigate the microstructure modification or failure pattern after testing, it is recommended to carry out certain microstructure analysis such as MIP, µ-CT scan, etc. Fundamental geotechnical properties (such as the water content) after testing need to be measured too in order to compare with the initial state.

Raw data of test results

In order to facilitate the further analysis and comparative study of all the existing test results performed in different laboratories, it is recommended to record and report all testing information and all raw data of test results.

4.3.3 NAGRA

In the following, an individual sample extracted from the conditioned core material and used in triaxial testing is referred to as the "specimen".

Triaxial Testing

Conform to the convention in the field of laboratory testing in soil and rock mechanics, Triaxial Testing here refers to a Specimen deformation test by means of a triaxial cell to apply confining pressure to the specimen and a loading device for applying and controlling axial load (e.g. ISRM, 1978; ASTM, 2004).

Balanced Pore Fluid

For those testing configurations requiring external pore fluid, the Operator will provide a detailed recipe of the pore fluid chemistry to prepare a Balanced Pore Fluid. The fluid contains variable amounts of commonly available chemicals such as NaCl, Na_2SO_4, $MgCl_2{\cdot}H_2O$ and $CaCl_2{\cdot}H_2O$ and possible KCl and $NaHCO_3$. The pH of the Balanced Pore Fluid should be fairly neutral (~7 – 8).

Minimum technical requirements

Specimen preparation and testing shall be performed in accordance with general international standards (e.g. ISRM 1978, ASTM 2004). Specifically, in view of the anticipated Triaxial Testing of Opalinus Clay, the following minimum technical requirements must be met:

Storage capacity

The Contractor should be able to accommodate up to 15 Cores of 10 cm diameter and 50 cm in length for the duration of the project. During storage, temperature should be fairly constant and exposure to extreme temperatures (lower than 10°C or greater than25 °C) must be avoided.

Specimen size and extraction

Specimens must be of cylindrical shape with length (L) to diameter (D) ratio L:D ≥ 2:1 and maximum dimensions of 38 mm ≤ L ≤ 76 mm.

The preferred method to extract the Specimen from the Core is by cutting a pre-defined (by the Operator) section of the Core tube through the PVC tube with a saw, and then to drill the Specimen. Coring and cutting should be done using a non-polar, non-wetting fluid (e.g. a hydrocarbon) cooling fluid. Air can be used if necessary, but there is an increased risk of drying and damaging the specimens. Water or brines cannot be used for extracting the Specimen or for any other step of Specimen preparation.

Native activity (i.e. total suction and/or relative humidity with corresponding temperature) of the Core must be determined upon extraction of the first section.

Triaxial Testing equipment and testing conditions

Choice of equipment and Specimen size must be done such that a total confining stress of up to 30 MPa and an axial load sufficient to fail the specimen (maximum of 120 MPa total axial stress) can be covered. For axial load measurements, the load cell must be inside the vessel and should have a maximum range of 350-400 kN. The pore fluid system (where applicable) must be able to handle the Balanced Pore Fluid chemistry and be designed to pressures up to 20 MPa. Pressure transducers are

also needed to monitor the fluid pressure in the drainage lines in case of undrained testing; a pressure range up to 20 MPa is required.

Strain measurements must be performed inside the vessel. Where LVDT transducers are being used, the maximum allowed range is 10 mm; and for all other system (e.g. strain gauges, cantilevers), a displacement resolution of 1 micron is required. Radial Specimen strain must be performed at mid height of the Specimen and at least one rig must be capable of performing two orthogonal measurements (for Specimens with bedding parallel to cylinder axis).

It is anticipated that most tests will be performed at room-temperature (~20°C). However, the equipment must also be capable to perform tests up to 80°C.

It is anticipated that most tests will be performed by axial compression with constant confinement (CTC stress path) and with loading at constant strain rate. However, alternative stress path will likely also be explored (e.g. extension, constant mean stress etc.), and the Contractor should specify in which alternative stress paths can be executed (including experience in doing so).

In the case of "conventional" testing, axial and radial stresses must be controlled independently such that a no displacement boundary can be maintained during the saturation phase. This is important to minimize volumetric changes to the specimen ("swelling").

The equipment must also routinely measure ultrasonic velocities for both P- and S-waves in axial direction.

A lateral drainage system, i.e. along lateral surface in addition to the end faces of the cylindrical Specimen is the preferred configuration for testing, but not a strict requirement. It is noted that depending on Specimen size and drainage configuration, strain rates for tests with drained boundary conditions are likely to be lower than $1 \cdot 10^{-8}$ s^{-1}. The estimated strain rates (i.e. test duration) must be compatible with the minimum loading rate capacity of the equipment.

Parameters to be derived from Core, Specimen and Triaxial Testing

Continuous measurements of stresses (axial and radial), deformations (axial and radial), and back fluid pressure are required from each test. The recorded data must enable the determination of the parameters listed in Table 4-36. In addition, the Table highlights the basic properties that are needed for the assessment of the initial conditions of the received Core and Specimen after preparation.

Determination of ultrasonic velocities (i.e. interpretation of P- and S-wave arrivals) must be done by the contractor.

Table 4-36. Parameters to be derived from Core, Specimen and Triaxial Testing

Test types	Symbol	Method
Core characterization upon opening		
Total suction or relative humidity	Ψ	Hygrometer / psychrometer
Bulk density	$\rho_{b,core}$	Caliper (regular shape) or fluid displacement (irregular shape)
Water content	w_{core}	Oven-drying (105°C)
Specimen characterization		
Initial specimen water content (before testing)	$w_{sp,i}$	Oven-drying (105°C) after testing
Bulk density	$\rho_{b,sp}$	Caliper measurements
Undrained / drained triaxial tests		

Test types	Symbol	Method
Swelling pressure (radial and axial)	σ_{axial}, σ_{radial}	Constant volume (independent control for axial and radial)
HM coupling parameters	Skempton *B*	Isotropic step-increase of pressure, undrained
Consolidation coefficient	c_v	isotropic consolidation
Void ratio after consolidation	e*	
Delta max pore pressure	$\Delta u_{w,max}$	Undrained testing
Deviator stress at failure	q'_f	
Effective mean stress at failure	p'_f	
Delta pore pressure at failure	Δu_{wf}	
Axial strain at failure	$\varepsilon_{a,f}$	
Volumetric strain at failure	$\varepsilon_{v,f}$	
Deviator stress (post-peak)	q_{pp}	
Effective mean (post-peak)	p'_{pp}	
Ultrasonic velocities	V_p/V_s	Axial direction
Tests dismantling		
Final specimen water content (after testing)	$w_{sp,f}$	Oven-drying (105°C)

4.4 State of models' development (modelling tools and approaches)

4.4.1 ANDRA

In order to validate the rheological models at the scale of an HLW cell and, and if possible, to improve the determination of the parameters used, Andra set up from 2003 an in situ experimental programme to progressively:

- Confirm the thermal design parameters for the disposal
- Provide a better quantification for the THM processes around the HLW cells
- Perform some experiments to validate the concepts for the HLW cells

The in-situ tests in the URL made it possible, through inverse analysis, to estimate certain THM parameters on a metric scale and to compare them with the measurements on samples (Garitte et al. 2014). For example, the inverse analysis of the thermal parameters (thermal conductivity, heat capacity) confirmed the measurements on samples.

The small-scale thermal tests (TER, TED) demonstrated that the numerical simulations conducted with a linear thermo-poro-elastic model could accurately reproduce the temperature and the pore pressure variations, while also taking into consideration the thermal, mechanical and hydraulic anisotropy. From these tests, the sensitivity analyses showed that the major parameters were the stiffness of the COx claystone, the permeability, and, to a lesser extent, the thermal conductivity and the Biot coefficient.

The first results from the full-scale HLW disposal cell demonstration test with the 2009 concept in the underground laboratory (ALC1604), show that the small-scale approach that was used, without considering the change in thermal parameters in the EDZ, enables a reasonable prediction of the temperature range. For the changes in the "far-field" pore pressure (several metres away from the heating cell), the influence of the modifications on the near-field hydro-mechanical properties caused

by the cell excavation, remain low. However, in the near-field, the purely linear poro-elastic approach is not good enough to correctly reproduce the change in pore pressure or the deformations. A more complete modelling approach is therefore required to better represent the physical processes in the fractured zone caused by cell excavation (variations in permeability, mechanical behaviour of fractured zone, etc.).

The analysis of the temperature, pressure and stress variations around the HLW cells as a function of the thermal load and of the inter-cell spacing was done internally using two well-known numerical simulation programs: Code-Aster and Code_Bright. UPC also performed the modelling on Code_Bright of the ALC1604 heating experiment.

In addition, some benchmarking exercises were carried out, they are briefly described below.

4.4.1.1 Constitutive model for the EDZ

A benchmark exercise was organised in 2012 to model the induced fracture networks around a drift. Several constitutive models were developed, divided in four main families: most were based on visco-elasto-plasticity, but damage-mechanics, rigid body spring and computational homogenised models were also tested. Nine teams took part in this exercise (Seyedi et al., 2017), a summary of the models used is given in Table 4-37.

Two series of test cases were defined. In the first one, simple stress paths similar to those that can be produced during the excavation of the tunnels were proposed. The second series of tests consisted in the modelling of underground drifts oriented in the two principal horizontal stress directions. These models were matched against in-situ data from URL drifts drilled parallel to σ_H and σ_h. This exercise showed that accounting for material anisotropy and strain localisation treatment techniques could improve the results when elasto-visco-plastic models were used.

4.4.1.2 THM modelling of the TED in-situ heating test

Another benchmark exercise was organised as part of the DECOVALEX 2019 international program. The following teams took part in the exercise: Andra, LBNL, Quintessa, NWMO and UFZ/BGR. The purpose of this benchmark was to upscale the THM modelling from small-size experiments (some cubic metres) to real-scale cell experiments (tens of cubic metres) and finally to the scale of the waste repository (cubic kilometres). It was based on the TED small-scale heating experiment and focused on the THM behaviour of the undisturbed claystone in the far-field. Some results are due to be published by Seyedi et al. (2020), but the general conclusion was that a good prediction of the evolution of both the temperature and the pore pressure can be achieved if an anisotropic poro-elastic behaviour is considered.

Table 4-37: Summary of the different models used in the framework of the "Transverse Action" benchmark exercise (Guayacan 2016, adapted from Seyedi et al. 2017)

Model	*Complementary description*	*Mechanical anisotropy*	*Failure criterion*	*Time-dependent behavior*	*References*
Elasto-visco-plasticity			Generalized Hoek et Brown criterion with hardening and softening functions	Perzyna type model, taking into account tertiary creep	Laigle 2004; Kleine 2007; Plassart 2011; Plassart et al. 2013
				Lemaitre type model, with creep threshold and damage-dependent creep strain rates	Souley et al. 2009; Souley et al. 2011
			Drucker-Prager including the effect of σ_{moy}	Lemaitre type model, with creep threshold	Hoxha et al. 2007a and 2007b
		Anisotropic elasticity	Power type failure function with hardening/softening	The creep is governed by a kinematic hardening law accounting for in-situ stress state	Hoxha et al. 2007a and 2007b
		Yes	Mohr-Coulomb criterion for the yield and failure limits and its anisotropic extension	Modified form of the Lemaitre law for visco-plastic strains	Mánica et al. 2015; Mánica et al. 2016
	with localisation traitment		Drucker-Prager with hardening law on friction angle/cohesion		Collin and Pardoen 2013; Pardoen et al. 2015a
		Yes	Drucker-Prager with hardening law on friction angle/cohesion, with anisotropic cohesion		Pardoen et al. 2015b; Pardoen 2015, Pardoen and Collin 2016
Elastoplasticity	with isotropic damage		Strain based criterion with distinction between compression and extension damage	Creep strain modeled as a retarded elastoplastic strain	Chiarelli et al. 2003; Shao et al. 2006a ; Jia 2006 ; Zhou et al. 2008 ; Jia et al. 2008
	with anisotropic damage	Yes	Strain based criterion with distinction between compression and extension damage and anisotropy accounted through a fabric tensor		Shao et al. 2005; Shao et al. 2006b ; Chen et al. 2010
Rigid Body-Spring Model(RBSM)		Yes	Isotropic/anisotropic criterion for interface failure		Yao et al. 2015, 2016a and 2016b
Anisotropic damage model		Yes	Double strain based criterion in extension/compression	Time-dependent strains calculated through a creep law calibrated based on creep tests	Robinet et al. 2015
Computational homogenized model (CHM)		Yes	FEM2* using a REV** (at the micro scale). The global response of this REV serves as a homogenized numerical constitutive law for the macro-scale		van den Eijnden 2015, van den Eijnden et al. 2016a and 2016b.

* FEM2 – Double scale finite element method ** REV – Representative elementary volume

4.4.2 BGE

To describe the mechanical behaviour of claystone, BGE is currently using a simple elasto-plastic material model based on Mohr-Coulomb. The model takes into account the material anisotropy typical for clay materials as well as strength softening when damage occurs in the rock. In order to consider the time-dependent behaviour of the rock during the dimensioning of concrete liner systems, a numerical approach has been developed. This approach considers a second set of material parameters corresponding to the state of the host rock at the end of the service life of disposal galleries and drifts. This state is characterized by incoming convergences and loads on the lining shell and is determined through calibration based on in situ measurements. This approach, which is well adapted for structural analyses, is not suitable for the numerical safety analyses of repository in clay since the time dependent behaviour of the rock plays an important role in the general thermo-hydro-mechanical phenomena that take place in a repository. Therefore, BGE envisages to incorporate the time dependent mechanical evolution of claystone into a basic model and to develop a thermal coupling necessary to simulate the thermal induced damage in the rock.

4.4.3 EURIDICE

This section presents the application of the main constitutive laws that are used to reproduce the Boom Clay behaviour. The hydro-mechanical behaviour of Boom Clay is reproduced with models such as the Drucker-Prager criterion or the Cam-Clay model. Many other constitutive mechanical laws have been developed to simulate the clay in various thermo-hydro-mechanical conditions. For example, the influence of the temperature with the development of thermo-plastic strains was taken into account in models such ACMEG-T (François 2008) and in other thermo-mechanical cap models (Cui et al. 2000, Dizier 2011).

After a short presentation of the Ducker-Prager model, the results of the simulation of triaxial tests are presented. The modelling of a hollow cylinder with a Drucker-Prager model taking into account the anisotropic properties is then showed. Finally, the modelling work performed within large scale PRACLAY Heater test is discussed.

4.4.3.1 Hydro-mechanical simulation

The Drucker-Prager model (Drucker & Prager 1952) is used for the Boom Clay. The elastic deformation is calculated by elastic modulus *E'*, and Poisson's ratio ν'. The following yield criterion was adopted to define the onset of yielding which can be written adopting the notation of Desai & Siriwardane (1984):

$$f \equiv \sqrt{J_{2D}} - \frac{2sin\phi\prime}{\sqrt{3}(3-sin\phi\prime)}\left(J_1 + \frac{3c'}{tan\phi\prime}\right) = 0 \qquad [7]$$

where:

J_1 is the first invariant of the stress tensor defined by $J_1 = \sigma_{ii}$;

J_{2D} is the second invariant of the deviatoric stress tensor defined by $J_{2D} = \frac{1}{2}\hat{\sigma}_{ij}\hat{\sigma}_{ij}$ with

$\hat{\sigma}_{ij} = \sigma_{ij} - \frac{J_1}{3}\delta_{ij}$ the deviatoric stress tensor;

ϕ' is the effective internal friction angle;

c' is the effective internal cohesion.

A non-associated plastic flow rule, taking into account the dilation angle, is assumed and the plastic flow induces hardening of the yield surface. This is introduced via a hyperbolic variation of the friction angle, ϕ', as a function of the Von Mises equivalent plastic strain ε_{eq}^{p} as it is defined in Barnichon (1998).

4.4.3.2 Simulation of experimental laboratory tests

Within the framework of the EC project TIMODAZ, a backanalysis of several triaxial tests were performed (Dizier 2011, TIMODAZ 2010) to determine a set of mechanical parameters. Figure 4-98 presents the results of the comparison between the observations and the simulations. This modelling work was performed step by step. A first set of parameters defined by Bernier et al. (2007a) was chosen as a reference set. Then, they were modified in different simulations to better fit the experimental results. Four cases of friction hardening angle or of the cohesion softening were tested. Modelling results put in evidence that deviatoric behaviour is well represented when considering hardening or softening, but the volumetric behaviour is more difficult to capture as seen in Figure 4-98.

Table 4-24 presents the different parameters set used to model the triaxial tests during the TIMODAZ project. The main conclusion of these modelling is that a classical elasto-plastic model may be used to simulate qualitatively the deviatoric behaviour of the clay under drained and undrained conditions. The smooth transition between the elastic and plastic part may be captured thanks to well adapted hardening parameter values. In that way, the elastic domain is reduced and the plastic strains are generated earlier.

Table 4-38. Parameters used to model the triaxial tests from TIMODAZ (Dizier, 2011, TIMODAZ, 2010). βc and βϕ are the hardening parameters controlling the cohesion softening and the friction angle hardening

	E' (MPa)	ν'	c' ($c_i' = c_f'$) (kPa)	ϕ_i' (°)	ϕ_f' (°)	β_ϕ	ψ' (°)
Bernier et al. 2007a	300	0.125	300	5	18	0.01	0
UJF	800	0.125	300	8	18	0.003	10
ENPC	300	0.125	300	7	18	0.02	0
GEO³	300	0.125	300	8	18	0.001	5

A Drucker-Prager model, taking into account the anisotropic nature of Boom Clay, was used to model a hollow cylinder test performed at EPFL that was performed during the TIMODAZ project (François et al. 2014). The anisotropy of the clay was considered by using a transverse elasticity and by an effective cohesion varying according to the angle between the stratification plane and the direction of the principal stress. This approach was implemented within the LAGAMINE finite element software (Collin 2003). Figure 4-99 presents the results of the 2D plane strain modelling. It is observed that by taking into account the anisotropic parameters, a general good agreement can be observed between the observations and the numerical results in the three directions which confirms the importance of the cross-anisotropy properties of the Boom Clay.

Table 4-39 presents the parameters used by François et al. (2014) for the cross-anisotropic Drucker-Prager model where a cross-anisotropic elastic model is used with an anisotropic plastic behaviour where the cohesion varies with the angle between the stratification and the direction of the principal stresses.

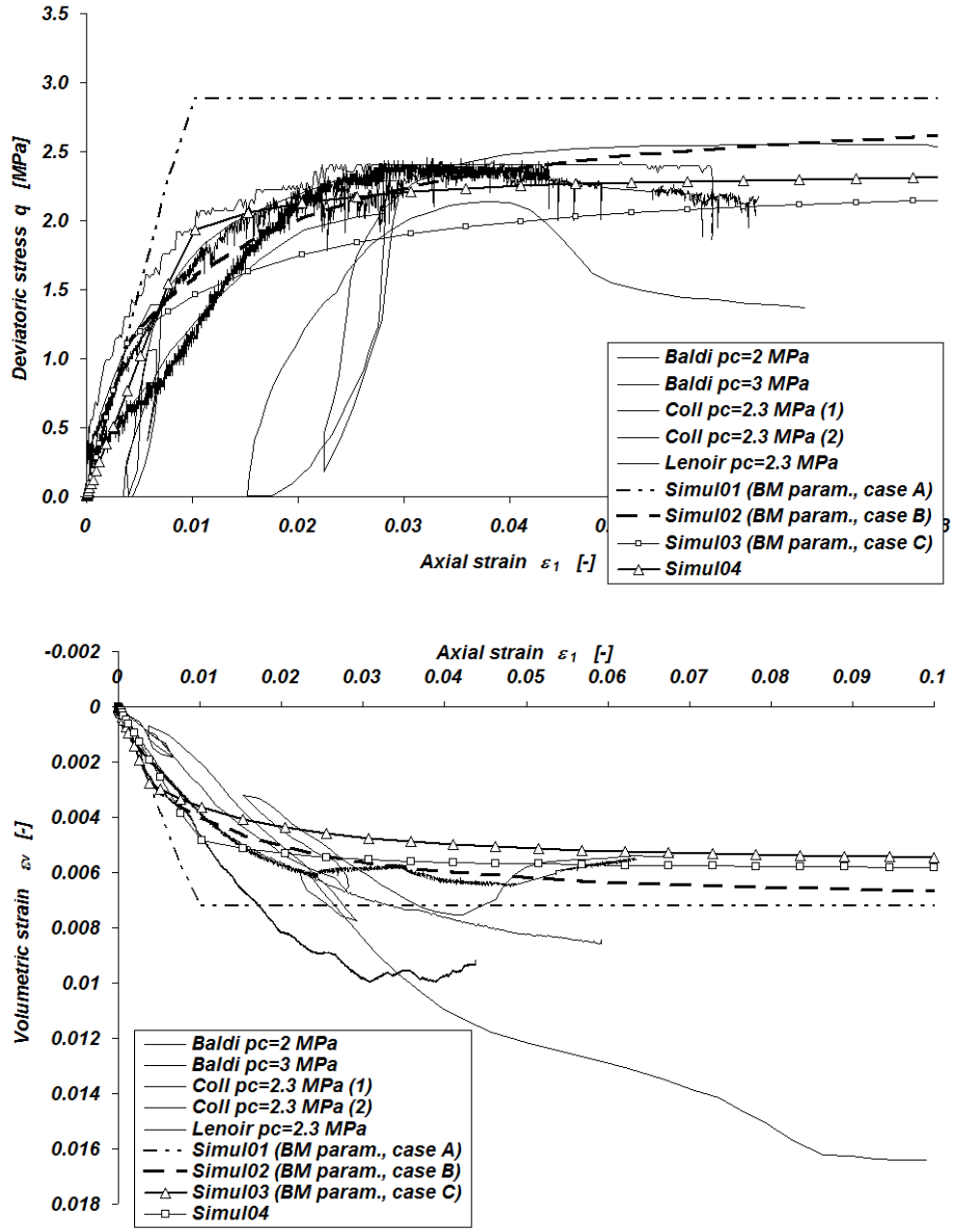

Figure 4-98. Summary of modelling work done in the framework of the TIMODAZ European project with the test performed by Baldi et al. (1991), Coll (2005) and Lenoir (TIMODAZ 2010)

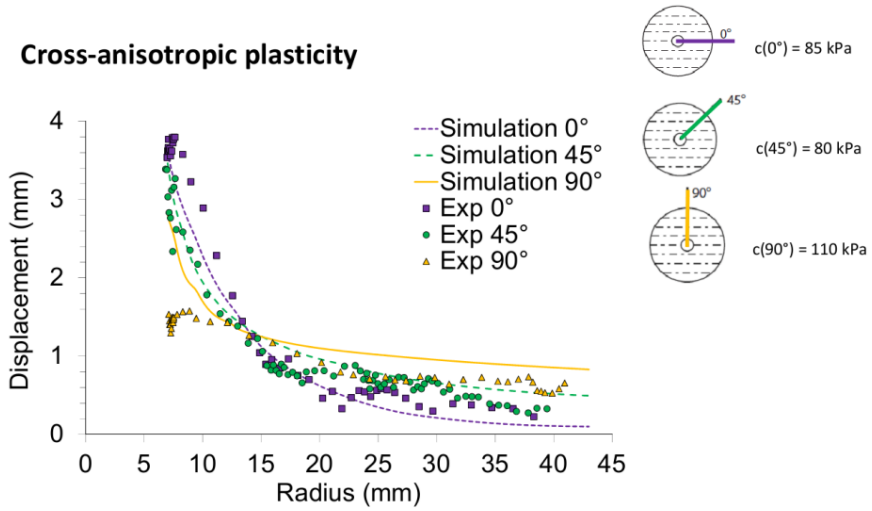

Figure 4-99. Modelling of the Boom Clay hollow cylinder test (François et al. 2014)

Table 4-39 : Parameters for the Drucker-Prager model with cross-anisotropic plasticity

Effective Young elastic modulus parallel to bedding (MPa)	$E_{//}$	400
Effective Young elastic modulus perpendicular to bedding (MPa)	$E_{\perp}$	200
Effective Poisson ratio (-)	$\nu'_{////}$	0.125
Effective Poisson ratio (-)	$\nu'_{//\perp}$	0.125
Shear modulus (MPa)	$G_{//\perp}$	178
Initial effective cohesion (kPa)	c'_0	255 (0°) 240 (45°) 330 (90°)
Final effective cohesion (kPa)	c'_f	85 (0°) 80 (45°) 110 (90°)
Softening parameter (-)	β_c	0.01
Initial effective friction angle (°)	ϕ'_{c0}	5
Final effective friction angle (°)	ϕ'_{cf}	18
Hardening parameter (-)	β_p	0.01
Effective dilation angle (°)	Ψ'	0

4.4.3.3 Thermo-hydro-mechanical modelling of laboratory experiments

As presented in the previous section, the increase of temperature induced thermo-plastic deformations. Many models have been developed to simulate these phenomena such as in François (2008), Sultan (1997), Cui et al. (2000) or Dizier (2011). Dizier (2011) developed a thermo-mechanical model consisting in an extension of the cap model to the thermo-plasticity. The model combines different plastic mechanisms, i.e. modified Cam-clay, friction angle criterion and a traction criterion. In addition to these three yield surfaces, a thermo-plastic mechanism is added based on the work realised by CERMES (Sultan 1997, Cui et al. 2000). The thermo-plastic model is based on the model developed by Hueckel & Borsetto (1990) in which two plastic mechanisms were added to represent the thermo-mechanical behaviour of soils. These mechanisms make possible to reproduce the volume change

induced by temperature and the decrease of the preconsolidation pressure with the increase of temperature. Figure 4-100 represents these mechanisms in the (*p', T*) plane. The thermal yield limit (TY) reproduces the generation of volumetric thermal strain depending on the stress state or OCR of the clay. This curve is close to the *p'* axis because the soil is assumed to be initially virgin of any temperature effects. The loading yield limit (LY) represents the decrease of the preconsolidation pressure with temperature. A more complete description can be found in Dizier (2011).

Concerning the THM parameters, the tests of Baldi et al. (1991) were modelled. Dizier (2011) performed the modelling of the laboratory experiment considering the model presented above. The comparisons between modelled and observed results are in a good agreement as it can be shown in Figure 4-101. François (2008) studied the thermo-plasticity of fine soils, such as the Boom Clay, and arrived to the same agreement using AGMEG-T law.

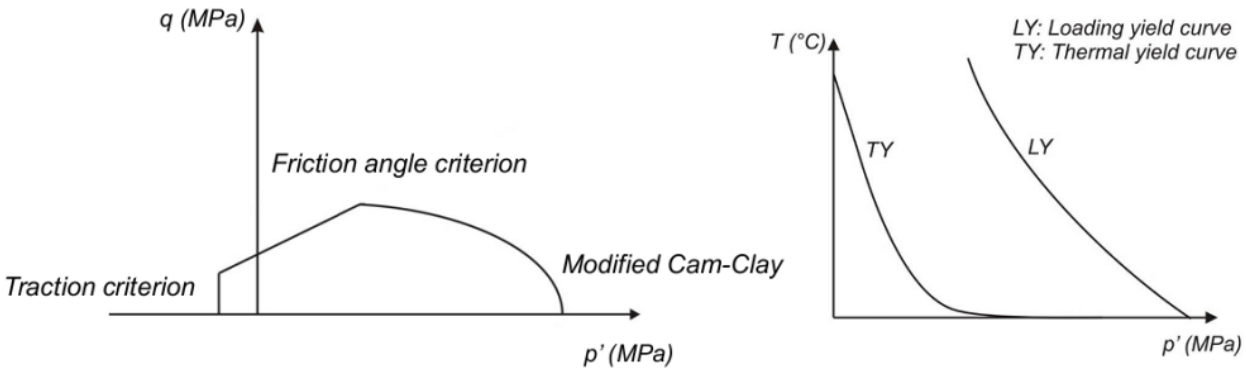

Figure 4-100. Thermal yield limit (TY) and loading yield limit (LY) in the *(p', T)* plane

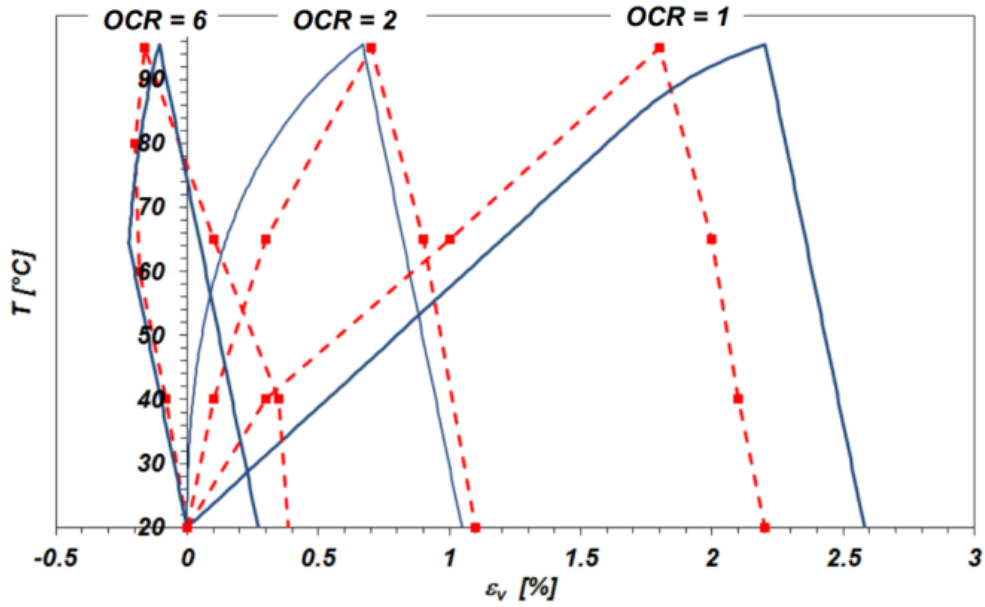

Figure 4-101. Thermo-mechanical tests. Comparisons between the numerical (continuous lines) and the experimental (dashed lines) results (Dizier 2011)

4.4.3.4 In-situ large scale PRACLAY Heater test modelling

This section presents the modelling of the large scale PRACLAY Heater test which was modelled considering a Drucker-Prager model with a cross-anisotropic elasticity (Dizier et al. 2016, 2017). In this model, the temperature induces thermal elastic strains only and the thermo-plasticity was not considered. As the geometry of the heater test is complex, the finite element model was simplified to correspond to a cross-section perpendicular to the PRACLAY gallery axis (Figure 4-102). This geometry includes the backfill sand of the PRACLAY gallery and the concrete lining. This model could consider the anisotropic behaviour of the Boom Clay and is most representative of a cross-section at the middle of the heated part of the PRACLAY gallery. The dissipation of heat and pore water pressure along the gallery axis cannot be represented with this configuration. A 2D axisymmetric model was also used to model the PRACLAY heater test, this model is not presented in this synthesis to simplify it but for more information, the reader can consult Dizier et al. (2017). The description of the simulation will focus only on Boom Clay properties and the results will concern the parameters driving the experiment i.e. the pore water pressure inside the backfill part of the gallery and the temperature at the extrados of the concrete lining.

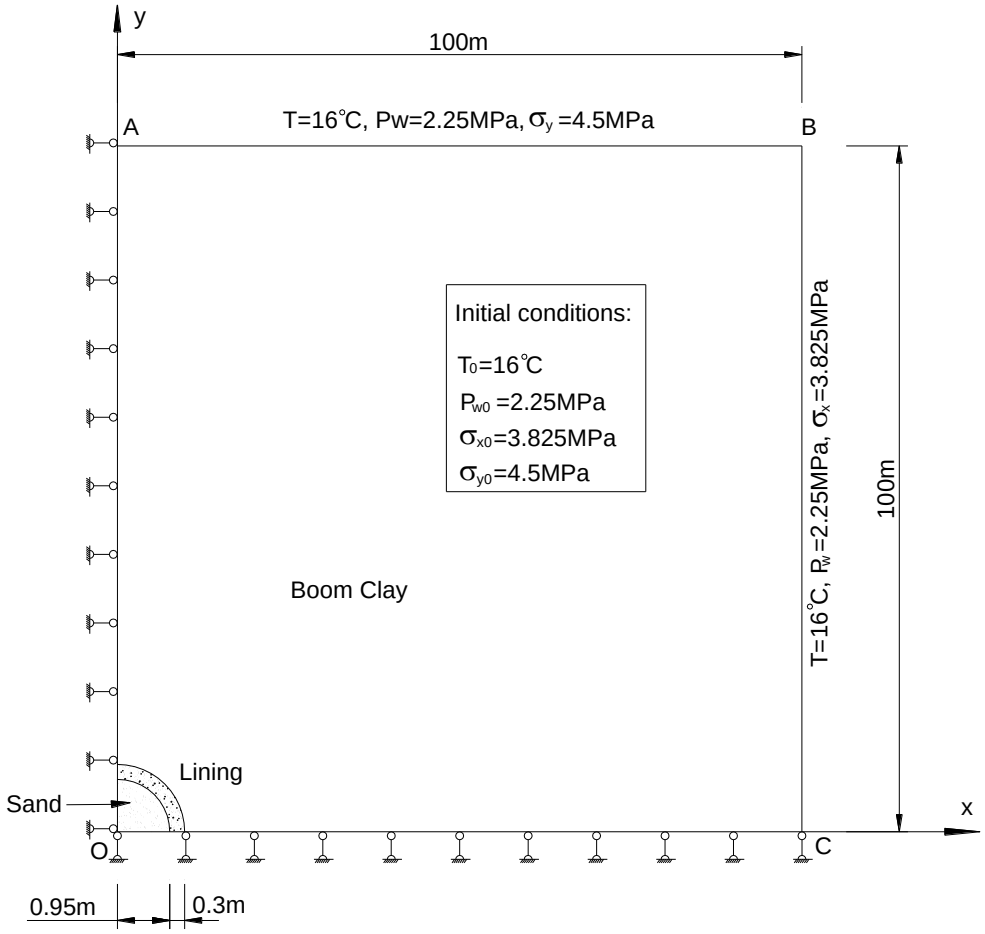

Figure 4-102. Description of the geometry of the 2D Plane Strain model (2D-PS) with the different components (sand, lining, Boom Clay). The boundary and initial conditions are described.

The initial conditions of the modelling depend on the geometry and are described in the following Tables. Distinct vertical and horizontal total stresses are imposed for this model and a coefficient of earth pressure at rest (K_0) of 0.7 is used in that case.

Table 4-40: Initial conditions for the Boom Clay for both models (based on Bernier et al. 2002, 2007a; Dehandschutter et al. 2004, Cornet 2009).

		2D Axisymmetric	2D Plane Strain
Pore water pressure (MPa)	P_w	2.25	2.25
Total stress (MPa)	σ	4.5	
Vertical total stress (MPa)	σ_v		4.5
Horizontal total stress (MPa)	σ_h		3.825
Temperature (°C)	T	16	16

Table 4-41: Initial conditions for the concrete lining, backfill sand and bentonite (MX80)

		Concrete lining	Backfill sand	Bentonite (MX80)
Pore water pressure (MPa)	P_w	0.1	0.1	-67[a]
Total stress (MPa)	σ	0.1	0.1	0.1
Temperature (°C)	T	16	16	16

[a] Based on measurements performed by CEA and EURIDICE

The main thermo-hydro-mechanical parameters of the materials (Boom Clay, sand, concrete lining and bentonite) are determined based on an extensive literature review, laboratory test results and in-situ measurements. The effective stresses are defined according to the Terzaghi's principle. The heat transfer is modelled using Fourier's law of conduction. The flow of water is reproduced using the classic Darcy's law. The thermo-hydraulic properties are defined in the tables below for the different materials, Table 4-42 for the Boom Clay.

Table 4-42. Main thermo-hydraulic properties of the Boom Clay (based on Bernier et al. 2007a, Bastiaens et al. 2006, Chen et al. 2011, Garitte et al. 2014, Horseman et al. 1987, Chen et al. 2014, Chen 2012)

Porosity (-)	n	0.39
Intrinsic permeability (m^2)	k_i	
Vertical intrinsic permeability (m^2)	k_{iv}	$3 \cdot 10^{-19}$
Horizontal intrinsic permeability (m^2)	k_{ih}	$6 \cdot 10^{-19}$
Thermal conductivity (W/mK)	λ	
Vertical thermal conductivity (W/mK)	λ_v	1.31
Horizontal thermal conductivity (W/mK)	λ_h	1.65

An elasto-plastic model using a Drucker-Prager criterion with a hardening behaviour of the effective friction angle is used for the Boom Clay. Because the excavation of the PRACLAY gallery caused the creation of an excavation damaged zone with a certain extension, the hydro-mechanical properties were modified during the modelling of the excavation (not described in this report), in order to take into account the damage caused by the excavation and the recovery of the transport properties with time (self-sealing, Bernier et al. 2007a). As a consequence, an increase of the permeability induced by the excavation was introduced in the model. The duration between the excavation and the start of heating was assumed to be sufficient (around seven years) to return to the undisturbed values of the permeability, as used for the modelling of the heating phase. The mechanical properties decreased in

this excavation-damaged zone due to the excavation and remained the same for the heating phase as their potential restoration requires a longer time (self-healing). The mechanical properties are given in the following table (Table 4-43).

Table 4-43. Mechanical properties of the Boom Clay (based on Bernier et al. 2007a, Chen 2012, Dizier 2011, Chen et al. 2011)

		Intact Boom Clay (undamaged zone)	**Damaged zone (<9.55 m from the extrados)**
Isotropic elastic modulus (GPa)	E'	1.05	0.3
Poisson's ratio (-)	ν'	0.125	
Vertical elastic modulus (GPa)	E'_v	0.7	0.2
Horizontal elastic modulus (GPa)	E'_h	1.4	0.4
Shear modulus (GPa)	G_v	0.28	0.08
Poisson's ratio (-)	ν'_{hh}	0.25	
Poisson's ratio (-)	ν'_{vh}	0.125	
Effective cohesion (MPa)	c'	0.3	
Initial effective friction angle (°)	$\phi'_{initial}$	5	
Final effective friction angle (°)	ϕ'_{final}	18	
Dilatancy angle (°)	ψ'	0	

In this section, only the parameters driving the experiment are compared with the numerical results. Figure 4-103 gives a comparison between the measurements and the 2D axisymmetric numerical predictions of the temperature evolution at the intrados (inner surface of the lining) and at the extrados (outer surface of the lining) of the three segments (S4, S6 and S8) located at the middle ring in the heated section until August 2017. The modelling results are in a good agreement with the observations.

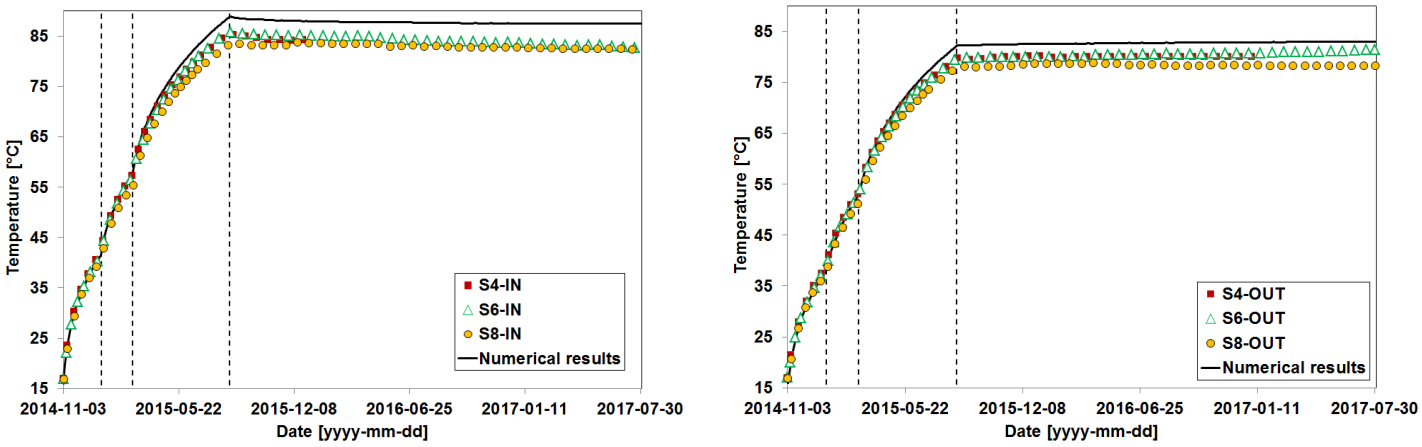

Figure 4-103. Temperature inside the concrete segments of Ring 50 since start-up of heating. Comparison with the 2D Axis model (black curve) at the intrados (left) and at the extrados (right)

The pore water pressure inside the PRACLAY gallery is an important hydraulic boundary for the PRACLAY Heater test, and the degree of agreement between its measured and predicted values may directly affect the prediction of thermo-hydro-mechanical responses in the surrounding clay. Figure 4-104 shows a comparison between the measurements and the predictions of the pore water pressure inside the PRACLAY gallery, for both models (2D-PS and 2D Axis). The overall agreement is very good for the 2D axisymmetric model, while the 2D-PS model overestimates the pore water pressure evolution. This can be explained by the fact that the 2D-PS model represents a vertical cross-section of the gallery where no axial drainage and no axial heat dissipation can be represented. As a consequence, higher pore water pressures are predicted compared with the 2D axis model.

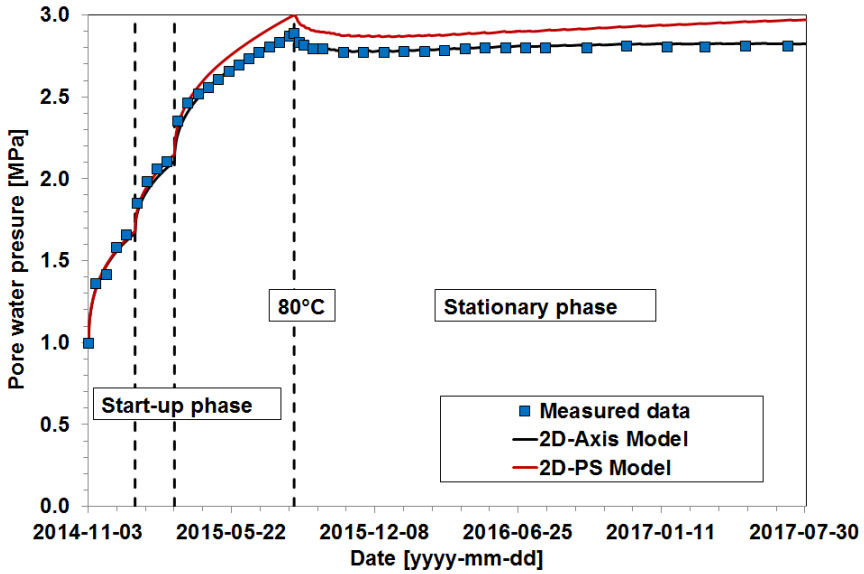

Figure 4-104. Comparison between the measurements and predictions of the pore water pressure inside the PG for both models (2D-Axis and 2D-PS)

4.4.3.5 Conclusion

This section has presented most of the simulations that were recently done on the THM behaviour of the Boom Clay. The Drucker-Prager model is mostly used to model both the hydro-mechanical and the THM behaviour of the Boom Clay from triaxial tests to large scale in-situ tests.

Considering cross-anisotropic models with anisotropic properties of the clay helps to have a better understanding of the Boom Clay behaviour. The first integration of this elasto-plastic anisotropy was done during the TIMODAZ project (Charlier et al. 2010). Even if the simple approach proposed at that time already provided very promising results, anisotropic models for Boom Clay still need further investigations to completely describe its elasto-plastic response.

In the modelling of the PRACLAY Heater test, the influence of the EDZ is limited to an abrupt variation of parameters with time. This description of the EDZ requires further investigations to improve the modelling of hydro-mechanical disturbances induced by the excavation.

So far, the thermo-plastic behaviour has not been taken into account in the modelling of the PRACLAY Heater test. Blind predictions of Dizier (2011) showed that at this scale the effect of thermo-plasticity should be very limited in comparison with thermo-elastic models. The temperature around PRACLAY heater tests should induce only reversible deformations. This conclusion needs to be reconsidered with the current knowledge of the PRACLAY Heater test which started in 2014.

In all the modelling presented above, the viscous characteristics were not taken into account while it is known that Boom Clay exhibits a visco-elasto-plastic behaviour. This effect needs to be integrated in the constitutive models to simulate the long-term behaviour of the Boom Clay.

4.4.4 NAGRA

4.4.4.1 HE-D Experiment

The HE-D experiment was a heater test aimed at characterising the THM behaviour of OPA in response to heating (Bossart et al. 2017). The HE-D experiment was intensively modelled (e.g. Gens et al. 2007, Garitte et al. 2017b). These modelling exercises are valuable to the modelling of the FE experiment because they allowed to classify the intensity of cross-coupling between the different THM processes in OPA in a hierarchical manner:

- The strongest coupling was found from thermal to hydraulic and mechanical behaviour. Pore water pressure generation is primarily controlled by the temperature increase and the largest contributor to strains and displacements is thermal expansion.
- Significant but more moderate effects were identified from the coupling of hydraulic to mechanical behaviour. The dissipation of pore pressures induces additional displacements and strains. However, these are smaller than thermally-induced deformations due to the large clay stiffness.
- In principle, mechanical damage could impact the hydraulic results due to the development of higher permeability caused by material damage. The size of the damaged zone, however, appeared to be very limited and its impact not very significant.
- There was no noticeable coupling from hydraulic to thermal behaviour. Practically all heat transport is by conduction and the thermal conductivity of the material does not change, as the material remains saturated throughout the heating sequence.
- The coupling from mechanical to thermal behaviour is negligible. The porosity variations in the clay host rock are so subtle that they do not affect thermal conductivity. In addition, mechanical energy dissipation is insignificant in the non-isothermal case of the HE-D experiment.

4.4.4.2 HE-E Experiment

The set-up and measurements of the HE-E experiment are described in detail in Gaus et al. (2014a and b) and above in section 3.2.3.2. The HE-E Experiment focuses on the early non-isothermal re-saturation period and its impact on the THM behaviour of the EBS. In the context of DECOVALEX-2015, seven THM codes were used to simulate the response of OPA and the EBS to thermal loading at 1:2.5 scale. Main results of the modelling exercise were (Garitte et al. 2017a):

- The initial conditions (especially hydraulic and mechanic) had a large impact on model outputs.
- The temperature at the heater surface was well reproduced by applying the power input as boundary condition. This indicates that the thermal conductivities of both buffer and host rock (as implemented in the models) were correct.
- The temperature evolution in the buffer and the general trends of the evolution of relative humidity were relatively well reproduced, except in the middle of the buffer. This issue could not be addressed by any of the different sensitivity analyses carried out to explore the different THM processes.
- The different relationships between relative permeability and water saturation, or the retention curves, implemented in different THM codes, led to a wide range of buffer re-saturation times.

4.4.4.3 The FE Experiment

In the context of the FE experiment, several modelling exercises have been carried out (e.g. Ewing & Senger 2011, Senger 2015, Garitte et al. 2014, 2018, NAGRA 2018). A set of scoping calculations aimed

at bracketing the main parameters and independent variables associated with the FE experiment (e.g. temperature at the different components, pore water pressure and strain in OPA, etc.) was carried out by Ewing & Senger (2011). Such exercise supported the design of the FE experiment and its monitoring system. Second, a calibration and validation exercise, which included uncertainty analysis, was carried out by different modelling teams (Alcolea et al 2019).

The experience and data from previous experiments, especially HE-E, were used to develop scoping estimates of key parameters and variables of the FE experiment, including 1) the evolution of temperature on the heater surface, in the bentonite and in the Opalinus Clay, 2) the degree of saturation and relative humidity in the bentonite and Opalinus Clay, 3) the pore water pressure in the Opalinus Clay, and 4) the strain in the Opalinus Clay. The scoping calculations were carried out using the THM code Code_Bright (Olivella et al. 1994, 1996) and are reported in Garitte et al. (2018). Key conclusions of the scoping calculations were:

- Peak temperatures at the heater surface vary between ~100°C and ~195°C, depending on the buffer properties.
- The maximum simulated temperature at the interface between buffer and rock in the direction of the bedding planes was 85°C, independently of buffer properties.
- The desaturation of the Opalinus Clay was limited.
- The combined effect of the pore water flux from the bentonite and the differential thermal expansion of the solid and liquid phases would lead to a maximum pore water pressure increase of ~3 MPa at a distance between 7 and 15 m from the tunnel axis.

Complementary scoping calculations of the TH evolution of the FE experimental site are presented in Ewing & Senger (2011) and Senger (2015). Key conclusions of the TH-scoping calculations were:

- Peak temperatures at the heater surface vary between ~130°C and ~140°C, depending on the buffer properties (sensitivity runs RC0 – RC2).
- The maximum simulated temperature at the interface between buffer and rock was 60-70°C, depending on the buffer properties.
- The combined effect of the pore water flux from the bentonite and the differential thermal expansion of the solid and liquid phases would lead to a maximum pore water pressure increase of ~1.8-2.2 MPa in the borehole interval FE-A2-I6. A significant impact of bedding anisotropy (thermal conductivity) on pore pressure evolution is expected.

4.4.4.4 Idealised behaviour of Opalinus in the FE Experiment

The description below of the THM behaviour of Opalinus Clay is related to the FE experiment at Mont Terri URL (NAGRA 2019). The THM physical phenomena driving the behaviour of the different experiment phases are fully coupled, and therefore complex. The main response to excavation and support installation (Figure 4-105) is mechanical and includes the development of the EDZ and convergence of the tunnel wall at an average rate approaching 1 mm per day. The rock is fully saturated, the tunnel has an ambient relative humidity of approximately 90%, the host rock has a temperature of approximately 18°C and the tunnel has a temperature of approximately 30°C.

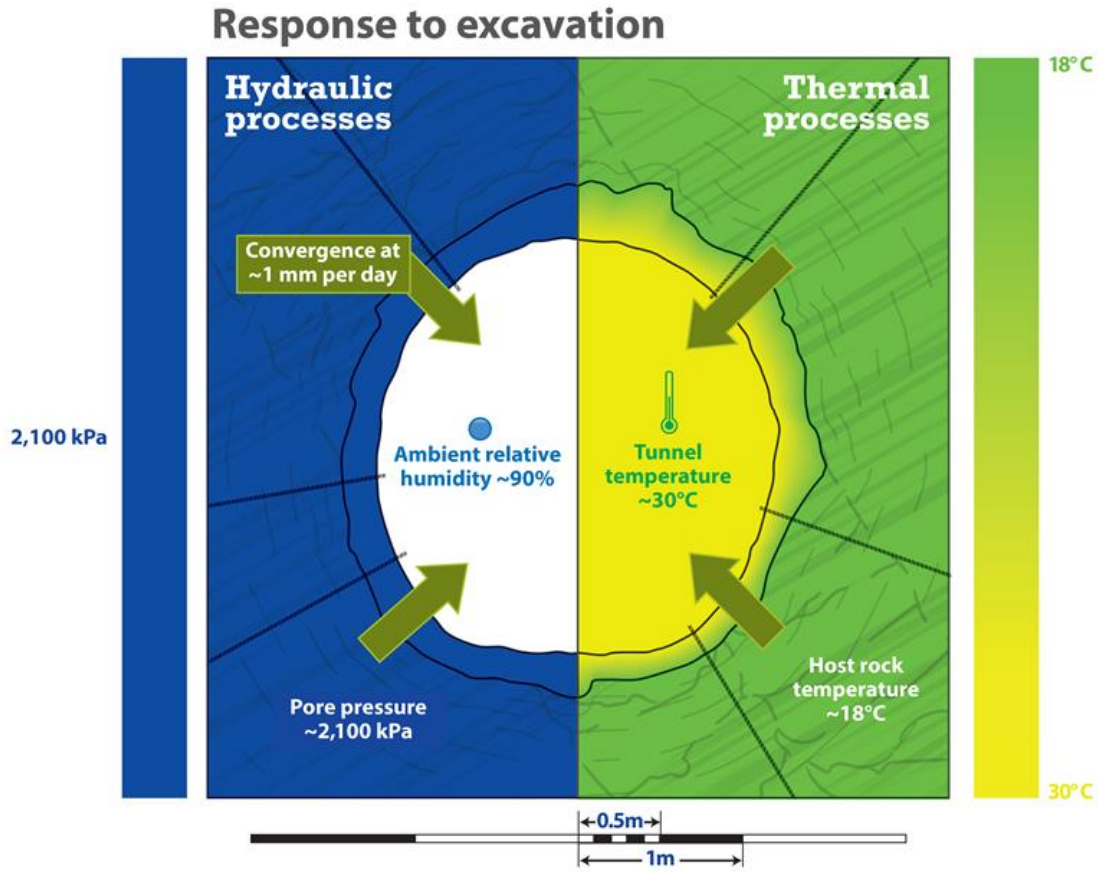

Figure 4-105. Illustration of the THM processes occurring in the FE Experiment following excavation and support installation (NAGRA, 2018). Hydraulic evolution (saturation in the rock and relative humidity in the tunnel and bentonite) is illustrated by the blue shading and mechanical evolution (displacement) by green arrows. The magnitude of processes is approximately scaled with darker colours and larger arrows indicating processes with greater magnitude

During the ventilation phase (Figure 4-106) there is on-going creep of the host rock inwards, translated into further tunnel convergence, but at significantly lower rates. The air in the tunnel is controlled by the ventilation system at approximately 60% relative humidity and 20°C. There is minor desaturation of the shotcrete and the host rock closest to the tunnel wall. The rock temperature remains unchanged.

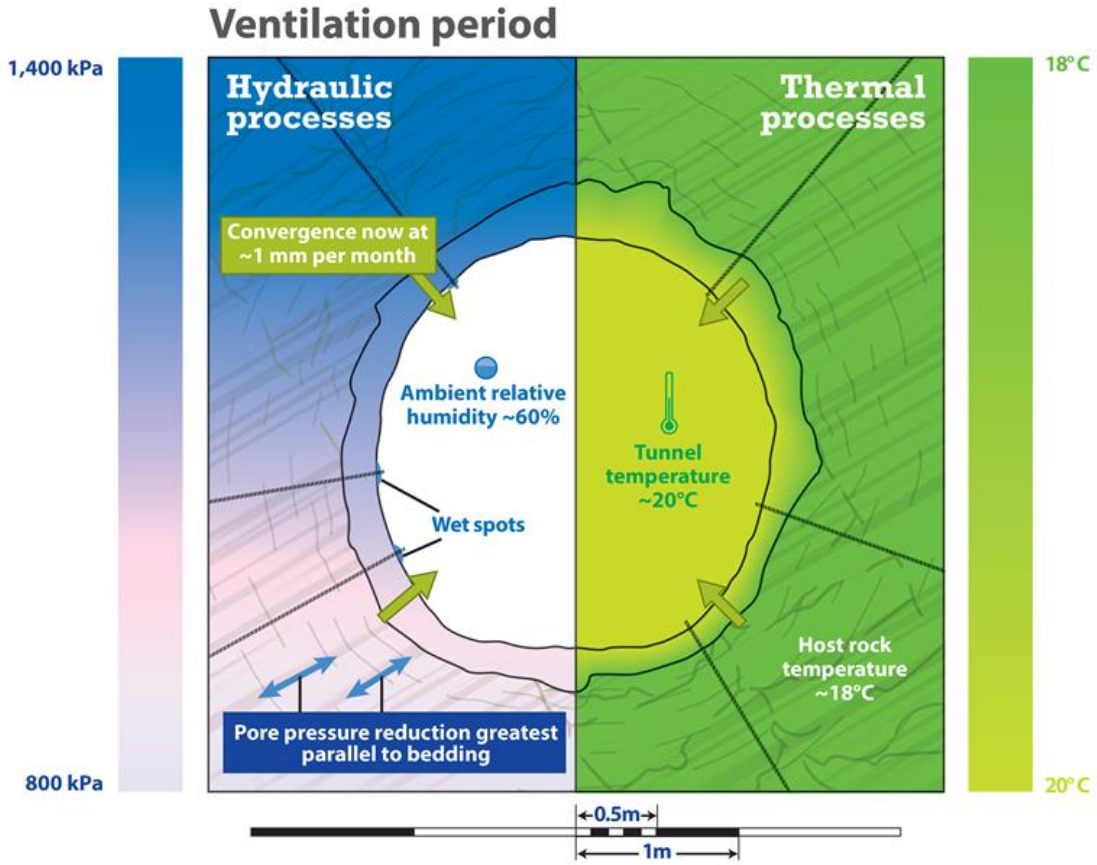

Figure 4-106. Illustration of the THM processes occurring in the FE Experiment during ventilation (NAGRA 2018). Hydraulic evolution (saturation in the rock and relative humidity in the tunnel and bentonite) is illustrated by the blue shading and mechanical evolution (displacement) by green arrows. The magnitude of processes is approximately scaled with darker colours and larger arrows indicating processes with greater magnitude

Following emplacement of the heaters and EBS, processes are mainly controlled by heat conduction and water movement away from the heaters. During the first few months (Figure 4-107, up), heater temperatures increase rapidly to values between 100 and 120°C. The bentonite is gradually heated, with higher temperatures observed in the GBM compared to the bentonite blocks forming the pedestals. However, temperatures in the GBM near the tunnel wall are lower than the corresponding temperatures in the bentonite blocks. The temperature increase in the GBM leads to a gradual reduction of relative humidity (and correspondingly to an increase of suction according to Kelvin's law). In this initial phase, vapour from water evaporation close to the heater surface migrates to the outer parts of the buffer where it condenses and locally increases the relative humidity. The relative humidity of the bentonite at any specific location first increases and then decreases as vapour moves away from the heaters. Relative humidity remains overall higher in the bentonite blocks, which were emplaced with a higher water content than the GBM. In response to heating, the bentonite block pedestal expands resulting in an uplift of the heater of 1-2 mm.

After more than one year of heating (Figure 4-107, down), the rock begins to heat up, with higher temperatures observed in the direction parallel to bedding compared to perpendicular to bedding. This results in an overall greater increase in the pore pressure in the rock parallel to bedding than perpendicular to bedding. However, this effect is offset by the greater hydraulic conductivity parallel to bedding which allows pressure dissipation through water movement into the tunnel. At the same time, the heaters begin to subside, owing to homogenisation of the buffer.

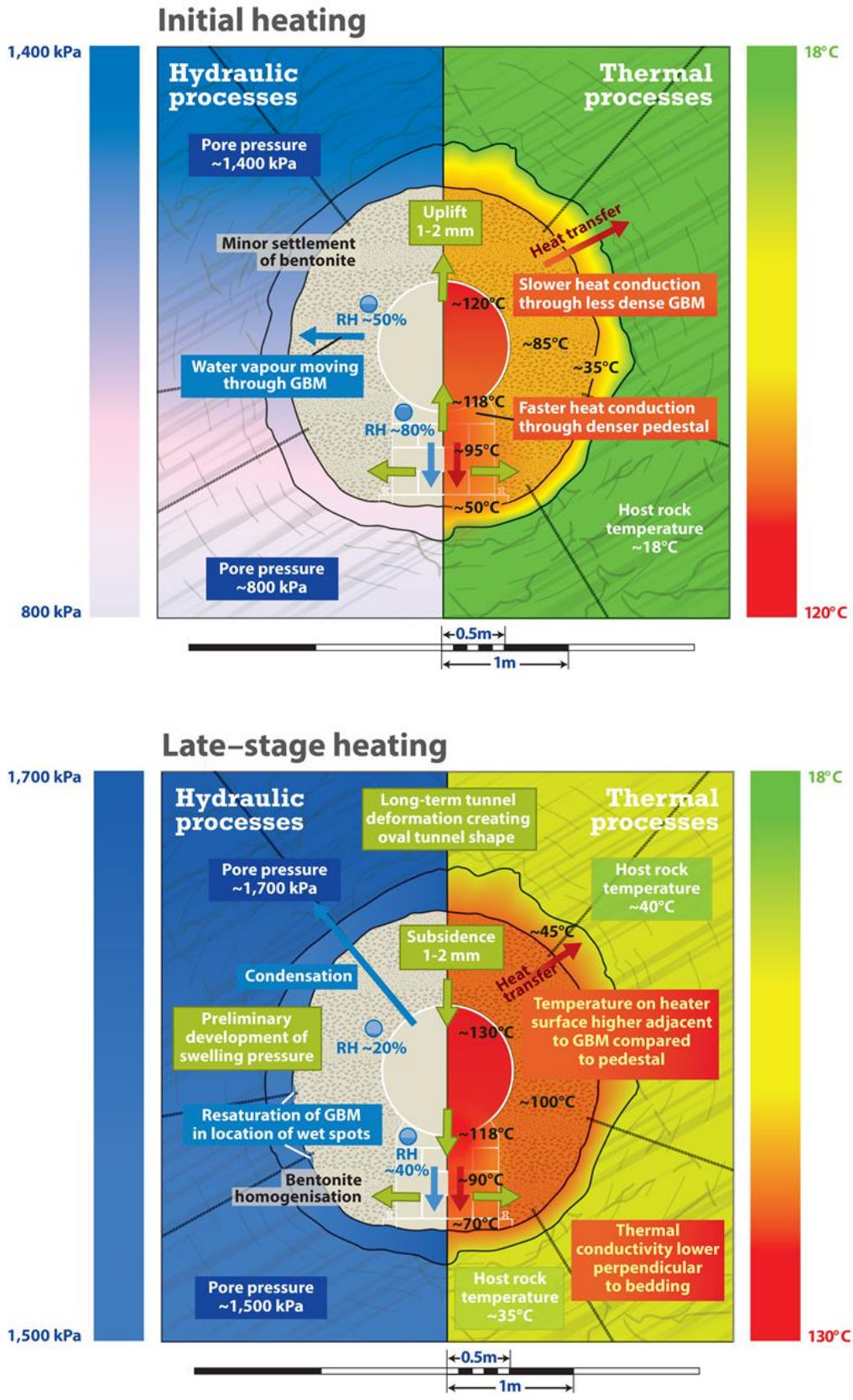

Figure 4-107. Illustration of the THM processes occurring in the FE Experiment during: up) the initial heating phase, i.e. approximately the first two months of heater operation; and down) during late-stage heating, i.e. up to 18 months after hater operation (NAGRA 2018)

4.5 Main conclusions from SotAs of previous related projects/reviews/relevant WMO documents

The TIMODAZ project analysed the evolution of the damaged zone (DZ) during the thermal transient in the context of a geological repository for heat-emitting waste in plastic and indurated clay host rocks. The project focused on the possible additional damage created by the thermal load. The knowledge gathered during the project (Yu et al. 2010) indicated that an increase in temperature due to the presence of heat-emitting wastes will induce strong and anisotropic THM coupled responses within the clay. The thermal expansion of pore water and the thermal-induced decrease of clay strength may pose a risk of additional mechanical damage. However, no evidence was found throughout the TIMODAZ experimental programme showing temperature-induced additional opening of fractures or a significant permeability increase of the DZ. Instead, the thermal-induced plasticity, swelling and creep of clay are likely beneficial to the sealing of fractures and recovery of the permeability of the DZ to the original state of the clay host rock. In the absence of plastic deformation, TIMODAZ demonstrated that elevated temperatures do not adversely affect the pore structure of the clay by showing that the intrinsic permeability remains constant or even decreases with the increase of temperature. Temporary increases of hydraulic conductivity of clay could be explained entirely by the decrease of water viscosity and are therefore reversible with temperature. In case where thermo-plasticity was observed, thermoconsolidation was most likely to occur resulting in a void ratio and intrinsic permeability decrease. Considering anisotropic properties of clay in the numerical simulations improved significantly the predictive capability of the numerical models. The anisotropy of thermal conductivity will have an impact on the temperature evolution near the disposal galleries, and should be taken into account in the final design of a geological repository.

The project also concluded that, with the current knowledge, the capacity of the repository host rock to perform its intended role as a barrier and to maintain the long-term safety functions of the system will be still preserved in spite of the combined effect of the inevitable EDZ and the thermal output from the waste (Yu et al. 2010). All the favourable properties of the clay host rock that guarantee the effectiveness of the safety functions of the repository system are expected to be maintained after the heating-cooling cycle. Those basic assumptions used in PA calculations still remain valid when considering the thermal impact on the evolution of DZ around a radioactive waste repository in clay host rock.

5 Conclusions (summary and knowledge gaps)

This report has first presented the main characteristics of the national concepts of the organizations involved in the project (ANDRA, BGE, ENRESA, EURIDICE, NAGRA, POSIVA, RWM, SKB and SÚRAO) and particularly of their thermal limits. An overview of what is known about the clay materials to be used in the project, both as buffer and as host rock, has been given, including the effect of temperature on the materials' behaviour. Large-scale tests relevant in terms of the temperatures involved have been identified and described, and they could be later used as benchmark exercises during the Project. The state of modelling approaches has been presented, mostly particularising their application to specific tests.

It has been shown that the effect of temperature on hydro-mechanical properties of bentonite has been systematically studied for temperatures of up to 100°C and is quite well established with respect to safety functions: temperature modifies some properties but they keep in values acceptable for complying with the safety functions. It is clear that temperature increases the hydraulic conductivity, although this increase cannot be explained in most cases solely by the increase in water kinematic viscosity, and other reasons, such as microstructural or pore fluid chemistry changes, have been

invoked. In contrast, the effect on swelling capacity seems to depend on the predominant exchangeable cations. Less work has been done on the effect of temperature on the water retention curve and thermal conductivity. Likewise, most laboratory studies have focused on compacted bentonite, therefore it cannot be stated if the effect of temperature on some properties is affected by the initial fabric (compacted powder, grains, pellets) or not.

Although the effect of temperatures higher than 100°C has been considerably studied concerning mineralogical transformations (unfortunately not always in clearly representative conditions), less is known with respect to HM properties for this range of temperatures, mainly because of the testing experimental issues.

Concerning the modelling of the buffer behaviour, it is considered that the THM formulations developed and validated for temperatures below 100°C can be extended without modifications to temperatures above that value.

For the clay host rock previous knowledge indicate that an increase in temperature due to the presence of heat-emitting wastes will induce strong and anisotropic THM coupled responses within the clay. Thermal expansion of pore water and thermal-induced decrease of clay strength are to be considered as a potential risk. In contrast, thermal-induced plasticity, swelling and creep of clay are likely beneficial to the sealing of fractures. Considering anisotropic properties of clay in the numerical simulations improves significantly the predictive capability of the numerical models. Current knowledge indicates that the capacity of the repository host rock to perform its intended role as a barrier and to maintain the long-term safety functions of the system will be still preserved in spite of the combined effect of the inevitable EDZ and the thermal output from the waste.

This report will be updated at the end of the Project. It is expected to enlarge the chapters describing the clay materials, particularly the effect of temperature on their properties (sections 3.1, 3.3 and 4.1), and add a final chapter about the impact of the improved understanding on the safety functions and remaining open issues with a future perspective.

6 References

Aertsens, M., Wemaere, I., Wouters, L. 2004. Spatial variability of transport parameters in the Boom Clay. Applied Clay Science 26: 37-45.

Åkesson, M., Kristensson, O., Börgesson, L., Dueck, A., Hernelind, J. 2010. THM modelling of buffer, backfill and other system components – Critical processes and scenarios. SKB TR-10-11. Svensk Kärnbränslehantering AB.

Åkesson, M., Olsson, S., Dueck, A., Nilsson, U., Karnland, O., Kiviranta, L., Kumpulainen, S., Lindén, J. 2012. Temperature buffer test. Hydro-mechanical and chemical/mineralogical characterizations. SKB Report P-12-06. Svensk Kärnbränslehantering AB.

Alcolea, A., Marschall, P., FE Team. 2019. FE-Modelling Task Force / Task 1: Validation of thermally induced THM effects in the rock around the FE-tunnel. NAGRA Arbeitsbericht NAB 19-040.

Alonso, E.E., Vaunat, J., Gens, A. 1999. Modeling the mechanical behaviour of expansive clays. Eng. Geol. 54: 173–183.

Alonso, J., García-Siñeriz, J.L., Bárcena, I., Alonso, M.C., Fernández Luco, L., García, J.L., Fries, T., Pettersson, S., Bodén, A., Salo, J.-P. 2008. ESDRED. Deliverable 9 of Module 4, WP4. Module 4 (Temporary Sealing Technology). Final Technical Report. 84 pp.

Amec 2016. Project Ankhiale: Disposability and full life cycle implications of high-heat-generating UK Wastes. Thermal analysis of disposal concepts for high-heat-generating wastes. Amec Report to RWM 103726-0011-UA00-TLN-0001. Issue 2, February 2016.

Amec 2018a. Vaults for High-heat-generating Waste – Integrated Report for Radioactive Waste Management, January 2018.

Amec 2018b. Mined Borehole Matrices for High-heat-generating Waste – Integrated Report for Radioactive Waste Management, January 2018.

ANDRA 2005. Dossier 2005 Argile - Synthesis - Evaluation of the feasibility of a geological repository in an argillaceous formation. Meuse/Haute-Marne site. https://international.andra.fr/sites/international/files/2019-03/3-%20Dossier%202005%20Argile%20Synthesis%20-%20Evaluation%20of%20the%20feasibility%20of%20a%20geological%20repository%20in%20an%20argillaceous%20formation_0.pdf

ANDRA 2009. Référentiel de site Meuse/Haute-Marne – Dossier 2009. Tome 2 : Caractérisation comportementale du milieu géologique sous perturbation - N° Andra : C.RP.ADS.09.0007.

ANDRA 2016. Safety Options Report - Post-Closure Part. Andra Technical Report CG-TE-D-NTE-AMOA-SR2-0000-r5-0062. https://international.andra.fr/sites/international/files/2019-03/Safety%20Options%20Report%20-%20Operations_2.pdf

ANDRA 2018. Le socle des connaissances scientifiques et techniques de CIGÉO. Les référentiels de connaissances du site de Meuse/Haute-Marne. Tome 4. Le comportement THM des formations géologiques sur le site de Meuse/Haute-Marne. CG.RP.AMFS.1 7.0031.

Arcos, D., Grandia, F., Domènech, C. 2006. Geochemical evolution of the near field of a KBS-3 repository. SKB TR-06-16. Svensk Kärnbränslehantering AB.

Armand, G., Bumbieler, F., Conil N., de la Vaissière, R., Bosgiraud, J.M., Vu, M.-N. 2017. Main outcomes from in situ thermo-hydro-mechanical experiments programme to demonstrate feasibility of radioactive high-level waste disposal in the Callovo-Oxfordian claystone. Journal of Rock Mechanics and Geotechnical Engineering 9(3): 415-427.

Autio, J., Hassan, Md.M., Karttunen, P., Keto, P. 2013. Backfill design 2012. Report POSIVA 2012-14, Posiva Oy, ISBN 978-951-652-196-4.

Baldi, G., Borsetto, M., Hueckel, T. 1987. Calibration of mathematical models for simulation of thermal, seepage and mechanical behaviour of Boom Clay. Commission of the European Communities. Nuclear science and Technology EUR 10924.

Baldi, G., Hueckel, T., Peano, A., Pellegrini, R., 1991. Developments in modelling of thermo-hydro-mechanical behaviour of Boom Clay and clay-based buffer (vol.2). Commission of the European Communities. Nuclear science and Technology EUR 13365/2.

Baldi, G., Hueckel, T., Pellegrini, R. 1988. Thermal volume changes of the mineral-water system in low-porosity clay soils. Canadian Geotechnical Journal 25(4): 807-825.

Bamforth, P., Chisholm, D., Gibbs, J., Harrison, T. 2008. Properties of Concrete for Use in Eurocode 2.

Bárcena, I., García-Siñeriz, J.L., Huertas, F., 2006. FEBEX Project Final Report. Addendum sensors data report. In situ experiment. Publicación Técnica ENRESA 05-5/2006. Madrid, 157 pp.

Barnichon, J.D. 1998. Finite Element Modelling in Structural and Petroleum Geology. PhD thesis. University of Liege.

Bass, J.D. 1995. Elasticity of Minerals, Glasses, and Melts. In: Thomas J.A. (eds). Mineral Physics and Crystallography: A Handbook of Physical Constants, American Geophysical Union Online Reference Shelf 2: 45-63.

Bastiaens, W., Bernier, F., Li, X.L. 2006. An overview of long-term HM measurements around HADES URF. In: EUROCK 2006 Multiphysics coupling and long term behaviour in rock mechanics, 15–26.

Basu S., Jones A., Mahzari P., 2020. Best Practices for Shale Core Handling: Transportation, Sampling and Storage for Conduction of Analyses. Journal of Marine Science and Engineering 8(2): 136. https://doi.org/10.3390/jmse8020136

Baxter, S., Holton, D., Williams, S., Thompson, S. 2018. Predictions of the wetting of bentonite emplaced in a crystalline rock based on generic site characterization data. Geological Society Special Publications 482: 285-300, London.

Beauheim, R.L. 2013. Hydraulic conductivity and head distributions in the host rock formations of the proposed siting regions. NAGRA Arbeitsbericht NAB 13-013.

Belmokhtar, M., Delage, P., Ghabezloo, S., Conil, N. 2017. Thermal volume changes and creep in the Callovo-Oxfordian claystone. Rock Mechanics and Rock Engineering, Springer Verlag, 50(9): 2297-2309.

Bernier, F., Li, X.L., Bastiaens, W. 2007a. Twenty-five years' geotechnical observation and testing in the Tertiary Boom clay formation. Géotechnique 57(2): 229-237.

Bernier, F., Li, X.L., Bastiaens, W., Ortiz, L. 2007b. SELFRAC: Fractures and self-healing within the excavation disturbed zone in clays. Final report. Euridice report, December 2007.

Bésulle, P., Viggiani, G., Desrues, J., Coll, C., Charrier, P. 2014. A laboratory study of the hydromechanical behaviour of Boom Clay. Rocks mechanics and Rock engineering 47(1): 143-155.

BGE 2020a. Zwischenbericht Teilgebiete gemäß § 13 StandAG, Stand 28.09.2020, Bundesgesellschaft für Endlagerung mbH (BGE) Peine.

BGE 2020b. Endlagerkonzepte Überblick über grundsätzliche Rahmenbedingungen in der ersten Phase des Standortauswahlverfahrens, Stand 28.09.2020, Report Number SG02302/3-1/1-2020#1 – Objekt-ID: 826885 – Revision: 000, Bundesgesellschaft für Endlagerung mbH (BGE), Peine.

Birgersson, M., Karnland, O. 2009. Ion equilibrium between montmorillonite interlayer space and an external solution – Consequences for diffusional transport. Geochimica et Cosmochimica Acta 73: 1908–1923.

Börgesson, L., Hökmark, H., Karnland, O. 1988. Rheological properties of sodium smectite clay. SKB TR-88-30. Svensk Kärnbränslehantering AB, 65 pp.

Bossart, P., Thury, M. 2008. Mont Terri Rock Laboratory. Project, Programme 1996 to 2007 and Results. Rep. Swiss Geol. Surv. 3, swisstopo, 3084 Wabern, Switzerland.

Braun, P. 2019. Thermo-hydro-mechanical behaviour of the Callovo-Oxfordian claystone Effects of stress paths and temperature changes. PhD Thesis. Université Paris-Est.

Braun, P., Ghabezloo, S., Delage, P., Sulem, J., Conil, N. 2018. Determination of multiple thermo-hydro-mechanical rock properties in a single transient experiment: application to shales. Rock Mechanics & Rock Engineering.

Brooks, R., Corey, A. 1964. Hydraulic properties of porous media. Hydrology paper 3. Colorado State University.

Burland, J. 1990. On the compressibility and shear strength of natural clays. Rankine Lecture, Géotechnique 40(3): 329-378.

Buyens, M., Put, M. 1984. Heat transfer experiment in Boom Clay. 9th European Conference on Thermophysical properties. 17-21 September, Manchester, UK.

Červinka, R., Vašíček, R., a kolektiv 2018. Kompletní charakterizace bentonitu. BCV 2017, SÚRAO TZ 419/2019.

Charlier, R., Chalandar, S., Collin F., Dizier, A. 2010. Delivrable D13 – Annex 4. In situ heating test ATLAS in Mol. TIMODAZ project, F16W-CT-2007-036449.

Chen, G.J. 2012. Modeling of PRACLAY tests: improved HM parameters of Boom Clay based on in-situ measured PWP around PG, SAC 41 meeting. Internal presentation.

Chen, G.J., Sillen, X., Verstricht, J., Li, X.L. 2011. ATLAS III in situ heating test in boom clay: Field data, observation and interpretation. Computers and Geotechnics 38(5): 683-696.

Chen, G.J., Maes, T., Vandervoort, F., Sillen, X. 2014. Thermal Impact on Damaged Boom Clay and Opalinus Clay: Permeameter and Isostatic Tests with µCT Scanning. Rocks mechanics and Rock Engineering 47(1): 87-99.

Chen, W.Z., Gong, Z., Ma, Y.S., Yu, H.D., Li, X.L. 2017. Temperature effect on the drained creep behavior of Boom Clay. Clay Conference, Davos, 2017.

Coll, C., Collin, F., Radu, J.P., Illing, P., Schroeder, C.H., Charlier, R. 2008. The report of long term behaviour of Boom clay – influence of clay viscosity on the far field pore pressure distribution. EURIDICE 2006: 154.

Coll, C. 2005. Endommagement des roches argileuses et perméabilité induite au voisinage d'ouvrages souterrains. Thèse de doctorat. Université Joseph Fourier, Grenoble 1.

Collin, F. 2003. Couplages thermo-hydro-mécaniques dans les sols et les roches tendres partiellement saturés. Thèse de doctorat. Université de Liège, Faculté des Sciences Appliquées.

Conil, N. 2012b. Essai de chauffe à surface libre – Rapport d'installation – Centre de Meuse / Haute-Marne, rapport Andra D.RP.AMFS.11. 0064.

Conil, N., Tallandier, J. 2019. Good practice guide for the use of claystone samples in hydromechanical tests. Rapport Andra D.NT.AMFS.19.0025.

Conil, N., Armand, G., Garitte, B., Jobmann, M., Jellouli, M., Fillipi, M., De La Vaissière, R., Morel, J. 2012a. In-situ heating test in the Callovo Oxfordian clay: measurement and interpretation. In: Clays in natural and engineered barriers for radioactive waste confinement. Proceedings of the 5th international meeting, Montpellier, France.

Conil N., Talandier J., Djizanne H., de La Vaissière R., Righini-Waz C., Auvray C., Morlot C., Armand G. 2018. How rock samples can be representative of in situ condition: a case study of Callovo-Oxfordian claystones. Journal of Rock Mechanics and Geotechnical Engineering 10(4): 613-623. https://doi.org/10.1016/j.jrmge.2018.02.004

Cornet F.H., 2009. In situ stress measurement campaign at SCK•CEN Underground Laboratory. École et Observatoire des Sciences de la Terre, Université de Strasbourg, Internal report.

Courdouan Merz, A. 2008. Nature and reactivity of dissolved organic matter in clay formations evaluated for the storage of radioactive waste. PhD thesis. ETH Zürich. Diss. ETH 17723, 111 pp.

Croisé, J., Mayer, G., Marschall, P., Matray, J.M., Tanaka, T., Vogel, P. 2006. Gas threshold pressure test performed at the Mont Terri Rock Laboratory (Switzerland): Experimental data and data analysis. Oil & Gas Science and Technology 61(5): 631-645.

Cuadros, J., Linares, J. 1996. Experimental kinetic study of the smectite-to-illite transformation. Geochim. Cosmochim. Acta 60: 439-453.

Cui, Y.J., Le, T.T., Tang, A.M., Delage, P., Li, X.L. 2009. Investigation the time dependent behavior of Boom Clay under thermo-mechanical loading. Géotechnique 59(4): 319-329.

Cui, Y.J., Sultan, N., Delage, P. 2000. A thermomechanical model for saturated clays. Canadian Geotechnical Journal 37: 607-620.

Daniels, K.A., Harrington, J.F., Zihms, S.J., Wiseall, A.C. 2017a. Bentonite Permeability at Elevated Temperature. Geosciences 7(3): 1 – 24.

Daniels, K.A., Harrington, J.F., Zihms, S.J., Wiseall, A.C. 2017b. Bentonite permeability: the effect of elevated temperature. Abstract from Clay Conference, Davos, 2017.

Dao, L.Q. 2015. Etude du comportement anisotrope de l'Argile de Boom. PhD thesis, CERMES, Ecole Nationale des Ponts et Chaussées, Paris.

Davies, C.W., Davie, C.T., Edward, C.A., White, M.L. 2017. Physiochemical and Geotechnical Alterations to MX80 Bentonite at the Waste Canister Interface in an Engineered Barrier System. Geosciences 7(3): 69.

De Beer, A., Carpentier, R., Manfroy, P., Heremans, R. 1977. Preliminary studies of an underground facility for nuclear waste burial in a tertiary clay formation. Rockstore Conference 3: 771-780, Stockholm.

De Bruyn, D., Labat, S. 2002. The second phase of ATLAS: the continuation of a running THM test in the HADES underground research facility at Mol. Engineering Geology 64: 309–316. ISSN 0013-7952.

De Craen, M., Wang, L., Van Geet, M., Moors, H. 2004. Geochemistry of Boom Clay pore water at the Mol site. Scientific report, SCK•CEN-BLG-990.

Dehandschutter, B., Vandycke, S., Sintubin, M., Vandenberghe, N., Gaviglio, P., Sizun, J.P., Wouters, L. 2004. Microfabric of fractured Boom Clay at depth: a case study of brittle-ductile transitional clay behaviour. Applied Clay Science 26: 389-401.

Dehandschutter, B., Vandycke, S., Sintubin, M., Vandenberghe, N., Wouters, L. 2005. Brittle fractures and ductile shear bands inargillaceous sediments: inferences from Oligocene Boom Clay (Belgium). Journal of Structural Geology 27: 1095-1112.

Delage, P., Sultan, N., Cui, Y.J. 2000. On the thermal consolidation of Boom Clay. Canadian Geotechnical Journal 37: 343-354.

De La Vaissière, R., Armand, G., Talandier, J. 2015. Gas and water flow in an excavation-induced fracture network around an underground drift: a case study for a radioactive waste repository in clay rock. J. Hydrol. 521: 141–156.

Deng, Y.F., Cui, Y.J., Tang, A.M., Li, X.L., Sillen, X. 2012. An experimental study on the secondary deformation of Boom Clay. Applied Clay Science 59(60): 19-25.

Desai, C.S., Siriwaradane, H.J. 1984. Constitutive laws for engineering materials with emphasis on geological materials, Prentice-Hall.

Dizier, A., Chen, G.J., Li, X.L., Rypens, J. 2017. The PRACLAY Heater test after two years of the stationary phase. EUR_PH_17_043. Mol, Belgium.

Dizier, A., 2011. Caractérisation des effets de température dans la zone endommagée autour des tunnels de stockage de déchets nucléaires dans des roches argileuses. PhD thesis. Université de Liège.

Dizier, A. 2018. Thermal analysis of C-Waste geological disposal facility in clay formations. ESV Euridice - European Underground Research Infrastructure for Disposal of nuclear waste in Clay Environment (Internal report).

Dizier, A., Chen, G., Li, X.L., Levasseur, S. 2020. Thermo-hydro-mechanical modelling of a C-Waste geological geological disposal. ESV Euridice - European Underground Research Infrastructure for Disposal of nuclear waste in Clay Environment (Internal report).

Dizier, A., Chen, G.J., Li, X.L., Leysen, J., Verstricht, J., Troullinos, I., Rypens, J. 2016. The Start-up Phase of the PRACLAY Heater Test. EUR_PH_16_025. Mol, Belgium.

Djéran, I., Bazargan, B., Giraud, A., Rousset, G. 1994. Etude expérimentale du comportement thermo-hydro-mécanique de l'Argile de Boom. Rapport G3S (Internal report).

Drucker, D.C., Prager, W. 1952. Soil mechanics and plasticity analysis or limit design. Quarterly Applied Mathematics 10(2): 157-165.

Dueck, A. 2014. Laboratory studies on stress-strain behavior. PEBS Deliverable D2.2-12.

Dueck, A., Johannesson, L.E., Kristensson, O., Olsson, S. 2011. Report on hydro-mechanical and chemical-mineralogical analyses of the bentonite buffer in Canister Retrieval Test. SKB Technical Report TR-11-07. Svenska Kärnbränslehanterin AB.

Eberl, D., Whitney, G., Khoury, H. 1978. Hydrothermal reactivity of smectite. American Mineralogist 63: 401–409.

Eberl, D.D., Velde, B., McCormick, T.D. 1993. Synthesis of illite-smectite from smectite at earth surface temperatures and high pH. Clays and Clay Minerals 28: 49-60.

Eng, A., Nilsson, U., Svensson, D. 2007. Äspö Hard Rock Laboratory. Alternative buffer material installation report. SKB report IPR-07-15.

ENRESA 2006. FEBEX Full-scale Engineered Barriers Experiment. Updated Final Report 1994-2004. Publicación Técnica ENRESA 05-0/2006, Madrid, 590 pp.

Ewing, J., Senger R. 2012. Evolution of Temperature, Pressure and Saturation in the Bentonite Buffer: Scoping Calculations in Support of the Design of the Full-Scale Emplacement Experiment at the Mont Terri URL. Unpubl. NAGRA Interner Bericht NIB 10-040.

Ewy, R.T. 2015. Shale/Claystone Response to Air and Liquid Exposure, and Implications for Handling, Sampling and Testing. International Journal of Rock Mechanics and Mining Sciences 80: 388–401. https://doi.org/10.1016/j.ijrmms.2015.10.009

Fei, Y. 1995. Thermal expansion. In: Thomas J.A. (ed.) Mineral physics and crystallography: a handbook of physical constants. American Geophysical Union Online References Shelf 2: 29 – 44.

Fernández, A.M. 2004. Caracterización y modelización del agua intersticial en materiales arcillosos: Estudio de la bentonita de Cortijo de Archidona. PhD thesis. CIEMAT, Madrid, 505 pp.

Ferrari, A., Laloui, L. 2012. Advances in testing the hydro-mechanical behaviour of shales. In L. Laloui and A. Ferrari editors. Multiphysical Testing of Soils and Shales, Springer, 57-68.

Ferrari, A., Favero, V., Manca, D., Laloui, L. 2013. Geotechnical characterization of core samples from the geothermal well Schlattingen SLA-1. NAGRA Arbeitsbericht NAB, NAGRA, Wettingen, Schweiz, 12-50.

Franče, J. 1992. Bentonity ve východní části Doupovských hor. Sborník geologických věd 30: 43-90.

Francois, B., Laloui, L., 2009. ACMEG-T: Soil Thermoplasticity Model. Journal of Engineering Mechanics 135(9).

François, B. 2008. Thermo-plasticity of soils at various saturation state: application to nuclear waste disposal. PhD thesis. École Polytechnique Fédérale de Lausanne.

François, B., Labiouse, V., Dizier, A., Marinelli, F., Charlier, R. 2014. Hollow Cylinder Tests on Boom Clay: Modelling of Strain Localization in the Anisotropic Excavation Damaged Zone. Rock Mechanics and Rock Engineering 47(1): 71-86.

François, B., Laloui, L., Laurent, C. 2009. Thermo-hydro-mechanical simulation of ATLAS in situ large scale test in Boom Clay. Computers and Geotechnics 36: 626-640. ISSN 0266-352X.

Frederickx, L. 2019. An advanced mineralogical study of the clay mineral fractions in the Boom Clay. PhD thesis. KU Leuven.

Fritz, B., Kam, M., Tardy, Y. 1984. Geochemical simulation of the evolution of granitic rocks and clay minerals submitted to a temperature increase in the vicinity of a repository for spent nuclear fuel. KBS TR 84-10. Svensk Kärnbränslehantering AB.

Garitte, B., Vaunat, J. 2008. Thermo-Hydro-mechanical Design calculation for the TED experiment. Laboratoire de recherche souterrain de Meuse/Haute-Marne, Rapport n°D.RP.0UPC.080001.

Garitte, B., Gens, A., Vaunat, J., Armand, G. 2014. Thermal conductivity of argillaceous rocks: Determination methodology using in situ heating tests. Rock Mechanics and Rock Engineering 47(1): 111–129.

Gatabin, C., Billaud, P. 2005. Bentonite THM mock up experiments. Sensors data report. CEA, Report NT-DPC/SCCME 05-300-A.

Gaucher, E.C., Blanc, P., Bardot, F., Braibant, G., Buschaert, S., Crouzet, C., Gautier, A., Girard, J. P., Jacquot, E., Lassin, A., Negrel, G., Tournassat, C., Vinsot, A., Altmann S. 2006. Modelling the porewater chemistry of the Callovian-Oxfordian formation at a regional scale. Comptes Rendus Geoscience 338: 917-930.

Gaus, I. (Ed.) 2011. Long term Performance of Engineered Barrier Systems (PEBS): Mont Terri HE-E experiment: detailed design. NAGRA-Arbeitsbericht NAB 11-01. NAGRA, Wettingen, Switzerland.

Gaus, I., Garitte, B., Senger, R., Gens, A., Vasconcelos, R., Garcia-Sineriz, J.L., Trick, T., Wieczorek, K., Czaikowski, O., Schuster, K., Mayor, J.C., Velasco, M., Kuhlmann, U., Villar, M.V. 2014. The HE-E Experiment: Lay-out, Interpretation and THM Modelling Combining D2.2-11. Final Report on the HE-E Experiment and D3.2-2: Modelling and Interpretation of the HE-E Experiment of the PEBS Project. NAGRA Working Report NAB 14-53, Wettingen, Switzerland and EU PEBS Project report downloadable from http://www.pebs-eu.de/

Gautschi 2017. Safety-relevant hydrogeological properties of the claystone barrier of a Swiss radioactive waste repository: An evaluation using multiple lines of evidence. (Grundwasser – Zeitschrift der Fachsektion Hydrogeologie).

Gens, A. 2019. Task Force on Engineered Barrier System (EBS). Task 1 Laboratory tests. SKB Technical Report TR-14-24. Stockholm, 141 pp.

Gens, A., Alonso, E.E. 1992. A framework for the behaviour of unsaturated expansive clays. Can. Geotech. J. 29: 1013–1032.

Gens, A., Valleján, B., Zandarín, M.T., Sánchez, M. 2013. Homogenization in clay barriers and seals: Two case studies. Journal of Rock Mechanics and Geotechnical Engineering 5(3): 191-199.

Gens, A., Vaunat, J., Garitte, B., Wileveau, Y. 2007. In-situ behaviour of a stiff layered clay subject to thermal loading. Observations and interpretation. Géotechnique 57(2): 207-228.

Georgiadis, K., Potts, D.M., Zdravkovic, L. 2005. Three-dimensional constitutive model for partially and fully saturated soils. International Journal of Geomechanics 5(3): 244-255.

Ghabesloo, S., Sulem, J. 2007. Pressurisation thermique d'une roche saturée. 18ème Congrès Français de Mécanique. http://hdl.handle.net/2042/16547

Ghiadistri 2019. Constitutive modelling of compacted clays for applications in nuclear waste disposal. PhD Thesis. Imperial College London, April 2019.

Göbel, I., Alheid, H.J., Alonso, E., Ammon, C.H., Bossart, P., Bühler, C.H., Emmerich, K., Fernandez, A.M., García-Siñeriz, J.L., Graf, A., Jockwer, N., Kaufhold, St. Kech, M., Klubertanz, G., Lloret, A., Mayor, J.C., Meyer, T., Miehe, R., Muñoz, J.J., Naumann, M., Nussbaum, C.H., Pletsch, T., Plischke, I., Ploetze, M., Rey, M., Schnier, H., Schuster, K., Sprado, K., Trick, Th., Weber, H., Wieczorek, K., Zingg, A. 2007. Heater Experiment: Rock and bentonite thermohydro-mechanical (THM) processes in the near field of a thermal source for development of deep underground high level radioactive waste repositories. In: Bossart, P., Nussbaum, P. (eds.). Mont Terri Project - Heater experiment, engineered barrier emplacement and ventilation experiment. Reports of the Swiss Geological Survey 1, Swisstopo, Wabern, 7-114.

Gómez-Espina, R., Villar, M.V. 2010. Geochemical and mineralogical changes in compacted MX-80 bentonite submitted to heat and water gradients. Applied Clay Science 47: 400–408.

Gómez-Espina, R., Villar, M.V. 2015. Effects of heat and humidity gradients on MX-80 bentonite geochemistry and mineralogy. Applied Clay Science 109-110: 39–48.

Gómez-Espina, R., Villar, M.V. 2016. Time evolution of MX-80 bentonite geochemistry under thermo-hydraulic gradients. Clay Minerals 51: 145-160.

Guayacan Carrillo, L.M. 2016. Analysis of long-term closure in drifts excavated in Callovo-Oxfordian claystone: roles of anisotropy and hydromechanical couplings. PhD thesis. Université Paris-Est.

Gudehus, G. 1996. A comprehensive constitutive equation for granular materials. Soils and Foundations 36 (1): 1–12.

Hanusová., I., Šťástka, J. 2017. Mock-Up Josef experiment – mineralogical study. Abstract for the 7th International Conference on Clays in Natural and Engineered Barriers for Radioactive Waste Confinement, Davos.

Hausmannová, L., Hanusová, I., a Dohnálková, M. 2018. Summary of the research of Czech bentonites for use in the deep geological repository – up to 2018, SÚRAO 309/2018/ENG.

Hill, R. 1952. The elastic behavior of crystalline aggregate. Proc. Physical Soc. A 65: 349–354, London.

Hinson, S. 2019. New Nuclear Power, Briefing Paper. House of Commons Library. Number CBP 8176, September 2019.

HökmarkK, H., Karnland, O., Pusch, R. 1997. A technique for modeling transport/conversion processes applied to smectite-to-illite conversion in HLW buffers. Engineering Geology 47: 367–378.

Horseman, S.T., Winter, M.G., Entwistle, D.C. 1987. Geotechnical characterisation of Boom clay in relation to disposal of radioactive waste. Publications of the European Communities, EUR 1087 EN, Luxembourg.

Horseman, S.T., Winter, M.G., Entwistle, D.C. 1993. Triaxial experiments on Boom clay. In: Cripps, J.C., Coulthard, J.M., Culshaw, M.G., Forster, A., Hencher, S.R., Moon, C.F. (eds). The engineering geology of weak rock. Rotterdam: Balkema, 36–43.

Horseman, S.T., Harrington, J.F. 2002. Laboratory experiments on gas migration in Opalinus Clay samples from the Benken borehole, Switzerland. Unpublublished NAGRA Interner Bericht.

Hoth, P., Wirth, H., Reinhold, K., Bräuer, V., Krull, P., Feldrappe, H. 2007. Endlagerung radioaktiver Abfälle in tiefen geologischen Formationen Deutschlands – Untersuchung und Bewertung von Tongesteinsformationen. Bundesanstalt für Geowissenschaften und Rohstoffe: 118 S. Berlin/Hannover.

Huang, W.L., Longo, J.M., Pevear, D.R. 1993. An experimentally derived kinetic model for smectite-to-illite conversion and its use as a geothermometer. Clays and Clay Minerals 41: 162–177.

Hueckel, T., François, B., Laloui, L. 2009. Explaining thermal failure in saturated clays. Géotechnique 53(3): 197-212.

Hueckel, T., Borsetto, M. 1990. Thermoplasticity of saturated clays: Experimental constitutive study. Journal of Geotechnical Engineering 116(12): 1765-1777, ASCE.

Ikonen, K., Kuutti, J., Raiko, H., 2018. Thermal dimensioning for the Olkiluoto Repository - 2018 update. Workreport 2018-26, Posiva Oy.

Inoue, A. 1983. Potassium fixation by clay minerals during hydrothermal treatment. Clays and Clay Minerals 31: 81-91.

Inoue, A. 1995. Formation of clay minerals in hydrothermal environments. In: Velde, B. (ed.). Origin and Mineralogy of Clays. Springer, 268-329.

Jacinto, A.C., Villar, M.V., Gómez-Espina, R., Ledesma, A. 2009. Adaptation of the van Genuchten expression to the effects of temperature and density for compacted bentonites. Applied Clay Science 42: 575–582.

Jobmann, M., Amelung, P., Billaux, D., Polster, M., Schmidt, H., Uhlig L. 2007. Untersuchungen zur sicherheitstechnischen Auslegung eines generischen Endlagers im Tonstein in Deutschland - GENESIS – Abschlussbericht. DBE TECHNOLOGY GmbH, Peine.

Jobmann, M., Breustedt, M., Li, S., Polster, M., Schirmer, S. 2013. Investigations on THM effects in buffer, EDZ and argillaceous host rock. Final Report. TEC-09-2012-AB, DBE TECHNOLOGY, Peine.

Jobmann, M., Bebiolka, A., Jahn, S., Lommerzheim, A., Maßmann, J., Meleshyn, A., Mrugalla, S., Reinhold, K., Rübel, A., Stark, L. Ziefle, G. 2017. Projekt ANSICHT - Sicherheits- und Nachweismethodik für ein Endlager im Tongestein in Deutschland. Synthesebericht. Förderkennzeichen 02E11061A/B, DBE TECHNOLOGY GmbH, TEC-19-2016-AB, Peine.

Jockwer, N., Wieczorek, K., Miehe, R., Fernández Diaz, A.M. 2006. Heater Test in the Opalinus Clay of the Mont Terri URL. Gas Release and Water Redistribution Contribution to Heater Experiment (HE). Rock and bentonite thermohydro- mechanical (THM) processes in the nearfield. GRS Report 223 ISBN 3-931995-93-3. http://www.grs.de/sites/ default/files/pdf/GRS-223.pdf

Johnson, L.H., Niemeyer, M., Klubertanz, G., Siegel, P., Gribi, P. 2002. Calculations of the Temperature Evolution of a Repository for Spent Fuel, Vitrified High-Level Waste and Intermediate Level Waste in Opalinus Clay. NAGRA TR 01-04.

Johnson, L., Gaus, I., Wieczorek, K., Mayor, J.C., Sellin, P., Villar, M.V., Samper, J., Cuevas, J., Gens, A., Velasco, M., Turrero, M.J., Montenegro, L., Martín, P.L., Armand, G. 2014. Integration of the short-

term evolution of the engineered barrier system (EBS) with the long-term safety perspective (Deliverable D4.1 of the PEBS project). NAGRA Arbeitsbericht NAB 14-079.

Juvankoski, M. 2013. Buffer design 2012. Report POSIVA 2012-14, Posiva Oy. ISBN 978-951-652-195-7.

Kamei, G., Mitsui, M.S., Futakuchi, K., Hashimoto, S., Sakuramoto, Y. 2005. Kinetics of long-term illitization of montmorillonite—a natural analogue of thermal alteration of bentonite in the radioactive waste disposal system. Journal of Physics and Chemistry of Solids 66 (2-4): 612-614.

Karnland, O., Birgersson, M. 2006. Montmorillonite stability. With special respect to KBS-3 conditions. SKB TR-06-11, Svensk Kärnbränslehantering AB.

Karnland, O., Sandén, T., Johannesson, L.E., Eriksen T.E., Jansson, M., Wold, S., Pedersen, K., Motamedi, M., Rosborg B. 2000. Long-term test of buffer material. Final report on the pilot parcels. SKB report TR-00-22, Svensk Kärnbränslehantering AB. Stockholm, 131 pp.

Karnland, O., Nilsson, U., Weber, H.P., Wersin, P. 2008. Sealing ability of Wyoming bentonite pellets foreseen as buffer material – Laboratory results. Physics and Chemistry of the Earth Parts A/B/C 33(1): S472-S475.

Karnland, O., Olsson, S., Dueck, A., Birgersson, M., Nilsson, U., Hernan-Hakansson, T., Pedersen, K., Nilsson, S., Eriksen, T.E., Rosborg, B. 2009. Long-term test of buffer material at the Äspö Hard Rock Laboratory, LOT project. Final report on the A2 test parcel. SKB report TR-09-29, Svensk Kärnbränslehantering AB. Stockholm, 295 pp.

Karnland, O., Olsson, S., Sandén, T., Fälth, B., Jansson, M., Eriksen, T.-E., Svärdström, K., Rosborg B., Muurinen, A. 2009. Long-term test of buffer material at the Äspö Hard Rock Laboratory, LOT project. Final report on the A0 test parcel. SKB report TR-09-31, Svensk Kärnbränslehantering AB. Stockholm, 123 pp.

Kiviranta, L., Kumpulainen, S. 2011. Quality Control and Characterization of Bentonite Materials, Workreport 2011-84, Posiva Oy.

Kiviranta, L., Kumpulainen, S., Pintado, X., Karttunen, P., Schatz, T. 2018. Characterization of Bentonite and Clay Materials 2012-2015. Workreport 2016-5, Posiva Oy.

Kotnour, P. 2017. Výzkum a vývoj ukládacího obalového souboru pro hlubinné ukládání vyhořelého jaderného paliva do stádia realizace vzorku 3. etapa, TZ SÚRAO, 2017.

Labiouse, V., Sauthier, C., You, S., 2014. Hollow cylinder experiments of galleries in Boom Clay Formation. Rock Mechanics and Rock Engineering 47(1): 43-55.

Laine, H., Karttunen, P. 2010. Long-Term Stability of Bentonite A Literature Review. POSIVA Working Report 2010-53: 128 pp.

Lanyon, G.W. 2019a. Update of synopsis regarding EDZ development and evolution at the Mont Terri Rock Laboratory. NAGRA Arbeitsbericht NAB 18-045.

Lanyon, G.W. 2019b. Update of synopsis regarding EDZ development and evolution at the Mont Terri Rock Laboratory. NAGRA Arbeitsbericht NAB 18-045.

Le, T.-T. 2008. Comportement thermo-hydro-mécanique de l'argile de Boom. PhD thesis. CERMES, Ecole Nationale des Ponts et Chaussées, Paris.

Leal-Olloqui, M. 2019. A study of alteration processes in bentonite. PhD thesis. University of Bristol. 328 pp.

Lenoir, N., Bornert, M., Desrues, J., Bésuelle, P., Viggiani, G. 2007. Volumetric digital image correlation applied to X-Ray microtomography images from triaxial compression tests on argillaceous rocks. Strain 43: 193-205.

Leonard, D. 2017. Design and construction of the supercontainer for category C waste. Technical report. NIROND-TR 2017-11 E V2 (Internal report ONDRAF/NIRAS).

Leupin, O., Lawrence, J. 2014. Requirements for buffer for a repository for SF/HLW in Opalinus Clay. NAGRA Working Report NAB 13-46. NAGRA, Wettingen.

Leupin, O.X. (Ed.), Birgersson, M., Karnland, O., Korkeakoski, P., Sellin, P., Mäder, U., Wersin, P. 2014. Montmorillonite stability under near-field conditions. NAGRA TR14-12. Wettingen, 104 pp.

Leupin, O.X., Smith, P., Marschall, P., Johnson, L., Savage, D., Cloet, V., Schneider, J., Senger, R.K. 2016. High-level waste repository-induced effects. NAGRA Technical Report NTB 14-13.

Li, X., Bernier, F., Vietor, T., Lebon, P. 2007. TIMODAZ. Deliverable 2. EC Contract: FI6W-CT-036449, 104 pp.

Lima, A. 2011. Thermo-hydro-mechanical behaviour of two deep Belgium clay formations: Boom Clay and Ypresian clays. PhD Thesis. Universitat Politècnica de Catalunya, Spain.

Lima, A., Romero, E., Piña, Y. 2011. Water retention properties of two deep Tertiary clay formations within the context of radioactive waste disposal. A: Simpósio Brasileiro de Solos Nao Saturados. VII Brazilian Symposium on Unsaturated Soil. Pirenópolis, Goiania, 315-321.

Mäder, U.K. 2009. Reference pore waters for the Opalinus Clay and "Brown Dogger" for the provisional safety-analysis in the framework of sectoral plan - interim results (SGT-ZE). NAGRA Arbeitsbericht NAB 09-014.

Madsen, F.T. 1998. Clay mineralogical investigations related to nuclear waste disposal. Clay minerals 33(1): 109-129.

Mair, R., Taylor, R., Clarcke, B. 1992. Repository tunnel construction in deep clay formations. Commission of the European Communities. Nuclear science and Technology EUR 13964.

Marschall, P., Horseman, S., Gimmi, T. 2005. Characterization of gas transport properties of the Opalinus Clay, a potential host rock formation for radioactive waste disposal. Oil & Gas Science and Technology 60(1): 121-139.

Martínez, V., Abós, H., García-Siñeriz, J.L. 2016. FEBEXe: Final Sensor Data Report (FEBEX 'In situ' Experiment). NAGRA Arbeitsbereicht NAB 16-019. Wettingen, 230 pp.

Mašín, D. 2005. A hypoplastic constitutive model for clays. International Journal for Numerical and Analytical Methods in Geomechanics 29(4): 311-336.

Mašín, D. 2010. Predicting the dependency of a degree of saturation on void ratio and suction using effective stress principle for unsaturated soils. International Journal for Numerical and Analytical Methods in Geomechanics 34 (1): 73-90.

Mašín, D. 2012. Hypoplastic Cam-clay model. Géotechnique 62(6): 549-553.

Mašín, D. 2013. Double structure hydromechanical coupling formalism and a model for unsatu-rated expansive clays. Engineering Geology 165: 73-88.

Mašín, D. 2014. Clay hypoplasticity model including stiffness anisotropy. Géotechnique 64(3): 232-238.

Mašín, D. 2017. Coupled thermohydromechanical double structure model for expansive soils. ASCE Journal of Engineering Mechanics 143(9).

Mašín, D., Khalili, N. 2008. A hypoplastic model for mechanical response of unsaturated soils. International Journal for Numerical and Analytical Methods in Geomechanics 32(15): 1903-1926.

Mašín, D., Khalili, N. 2016. Swelling phenomena and effective stress in compacted expansive clays. Canadian Geotechnical Journal 53(1): 134-147.

Mayor, J.C., García-Siñeriz, J.L., Alonso, E. Alheid, H.J., Blümling P. 2005. Engineered barrier emplacement experiment in Opalinus Clay for the disposal of radioactive waste in underground repositories. Report EUR 21920.

Mazurek, M., Pearson, F.J., Volckaert, G., Bock, H. 2003. Features, Events and Processes Evaluation Catalogue for Argillaceous Media. Radioactive Waste Management. OECD Nuclear Energy Agency (NEA), France, 380 pp. ISBN 92-64-02148-5.

McTigue, D.F. 1986. Thermoelastic response of fluid-saturated porous rock. Journal of Geophysical Research 91(B9): 9533—9542.

Mertens, J., Wouters, L. 2003. 3D Model of the Boom Clay around the HADES-URF, Construction of an AUTOCAD 3D-model of the URF, together with the internal clay layering. NIROND 2003-02, 31 pp.

Mertens, J., Vandenberghe, N., Wouters, L., Sintubin, M. 2003. The origin and development of joints in the Boom Clay Formation (Rupelian) in Belgium. In: Van Rensbergen, P., Hillis, R.R., Maltman, A.J., Morley, C.K. (eds). Subsurface Sediment Mobilization. Geological Society Special Publication 217: 311-323, London.

Mertens, J., Bastiaens, W., Dehandschutter, B. 2004. Characterisation of induced discontinuities in the Boom Clay around the underground excavations (URF, Mol, Belgium). Applied Clay Science 26: 413-428.

Mohajerani, M., Delage, P., Sulem, J., Monfared, M., Tang, A.M., Gatmiri, B. 2012. "A laboratory investigation of thermally induced pore pressures in the Callovo-Oxfordian claystone". International Journal of Rock Mechanics and Mining Sciences 52: 112–121.

Monfared, M. 2011. Couplages température-endommagement-perméabilité dans les sols et les roches argileuses. PhD thesis. École Nationale des Ponts et Chaussées.

Morodome, S., Kawamura, K. 2009. Swelling behaviour of Na- and Ca- montmorillonite up to 150◦C by in situ X-ray diffraction experiments. Clays and Clay Minerals 57(2): 150–160.

Müller, H.R., Garitte, B., Köhler, S., Vogt, T., Sakaki, T., Weber, H., Vietor, T. 2015. LUCOEX (EURATOM Grant Agreement 269905). Deliverable D2.6 Final Report of WP2. 56 pp.

Müller-Vonmoos, M., Kahr, G. 1983. Mineralogische Untersuchungen von Wyoming bentonit MX-80 und Montigel. NAGRA. Technischer Bericht 83-12.

Muñoz, J.J., Lloret, A., Alonso, E. 2003. "VE" Experiment - Laboratory Report: Characterization of hydraulic properties under saturated and non-saturated conditions Project Deliverable 4, EC contract FIKW-CT2001-00126.

Muurinen, A., Karnland, O., Lehikoinen, J. 2004. Ion concentration caused by an external solution into the porewater of compacted bentonite. Physics and Chemistry of the Earth 29: 119–127.

Muurinen, A. 2011. Measurements on Cation Exchange Capacity of Bentonite in the Long-Term Test of Buffer Material (LOT) Posiva Working Report 10 : 26 pp, January 2011.

NAGRA 2002a. Project Opalinus Clay: Safety report: Demonstration of disposal feasibility for spent fuel, vitrified high-level waste and long-lived intermediate-level waste (Entsorgungsnachweis). NAGRA Technical Report NTB 02-05.

NAGRA 2002b. Projekt Opalinuston: Synthese der geowissenschaftlichen Untersuchungsergibnisse - Entsorgunsnachweis für abgebrannte Brennelemente, verglaste hochaktive sowie langlebige mittelaktive Abfälle. NAGRA Technischer Bericht NTB 02-03.

NAGRA 2008. Vorschlag geologischer Standortgebiete für ein SMA- und ein HAA-Lager: Begründung der Abfallzuteilung, der Barrierensysteme und der Anforderungen an die Geologie (Bericht zur Sicherheit und Machbarkeit). NAGRA Technischer Bericht NTB 08-05.

NAGRA 2014a. An Assessment of the Impact of the Long Term Evolution of Engineered Structures on the safety-Relevant Functions of the Bentonite Buffer in a HLW Repository. NAGRA Technical Report. NTB 13-02.

NAGRA 2014b. Montmorillonite stability under near-field conditions. NAGRA Technical Report. NTB 14-12.

NAGRA 2014c. SGT Etappe 2: Vorschlag weiter zu untersuchender geologischer Standortgebiete mit zugehörigen Standortarealen für die Oberflächenanlage: Geologische Grundlagen Dossier VI Barriereneigenschaften der Wirt- und Rahmengesteine. Nagra Technischer Bericht. NTB 14-02 Dossier VI.

NAGRA 2015. Thermo-hydro-mechanical characterization and modelling of Wyoming granular bentonite. NAGRA Technical Report NTB 15-05. NAGRA, Wettingen, Switzerland.

NAGRA 2016a. High-level waste repository-induced effects. NAGRA Technical report. NTB 14-13.

NAGRA 2019. Implementation of the Full-scale Emplacement Experiment at Mont Terri: Design, Construction and Preliminary Results. NAGRA Technical Report. NTB 15-02. Wettingen, 147 pp.

Nguyen, X.P., Cui, Y.J, Tang, A.M., Deng, Y.F., Li, X.L., Wouters, L. 2013. Effects of pore water chemical composition on the hydro-mechanical behavior of natural stiff clays. Engineering Geology 166: 52-64.

Olivella, S., Gens, A., Carrera, J., Alonso, E.E. 1996. Numerical formulation for a simulator (CODE_BRIGHT) for the coupled analysis of saline media. Engineering Computations 13(7): 87-112.

Olsson, S., Jensen, V., Johannesson, L.E., Hansen, E., Karnland, O., Kumpulainen, S., Kiviranta, L., Svensson, D., Hansen, S., Lindén, J. 2013. Prototype Repository. Hydro-mechanical, chemical and mineralogical characterization of the buffer and tunnel backfill material from the outer section of the Prototype Repository. SKB report TR-13-21.

ONDRAF/NIRAS 2013. Research, Development and Demonstration (RD&D) plan for the geological disposal of high level and / or long-lived radioactive waste including irradiated fuel if considered as waste. State-of-the-art report as of December 2012. Belgian Agency for Radioactive Waste for Enriched Fissile Materials. NIROND-TR 2013-12 E.

Ouvry, J.F. 1983. Caractéristiques géotechniques de l'argile de Boom (Belgique) à partir des essais de laboratoires communiqués par le CEN/SCK. Service géologique régional du Nord-Pas-de-Calais, Lille, France.

Pellet, F. 2007. Expertise sur le comportement différé des argilites. Rapport interne ANDRA N° CRP0FLO070024.

Petley, D.N. 1999. Failure envelopes of mudrocks at high effective stresses. In: Aplin, A.C., Fleet, A.J., Macquaker, J.H.S. (eds). Physical Properties of Muds and Mudstones. Special Publication of the Geological Society of London 158: 61-71.

Pintado, X., Ledesma, A., Lloret, A. 2002. Backanalysis of thermohydraulic bentonite properties from laboratory tests. Engineering Geology 64(2): 91–115

Pintado, X., Mamunul, H.M., Martikainen, J. 2013. Thermo-Hydro-Mechanical Tests of Buffer Material. POSIVA 2012-49. Olkiluoto, 152 pp. ISBN 978-951-652-231-2.

Pöhler, M., Amelung, P., Bollingerfehr, W., Engelhardt, H.J., Filbert, W., Tholen, M. 2010. Referenzkonzept für ein Endlager für radioaktive Abfälle im Tongestein. ERATO. Abschlussbericht. Förderkennzeichen 02E 10288, DBE TECHNOLOGY GmbH, TEC-28-2008-AB, Peine.

Poller, A., Mayer, G., Croisé, J. 2007. Two-phase Flow Analysis of Gas Tests in Opalinus Clay Core Specimen: Complementary Analysis. Mont Terri TN 2007-01.

POSIVA, 2013. Safety Case for the Disposal of Spent Nuclear Fuel at Olkiluoto – Performance Assessment 2012. Posiva report 2012-04, ISBN 978-951-652-185-8.

Potts, D.M., Zdravkovic, L. 1999. Finite element analysis in geotechnical engineering: Theory. Thomas Telford, London.

Pusch, R. 2001. The buffer and backfill handbook. Part 2: Materials and techniques: Swedish Nuclear Fuel and Waste Management Co. SKB TR-02-12. 197 pp.

Pusch, R., Kasbohm, J., Thao, H.M. 2010. Chemical stability of montmorillonite buffer clay under repository-like conditions - A synthesis of relevant experimental data. Applied Clay Science 47(1–2): 113–119.

Raymaeckers, D., D'Orazio, D., Leonard, D. 2019. Les déchets de forte activite et/ de longue durée de vie. Le design et l'architecture du stockage géologique. Journée d'étude du SBGIMR – Le stockage des déchets nucléaires, Liège 21 Février 2009 (Presentation).

Rebours, H., Andre, G., Cruchaudet, M., Dewonck, S., Distinguin, M., Drouiller, Y., Morel, J., Wileveau, Y., Vinsot, A., 2005. Callovo-Oxfordien - Rapport de synthèse. D.RP.ADPE.04.1110, Andra, Paris, France.

Reinhold, K., Sönnke, J. 2012. Geologische Referenzprofile in Süd- und Norddeutschland. Projekt ANSICHT: Methodik und Anwendungsbezug eines Sicherheits- und Nachweiskonzeptes für ein HAW-Endlager im Tonstein, Bundesanstalt für Geowissenschaften und Rohstoffe (BGR), Berlin und Hannover.

Reinhold, K., Stark, L., Kühnlenz, T., Ptock, L. 2016. Endlagerstandortmodell SÜD – Teil I: Be-schreibung des geologischen Endlagerstandortmodells. Projekt ANSICHT: Methodik und Anwendungsbezug eines Sicherheits- und Nachweiskonzeptes für ein HAW-Endlager im Ton-stein, Bundesanstalt für Geowissenschaften und Rohstoffe (BGR), Berlin und Hannover.

Roaldset, E., Wei, H., Grimstad, S. 1998. Smectite to illite conversion by hydrous pyrolysis. Clays and Clay Minerals 33: 147-158.

Robinet, J.C., Sardini, P., Coelho, D., Parneix, J.-C., Prêt, D., Sammartino, S., Boller, E., Altmann S. 2012. Effects of mineral distribution at mesoscopic scale on solute diffusion in a clay-rich rock. Example of the Callovo-Oxfordian mudstone of Bure (France), Water Ressources Research (48), W05554.

Romero, E., Gens, A., Lloret, A. 2001. Temperature effects on the hydraulic behaviour of an unsaturated clay. Geotechnical and Geological Engineering 19: 311–332.

Romero, E. Gens, A. Lloret, A. 2003. Suction effects on a compacted clay under non-isothermal conditions. Geotechnique 53(1): 65–81.

Romero, E., Gómez, R. 2013. Water and air permeability tests on deep core samples from Schlattingen SLA-1 borehole. NAGRA Arb. Ber. NAB 13-51. NAGRA, Wettingen, Switzerland.

Rousset, G. 1988. Comportement mécanique des argiles profondes, application au stockage de déchets radioactifs. PhD thesis. École Nationale des Ponts et Chaussées.

RWM 2016. Geological Disposal Part B: Technical Specification Generic Disposal System Specification. NDA Report no. DSSC/402/01.

RWM 2017. Geological Disposal GEOWASTE Project: Summary of Output from a Joint EPSRC NDA RWMD Co-funded Project. January 2017. NDA Report no. NDA/RWM/152.

Salager, S., Rizzi, M., Laloui L. 2011. An innovative device for determining the soil water retention curve under high suction at different temperatures. Acta Geotechnica 6(3): 135-142.

Sandén, T., Nilsson, U., Andersson, L., Svensson, D., 2018. ABM45 experiment at Äspö Hard Rock Laboratory. Installation report. SKB Report P-18-20.

Sarikaya, Y., Onal, M., Baran, B., Alemdaroglu, T. 2000. The effect of thermal treatment on some of the physicochemical properties of a bentonite. Clays and Clay Minerals 48(5): 557–562.

Sena, C., Salas, J., Arcos, D. 2010. Thermo-hydro-geochemical modelling of the bentonite buffer. The LOT-A2 experiment. SKB TR-10-65. Svensk Kärnbränslehantering AB.

Seiphoori, A., Ferrari, A., Laloui, L. 2014. Water retention behaviour and microstructural evolution of MX-80 bentonite during wetting and drying cycles. Géotechnique 64(9): 721-734.

Sellin, P., Leupin, O. 2013. The Use of Clay as an Engineered Barrier in Radioactive-Waste Management – A Review. Clays and Clay Minerals 61: 477-498.

Senger, R.K., Ewing, J. 2008. Evolution of temperature and water content in the bentonite buffer: Detailed modelling of two-phase flow processes associated with the early closure period – Complementary simulations. NAGRA Working Report NAB 08-53. NAGRA, Wettingen.

Senger, R.K., Papafotiou, A., Marschall, P. 2014. Thermo-hydraulic simulations of the near-field of a SF/HLW repository during early- and late-time post-closure period. NAGRA Arbeitsbericht NAB 14-011.

Seyedi, D.M., Armand, G., Noiret, A. 2017. "Transverse Action" – A model benchmark exercise for numerical analysis of the Callovo-Oxfordian claystone hydromechanical response to excavation operations. Computers and Geotechnics 85: 287-305.

Seyedi, D.M., Plua, C., Vitel, M., Armand, G., Rutqvist, J., Birkholzer, J., Xu, H., Guo, R., Thatcher, K.E., Bond, A.E., Wang, W., Nagel, T., Shao H., Kolditz, O. 2020. A numerical benchmark exercise for thermo-hydro-mechanical modeling of an in situ heating test in the Callovo-Oxfordian claystone. Submitted to the International Journal of Rock Mechanics and Mining Sciences.

Sillen, X., Marivoet, J. 2007. Thermal impact of a HLW repository in clay. Deep disposal of vitrified high-level waste and spent fuel. Mol, Belgium: SCK•CEN. 59 p. (External Report of the Belgian Nuclear Research Centre, ER-38, CCHO 2004-2470/00/01, DS 251.SAF). ISSN 1782-2335.

SKB 2011. Long-term safety for the final repository for spent nuclear fuel at Forsmark. Main report of the SR-Site project – Volume I. TR-11-01. Svensk Kärnbränslehantering AB.

Spang, B. 2002. Excel Add-In for Properties of Water and Steam in SI-Units. http://www.cheresources.com/iapwsif97.shtml

Špinka, O., Grunwald, L., Zahradník, O., Veverka, A., Fiedler, F., Nohejl, J. 2018. Siting study – Březový potok FINAL report, SÚRAO 139/2017.

Šťástka, J., Hausmannová, L., Hanusová, I. 2017. The Mock-Up Josef In-Situ Physical Model after 4 Years of Operation. Abstract for the 7th International Conference on Clays in Natural and Engineered Barriers for Radioactive Waste Confinement, Davos.

Šťástka, J. 2014. MOCK-UP Josef demonstration experiment. Tunel 23(2) : 65-73. http://www.ita-aites.cz/files/tunel/2014/2/tunel_2_14-12.pdf

Sultan, N. 1997. Etude du comportement thermo-mécanique de l'Argile de Boom: Expériences et modélisation. PhD thesis, École Nationale des Ponts et Chaussées.

Sultan, N., Delage, P., Cui, Y.J. 2000. Comportement thermomécanique de l'Argile de Boom. C. R. Acad. Sci. Paris 328, Série II *b*: 457–463.

Svensson, D., 2015. The Bentonite barrier. Swelling properties, redox chemistry and mineral evolution. Doctoral thesis. Lund. ISBN 978-91-7422-385-9.

Svensson, D., Dueck, A., Nilsson, U., Olsson, S., Sandén, T., Lydmark, S., Jägerwall, S., Pedersen, K., Hansen, S. 2011. Alternative Buffer Material, Status of the ongoing laboratory investigation of reference materials and test package 1. SKB Technical Report TR-11-06. Svensk Kärnbränslehantering.

Svensson, D., Hansen, S. 2013. Redox chemistry in two iron-bentonite field experiments at Äspö hard rock laboratory, Sweden: An XRD and Fe-K edge XANES study. Clays and Clay Minerals 61: 566-579.

Tang, A.M., Cui, Y.J. 2007. "Controlling suction by vapour equilibrium technique at different temperatures, application to the determination of the water retention properties of MX80 clay." Can. Geotech. J. 42(1): 287–296.

Tang, A.M., Cui, Y.J., Le, T.T. 2008a. A study on the thermal conductivity of compacted bentonites. Appl. Clay Sci. 41 (3): 181–189.

Tang, A.M., Cui, Y.J., Barnel, N. 2008b. Thermo-mechanical behaviour of a compacted swelling clay. Géotechnique 58(1): 45-54.

Teodori, S.P., Gaus, I. (Eds.) (2012): Report of the construction of the HE-E experiment. Deliverable D2.2-3 of the PEBS Project. EU report downloadable from http://www.pebseu.de/.

Terzaghi, K., Peck, R., Mesri, G. 1996. Soil Mechanics in Engineering Practice. Third edition, John Wiley & sons.

Thatcher, K.E., Newson, R.K., Watson, S.P., Norris, S. 2017. Review of data and models on the mechanical properties of bentonite available at the start of Beacon. Deliverable D2.2.

Thatcher, K. 2017. FEBEX-DP: THM modelling, Contractor Report to RWM no. QRS-1713A-R2, V1.8, March 2017.

TIMODAZ 2010. Deliverable D13 – Simulation of lab and in situ tests. European commission.

Toprak, E. 2018. Long term response of multi-barrier schemes for underground radioactive waste disposal. Doctoral thesis, Universitat Politècnica de Catalunya.

Toprak, E., Mokni, N., Olivella, S., Pintado, X. 2013. Thermo-hydraulic-mechanical modelling of buffer and backfill. Report POSIVA 2012-47, Posiva Oy. ISBN 978-951-652-230-5.

Tourchi, S., Vaunat, J., Gens, A. 2019. THM modelling of the ALC1604 experiment. Rapport Andra n°CGRPCMFS190016.

Traber, D., Blaser, P. 2013. Gesteinsparameter der Wirtgesteine Opalinuston, 'Brauner Dogger', Effinger Schichten und Helvetische Mergel als Grundlage für die Sorptionsdatenbank. NAGRA Arbeitsbericht NAB 12-039.

Tripathy, S., Thomas, H.R., Stratos, P. 2017. Response of Compacted Bentonites to Thermal and Thermo-Hydraulic Loadings at High Temperatures. Geosciences 7(53): 1 – 23.

Tsiampousi, A., Zdravković, L., Potts, D.M. 2013. A new Hvorslev surface for critical state type unsaturated and saturated constitutive models. Computers and Geotechnics 48: 156–166.

Tsitsopoulos, V., Baxter, S., Holton, D., Dodd, J., Williams, S., Thompson, S. 2018. Modelling the Prototype Repository. Geological Society Special Publications 482: 241-260, London, 7 December 2018.

Valter, M., Plötze, M. 2013. Characteristics of variably saturated granular bentonite after long-term storage at near-field relevant temperatures. Clay Minerals 48(2): 343-361.

Van Geet, M., Lalieux, P., Van Humbeek, H., Dierckx, A., De Preter, P., Gens, R., Bernier, F. 2007. PRACLAY success criteria. NIROND note 2007-1144 (internal report).

Van Humbeeck, H., Verstricht, J., Li, X.L., De Cannière, P., Bernier, F., Kursten, B. 2009. The OPHELIE mock-up. Final report. EURIDICE report 09-134. 197 pp. http://www.euridice.be/sites/default/files/scientific/OPHELIE%20mockup%20final%20report%20low%20resolution.pdf

Van Marcke, P., Li, X.L, Bastiaens W., Verstricht J., Chen G., Leysen J., Rypens J., 2013. The design and installation of the PRACLAY In-Situ Experiment. EURIDICE report 13-129.

Vandenberghe, N., De Craen, M., Wouters, L. 2014. The Boom Clay geology, from sedimentation to present-day occurrence, a review. Royal Belgian institute of natural sciences. Memoirs of the geological survey of Belgium, N.60-2014.

Večerník, P., Trpkošová, D., Hofmanová, E. 2014. Vývoj aparatur pro charakterizaci materiálů inženýrských bariér hlubinného úložiště radioaktivních odpadů a vyhořelého jaderného paliva - TA04021378. Zpráva ÚJV Řež, a. s. číslo 14422.

Velde, B., Vasseur, G. 1992. Estimation of the diagenetic smectite to illite transformation in time-temperature space. American Mineralogist 77: 967–976.

Villar, M.V. 2002. Thermo-hydro-mechanical characterisation of a bentonite from Cabo de Gata. A study applied to the use of bentonite as sealing material in high level radioactive waste repositories. Publicación Técnica Enresa 01/2002, Madrid, 258 pp.

Villar, M.V. 2005. MX-80 bentonite. Thermo-hydro-mechanical characterisation performed at CIEMAT in the context of the Prototype Project. Informes Técnicos CIEMAT 1053. CIEMAT, Madrid, 39 pp. Febrero 2005.

Villar, M.V. (Ed.) 2006. FEBEX Project Final report. Post-mortem bentonite analysis. Publicación Técnica ENRESA 05-1/2006, Madrid, 183 pp.

Villar, M.V. 2007. Water retention of two natural compacted bentonites. Clays and Clay Minerals 55(3): 311-322.

Villar, M.V. 2013. Long-term THM tests reports: Isothermal infiltration tests with materials from the HE-E. PEBS Deliverable 2.2-7.2. CIEMAT Technical Report CIEMAT/DMA/2G210/07/2013. Madrid, 32 pp.

Villar, M.V. 2017. FEBEX-DP Postmortem THM/THC Analysis Report. Technical Report NAB 16-017. 147 pp.

Villar, M.V., Lloret, A. 2004. Influence of temperature on the hydro-mechanical behaviour of a compacted bentonite. Applied Clay Science 26(1–4): 337–350.

Villar, M.V., Gómez-Espina, R. 2008. Effect of temperature on the water retention capacity of FEBEX and MX-80 bentonites. In: Toll, D.G., Augarde, C.E., Gallipoli, D., Wheeler, S.J. (eds.). Unsaturated soils: Advances in Geo-engineering. Proceedings of the first European Conference on unsaturated soils, E-UNSAT 2008. Durham, UK, July 2-4 2008. CRC Press/Balkema. Taylor & Francis Group, London, 257-262.

Villar, M.V., Gómez-Espina, R. 2009. Report on thermo-hydro-mechanical laboratory tests performed by CIEMAT on FEBEX bentonite 2004 – 2008. Informes Técnicos CIEMAT 1178. Madrid, 67 pp. Agosto 2009.

Villar, M.V., Gómez-Espina, R., Martín, P.L. 2006. Behaviour of MX-80 bentonite at unsaturated conditions and under thermo-hydraulic gradient. Work performed by CIEMAT in the context of the TBT project. Informes Técnicos CIEMAT 1081. CIEMAT, Madrid, 45 pp. July 2006. DOI: 10.13140/RG.2.2.30062.92482

Villar, M.V., Sánchez, M., Gens, A. 2008. Behaviour of a bentonite barrier in the laboratory: Experimental results up to 8 years and numerical simulation. Physics and Chemistry of the Earth 33: S476–S485.

Villar, M.V., Gómez-Espina, R., Martín, P.L., Barcala, J.M. 2012. Tests in thermo-hydraulic cells to simulate the behaviour of engineered barriers. In: Laloui, L., Ferrari, A. (eds). Multiphysical Testing of Rocks and Shales. Springer Series in Geomechanics and Geoengineering, Springer, Berlin, 137-142. ISBN: 978-3-642-32491-8.

Villar, M.V., Iglesias, R.J., Abós, H., Martínez, V., de la Rosa, C., Manchón, M.A. 2016a. FEBEX-DP onsite analyses report. NAB 16-12. 106 pp.

Villar, M.V., Martín, P.L., Romero, F.J., Iglesias, R.J., Gutiérrez-Rodrigo, V. 2016b. Saturation of barrier materials under thermal gradient. Geomechanics for Energy and the Environment 8: 38-51. https://doi.org/10.1016/j.gete.2016.05.004

Von Wolffersdorff, P.A. 1996. A hypoplastic relation for granular materials with a predefined limit state surface. Mechanics of Cohesive-Frictional Materials 1: 251–271.

Wan, M., Ye, W.M., Chen, Y.G., Cui, Y.J. 2015. Influence of temperature on the water retention properties of compacted GMZ01 bentonite. Environmental Earth Science 73: 4053-4061.

Wang, L., Bornert, M., Chanchole, S. 2013. Micro-Scale Experimental Investigation of Deformation and Damage of Argillaceous Rocks under Hydric and Mechanical Loads. Poromechanics V: 1635-1643.

Wemaere, I., Marivoet, J., Labat, S. 2008. Hydraulic conductivity variability of the Boom Clay in the north-east Belgium based on four core drilled boreholes. Physics and Chemistry of the Earth 33(s1): 24-36.

Wersin, P., Johnson, L.H., McKinley, I.G. 2007. Performance of the bentonite barrier at temperatures beyond 100°C: A critical review. Physics and Chemistry of the Earth 32(8–14): 780–788.

Wigger, C., (Ed.), Hanusová, I., Hausmannová, L., Heino, V., Lavikainen, L., Leupin, O.X., Marshall, P., Mayor, J.C., Meleshyn, A., Pusch, R., Sellin, P., Swahn, J., Talandier, J., Wendling, J., Wieczorek, K. 2017. Beacon - Bentonite Mechanical Evolution. State-of-the-Art Report. Deliverable D1.1.

Wileveau, Y. 2005. THM behaviour of host rock (HE-D) experiment: Progress report. Part 1, Technical Report TR 2005-03. Mont Terri Project.

Wileveau, Y., Rothfuchs, T. 2007. THM behaviour of host rock (HE-D). Experiment: Study of Thermal effects on Opalinus Clay. Mont Terri Technical Report 2006-01.

Wilson, J. 2017. FEBEX-DP: Geochemical Modelling of Iron-Bentonite Interactions, Contractor Report to RWM no. QRS-1713A-R3, May 2017P.

Wilson, J., Savage, D., Bond, A., Watson, S., Push, R., Bennett, D. 2010. Bentonite: a review of key properties, processes and issues for consideration in the UK context. Quintessa 1.1: 145 pp. QRS-1378ZG-1.1.

Xu, Y., Sun, D., Zeng, Z., Lv, H. 2019. Temperature dependence of apparent thermal conductivity of compacted bentonites as buffer material for high-level radioactive waste repository. Applied Clay Science 174: 10-14.

Ye, W.M., Wan, M., Chen, B., Chen, Y.G., Cui, Y.J., Wang, J. 2012. Temperature effects on the unsaturated permeability of the densely compacted GMZ01 bentonite under confined conditions. Engineering Geology 126: 1–7.

Yu, L., Weetjens, E., Vietor, T., Hart, J. 2010. TIMODAZ (Contract Number: FI6W-CT-2007-036449). Integration of TIMODAZ results within the safety case and recommendations for repository design (D14). Final report of WP6, 48 pp.

Yu, L., Rogiers, B., Gedeon, M., Marivoet, J., De Craen, M., Mallants, D. 2013. A critical review of laboratory and in-situ hydraulic conductivity measurements for the Boom Clay in Belgium. Applied Clay Science 75-76: 1-12.

Zhang, C.L., Rothfuchs, T. 2007. Laboratory Experiments on the THM Behaviour of Clay Rocks, TIMODAZ, Report D.2.

Zhang, C.L., Rothfuchs, T., Jockwer, N., Wieczorek, K., Dittrich, J., Müller, J., Hartwig, L., Komischke, M. 2007. Thermal Effects on the Opalinus Clay. A Joint Heating Experiment of ANDRA and GRS at the Mont Terri URL (HE-D Project). Final Report. Mont Terri Project Technical Report TR 2007-02 and GRS Report 224, ISBN 3-931995-98-4. https://www.grs.de/sites/default/files/fue/grs_224_thermeff_clay.pdf.

Zhang, C.L., Czaikowski, O., Rothfuchs, T. 2010. Thermo-Hydro-Mechanical behaviour of the Callovo-Oxfordian clay rock, GRS – 266, 2010.

Zhang, C.L., Armand, G., Conil, N. 2015. Investigation on the Anisotropic Mechanical Behavior of the Callovo-Oxfordian Clay Rock. Final report GRS 360.

Zhang, F., Xie, S.Y., Shao, J.F. 2012. Groupement de Laboratoires-Géomécanique, Fiche GM6: Effets de la température sur le comportement des argilites. Etude expérimentale et modélisations des effets de la température sur le comportement des argilites. Rapport Andra n° C.RP.0LML.11.0004.

Zheng, L., Rutqvist, J., Birkholzer, J.T., Liu, H.H. 2015. On the impact of temperatures up to 200°C in clay repositories with bentonite engineer barrier systems: A study with coupled thermal, hydrological, chemical, and mechanical modeling. Engineering Geology 197: 278–295.

Zihms, S.G., Harrington, J.F. 2015. Thermal cycling: impact on bentonite permeability. Mineralogical Magazine 79(6): 1543–1550, November 2015